UNIVERSIDADE ESTADUAL DE CAMPINAS

FACULDADE DE ENGENHARIA DE ALIMENTOS

DEPARTAMENTO DE ENGENHARIA DE ALIMENTOS

SIMULAÇÃO COMPUTACIONAL DE PROCESSOS DE DESODORIZAÇÃO E DESACIDIFICAÇÃO DE ÓLEOS VEGETAIS

Roberta Ceriani

Engenheira de Alimentos

Prof. Dr. Antonio José de Almeida Meirelles

Orientador

Tese apresentada à Faculdade de Engenharia de Alimentos da Universidade Estadual de Campinas, para obtenção do título de Doutor em Engenharia de Alimentos.

Campinas, outubro de 2005

FICHA CATALOGRÁFICA ELABORADA PELA
BIBLIOTECA DA F.E.A. – UNICAMP

Ceriani, Roberta
C335s Simulação computacional de processos de desodorização e desacidificação de óleos vegetais / Roberta Ceriani. – Campinas, SP: [s.n.], 2005.

Orientador: Antonio José de Almeida Meirelles
Tese (doutorado) – Universidade Estadual de Campinas. Faculdade de Engenharia de Alimentos.

1. Óleos vegetais. 2. Simulação. 3. Equilíbrio líquido-vapor. 4. Desodorização. 5. Modelagem. I. Meirelles, Antonio José de Almeida. II. Universidade Estadual de Campinas. Faculdade de Engenharia de Alimentos. III. Título.

Título em inglês: Computational simulation of deodorization and deacidificaction of vegetable oils.
Palavras-chave em inglês (Keywords): Vegetable oils, Simulation, Vapor-liquid equilibria Deodorization, Modeling
Titulação: Doutor em Engenharia de Alimentos
Banca examinadora: Antonio José de Almeida Meirelles
Eduardo Caldas Batista
Lireny Aparecida Guaraldo Gonçalves
Maria Regina Wolf Maciel
Claudio Augusto Oller do Nascimento
Luiz Antonio Minim

BANCA EXAMINADORA

_____

Prof. Dr. Antonio José de Almeida Meirelles
DEA/FEA/UNICAMP
Orientador

_____

Prof. Dr. Eduardo Caldas Batista
DEA/FEA/UNICAMP
Membro titular

_____

Profa. Dra. Lireny Aparecida Guaraldo Gonçalves
DTA/FEA/UNICAMP
Membro titular

_____

Profa. Dra. Maria Regina Wolf Maciel
DPQ/FEQ/UNICAMP
Membro titular

_____

Prof. Dr. Claudio Augusto Oller do Nascimento
PQI/POLI/USP
Membro titular

_____

Prof. Dr. Luiz Antonio Minim
CCE/DTA/UFV
Membro titular

Não sei...

se a vida é curta ou longa demais para nós.

Mas sei que nada do que vivemos tem sentido, se não tocarmos o coração das pessoas. Muitas vezes basta ser: colo que acolhe, braço que envolve, palavra que conforta, silêncio que respeita, alegria que contagia, lágrima que corre, olhar que sacia, amor que promove. E isso não é coisa de outro mundo: é o que dá sentido à vida. É o que faz com que ela não seja nem curta, nem longa demais, mas que seja intensa, verdadeira e pura ... enquanto durar.

Não sei - Cora Coralina

Agradecimentos

Ao Prof. Dr. Antonio José de Almeida Meirelles, pela orientação cuidadosa, paciente e entusiástica, pelas inúmeras idéias frutíferas e pelo exemplo de dedicação ao seu trabalho como orientador, pesquisador e professor.

Ao Departamento de Engenharia de Alimentos, por permitir e fazer tênue a transição do mestrado para o doutorado direto.

À UNICAMP por toda a sua estrutura e pelo ambiente agradável do campus.

À FAPESP pela concessão da bolsa e financiamento deste projeto de pesquisa.

Aos membros da banca examinadora pelas sugestões e por aceitarem o convite de participar da etapa final deste trabalho.

Aos meus amigos, por estarem sempre presentes nos momentos importantes, sejam eles alegres ou difíceis. Agradeço pelos conselhos e problemas divididos, por compartilharem almoços, saraus, cantorias, churrascos, *fondues*, cafezinhos, momentos "shopping", cabeleireiro, natação, Via Roça, inaugurações das casas, aniversários, viagens, enfim tudo há de bom!

À minha mãe, companheira de todos os momentos, ao meu marido, Luiz Carlos, pelo amor e sonhos compartilhados, ao meu irmão Rodolfo, pelo carinho, amor e admiração, e ao meu pai, Carlo Ceriani, que me deixou seu exemplo de vida.

Aos amigos e colegas do DEA, do novo EXTRAE (Laboratório de Extração, Termodinâmica Aplicada e Equilíbrio) e da salinha 17. Em especial, agradeço às amigas Cintia e Christianne pela companhia agradável no dia-a-dia, pela amizade e pelas contribuições ao meu trabalho, à amiga Juliana, à Helena e à aluna de iniciação científica Ana Cristina, pelos trabalhos em conjunto.

À Deus, pela vida e pelas pessoas que colocou no meu caminho.

Sumário

RESUMO xiii
ABSTRACT xiv
CAPÍTULO 1. INTRODUÇÃO 1
CAPÍTULO 2. REVISÃO BIBLIOGRÁFICA 7
2.1 Óleos vegetais 7
2.1.1 Óleo de algodão 10
2.1.2 Óleo de amendoim 10
2.1.3 Óleo de canola 11
2.1.4 Óleo de coco 11
2.1.5 Óleo de gérmen de trigo 12
2.1.6 Óleo de palma 12
2.1.7 Óleo de soja 13
2.2 Processamento de óleos vegetais 13
2.2.1 Extração com solvente: recuperação de solvente da miscela 14
2.2.2 Refino 15
2.2.3 Desodorização 16
2.2.4 Princípios da desodorização 17
2.2.5 Perdas no processamento de óleos 21
2.2.5.1 Perdas por destilação (volatilização) 21
2.2.5.2 Perdas por arraste mecânico 22
2.2.5.3 Perdas por reações de degradação térmica e oxidação 23
2.2.5.3.1 Isomerização *cis-trans* 24
2.2.5.3.2 Hidrólise 26
2.2.6 Eficiência de vaporização 28
2.3 Simulação computacional de processos de contato-gás-líquido 29
2.3.1 Destilação diferencial (batelada) 30
2.3.2 Desodorização/desacidificação por via física (equipamento contínuo) 31
2.3.2.1 Regime permanente 31
2.3.2.2 Regime dinâmico 33
2.3.2.3 Estimativa da eficiência de Murphree 35
2.3.2.4 Estimativa do arraste mecânico 36
2.3.3 Equilíbrio de fases 38
2.3.3.1 Ponto de bolha 39
2.3.4 Propriedades termodinâmicas 40
2.3.4.1 Pressão de vapor 41
2.3.4.2 Método UNIFAC para o cálculo do coeficiente de atividade 42
2.3.4.3 Calor específico do líquido e vapor 42
2.3.4.4 Entalpia de vaporização 45
2.3.5 Estimativa da composição de óleos vegetais 46
Referências 47
CAPÍTULO 3. PREDICTING VAPOR-LIQUID EQUILIBRIA OF FATTY SYSTEMS 53
Key words 54
Abstract 54
3.1 Introduction 54
3.2 Vapor pressure model development 56
3.3 Thermodynamic of fatty mixtures 60
3.4 Results and discussion 64
3.5 Conclusion 74

List of symbols 75
Acknowledgements 77
Appendix: Calculation of vapor pressure of propil-laureate ester at 396.85K. 77
References 77
CAPÍTULO 4. SIMULATION OF BATCH PHYSICAL REFINING AND DEODORIZATION PROCESSES 81
Key words 82
Abstract 82
4.1 Introduction 82
4.2 Modeling a batch deodorizer 84
4.3 Results and discussion 88
Acknowledgements 98
References 98
CAPÍTULO 5. SIMULATION OF CONTINUOUS DEODORIZERS: EFFECTS ON PRODUCT STREAMS 101
Key words 102
Abstract 102
5.1 Introduction 102
5.2 Modeling continuous deodorizers: plant and lab-scale 104
5.3 Estimation of oil composition, physical properties, Murphree efficiencies and entrainment 106
5.4 Results and discussion 113
Acknowledgements 126
Appendix I: Equations for the continuous multitray countercurrent flow design 126
Appendix II: Equations for the continuous multitray cross-flow design 127
References 128
CAPÍTULO 6. SIMULATION OF PHYSICAL REFINERS FOR EDIBLE OIL DEACIDIFICATION 131
Abstract 132
Key words 132
6.1. Introduction 132
6.2. Modeling a continuous physical refiner 134
6.2.1 Vapor-liquid equilibria 136
6.2.2 Estimation of oil composition and physical properties 137
6.2.3 Murphree efficiencies and entrainment (or mechanical carry-over) 140
6.3. Results and discussion 142
6.4. Conclusion 150
Acknowledgements 151
Appendix I: Equations for the continuous multitray countercurrent flow design 151
Appendix II: Equations for the continuous multitray cross-flow design 152
References 153
CAPÍTULO 7. MODELING VAPORIZATION EFFICIENCY FOR STEAM REFINING AND/OR DEODORIZATION 157
Abstract 158
Key words 158
7.1. Introduction 158
7.2. Developing a model for steam refining and/or deodorization 160

7.2.1 Physical Situation and Simplifying Hypothesis 160
7.2.2 Mathematical Model Formulation 163
7.2.3 Theory of Steam Stripping from Bailey[5] 169
7.2.4 Steam or Gas Consumption in Stripping Processes 170
7.2.5 Estimation of Physical Properties of the Oil 172
7.3. Results and discussion 173
7.4. Conclusion 182
Nomenclature 182
Acknowledgments 184
Literature cited 184
CAPÍTULO 8. STUDY OF CANOLA OIL DEODORIZATION COMBINING COMPUTATIONAL SIMULATION WITH RESPONSE SURFACE METHODOLOGY 187
Key words 188
Summary 188
8.1. Introduction 188
8.2. Materials and methods 190
8.2.1 Response surface methodology (RSM) 190
8.2.2 Modeling a batch deodorizer 191
8.2.3 Composition of canola oil and reaction features 197
8.3. Results and Discussion 198
Conclusion 207
Acknowledgements 207
References 207
CAPÍTULO 9. CONCLUSÕES GERAIS 211
SUGESTÕES PARA TRABALHOS FUTUROS 215
APÊNDICE I: DINÂMICA NA DESACIDIFICAÇÃO DE ÓLEOS VEGETAIS 217
Referências 225
APÊNDICE II: BANCO DE DADOS DE PRESSÃO DE VAPOR DE COMPOSTOS GRAXOS (REFERENTE AO CAPÍTULO 3) 227
APÊNDICE III: INFORMAÇÕES A RESPEITO DOS PROGRAMAS DE SIMULAÇÃO 237

Lista de Tabelas

Tabela 2.1.1. Classes de óleos vegetais e alguns de seus exemplares (ORTHOEFER, 1996). 7
Tabela 2.1.2. Composição em ácidos graxos de óleos vegetais (FIRESTONE, 1999; BASIRON, 1996). 8
Tabela 2.2.5.1.1. Volatilidade relativa de alguns componentes-chaves de óleos vegetais em relação ao tocoferol (WOERFEL, 1995). 22
Tabela 2.3.3.1.1. Banco de dados de equilíbrio 40
Table 3.2.1. Experimental vapor pressure data bank of fatty compounds 57
Table 3.2.2. Adjusted parameters for Equations 3.2.1 to 3.2.5 60
Table 3.3.1. Differences between the versions of UNIFAC used 64
Table 3.4.1. Average Relative Deviation (ARD) for vapor pressure of fatty compounds . 65

Table 3.4.2. Calculation of the equilibrium vapor composition (Δy^{abs}(mole%))[a] for fatty acids and fatty esters binary mixtures[b] 68

Table 3.4.3. Average Relative Deviation (ARD) for boiling point of triacylglycerols mixtures (ΔT(%))[a] 69

Table 3.4.4. Fatty acid composition of cottonseed oil 70

Table 3.4.5. Estimated composition of cottonseed oil 70

Table 4.3.1. FA composition of coconut oils 89

Table 4.3.2. Estimated composition of coconut oil 90

Table 4.3.3. Comparison of calculated neutral oil loss and refined oil acidity by Petrauskaitè et al. (2) and this work using Model 3 as the simulation tool [a,b] 92

Table 5.3.1. General composition of soybean, wheat germ and canola oils. 108

Table 5.3.2. Estimated composition of soybean oil 109

Table 5.4.1. Operating conditions for the continuous deodorizer simulations. 114

Table 5.4.2. Composition of the deodorizer distillate (%) of soybean oil and the corresponding final oil acidity for different temperatures and pressures [a, b]. 117

Table 5.4.3. Effects of deodorization conditions on final oil acidity and tocopherol retention in soybean oil 121

Table 5.4.4. Comparison between cross-flow and countercurrent flow in multitray deodorizers. 124

Table 6.2.2.1. Simplified composition of palm and coconut oils. 138

Table 6.2.2.2. Complete estimated composition of the more volatile palm oil (MVPO) 138

Table 6.3.1. Operating conditions for the continuous physical refiner simulations 143

Table 6.3.2. Effects of processing conditions on OA and NOL in the physical refining of coconut oil (MVCO and LVCO) with 1% of stripping steam. 148

Table 7.3.1. VLE for components A, B and C at selected conditions of temperature and pressure for soybean oil with 1.1% of acidity. 174

Table 7.3.2. VLE constants for Equations 7.2.2.19, 7.2.2.20 and 7.2.2.24 for soybean oil with 1.1% of acidity. 174

Table 7.3.3. Average Vaporization Efficiencies for steam refining, ε_{1-2}, at Experimental Conditions of Decap et al.[3] $\left(w_{FFA_1} = 1.1\%\right)$. 180

Table 8.2.1.1 Factorial design and coded variables of the deodorization of canola oil using RSM. 191

Table 8.2.3.1. Overall composition of canola oil 197

Table 8.3.1. Simulation results and estimated values for the deodorization of canola oil using RSM. 203

Table 8.3.2. Analysis of variance (ANOVA) 203

Lista de Figuras

Figura 2.2.4.1. Desodorização em batelada em (A) escala industrial (DAVIDSON et al., 1996) e (B) escala laboratorial. 18

Figura 2.2.4.2. Sistema de pratos de desodorização contínua (AHRENS, 1998; CARLSON, 1996). 20

Figura 2.2.5.3.1.1. Configurações *cis* (A) e *trans* (B) em ácidos graxos insaturados..... 25

Figura 2.2.5.3.2.1. Hidrólise do óleo de amendoim contendo ácido esteárico (SZABO SARKADI, 1959). 28

Figura 2.3.2.1.1. Estágio de equilíbrio 32

Figura 2.3.2.2.1. Algoritmo de resolução 34

Figura 2.3.2.4.1. Correlação para o arraste mecânico (FAIR & MATTHEWS, 1958). 37

Figure 3.4.1. Comparative vapor pressure of linear fatty compounds. Code for experimental data: caproic acid (■); lauric acid (□); caproic alcohol (●); lauryl alcohol (○); caproic methyl ester (▲), lauryl methyl ester (Δ). 66

Figure 3.4.2. Experimental and predicted values of short chain triacylglycerols vapor pressure. Code for experimental data: tributirin (□); tricaproin (◆); tricaprilin (Δ) and tricaprin (■). 66

Figure 3.4.3. Comparative vapor pressure of short-chain monoacylglycerols and long-chain fatty acids. Code for experimental data: stearic acid (■); arachidic acid (□) and monomiristate (◆). 67

Figure 3.4.4. Comparison between experimental boiling temperatures of commercial hexane-cottonseed oil miscellas and predicted values by different UNIFAC versions at 310 mmHg (option 1 for the vapor phase behavior). Code for experimental data (■). 72

Figure 3.4.5. Absolute errors in the boiling temperatures as predicted by the methodology proposed in this work using UNIFAC $r^{3/4}$ for mixtures of commercial hexane with cottonseed and peanut oils (option 1 for the vapor phase behavior). Code for predicted values (■). 73

Figure 4.3.1. Relative volatility $(\alpha_{i,TAG})$ of the FFA, MAG and DAG classes for coconut oil (OC2) calculated during Experiment 6 simulation (Model 1). Code: FFA (▽); MAG (Δ) and DAG (○). OC2 oil composition. 91

Figure 4.3.2. Variation of (A) the boiling temperatures, (B) FFA content of the distillate (DA), and (C) FFA content of the oil (OA) with time for the physical refining of coconut oil (OC2, 1.16% of partial acylglycerols) for Experiment 6 (see Table 4.3.3). Code: Model 1 (○); Model 2 (Δ); Model 3 (●) and experimental points (□). The experimental temperature shown is the oven temperature. OA, oil acidity; DA distillate acidity; for other abbreviation see Figure 4.3.1 94

Figure 4.3.3. Main classes of (A) FFA in the oil acidity and (B) acidity and acylglycerols in the distillate for Experiment 6 (see Table 4.3.3). Code: (A) C6:0 to C12:0 (□); C14:0 to C18:0 (○); C18:1 and C18:2 (Δ); (B) DA (▼); TAG (■); DAG (●) and MAG (▲). For other abbreviations see Figure 4.3.2. 95

Figure 4.3.4. Variation in DA, NOL and OA as a function of the FA composition of the coconut oil and its volatility. Code: More-volatile DA (Δ); OA (□) and NOL (○); less-volatile DA (▲); OA (■) and NOL (●). NOL, neutral oil loss; for other abbreviations see Figure 4.3.2. 97

Figure 5.2.1. Continuous tray design: (A) cross-flow, and (B) countercurrent flow. 104

Figure 5.4.1. Profiles for the mass fractions of acylglycerols, FFA, squalene, β-sitosterol and δ-tocopherol (A) in the liquid phase and (B) in the vapor phase; (C) enthalpies and

flows for a typical deodorizing condition (3). Code: (♦) Liquid phase acylglycerols, (■) FFA, (▼) β-sitosterol, (▲) δ-tocopherol and (•) squalene. (◇) Vapor phase acylglycerols, (□) FFA, (▽) β-sitosterol, (△) δ-tocopherol (○) and squalene. Liquid (◀) and vapor (◁) enthalpies. Liquid (★) and vapor (×) flows. 116

Figure 5.4.2. Contribution of distillative and entrainment effects to the total loss of neutral oil (NOL), squalene, β-sitosterol and tocopherol at 2.775 mmHg, 250 °C and 1.3% of stripping steam. 119

Figure 6.2.1. Schematic flow diagram of a continuous tray design: (a) in countercurrent flow, and (b) in cross-flow. 135

Figure 6.3.1. Profiles for the mass flow rates of FFA and acylglycerols in the liquid phase for the (a) CCF and (d) CRF design, in the vapor phase for the (b) CCF and (e) CRF design, and for the temperature in the (c) CCF and (f) CRF stripping column. Code: Vapor phase FFA (▽), TAG (□), DAG (○) and MAG (△); Liquid phase FFA (▼), TAG (■), DAG (•) and MAG (▲). 145

Figure 6.3.2. Final oil acidity (OA) and neutral oil loss (NOL) for physical refining of the MVPO with 1% of stripping steam for (a) CCF and (b) CRF patterns. Code: OA (□) and NOL (△). 146

Figure 6.3.3. Contribution of distillation and entrainment to (a) the total loss of neutral oil (NOL) at 133 Pa and to (b) the loss of TAG at 210°C in the physical refining MVCO. 149

Figure 7.2.1.1. Diagram of continuous bubbling in a steam deodorization and/or steam refining under vacuum through a single orifice. 161

Figure 7.3.1. Predicted profiles of p_A as a function of h. Conditions: 260g of soybean oil, P^O = 300 Pa, T= 250°C, $\dot{m}_G$ = 0.016g/min (1.5%) and H = 0.8 m. (a) Equation 7.2.2.20 (△) and Coelho Pinheiro and Guedes de Carvalho[7] (▽); (b) Equation 7.2.2.24 (□) and Equation 7.2.3.3 (○). 175

Figure 7.3.2. Bubble properties as a function h. Conditions: 260g of soybean oil, P^O = 300 Pa, T= 250°C, $\dot{m}_G$ = 0.016g/min (1.5%) and H = 0.8 m. D_G (○) from Equation 7.2.2.11 and d_b (□) from Equation 7.2.2.5. 176

Figure 7.3.3. Vaporization efficiency $\varepsilon^{h=H}$ as a function of $x_{FFA}(\%)$. Conditions: 260 g of soybean oil, T= 210°C, P^O=300 Pa, 1.5% of steam and H= 0.03 m. 181

Figure 8.2.2.1. Scheme of a lab-scale batch deodorizer. 192

Figure 8.3.1. Variation of the (A) temperature and vaporization rate, and (B) C18:2 *trans*, C18:3 *trans* (% mass) and OA (%) with time for the deodorization of canola oil for trial number 25. 199

Figure 8.3.2. (A) C18:2 *trans* (% mass) and (B) C18:3 *trans* (% mass) as predicted, respectively, by Eqs. 8.3.1 and 8.3.2, and the models of Hénon *et al.* [8]. 201

Figure 8.3.3. Response surface and contour curves of (A) C18:2 *trans* (% mass) and (B) C18:3 *trans* (% mass) as a function of T (°C) and duration (h). 205

Fig. 8.3.4. Superposed contour curves of final OA (%) and total *trans* (% mass) as a function of T (°C) and duration (h). 206

Figura A1. Vazões (a) de líquido e (b) de vapor no desodorizador. 220

Figura A2. Frações molares (a) no líquido (Estágio 1) e (b) no vapor (Estágio N). 221

Figura A3. Frações molares no líquido para (a) água, (b) ácido oléico e (c) trioleína. 223

Figura A4. Frações molares no vapor para (a) água, (b) ácido oléico e (c) trioleína. ... 224
Figura A5. Perfil da temperatura de equilíbrio. 224
Figura A6. Resíduos para o banco de dados de pressão de vapor utilizado no Capítulo 3. 235
Figura A7. Algoritmo de resolução: cálculo do ponto de bolha. 237
Figura A8. Algoritmo de resolução: destilação diferencial. 238
Figura A9. Algoritmo de resolução: destilação diferencial com reação química e balanço de energia. 239
Figura A10. Algoritmo de resolução: processo contínuo em regime permanente..... 240

RESUMO

Este trabalho de tese teve como objetivo o estudo por simulação computacional de processos de desacidificação por via física e de desodorização presentes na indústria de óleos vegetais. A modelagem foi desenvolvida tanto para o estudo dos processos em batelada como contínuo em regimes permanente e dinâmico. Para a descrição dos balanços de massa, energia e das relações de equilíbrio, são necessárias equações empíricas e/ou modelos preditivos para o cálculo das propriedades físicas dos componentes da mistura, como a pressão de vapor, calores específicos, entalpias de vaporização, coeficientes de atividade, coeficientes de fugacidade e propriedades críticas. Em vista da grande variedade de dados experimentais de pressão de vapor de compostos graxos disponível na literatura, a primeira etapa deste trabalho foi ajustar uma equação preditiva desta propriedade utilizando o conceito de contribuição de grupos. Em conjunto com o modelo UNIFAC (UNIquac Functional group Activity Coefficients), diversos dados de equilíbrio líquido-vapor de misturas binárias (ácidos graxos, ésteres graxos e triacilgliceróis) e multicomponentes (miscelas de óleo/solvente) foram preditos com sucesso utilizando um programa computacional desenvolvido para o cálculo do ponto de bolha. A segunda etapa foi estudar a desacidificação por via física em batelada, modelando o processo como uma destilação diferencial. O programa computacional desenvolvido foi utilizado na simulação de um trabalho experimental com óleo de coco. O passo seguinte foi a elaboração do programa completo de simulação de uma coluna de dessorção multicomponente, formado por sub-rotinas para o cálculo dos coeficientes de atividade e fugacidade, pressões de vapor, calores específicos e entalpias de vaporização para cada um dos componentes do óleo e do vapor, além do algoritmo de convergência pelo método de Newton-Raphson. Com a implementação do programa e a seleção de alguns óleos vegetais, diversas condições de processamento foram testadas para avaliação da influência das mesmas na composição das correntes de saída (óleo refinado e destilado), em termos da acidez final, perda de óleo neutro e de compostos nutracêuticos. Incorporou-se também ao programa os parâmetros da eficiência de Murphree e arraste mecânico. Reações químicas de degradação ocasionadas pelas altas temperaturas empregadas nestes processos, como a isomerização de ácidos graxos polinsaturados, também foram avaliadas no processo em batelada. Em uma etapa complementar foi modelada a eficiência de vaporização do processo de desodorização de óleos vegetais, associada ao fenômeno da transferência da acidez livre presente no líquido para uma bolha de vapor ascendente, que se expande devido a variação na pressão hidrostática ao longo do leito. Para a conclusão deste trabalho, foi feita uma análise dinâmica do processo de desacidificação por via física. Todos os programas computacionais foram desenvolvidos no software MatLab®.

ABSTRACT

This work was developed in order to study through simulation, the processes of deacidification by steam refining and deodorization, present in the vegetable oil industry. The modeling was developed for batch and continuous processes in steady-state and dynamic regime. To describe mass and energy balances, and equilibrium relationships, it was necessary to use empirical equations and/or predictive models to calculate physical properties of all compounds of the mixture, as vapor pressure, heat capacities, vaporization enthalpies, activity coefficients, fugacity coefficients and critical properties. Because of the great variety of experimental data for the vapor pressure of fatty compounds available in the literature, the first step of this work was to adjust a predictive equation for this property using the concept of group contribution. In combination with the UNIFAC model (UNIquac Functional group Activity Coefficients), several vapor-liquid equilibrium data for binary (fatty acids, fatty esters and triacylglycerols) and multicomponent (oil/solvent miscellas) mixtures were predicted with success using a computational program developed to calculate the boiling points. The second step was to study the batch steam refining, modeling the process as a differential distillation. The computational program was used in the simulation of an experimental work with coconut oil. In the next step, the elaboration of the complete simulation program for a multicomponent stripping column was carried out through the use of subroutines for calculation of activity and fugacity coefficients, vapor pressures, heat capacities and vaporization enthalpies for each of the oil compounds and of vapor, besides the convergence algorithm using the Newton-Raphson method. Some vegetable oils were selected and their processing conditions were simulated to evaluate their influence on the composition of the product streams (refined oil and distillate), in terms of final oil acidity, neutral oil loss and losses of nutraceutical compounds. Murphree efficiency and entrainment were also included in the program. Degradative chemical reactions, occasioned by the high temperatures of these processes, as polyunsaturated fatty acid isomerization, were also evaluated in the batch process. A complementary task was modeling the vaporization efficiency of the deodorization process of vegetable oils, associated with the transfer of the free acidity present in the liquid phase to an ascending bubble of steam, that expands due to a variation in the hydrostatic pressure throughout the liquid height. To end this work, the steam refining was simulated dynamically. All computational programs were developed using MatLab®.

CAPÍTULO 1. INTRODUÇÃO

A importância nutricional dos óleos vegetais se deve ao seu alto valor energético e à presença de vitaminas, ácidos graxos essenciais e antioxidantes naturais. De sementes oleaginosas ou de polpa de frutas extrai-se o óleo bruto, composto predominantemente por triacilgliceróis. Para ser consumido, o óleo bruto deve passar por um processamento cujo objetivo é remover as impurezas e compostos indesejáveis, com menor dano possível aos triacilgliceróis e compostos nutracêuticos, como tocoferóis e ácidos graxos polinsaturados. As etapas envolvidas neste processamento são: preparação, extração mecânica e/ou com solvente, degomagem, branqueamento, desacidificação por via física (refino físico) ou por adição de soda cáustica (refino químico) e desodorização.

Os óleos vegetais brutos são extraídos mecanicamente por prensagem e/ou pelo contato com um solvente. Neste caso, após a extração, o óleo forma uma mistura denominada miscela, da qual é possível se recuperar o solvente (em geral, hexana) por evaporação seguida de esgotamento com vapor de arraste. Já a corrente de óleo bruto, ainda ligeiramente contaminada com o solvente, segue para o processo de refino.

O refino é a purificação de óleos vegetais brutos. É o processo de remoção de impurezas indesejáveis e acidez, presentes naturalmente nos óleos ou formadas em etapas anteriores do processamento. A perda de óleo neutro (triacilgliceróis e acilgliceróis parciais) associada a algumas etapas do refino tem um efeito significativo no custo do processo.

A desacidificação do óleo pode ser feita quimicamente por adição de soda cáustica, formando sabões. O refino químico auxilia também na remoção de fosfolipídeos, responsáveis pelo escurecimento do óleo quando submetido a elevadas temperaturas nos processos subseqüentes. A desacidificação por via física (etapa do refino físico), além de remover ácidos graxos livres também remove outras impurezas do óleo, mantendo a perda de óleo neutro a um nível

reduzido. Está baseada na grande diferença de volatilidade entre estes compostos e o óleo.

O processo de desodorização, cujo principal objetivo é a remoção de odores, está quase sempre presente no refino dos óleos. É a etapa subseqüente ao refino químico e ocorre em conjunto com a desacidificação por via física.

As etapas de processamento descritas acima podem ser aproximadas a um processo de separação (esgotamento) com arraste de vapor, cujo principal objetivo é a volatilização de substâncias que possuem pontos de ebulição diferentes.

Os processos de contato líquido-vapor, como por exemplo, a destilação, a absorção, a dessorção e o esgotamento, foram amplamente modelados computacionalmente para simulações de processos tradicionais da Engenharia Química, sendo vastas as fontes de algoritmos e sub-rotinas de cálculo na literatura. Na área de Engenharia de Alimentos, a simulação computacional de processos não é tão freqüente, embora seu emprego esteja crescendo e represente, sem dúvida, uma ferramenta indispensável para a investigação e otimização de processos bem complexos. No caso específico do processamento de óleos, a obtenção de dados experimentais em laboratório é muito difícil em função das elevadas temperaturas e baixas pressões, e o estudo diretamente em planta industrial sofre as restrições naturais de um processo que está sendo empregado para a produção, não para fins de investigação. O emprego da simulação computacional nos processos de desacidificação por via física e desodorização de óleos vegetais comestíveis vem, deste modo, constituir uma ferramenta importante para a sua investigação e otimização.

Este trabalho de tese teve como objetivo o estudo por simulação computacional de processos de contato líquido-vapor presentes na indústria de óleos vegetais, como a desacidificação por via física e a desodorização. A modelagem foi desenvolvida tanto para o estudo dos processos em batelada como contínuo em regimes permanente e dinâmico. Para a descrição dos balanços de massa, energia e das relações de equilíbrio, são necessárias equações empíricas

e/ou modelos teóricos para o cálculo das propriedades físicas dos componentes da mistura, como a pressão de vapor, calores específicos, entalpias de vaporização, coeficientes de atividade, coeficientes de fugacidade e propriedades críticas. Esta tese foi organizada na forma de artigos, que individualmente abrangem cada um dos objetivos estabelecidos.

O **Capítulo 1 (Introdução)** insere o leitor ao tema central desta tese, colocando, de forma sucinta, os pontos mais relevantes.

O **Capítulo 2 (Revisão Bibliográfica)** contextualiza o leitor no estado da arte referente a este trabalho de tese.

O **Capítulo 3** traz o artigo intilulado "Predicting vapor-liquid equilibria of fatty systems", que descreve o desenvolvimento e aplicação de uma equação para a predição da pressão de vapor de compostos graxos, como ácidos, ésteres, álcoois e acilgliceróis, utilizando o conceito de contribuição de grupos. Diferentes versões do modelo UNIFAC foram testadas na descrição de diversos dados de equilíbrio líquido-vapor de misturas binárias (ácidos graxos, ésteres graxos e triacilgliceróis) e multicomponentes (miscelas de óleo/solvente) a partir de um programa computacional desenvolvido para o cálculo do ponto de bolha. De uma maneira geral, este capítulo relata uma etapa fundamental para o sucesso no desenvolvimento do restante do trabalho, uma vez que os resultados obtidos permitiram estimar a volatilidade de compostos graxos, destacando-se acilgliceróis e ácidos graxos, parâmetro fundamental na análise dos processos de desacidificação por via física e/ou desodorização de óleos vegetais.

O trabalho seguinte foi utilizar a equação preditiva da pressão de vapor de compostos graxos e a modelagem do equilíbrio líquido-vapor, discutidas no Capítulo 3, no estudo do processo de desacidificação do óleo de coco por via física, em escala laboratorial, seguindo dados experimentais da literatura. Neste contexto, o artigo relatado no **Capítulo 4,** intitulado "Simulation of batch physical refining and deodorization processes", investiga e modela o processo em batelada como uma destilação diferencial. Seguindo as conclusões relatadas no Capítulo 3, o problema do equilíbrio de fases foi modelado de três formas diferentes com

crescente grau de complexidade. Os resultados das simulações foram comparados com trabalho experimental da literatura em termos da acidez final do óleo e do destilado, e da perda de óleo neutro.

Passando para uma modelagem bem mais complexa, o **Capítulo 5,** intitulado "Simulation of continuous deodorizers: effects on product streams", traz um artigo que apresenta a simulação da desodorização contínua de diferentes óleos vegetais, a partir do desenvolvimento e implementação de um programa completo de simulação de uma coluna de desodorização multicomponente, formado por sub-rotinas para o cálculo dos coeficientes de atividade e fugacidade, pressões de vapor, calores específicos e entalpias de vaporização para cada um dos componentes do óleo e do vapor, além do algoritmo de convergência pelo método de Newton-Raphson. Foram estudadas duas configurações diferentes para o desodorizador: contracorrente e corrente cruzada. O impacto dos parâmetros de processamento na composição das correntes de saída (óleo refinado e destilado) foi investigado para os óleos de soja, canola e gérmen de trigo, em termos da acidez final, perda de óleo neutro e retenção de tocoferol e outros compostos de interesse. Incorporaram-se os parâmetros da eficiência de Murphree e arraste mecânico ao programa.

Continuando com a mesma abordagem descrita no Capítulo 5, o artigo exposto no **Capítulo 6,** intitulado "Simulation of physical refiners for edible oil deacidification", traz os resultados obtidos para a simulação da desacidificação dos óleos de coco e palma por via física, para diferentes condições de temperatura, pressão e quantidade de vapor de arraste injetada. Neste caso, as análises foram concentradas nos valores da acidez final e da perda de óleo neutro para duas composições de cada óleo, uma mais volátil (rica em ácidos graxos de menor peso molecular) e outra menos volátil (rica em ácidos graxos de cadeia longa), uma vez que tanto o óleo de coco como o óleo de palma apresentam a porção glicerídica expressivamente volátil.

O artigo descrito no **Capítulo 7,** intitulado "Modeling vaporization efficiency for steam refining and/or deodorization", modela e analisa a eficiência de

vaporização em processos de desacidificação por via física de óleos vegetais. Este trabalho está ligado ao escopo desta tese pela importância do conceito da eficiência de vaporização na determinação da quantidade de vapor necessária para que uma determinada acidez final seja atingida, conhecida a carga inicial de óleo do equipamento. A modelagem cuidadosa do problema permitiu que bons resultados fossem obtidos na predição da eficiência de vaporização em condições experimentais testadas em escala laboratorial em trabalhos recentes encontrados na literatura (óleo de soja com 1% de acidez inicial).

O artigo apresentado no **Capítulo 8,** intitulado "Study of canola oil deodorization combining computational simulation with response surface methodology", avalia o efeito das reações de isomerização de ácidos graxos polinsaturados (ácidos linoléico e linolênico) durante a desodorização do óleo de canola em batelada. De uma maneira geral, este capítulo encerra os objetivos previstos para este trabalho de tese, introduzindo reações químicas e o balanço de energia na modelagem da destilação diferencial, aperfeiçoando a abordagem apresentada no Capítulo 4. A metodologia de superfície de resposta foi utilizada na análise dos efeitos das variáveis independentes (temperatura, pressão, percentagem de vapor de arraste, tempo de desodorização) nas respostas. Os resultados foram comparados com o trabalho experimental de HÉNON et al. (2001).

O **Capítulo 9 (Conclusões gerais)** discorre sobre os principais resultados obtidos em cada um dos artigos apresentados nesta tese.

No **Apêndice I** estão colocados os resultados das primeiras investigações do processo de desacidificação por via física por simulação dinâmica e os problemas encontrados. Já o **Apêndice II** traz o banco de dados utilizado no desenvolvimento do modelo por contribuição de grupos para a predição da pressão de vapor de compostos graxos apresentado no Capítulo 3. O **Apêndice III** traz algumas informações adicionais a respeito dos programas implementados no MatLab®.

CAPÍTULO 2. REVISÃO BIBLIOGRÁFICA

2.1 Óleos vegetais

A importância do Brasil como país produtor e exportador de oleaginosas é evidenciada pelos números do mercado internacional. Atualmente, ocupa a primeira posição no *ranking* dos países produtores e exportadores de soja (cerca de 26% da produção mundial), o que contribui positivamente com US$ 8 bilhões na Balança Comercial Brasileira (ABIOVE, 2005). O país é considerado também o segundo maior exportador de óleo de algodão (ABIOVE, 2005).

Os óleos vegetais são predominantemente formados por triésteres de ácidos graxos (AG) e glicerol, conhecidos como triacilgliceróis (TAG). A combinação de ácidos graxos ligados ao glicerol dá ao óleo características diferenciadas, tanto nutricionais quanto em relação às suas propriedades físicas (SWERN, 1964). Os óleos vegetais podem ser divididos de acordo com o principal ácido graxo presente em sua composição. As principais classes de óleos vegetais estão colocadas na Tabela 2.1.1 (ORTHOEFER, 1996).

Tabela 2.1.1. Classes de óleos vegetais e alguns de seus exemplares (ORTHOEFER, 1996).

Principal ácido graxo (AG)	Óleo vegetal
Láurico	Óleo de coco (cerca de 90% de AG saturados)
Palmítico	Óleo de palma (cerca de 50% de AG saturados e 40% de AG monoinsaturados)
Oléico	Óleo de oliva (cerca de 69% de AG monoinsaturados)
	Óleo de canola (cerca de 61% de AG monoinsaturados)
	Óleo de amendoim (cerca de 53% de AG monoinsaturados)
Linoléico	Óleo de algodão (cerca de 52% de AG polinsaturados)
	Óleo de soja (cerca de 60% de AG polinsaturados)
Linolênico	Óleo de girassol (cerca de 60% de AG polinsaturados)
Erúcico	Óleo de colza (industrial)

A Tabela 2.1.2 apresenta a composição percentual média em AG de alguns dos óleos vegetais mais conhecidos (FIRESTONE, 1999; BASIRON, 1996).

Tabela 2.1.2. Composição em ácidos graxos de óleos vegetais (FIRESTONE, 1999; BASIRON, 1996).

Ácido graxo		Óleo vegetal (% ácidos graxos, m/m)						
		Algodão	Amendoim	Canola	Coco	Gérmen de Trigo	Palma	Soja
Capróico (Co)	C6:0	---	---	---	0-0,6	---	---	---
Caprílico (Cp)	C8:0	---	---	---	4,6-9,4	---	---	---
Cáprico (C)	C10:0	---	---	---	5,5-7,8	---	---	---
Láurico (L)	C12:0	0-0,2	0-0,1	---	45,1-50,3	---	0,1-1,0	0-0,1
Mirístico (M)	C14:0	0,6-1,0	0-0,1	0-0,2	16,8-20,6	0-0,2	0,9-1,5	0-0,2
Palmítico (P)	C16:0	21,4-26,4	8,3-14,0	3,3-6,0	7,7-10,2	12,0-20,0	41,8-46,8	9,7-13,3
Palmitoléico (Po)	C16:1	0-1,2	0-0,2	0,1-0,6	---	0,2-0,5	0,1-0,3	0-0,2
Esteárico (E)	C18:0	2,1-3,3	1,9-4,4	1,1-2,5	2,3-3,5	0,3-3,0	4,2-5,1	3,0-5,4
Oléico (O)	C18:1	14,7-21,7	36,4-67,1	52,0-67,0	5,4-9,9	13,0-23,0	37,3-40,8	17,7-28,5
Linoléico (Li)	C18:2	46,7-58,3	14,0-43,0	16,0-25,0	0,8-2,1	50,0-59,0	9,1-11,0	49,8-57,1
Linolênico (Ln)	C18:3	0-0,4	0-0,1	6,0-14,0	0-0,2	2,0-9,0	0-0,6	5,5-9,5
Araquídico (A)	C20:0	0,2-0,5	1,1-1,7	0,2-0,8	0-0,2	0,3	0,2-0,7	0,1-0,6
Gadoléico (Ga)	C20:1	0-0,1	0,7-1,7	0,1-3,4	0-0,2	0,3	---	0-0,3
Gadolênico (Ge)	C20:2	0-0,1	---	0-0,1	---	---	---	0-0,1
Behênico (Be)	C22:0	0-0,6	2,1-4,4	0-0,5	---	0-0,1	---	0,3-0,7
Erúcico (Er)	C22:1	0-0,3	0-0,3	0-4,7	---	0,3	---	0-0,3
Docosadienóico (Do)	C22:2	0-0,1	---	0-0,1	---	---	---	---
Lignocérico (Lg)	C24:0	0-0,1	1,1-2,2	0-0,2	---	0-1,0	---	0-0,4
Nervônico (Ne)	C24:1	---	0-0,3	0-0,4	---	---	---	---
Índice de Iodo		96-115	83-107	110-126	5-13	115-128	49-55	118-139

Devido a hidrólise ao longo do processo de extração do óleo, que pode ser feita a partir de sementes oleaginosas (soja, algodão, milho, amendoim, girassol, canola) ou polpas de frutas (coco, palma, babassu, oliva), uma porção dos ácidos graxos ligados ao glicerol passa a fazer parte do que é conhecido como acidez livre. Da reação de hidrólise resultam também monoacilgliceróis (MAG) e diacilgliceróis (DAG), compostos formados por uma molécula de glicerol ligada a uma ou duas moléculas de AG, respectivamente (SWERN, 1964).

Os ácidos graxos livres (AGL) são ácidos carboxílicos (R-COOH) alifáticos saturados ou insaturados com cadeia carbônica entre C_6 e C_{24} (BROCKMANN et al, 1987). Sua concentração no óleo bruto varia fortemente, dependendo da fonte e das técnicas de extração, e é considerada uma boa medida da qualidade tanto do óleo bruto como do óleo refinado. Como exemplos, a acidez livre do óleo bruto de soja gira em torno de 0,7%(m/m) (MAZA et al., 1992); no óleo de palma, fica

entre 2 e 3% (CHUAN HO, 1976), enquanto que no óleo de gérmen de trigo, em casos extremos, pode chegar a 25% (WANG & JOHNSON, 2001). Durante o refino, o teor de AGL deve ser reduzido a 0,3%, limite máximo de acidez, em massa, expresso em ácido oléico, permitido pela Legislação Brasileira (ANVISA, 1999).

Além dos TAG, DAG e MAG, e dos AGL, compostos minoritários constituem os óleos vegetais. Em média, os óleos vegetais brutos contêm 5% de material não-glicerídico, formado por diferentes quantidades de AGL, gomas (fosfatídeos), metais (principalmente ferro, cobre, cálcio e magnésio), peróxidos e outros produtos de reações de oxidação, pigmentos, esteróis, tocoferóis, ceras e umidade (O'BRIEN, 1998).

Parte destas impurezas afetam a estabilidade do produto final em termos de cor, sabor e odor e podem gerar problemas durante o processamento, como a formação de espuma e fumaça, quando não retiradas. Os fosfatídeos, por exemplo, são responsáveis pelo escurecimento do óleo quando submetido a elevadas temperaturas. Tanto a etapa de degomagem como o refino químico (em menor escala) são responsáveis por diminuir o teor destes compostos.

Deve-se ressaltar, porém, que nem todos os compostos não-glicerídicos são indesejáveis e, muitas vezes, é interessante mantê-los no óleo refinado. A seguir, será discutida a importância de alguns destes compostos.

Os esteróis são os principais constituintes da matéria insaponificável dos óleos vegetais, que também possui hidrocarbonetos, como o esqualeno. Os esteróis são compostos sem cor, termicamente estáveis e relativamente inertes. No óleo de soja, o principal esterol é o β-sitosterol (PRYDE, 1995). As altas temperaturas da desacidificação por via física e da desodorização são capazes de removê-los de forma efetiva, concentrando-os no destilado (O'BRIEN, 1998). Os esteróis são utilizados na indústria farmacêutica, na produção de hormônios e corticóides (WOERFEL, 1995).

Os tocoferóis são antioxidantes naturais e têm ação sobre os radicais livres. Sua presença no óleo é altamente desejável (O'BRIEN, 1998), mas, em alguns casos, o processo de desodorização é delineado de forma a recuperá-lo no

destilado (AHRENS, 1998). Dependendo de quão drástico for o tratamento térmico sofrido pelo óleo durante a desodorização, a concentração final de tocoferóis no destilado pode chegar a 14% (WALSH et al., 1998).

Como já foi salientado, a variabilidade na composição dos óleos vegetais é alta, tanto nos AG ligados aos acilgliceróis, quanto na porção não-glicerídica. Este fator gera diferenças no processamento a ser seguido nas refinarias. A seguir, é apresentada uma breve introdução dos principais óleos vegetais estudados neste projeto, evidenciando sua composição e etapas mais comuns do seu processamento.

2.1.1 Óleo de algodão

O óleo extraído do caroço de algodão é um óleo vegetal comestível, apesar de não ter uso doméstico tradicional no Brasil. Mesmo assim, o país é o segundo maior exportador deste óleo (ABIOVE, 2005). Hoje em dia já é possível se encontrar o óleo de algodão nas prateleiras dos supermercados brasileiros.

O óleo bruto de algodão apresenta uma intensa coloração vermelha devido a presença de diversos componentes não-glicerídicos caracterizados como gossipol (0,05 a 0,42%), fosfatídeos (0,7 a 0,9%), tocoferóis (1000 mg/kg), esteróis (3800mg/kg) e carboidratos. Estas substâncias podem totalizar cerca de 2% da composição do óleo (JONES & KING, 1996).

A extração do óleo de algodão pode ser feita por prensagem, por adição de solvente ou por uma combinação das duas etapas (mais econômico). O refino é feito por adição de soda cáustica (refino químico), removendo AGL e a quase totalidade de gossipol. A etapa de desodorização remove os AGL e componentes da auto-oxidação das gorduras (aldeídos, cetonas, álcoois e hidrocarbonetos) (JONES & KING, 1996).

2.1.2 Óleo de amendoim

O óleo de amendoim é fruto da extração sob prensagem das sementes. Associada à extração mecânica, faz-se a extração com solvente já que o alto teor

de óleo na semente dificulta a quebra dos grãos. É altamente insaturado, podendo ser utilizado como componente alimentar e como biodiesel. O teor de AGL varia de 0,02 a 0,6% (YOUNG, 1996). Após a extração, o óleo é degomado, refinado quimicamente e desodorizado (SALUNKHE et al., 1992).

2.1.3 Óleo de canola

O óleo de canola é obtido da semente da espécie *Brassica napus* desenvolvida por melhoramento genético convencional da semente de colza. O óleo de colza é rico em ácido erúcico (C22:1) (fatores antinutricionais), sendo utilizado apenas como óleo industrial (MICHAEL ESKIN et al., 1996). A redução do teor de ácido erúcico resultou num grande aumento nos níveis de ácido oléico e, em menor escala, de ácido linolênico. Este óleo tem uma composição similar ao óleo de amendoim e oliva, com exceção do baixo teor de ácido palmítico e alto teor de ácido linolênico (SALUNKHE et al, 1992).

A extração do óleo de canola é feita por uma combinação da extração mecânica seguida pela adição de solvente. Após a degomagem, o óleo pode ser refinado quimicamente e desodorizado, ou refinado fisicamente (HÉNON et al., 2001). Seu teor inicial de AGL é baixo, não superior a 1,2% (MICHAEL ESKIN et al., 1996).

2.1.4 Óleo de coco

O óleo de coco é produzido principalmente na Ásia, Ilhas do Oceano Pacífico, África, América Central e América do Sul. No Brasil, não há produção de óleo de coco, sendo o fruto destinado apenas para a obtenção da água de coco. Pertence ao grupo dos óleos láuricos, uma vez que este é o principal AG em sua composição. Mais de 90% de seus AG são saturados (CANAPI et al., 1996), fazendo com que o óleo de coco tenha um baixo valor de índice de iodo (entre 5 e 13). Esta característica impõe ao óleo uma grande resistência à rancidez oxidativa (CANAPI et al., 1996), além do fato de mudar do estado fortemente sólido para o líquido com um leve aumento de temperatura (O'BRIEN, 1998).

A extração do óleo de coco pode ser feita mecanicamente ou por adição com solvente. O óleo bruto é desacidificado pela adição de soda cáustica (batelada ou contínuo) ou por contato com vapor (refino físico) (CANAPI et al., 1996).

2.1.5 Óleo de gérmen de trigo

O óleo de gérmen de trigo é uma excelente fonte de AG polinsaturados e vitamina E. É um dos óleos naturais com maior nível de α-tocoferol. É conhecido por seu poder na redução do colesterol e no retardamento do envelhecimento precoce (WANG & JOHNSON, 2001).

A extração do óleo de gérmen de trigo pode ser feita tanto mecanicamente como por adição de solvente. Ainda que a extração com solvente seja muito mais eficiente, extraindo até 90% do óleo, a extração por prensagem, que extrai cerca de 50%, é preferida pelos consumidores por causa do apelo mercadológico de "produto natural" (SINGH & RICE, 1979).

O teor de AGL no óleo de gérmen de trigo varia entre 5% e 25%, dependendo das condições de extração e armazenagem (WANG & JOHNSON, 2001).

Degomagem, neutralização, branqueamento e desodorização são as etapas usuais do seu processamento (WANG & JOHNSON, 2001).

2.1.6 Óleo de palma

Atualmente, o óleo de palma representa cerca de 21% da produção mundial de óleos vegetais, com um volume de produção de 17 milhões de toneladas/ano concentrada principalmente na Malásia (ABEQ, 2005).

O óleo de palma bruto é caracterizado por uma intensa cor alaranjada devido ao elevado teor de carotenos (0,03 a 0,15%). Sua porção glicerídica é formada basicamente por TAG, dos quais 7,9% são trisaturados (CHUAN HO, 1976). Difere dos demais óleos devido ao seu alto teor de ácido palmítico (vide Tabela 2.1.2). Carotenóides (500 a 700 mg/kg), tocoferóis (600 a 1000 mg/kg),

esteróis, fosfatídeos, peróxidos e produtos de oxidação formam a porção não-glicerídica (O'BRIEN, 1998).

A extração do óleo de palma é feita por prensagem. No Brasil e na África, o óleo de palma ou azeite de dendê é consumido na forma bruta (BASIRON, 1996).

O refino físico é o método de purificação mais empregado na indústria de óleo de palma e compreende as etapas de degomagem, branqueamento e desodorização/desacidificação que utiliza altas temperaturas (240 a 260 ºC) e pressões entre 1 e 3 mmHg (ROSSI et al., 2001). Sob estas condições de operação, os carotenóides são decompostos termicamente. (BASIRON, 1996).

2.1.7 Óleo de soja

O óleo de soja é o óleo vegetal mais importante produzido no mundo, totalizando 24% da produção mundial (ABEQ, 2005), devido a sua alta qualidade e baixo custo.

Algumas de suas principais características são: alto teor de insaturações, a presença de antioxidantes naturais (tocoferóis) e de cerca de 2% de fosfatídeos, que devem ser removidos durante o processamento (SIPOS & SZUHAJ, 1996).

O método mais comum de extração do óleo de soja é por adição de hexana. O refino pode ser químico ou físico. Neste último, o óleo, livre de fosfatídeos após o pré-tratamento, é desodorizado e desacidificado (SIPOS & SZUHAJ, 1996) em equipamento contínuo. O destilado resultante da desodorização do óleo de soja pode conter altos níveis de tocoferol, de acordo com as condições estabelecidas na desodorização (AHRENS, 1998).

2.2 Processamento de óleos vegetais

Quase a totalidade dos óleos vegetais brutos, como visto no item 2.1, passa por algum tipo de processamento antes de ser destinada ao consumo humano. Os objetivos do processamento são diversos: remoção de odor e acidez,

alterações no sabor e na cor do óleo, modificações em sua estrutura molecular e de suas propriedades termodinâmicas (O'BRIEN, 1998).

Resumidamente, as etapas que compõem o processamento de óleos vegetais são: preparação, extração mecânica e/ou com solvente, degomagem, branqueamento, desacidificação por via física (refino físico) ou por adição de soda cáustica (refino químico) e desodorização. Neste trabalho de tese, serão discutidas apenas as etapas que envolvem a separação de compostos por arraste com vapor. São elas, recuperação de solvente da miscela, desodorização e desacidificação por via física.

2.2.1 Extração com solvente: recuperação de solvente da miscela

O processo de extração do óleo de sementes oleaginosas ou polpas de frutas pode ser feito de três maneiras distintas: extração mecânica, extração com solvente ou uma combinação das duas. Na extração mecânica, as sementes são prensadas sob altas temperaturas, de forma que o óleo é forçado a sair das células. Em muitos casos, a torta (massa de sementes) resultante contém um certo teor de óleo residual (em geral, de 15 a 18%), que pode ser removido por contato com um solvente (O'BRIEN, 2004). Este processo combinado (extração mecânica + extração com solvente) resulta em um maior rendimento (WILLIANS & HRON, 1996).

A extração com solvente apresenta algumas vantagens frente à extração mecânica, como o emprego de temperaturas mais amenas. Além disso, o solvente consegue extrair mais componentes não-glicerídicos, que não são retirados pela ação mecânica (WILLIANS & HRON, 1996). O solvente normalmente empregado neste processo é a hexana, uma mistura de hidrocarbonetos de petróleo (principalmente C_6H_{14}) de pontos de ebulição próximos a 65 °C (FORNARI et al., 1994). Em vista de suas características de flamabilidade e impacto ambiental, vários outros solventes estão sendo investigados como possíveis substitutos.

No processo de extração combinada, o material sólido move-se em sentido contrário à miscela (óleo+solvente), de forma que, ao entrar no equipamento,

contata uma miscela rica em óleo. Após esta primeira lavagem, a miscela, que contém cerca de 25 a 30% de óleo, deixa o extrator para ser destilada e recuperada. Depois de passar através dos vários estágios de lavagem e, finalmente, entrar em contato com o solvente puro, o material sólido é destinado à etapa de desolventização (ANDERSON, 1996).

Ao deixar o extrator, a miscela é previamente concentrada em evaporadores, chegando a cerca de 90% ou mais de óleo em solvente, sendo então destinada à coluna de destilação ou *stripping* (MILLIGAN & TANDY, 1974).

O óleo bruto, em geral, contém de 500 a 1000 mg/kg de resíduo de solvente, que são eliminados durante o refino físico ou desodorização. O teor de n-hexano no óleo refinado não deve exceder 1 mg/kg (KARLESKIND, 1996).

A partir da miscela pode-se obter dois produtos em duas correntes distintas: uma de solvente e outra de óleo. O solvente é recuperado e o óleo destinado às etapas subseqüentes do seu processamento.

2.2.2 Refino

O refino é a purificação de óleos vegetais brutos. É o processo de remoção das impurezas presentes naturalmente nos óleos ou formadas em etapas anteriores do processamento.

O refino de óleos vegetais pode seguir por duas vias distintas: química ou física. No refino químico, a etapa de desacidificação é efetuada por neutralização com soda cáustica, ocasionando a conversão dos AGL em sabões, que são removidos posteriormente por meio de centrifugação ou decantação. O principal problema associado à etapa de neutralização é a perda de óleo neutro devido à saponificação e ao arraste mecânico do mesmo na emulsão, principalmente em óleos com alto teor de AGL. ANTONIASSI et al. (1998) reportam perdas de até 14% de óleo neutro para óleo de milho com 4% de acidez. O óleo refinado quimicamente deve seguir para uma etapa subseqüente, denominada de desodorização, onde ocorre a eliminação de odores indesejáveis.

Já no refino físico, as etapas de branqueamento, desodorização e desacidificação ocorrem conjuntamente pela ação de elevadas temperaturas, que causam a degradação térmica e a volatilização de compostos. O processo de refino físico é projetado para cumprir os seguintes objetivos: (a) redução do teor de AGL para níveis aceitáveis; (b) obtenção de um produto totalmente desodorizado; (c) operação com aproximadamente os mesmos gastos de utilidades que o processo de desodorização convencional; (d) recuperação de uma corrente de AGL do destilado (GAVIN, 1978).

Para ser bem sucedido, o refino físico deve ser executado em óleos com baixo teor de fosfatídeos ou que tenham passado pela etapa de remoção destes compostos (máximo de 10 mg/kg).

2.2.3 Desodorização

A desodorização é um processo quase sempre presente no refino de óleos vegetais e vem sendo utilizado desde o final do século XIX, quando foi idealizado com o objetivo de retirar odores de óleos vegetais, que seriam utilizados como substitutos de gorduras animais em formulações de margarinas (GAVIN, 1978). Os óleos de soja e palma, principais fontes de gorduras em alimentos, apresentam forte odor e sabor naturais; óleos hidrogenados também são bastante comuns e os odores formados por este processo são retirados pela desodorização. Até em casos onde a desodorização não é desejável, como quando se quer reter características naturais do óleo, este processo ainda pode ser necessário para garantir a completa remoção de traços de hexana (da extração), herbicidas e pesticidas. Com a crescente prática do refino físico, grande parte dos sistemas de desodorização é projetada de forma versátil, permitindo a execução dos dois processos (CARLSON, 1996).

O processo de desodorização está baseado na grande diferença de volatilidade entre o óleo e a maioria das substâncias indesejáveis que afetam o sabor, odor, cor e a estabilidade dos óleos. Nos desodorizadores, o vapor de arraste é utilizado para facilitar a mistura, de forma que todo o óleo fique exposto

às condições de superfície, onde a vaporização acontece. Na prática, para que a diferença entre a pressão de vapor dos TAG e dos componentes indesejáveis seja suficientemente grande, a temperatura do óleo deve chegar a valores entre 200 ºC e 275 ºC (CARLSON, 1996), e o vácuo estar na faixa de 4 a 6 mmHg.

A desodorização é a última etapa do processo de refino do óleo e, por isso, é altamente dependente da qualidade das correntes de entrada. Os componentes removidos ou inativados pelo processo são aldeídos, cetonas, álcoois, esteróis, hidrocarbonetos, diversas substâncias formadas pela degradação térmica de peróxidos e pigmentos, além de compostos odoríferos causados por hidrogenação. Os tocoferóis, antioxidantes naturais, infelizmente também são parcialmente removidos. A concentração total destes compostos menores (excluindo os AGL) varia entre 0,02 e 0,2%. Em geral, a maior parte dos compostos odoríferos é eliminada quando o teor de AGL é reduzido abaixo de 0,03% (CARLSON, 1996).

Quando associada à desacidificação no refino físico, os principais componentes removidos são os AGL, cujo teor normalmente varia de 0,5 a 5,0%. Já em óleos refinados quimicamente, a acidez livre do óleo a ser desodorizado é bem menor, ficando entre de 0,1 a 0,5%. Para bons resultados, as impurezas não-voláteis na alimentação devem ser as menores possíveis. Fosfatídeos e ferro devem estar presentes em teores inferiores a 3 mg/kg (preferencialmente menos que 1 mg/kg) e 0,1 mg/kg, respectivamente.

2.2.4 Princípios da desodorização

A desodorização e/ou desacidificação por via física podem ser definidas como a purificação da fase líquida graxa pela mistura com um gás de arraste, que facilita a transferência de massa das impurezas voláteis para a fase gasosa. Esta fase é continuamente removida do equipamento, evitando que parte dos voláteis retorne ao líquido (BALCHEN et al., 1999). Praticamente todas as suas aplicações comerciais utilizam vapor como o agente de arraste, devido a habilidade deste gás

de se condensar em condições moderadas, diminuindo desta forma o custo do sistema de vácuo (BALCHEN et al., 1999).

Os processos de desacidificação por via física e desodorização podem ser efetuados em equipamentos contínuos ou em batelada. A Figura 2.2.4.1 traz esquemas de desodorizadores em batelada, em escala industrial (DAVIDSON et al., 1996) (A) e laboratorial (B).

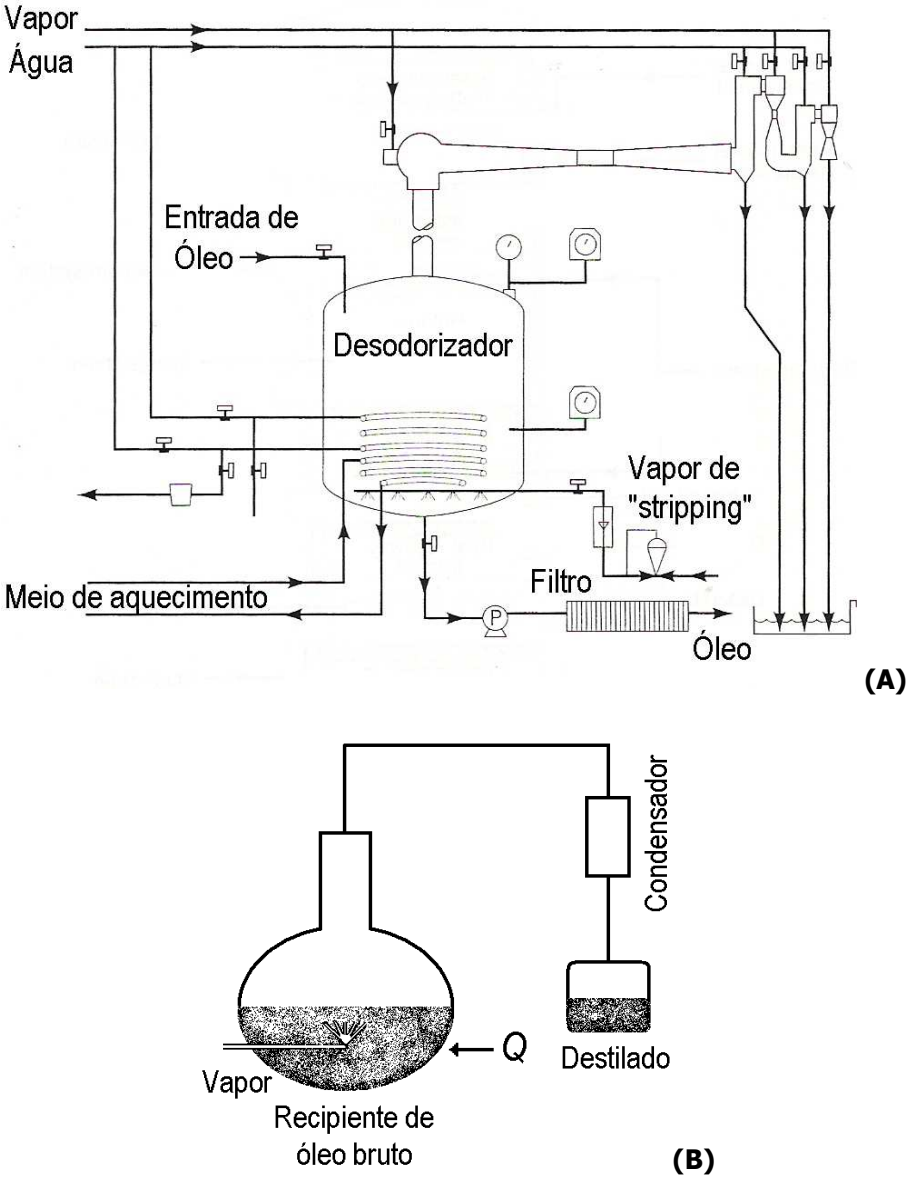

Figura 2.2.4.1. Desodorização em batelada em (A) escala industrial (DAVIDSON et al., 1996) e (B) escala laboratorial.

De acordo com ANDERSON (1996), o processo em batelada foi o primeiro a ser desenvolvido para realizar a desodorização de óleos vegetais e, em geral, é indicado para processar até 60 metros cúbicos de óleo (≈ 55 toneladas) em 24 horas. No processo industrial, o óleo é aquecido indiretamente pelo contato com serpentinas (ANDERSON, 1996) até que seja atingida a temperatura requerida, quando passa a haver a injeção de vapor de arraste. Após um período de várias horas, quando o teor de acidez requerido pela Legislação é atingido, o óleo é resfriado, sob vácuo, e destinado ao estoque (ANDERSON, 1996).

No equipamento industrial, a capacidade do tanque é, em geral, duas vezes maior que sua capacidade de operação. É equipado com serpentinas para aquecimento e resfriamento das cargas de óleo, além de uma tubulação perfurada (furos com 3,2 mm de diâmetro), por onde é introduzido o vapor de arraste (DAVIDSON et al., 1996).

Já os processos de desacidificação por via física e desodorização feitos em equipamento contínuo, possuem seções individuais para o aquecimento do óleo, arraste dos compostos voláteis e resfriamento. O sistema de desodorização contínua está esquematizado na Figura 2.2.4.2 (AHRENS, 1998; CARLSON, 1996).

Neste equipamento, o óleo, previamente tratado, é bombeado continuamente através de um filtro e aspergido num desaerador a vácuo. É então conduzido através de uma seção de recuperação de calor para uma seção de aquecimento, onde atinge a temperatura de processo, pelo contato indireto com um sistema de espirais aquecidas com vapor. O óleo é então desacidificado e desodorizado, fluindo sobre as bandejas e entrando em contato direto com o vapor de arraste. Ao sair do equipamento, o óleo já refinado passa pela seção de recuperação de calor, onde transfere calor para o óleo que entra no equipamento. É então resfriado sob vácuo por contato indireto com água e bombeado através de filtros para a estocagem (ZEHNDER, 1995).

A agitação é proporcionada pelo vapor de arraste que é injetado na base de cada seção através de tubos de distribuição. O tempo de permanência em cada

seção gira em torno de 10 a 30 minutos e o nível de líquido fica entre 0,3 e 0,8 m (AHRENS, 1998).

Acoplado ao desodorizador está o sistema de recuperação de destilado no qual toda a corrente de vapor proveniente do equipamento é condensada, permitindo a recuperação da fração volátil presente no óleo.

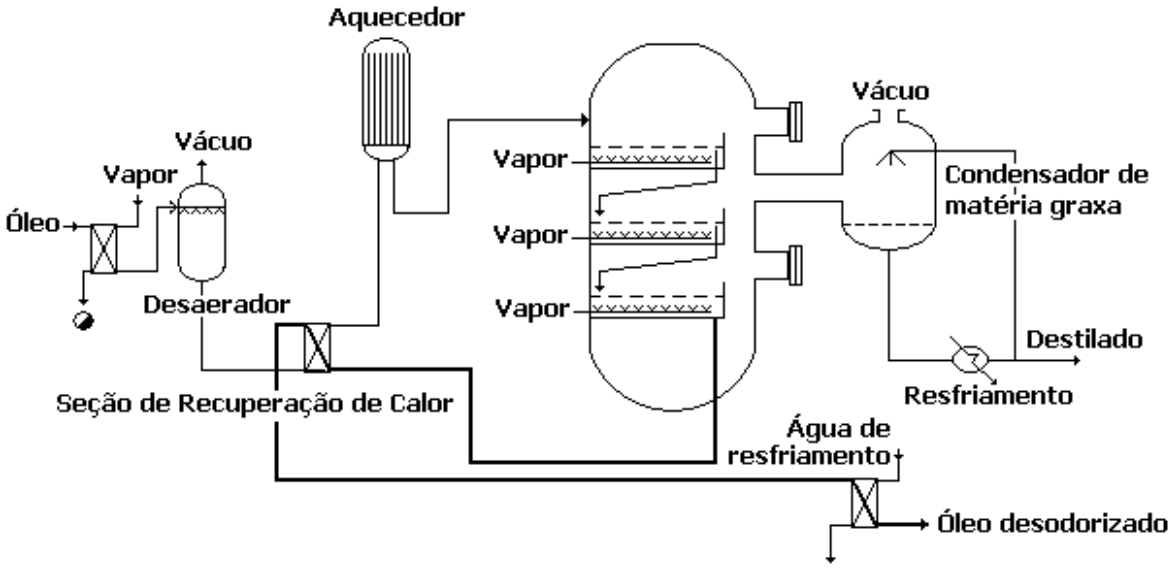

Figura 2.2.4.2. Sistema de pratos de desodorização contínua (AHRENS, 1998; CARLSON, 1996).

Em desodorizadores contínuos comerciais, duas configurações são utilizadas: (i) corrente cruzada, na qual as direções das correntes se cruzam dentro do equipamento, e (ii) contracorrente, na qual a entrada de vapor é feita junto à saída de líquido, e vice-versa (BALCHEN et al., 1999). Desodorizadores de contato diferencial (*thin-film* ou *Softcolumn*^{TM}) são baseados na configuração contracorrente enquanto que desodorizadores de estágios são principalmente configurados em corrente cruzada. AHRENS (1999) apresenta uma boa revisão a respeito de desodorizadores do tipo *Softcolumn*^{TM}, e ressalta que neste tipo de equipamento o consumo de vapor pode ser reduzido em até $\frac{1}{3}$ do total requerido em desodorizadores convencionais. WANG & JOHNSON (2001) investigaram em escala laboratorial a performance de um desodorizador de estágios em contracorrente.

Neste trabalho de tese foram investigadas as configurações contracorrente e corrente cruzada para os desodorizadores contínuos de estágios. Alguns resultados interessantes foram obtidos na avaliação das diferenças das correntes de óleo refinado e destilado provenientes destas duas configurações, quando utilizadas as mesmas condições de processamento.

2.2.5 Perdas no processamento de óleos

A quantidade de compostos odoríferos removida durante a desodorização é pequena e raramente excede 0,1% da massa de óleo. No entanto, existe uma perda indesejável de óleo neutro e outros compostos que torna o total de perdas muito maior. As condições de operação, teores iniciais de AGL e insaponificáveis, e a composição da porção glicerídica influem diretamente nas perdas dos processos de desodorização e refino físico (CARLSON, 1996). Artigos publicados nas décadas de 50 e 60 reportam perdas entre 0,2 e 0,8% para óleos com menos de 0,1% de AGL, processados em desodorizadores semi-contínuos (MATTIL, 1964; WHITE, 1953). Atualmente, com o uso de quantidades menores de vapor de arraste e meios mais eficientes de se evitar o arraste mecânico, as perdas giram em torno de 0,2 a 0,4%. Fornecedores de sistemas de desodorização e refino físico oferecem garantias de perdas mínimas, baseando-se na acidez livre da alimentação. Desta forma, as perdas totalizariam 0,2 a 0,4% mais 1,05 a 1,2 vezes a porcentagem de AGL na alimentação (CARLSON, 1996).

As perdas geradas nas etapas de desodorização e refino físico de óleos vegetais podem ser divididas em duas frações: por destilação (evaporação) ou por arraste mecânico (CARLSON, 1996). Há também, perdas relacionadas a reações de degradação. A seguir estão discutidas suas decorrências.

2.2.5.1 Perdas por destilação (volatilização)

Os AGL estão entre os compostos mais facilmente evaporados durante a desacidificação de óleos vegetais por via física (vide Tabela 2.2.5.1.1). Em grande parte, estão presentes na alimentação da coluna, mas também podem ser

formados durante o processamento, por hidrólise de acilgliceróis (CARLSON, 1996; BAILEY, 1941; SZABO SARKADI, 1959; PETRAUSKAITÈ et al, 2000).

Tabela 2.2.5.1.1. Volatilidade relativa de alguns componentes-chaves de óleos vegetais em relação ao tocoferol (WOERFEL, 1995).

Componente	Peso Molecular	Volatilidade Relativa
Ácidos graxos	280	2,5
Esqualeno	411	5,0
Tocoferol	415	1,0
Esterol	410	0,6
Ésteres de esteróis	675	0,038
Óleo	885	pequena

Esteróis e outros componentes da matéria insaponificável são menos voláteis que os AGL. Porém, dependendo do tipo de óleo e da temperatura de operação, até 60% da concentração da alimentação pode ser perdida (CARLSON, 1996).

A porção glicerídica é menos volátil que os demais componentes do óleo, mas existe alguma perda por evaporação (em torno de 0,1%). MAG e DAG, por terem um peso molecular menor, são mais voláteis que os TAG e constituem grande parte deste total. É interessante, porém, estudar também o comportamento dos TAG frente às elevadas temperaturas empregadas neste processo, sendo este um dos objetivos deste trabalho, que pretende investigar se as perdas de óleo neutro são causadas exclusivamente por arraste mecânico ou também por volatilização.

2.2.5.2 Perdas por arraste mecânico

O arraste mecânico ou *entrainment* pode ser definido como o arraste de partículas de líquido, de um prato a outro, causado pelo escoamento do vapor. As bolhas de vapor de arraste despendem considerável quantidade de energia cinética atravessando a superfície do óleo, suficiente para carregar gotas de líquido até a saída do equipamento (CARLSON, 1996).

As perdas de óleo neutro causadas por arraste mecânico são altamente indesejáveis nos processos de desodorização e desacidificação por via física,

principalmente porque podem ser evitadas com um projeto apropriado do desodorizador. A velocidade do vapor acima da superfície do óleo, em geral, gira em torno de 2 m/s. No entanto, este valor pode chegar próximo dos 50 m/s na saída do equipamento devido às condições de processo (CARLSON, 1996).

Os desodorizadores mais atuais possuem sistemas eficientes para se evitar perdas por arraste, reduzindo-as à valores entre 0,1 e 0,2%. Para o refino físico, a esse valor acrescenta-se 10% da porcentagem de AGL na alimentação (CARLSON, 1996).

PETRAUSKAITÈ et al (2000) quantificou as perdas de óleo neutro (arraste mecânico e por destilação) durante a desacidificação de óleo de coco por via física em batelada, em escala laboratorial, correlacionando com a qualidade do óleo bruto e as condições de operação.

2.2.5.3 Perdas por reações de degradação térmica e oxidação

Durante a desodorização e/ou desacidificação por via física, simultaneamente à remoção de compostos indesejáveis, existe uma perda inevitável de outros componentes por degradação. De fato, estes dois processos geram grandes mudanças nos óleos vegetais em decorrência do emprego de elevadas temperaturas e baixas pressões. A presença de insaturações, oxigênio dissolvido e água, em conjunto com estas condições drásticas de processamento, tornam o óleo uma mistura passível de sofrer reações de degradação, tanto térmica como por oxidação. A hidrólise de acilgliceróis e a isomerização de ácidos graxos polinsaturados são exemplos de reações de degradação térmica, ou seja, reações que ocorrem devido a ação exclusiva da temperatura. Em ambos os casos, a constante de reação é dependente da temperatura do sistema e aumenta de acordo com a equação de Arrhenius (BENSON, 1960).

Devido à sua importância nutricional, esta pesquisa estudou a reação de isomerização de ácidos graxos polinsaturados durante as etapas de desacidificação por via física e/ou desodorização de óleos vegetais. Os detalhes desta reação estão discutidos no item 2.2.5.3.1. Algumas informações sobre a reação de hidrólise de

acilgliceróis, que também ocorre durante estas etapas, estão colocadas no item 2.2.5.3.2, apesar de serem insuficientes para a introdução desta reação nos programas de simulação. A importância da reação de hidrólise de acilgliceróis está no fato de gerar acidez justamente quando se quer retirá-la, devido as altas temperaturas empregadas durante a desacidificação por via física e/ou desodorização.

2.2.5.3.1 Isomerização *cis-trans*

Os TAG provenientes de fonte vegetal ou animal são classificados em saturados, monoinsaturados e polinsaturados, de acordo com o número de insaturações em seus AG. Em sua maioria, a configuração *cis* (Figura 2.2.5.3.1.1A) é predominante (SCHWARZ, 2000a). Estudos mostram que a configuração *trans* (Figura 2.2.5.3.1.1B) gera diferenças nas propriedades físicas do AG, como o aumento do ponto de fusão, maior resistência à oxidação e maior similaridade do mesmo com AG saturados. Atualmente, AG insaturados de conformação *trans* são considerados como substâncias com um certo efeito indesejável sobre o nível do colesterol HDL (o "mau" colesterol) no sangue (SCHWARZ, 2000a). De acordo com a Agência Nacional de Vigilância Sanitária (ANVISA), não há um Valor Diário de Ingestão (VDI%) determinado para gorduras *trans*. No entanto, a Agência recomenda que não seja consumido mais que dois gramas ao dia (ANVISA, 2005). Até julho de 2006, as indústrias de alimentos deverão adequar os seus rótulos, informando a quantidade de gorduras *trans* em todos os seus produtos (ANVISA, 2005). De acordo com ARO et al. (1998), um dos parâmetros de qualidade em países europeus para óleos vegetais refinados comestíveis é que o teor de AG *trans* deve ser inferior a 1%. A importância deste novo parâmetro de qualidade é, portanto, evidente.

Os óleos hidrogenados podem constituir uma fonte importante de AG *trans* na dieta humana, uma vez que são largamente utilizados na formulação de alimentos industrializados. De acordo com o método e o grau de hidrogenação, o

teor destes ácidos em óleos hidrogenados varia entre 5 e 70%. Óleos refinados também apresentam uma certa quantidade de AG *trans*, porém em menor escala.

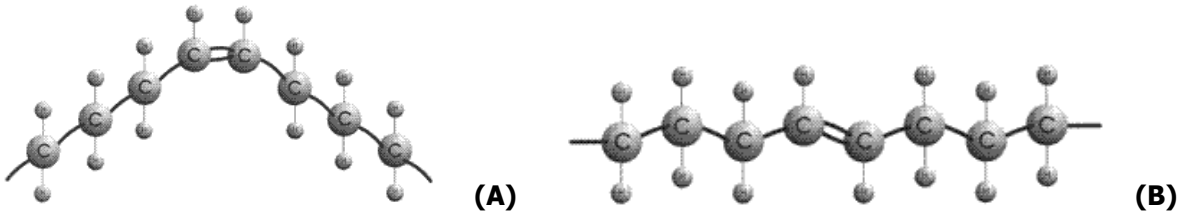

Figura 2.2.5.3.1.1. Configurações *cis* (A) e *trans* (B) em ácidos graxos insaturados.

O principal fator que afeta a taxa da reação de isomerização, e conseqüentemente, o teor de AG *trans* no óleo refinado é, sem dúvida, a temperatura empregada na etapa de desodorização, uma vez que esta reação não ocorre em etapas precedentes e os valores iniciais de AG polinsaturados de conformação *trans* no óleo bruto (0,1 a 0,3%) podem aumentar consideravelmente no óleo refinado, atingindo valores superiores à 5,0% (SCHWARZ, 2000b). Para temperaturas ao redor de 250 °C, o teor de isômeros *trans* pode variar entre 2,0 e 2,4% (SCHWARZ, 2000b).

Diversos trabalhos na literatura investigaram a formação de isômeros *trans* durante o aquecimento e as etapas de desodorização de óleos vegetais nos últimos anos (WOLFF, 1993; CAMACHO et al., 2001; O´KEEFE et al., 1993; HENÓN et al., 1997, 1999, 2001; KÉMENY et al. 2001), evidenciando a importância desta reação para a indústria de óleos vegetais. O'KEEFE et al. (1993) avaliaram o efeito da temperatura na perda de ácido linolênico *cis* em óleo de soja comercial. De acordo com os autores, o teor inicial de C18:3*cis* diminuiu com o tempo e com o aumento na temperatura (160 a 240°C). A cinética da reação foi de primeira ordem, ou seja, a taxa de reação é proporcional à concentração do reagente $\left(dc/dt = k \cdot c\right)$ (BENSON, 1960). Os principais isômeros *trans* identificados para o ácido C18:3 são: C18:3 Δ9-*cis*, Δ12-*cis*, Δ15-*trans*, C18:3 Δ9-*trans*, Δ12-*cis*, Δ15-*cis* e C18:3 Δ9-*trans*, Δ12-*cis*, Δ15-*trans*. Os autores não apresentaram a equação de Arrhenius para esta reação. WOLFF (1993) obteve conclusões semelhantes, trabalhando com óleo de linhaça para temperaturas entre 190 e 260°C.

HENÓN et al. (1997, 1999) estudaram a cinética das reações de degradação e isomerização dos ácidos linoléico e linolênico durante a desodorização em batelada do óleo de canola. Os modelos matemáticos apresentados pelos autores também evidenciaram que as reações de isomerização são de primeira ordem, e que o ácido linolênico (C18:3) é mais susceptível à isomerização do que o ácido linoléico (C18:2). Os autores identificaram que o teor de ácido linolênico decresce também devido à reações de degradação, cuja cinética foi estabelecida em trabalho anterior (HÉNON et al., 1997). No entanto, os compostos resultantes não foram identificados.

O trabalho de CAMACHO et al. (2001) trata da isomerização do ácido linoléico durante a desacidificação por via física e/ou desodorização de três óleos distintos: óleo de girassol, azeite de oliva e óleo de soja. Os autores estudaram a cinética de reação em equipamento descontínuo para temperaturas entre 240 °C e 265 °C, vazões distintas de nitrogênio e quantidades diferentes de óleo em cada batelada. Os resultados são expressos em frações molares do conjunto de isômeros do ácido linoléico. Ao contrário dos demais trabalhos, a reação de isomerização foi tida como sendo de ordem zero.

Pela qualidade das informações, este projeto de pesquisa selecionou os trabalhos de HÉNON et al. (1997, 1999, 2001) como fontes para o estudo das reações de isomerização durante a desodorização em batelada de óleos vegetais.

2.2.5.3.2 Hidrólise

Acilgliceróis totais (TAG) ou parciais (DAG e MAG) podem ser hidrolisados à AG e glicerol, ou acilgliceróis parciais (DAG e MAG), durante a desacidificação por via física e/ou desodorização de óleos vegetais (BROCKMANN et al., 1987). A reação geral é dada por:

$$\begin{array}{l} CH_2OCOR \\ | \\ CHOCOR + 3H_2O \Leftrightarrow \\ | \\ CH_2OCOR \end{array} \quad \begin{array}{l} CH_2OH \\ | \\ CHOH + 3RCOOH \\ | \\ CH_2OH \end{array} \qquad (2.2.5.3.2.1)$$

$$TAG + 3H_2O \Leftrightarrow GLICEROL + 3RCOOH$$

Os passos desta reação são:

$$\begin{array}{l} TAG + H_2O \Leftrightarrow DAG + RCOOH \\ DAG + H_2O \Leftrightarrow MAG + RCOOH \\ MAG + H_2O \Leftrightarrow GLICEROL + RCOOH \end{array} \qquad (2.2.5.3.2.2)$$

A reação de hidrólise é tão importante que, na fase final destes processos, chega a igualar a volatilização de AG. Como ressaltado por CARLSON (1996), a acidez final de óleos desodorizados não é inferior a 0,005%, devido à hidrólise do óleo causada pelo vapor de arraste. SZABO SARKADI (1959) enfatizou também a ação catalítica de AG na reação de hidrólise.

De acordo com BROCKMANN et al. (1987) a reação de hidrólise segue uma cinética de primeira ordem em relação à concentração do TAG e o fator pré-exponencial é altamente dependente da temperatura.

Infelizmente nenhum artigo, que discutisse a cinética da reação de hidrólise durante as etapas de desodorização, e fornecesse os valores do fator pré-exponencial e da energia de ativação necessários na equação de Arrhenius, foi encontrado na literatura. Uma informação relevante porém, pode ser obtida no artigo de SZABO SARKADI (1959).

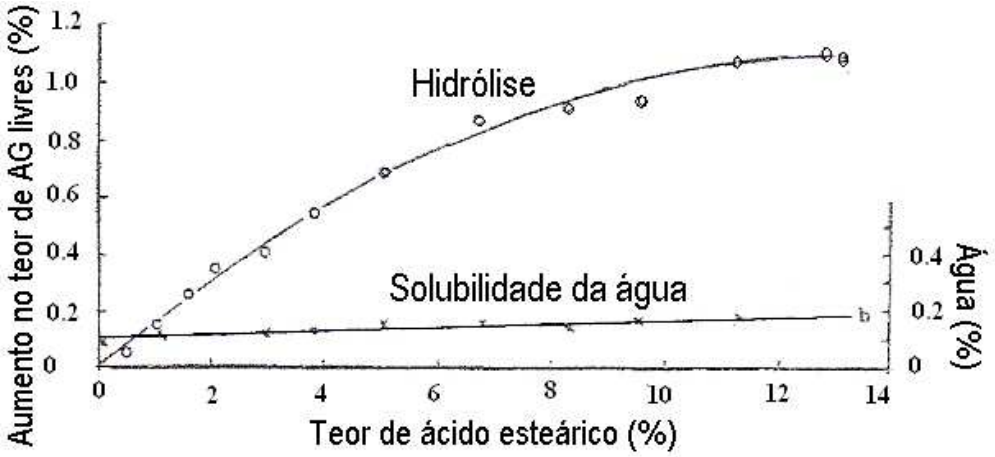

Figura 2.2.5.3.2.1. Hidrólise do óleo de amendoim contendo ácido esteárico (SZABO SARKADI, 1959).

Como pode ser observado na Figura 2.2.5.3.2.1 (SZABO SARKADI, 1959), para a desodorização do óleo de amendoim (em batelada) a 180 °C, 400 mmHg e 4½ h, a hidrólise gera um aumento de até 1,1% na acidez do óleo. Nenhuma informação foi encontrada para a dependência da constante de reação (*k*) com a temperatura, para a reação de hidrólise nas condições usuais da desodorização e/ou desacidificação por via física.

2.2.6 Eficiência de vaporização

O refino físico e/ou desodorização de óleos vegetais em batelada podem ser classificados como uma destilação diferencial na qual compostos voláteis (AGL e odores) são volatilizados pela ação de altas temperaturas e alto vácuo. Um conceito associado à destilação diferencial é a eficiência de vaporização (ε), uma medida do quão saturada de compostos voláteis, uma bolha de vapor torna-se ao longo de sua passagem através da camada de líquido.

BAILEY (1941) foi o primeiro pesquisador a discutir teoricamente a desodorização de óleos vegetais em batelada e apresentar um modelo relacionando a quantidade de vapor de arraste com a eficiência de vaporização. Ainda hoje, este modelo é largamente empregado (CARLSON, 1996; CONSTANTE et al., 1991; RUIZ-MÉNDEZ et al., 1996; DECAP et al., 2004) para a avaliação

deste tipo de processo. Em seu trabalho, BAILEY (1941) já discutia a necessidade de se considerar o efeito da pressão hidrostática na bolha.

Um trabalho recente (COELHO PINHEIRO & GUEDES DE CARVALHO, 1994) abordou este tema, apresentando um estudo teórico detalhado, acompanhado de experimentos para o arraste de pentano de *n*-parafinas e de óleo de girassol com nitrogênio. De acordo com os autores, quando a pressão acima da superfície do líquido é suficientemente pequena, as bolhas formadas no orifício de injeção do agente de arraste crescem consideravelmente, conforme ascendem num campo de pressão variante devido à pressão hidrostática exercida pela coluna de líquido. A equação sugerida pelos autores é integrável numericamente e fornece a relação entre a pressão parcial do composto volátil (A), p_A, com a altura do leito de líquido, h. O modelo informa que há uma redução de p_A conforme a bolha se aproxima da superfície, principalmente para pressões reduzidas (300Pa). Embora os autores tenham considerado os efeitos da pressão hidrostática (expansão da bolha e da pressão interna), o equacionamento e as hipóteses sugeridas são aplicáveis para arraste com gás inerte (como o nitrogênio).

Em vista da importância deste conceito, este trabalho buscou desenvolver uma equação para estimar a eficiência de vaporização que levasse em conta tanto a pressão hidrostática quanto a solubilidade da água no óleo, evidenciada pela reação de hidrólise durante a desodorização de óleos vegetais (vide item 2.2.5.3.2).

2.3 Simulação computacional de processos de contato-gás-líquido

A simulação computacional de processos tem grande possibilidade de aplicação na área de processamento de óleos, já que permite a obtenção de dados de processo em diversas situações operacionais. Esta ferramenta computacional possibilita ajustes de entradas, de condições de operação e de projeto do equipamento que não poderiam ser feitos em um processamento em escala industrial. Isto porque, variações em condições de operação gerariam alterações indesejáveis à rentabilidade do processo na planta de processamento.

O desenvolvimento de pacotes de simulação vem ganhando espaço também na indústria de alimentos, uma vez que o conhecimento prévio do comportamento do processo possibilita um melhor projeto dos equipamentos envolvidos (ALFA LAVAL).

Este item, bem como os seus subitens, apresentam de forma sucinta a modelagem necessária para a implementação de programas de simulação capazes de descrever os processos de interesse deste trabalho de tese.

2.3.1 Destilação diferencial (batelada)

Para uma destilação diferencial multicomponente, os balanços de massa global e por componentes são dados por (INGHAM et al., 1994):

$$\frac{dL}{dt} = -\nu \qquad (2.3.1.1a)$$

$$\frac{d(L \cdot x_i)}{dt} = -\nu \cdot y_i \qquad (2.3.1.1b)$$

onde L é o número total de moles de líquido no recipiente (vide Figura 2.2.4.1B), ν é a taxa de vaporização molar em moles/tempo e x_i e y_i são, respectivamente as frações molares no líquido e no vapor para cada componente *i*.

Assumindo que as fases líquida e vapor estão em equilíbrio para cada tempo, ou seja, que o recipiente de óleo bruto age como um estágio de equilíbrio teórico, as relações de equilíbrio, em termos da composição da fase vapor, são função da pressão de vapor, coeficientes de atividade, temperatura e composição da fase líquida.

Para o recipiente de destilado, os balanços de massa global e por componente são dados por (INGHAM et al., 1994):

$$\frac{dD}{dt} = \nu \qquad (2.3.1.2a)$$

$$\frac{dD_i}{dt} = \nu \cdot y_i \qquad (2.3.1.2b)$$

onde D é o número de moles do destilado e D_i é o número de moles do componente i no recipiente.

Combinando as Equações 2.3.1.1 e 2.3.1.2, em conjunto com as relações de equilíbrio, tem-se um sistema que pode ser facilmente resolvido por integração numérica direta.

A taxa de vaporização, ν, pode ser obtida a partir do balanço de energia no recipiente de líquido, onde o calor proveniente do meio de aquecimento, é adicionado ao sistema.

Este trabalho de tese utilizou a modelagem descrita acima para investigar a desacidificação por via física e a desodorização de óleos vegetais, com a inclusão ou não de reações químicas e do balanço de energia às equações supramencionadas.

2.3.2 Desodorização/desacidificação por via física (equipamento contínuo)

2.3.2.1 Regime permanente

Colunas de separação multi-estágio, com sistemas multicomponentes constituem um exemplo de processo cuja simulação envolve a solução de sistemas de equações não-lineares de elevada dimensão. O elemento básico da modelagem deste tipo de problema é o estágio de equilíbrio (vide Figura 2.3.2.1.1).

Um estágio de equilíbrio genérico **n** admite:

- uma alimentação, F_n, cuja composição z_i, temperatura T_n e pressão P_n são conhecidas;
- duas entradas: uma corrente de vapor vinda do estágio inferior (n-1), com uma vazão molar V_{n-1}, uma composição $y_{i,n-1}$ e à temperatura T_{n-1} e pressão P_{n-1}; uma corrente de líquido proveniente do estágio n+1, com uma vazão molar L_{n+1}, uma composição $x_{i,n+1}$ e à temperatura T_{n+1} e pressão P_{n+1}.

- duas saídas: uma corrente de vapor para o estágio seguinte (n+1), com uma vazão molar V_n, uma composição $y_{i,n}$ e à temperatura T_n e pressão P_n; uma corrente de líquido para o estágio anterior (n-1), com uma vazão molar L_n, uma composição $x_{i,n}$ e à temperatura T_n e pressão P_n.
- troca de calor do estágio com o exterior Q_n.

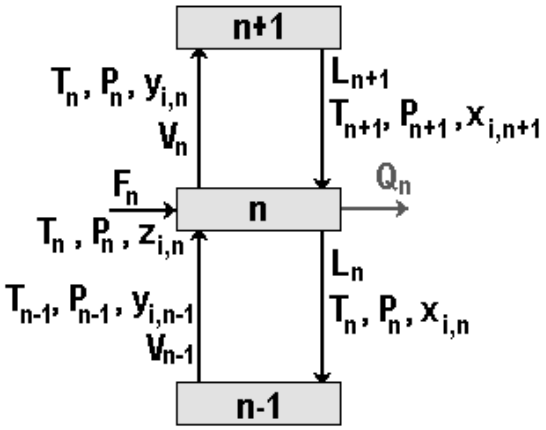

Figura 2.3.2.1.1. Estágio de equilíbrio

Neste trabalho. o método escolhido para a simulação computacional, em regime estacionário, foi o método de cálculo de separação multicomponente por linearização, sugerido por NAPHTALI & SANDHOLM (1971). Este método emprega a técnica de particionamento de matrizes em vista da elevada esparsicidade da matriz resultante em sistemas formados pela cascata dos **N** estágios. Para cada estágio **n** da coluna tem-se um sistema formado por (2*m*+1) equações, onde *m* representa o número de componentes: balanços de massa $M_{n,i}$ (i=1,..., m), condições de equilíbrio $E_{n,i}$ (i=1,..., m) e o balanço de energia H_n. As variáveis em cada estágio são: $l_{n,i}$, $v_{n,i}$ e T_n, respectivamente, as vazões de líquido e de vapor de cada componente *i* e a temperatura do estágio.

Os balanços de massa, energia e a condição de equilíbrio do estágio genérico **n** são relativos apenas aos estágios n-1 e n+1. Desta forma, a matriz Jacobiana $\left(\frac{\partial F}{\partial x}\right)$ formada é altamente esparsa e de estrutura tridiagonal. Esta característica facilita sua resolução pelo método de Newton-Raphson.

As vantagens deste algoritmo são: (a) a volatilidade de cada um dos componentes não afeta a convergência do método; (b) a presença de soluções não-ideais é considerada e não afeta o modelo; (c) a eficiência dos pratos (eficiência de Murphree) pode ser levada em conta de forma rigorosa; (d) a quantidade de alimentações e saídas laterais é ilimitada; (e) o método é baseado na linearização das equações, acelerando a convergência conforme se aproxima da solução.

Maiores detalhes sobre o equacionamento do modelo empregado neste trabalho podem ser encontrados nos Apêndices I e II dos Capítulos 5 e 6.

2.3.2.2 Regime dinâmico

O modelo para a simulação dinâmica de uma coluna de destilação consiste em um grupo de equações diferenciais ordinárias (EDO), que correspondem aos balanços de massa e energia, e outro de equações algébricas, que descrevem o equilíbrio e a hidráulica do prato. Para cada estágio *n*, balanços molares global e por componentes, e o balanço de energia podem ser estabelecidos.

De acordo com RAMIREZ (1997), algumas simplificações podem ser feitas na modelagem dinâmica de colunas de destilação: (1) o hold-up da fase vapor é desprezível; (2) o hold-up da fase líquida é constante; (3) a variação na entalpia de cada estágio é aproximadamente nula.

O balanço molar por componente é resolvido para a composição da fase líquida, uma vez que o hold-up da fase vapor é nulo. Desta forma, a variação nos moles do componente *i* na fase líquida depende das vazões de entrada e saída no estágio *n*.

Uma vez conhecida a composição do líquido, a temperatura de equilíbrio e a composição da fase vapor podem ser obtidas pelas relações de equilíbrio, através de um método como Newton-Raphson, de forma que $\sum y_i = 1$. A estratégia computacional para resolver o modelo dinâmico está mostrada na Figura 2.3.2.2.1.

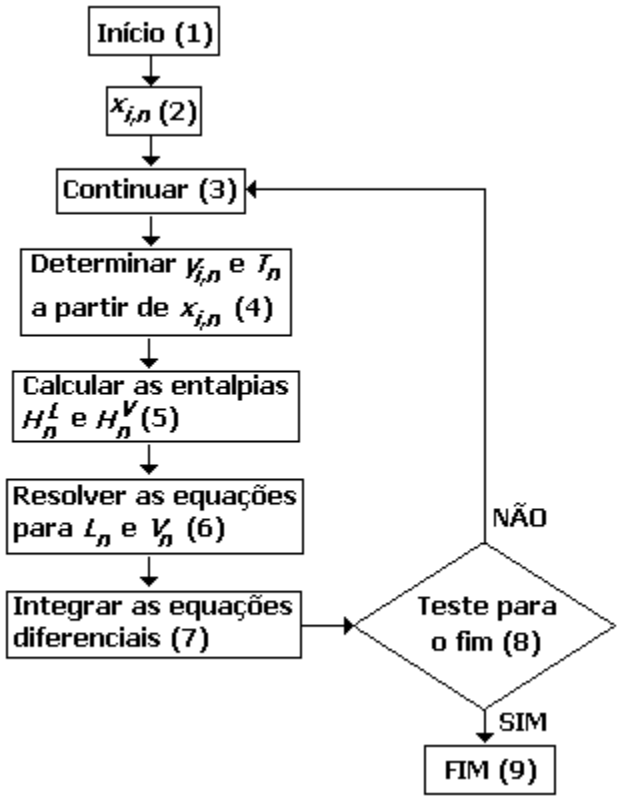

Figura 2.3.2.2.1. Algoritmo de resolução.

Conhecida a composição da fase líquida ($x_{i,n}$) em cada estágio (BLOCO 2), as temperaturas de equilíbrio (T_n), e a composição da fase vapor ($y_{i,n}$) são determinadas (BLOCO 4). As entalpias das fases líquida ($H^L{}_n$), e vapor ($H^V{}_n$) são calculadas através de equações algébricas (BLOCO 5). Com estas informações é possível resolver os balanços molares globais e de energia para cada estágio utilizando técnicas de resolução simultânea de matrizes (BLOCO 6). Finalmente, as equações diferenciais dos balanços molares por componente são integradas, fornecendo as composições das fases líquidas para o novo tempo t (RAMIREZ, 1997).

Vale ressaltar que para problemas mal-comportados (rígidos) recomenda-se um método de integração de passo variável, como o método de GEAR (1971) ou ode15s no MatLab®. Nestes casos, o método de Runge-Kutta é pouco eficiente (RAMIREZ, 1997). Seguindo esta sugestão, este trabalho utilizou o método de integração de passo variável.

Maiores detalhes sobre o equacionamento do modelo empregado podem ser encontrados no Apêndice I desta tese.

2.3.2.3 Estimativa da eficiência de Murphree

Em processos de separação, onde as fases líquida e vapor estão perfeitamente misturadas, a eficiência na transferência de massa de um componente é dada pela eficiência de Murphree. Como sugerido por LUDWIG (1995), a eficiência de Murphree pode ser estimada facilmente pelas equações sugeridas por MACFARLAND et al. (1972). Estes autores ajustaram 806 pontos experimentais de sistemas binários à duas equações de correlação para a eficiência de Murphree (η) colocadas a seguir. Ambas são funções dos adimensionais N_{DG} (número de tensão superficial), N_{Re} (número de Reynolds) e N_{SC} (número de Schmidt).

$$\eta = 7{,}0 \cdot (N_{DG})^{0{,}14} \cdot (N_{SC})^{0{,}25} \cdot (N_{\mathrm{Re}})^{0{,}08} \qquad (2.3.2.3.1)$$

$$\eta = 6{,}8 \cdot (N_{\mathrm{Re}} \cdot N_{SC})^{0{,}1} \cdot (N_{DG} \cdot N_{SC})^{0{,}115} \qquad (2.3.2.3.2)$$

Para a primeira equação (Equação 2.3.2.3.1), os autores obtiveram um desvio médio de 13,2%, o que pode ser considerado tão preciso quanto outras metodologias muito mais complicadas (LUDWIG, 1995). Já para a segunda equação, o desvio médio obtido foi de 10,6%, para o mesmo banco de dados. Os adimensionais estão definidos a seguir.

$$N_{DG} = 28572{,}06 \cdot \frac{\sigma_L}{\mu_L \cdot U_{VN}} \qquad (2.3.2.3.3)$$

$$N_{SC} = \frac{\mu_L}{\rho_L \cdot D_{LK}} \qquad (2.3.2.3.4)$$

$$N_{Re} = \frac{\rho_V \cdot U_{VN} \cdot h_w}{\mu_L} \qquad (2.3.2.3.5)$$

onde: σ_L = tensão superficial do líquido (dinas/cm), μ_L = viscosidade do líquido (lb/h.pés), U_{VN} = velocidade do vapor (pés/h), ρ_L = densidade do líquido (lb/pés^3), h_w = altura da barreira de saída (parâmetro de projeto dos pratos) e D_{LK}

= difusividade do componente mais volátil na fase líquida. Segundo CARLSON (1996), o valor de U_{VN} em desodorizadores é igual a 6,6 pés/s.

Um outro método que possibilita o cálculo da eficiência de Murphree é o método AIChE, recomendado pelo *The Distillation Subcommittee of the American Institute of Chemical Engineering* (AIChE) e incluso no livro *AIChE Bubble Tray Design Manual* de 1958. Uma desvantagem relacionada ao seu uso é a grande quantidade de dados de projeto dos pratos necessária nos cálculos. Na área de óleos vegetais, este tipo de informação não é facilmente acessível. Levando-se em consideração esta dificuldade e o fato de LUDWIG (1995) recomendar o método de MACFARLAND et al. (1972), este trabalho utilizou-o no cálculo da eficiência de Murphree.

2.3.2.4 Estimativa do arraste mecânico

A correlação de arraste mecânico apresentada na Figura 2.3.2.4.1 foi desenvolvida por FAIR & MATTHEWS (1958) para pratos de campânulas e pratos perfurados a partir de dados da literatura para diversas colunas sob diferentes condições e sistemas.

A correlação relaciona a porcentagem de inundação, o arraste mecânico fracional ψ (moles de líquido arrastado no vapor/moles de liquido), vazões de líquido e vapor (L e V), e suas densidades (ρ_L e ρ_V).

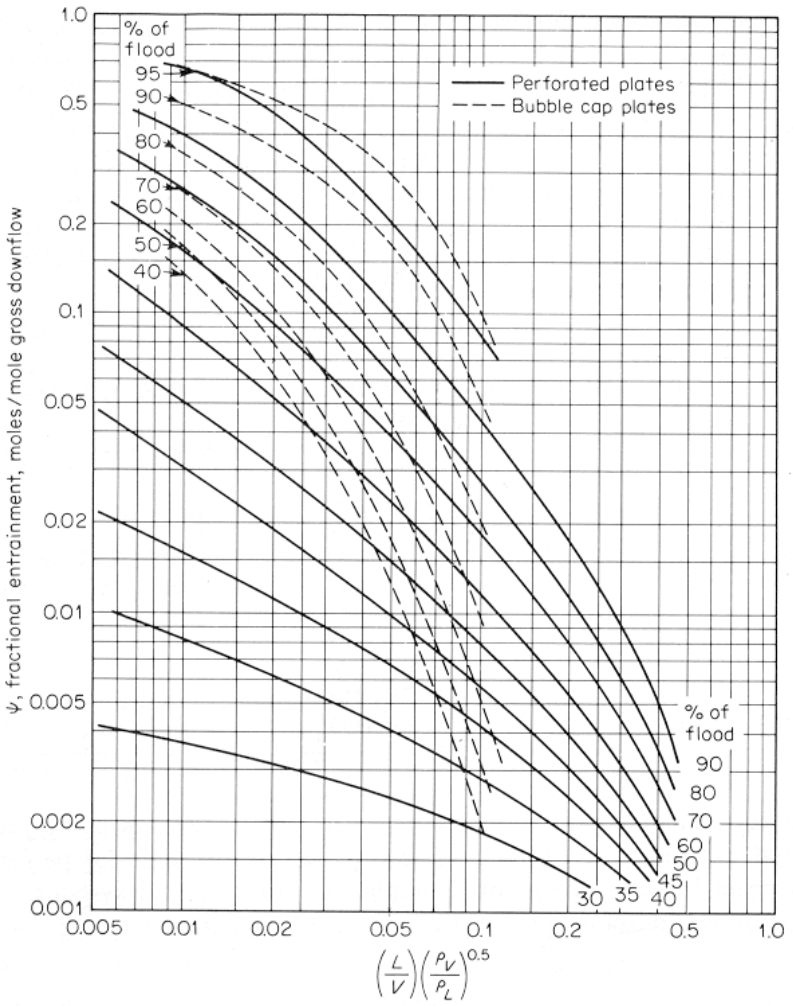

Figura 2.3.2.4.1. Correlação para o arraste mecânico (FAIR & MATTHEWS, 1958).

Usando as restrições especificadas a seguir, assume-se uma precisão de 15%.

1. O sistema de destilação não produz ou produz pouca espuma.
2. A altura da barreira de saída é menor que 15% do espaçamento entre os pratos.
3. Os diâmetros das perfurações são menores ou iguais a 0,25 polegada.
4. O espaçamento entre pratos de 6 a 9 polegadas não se aplica aos pratos de campânulas.

5. A tensão superficial (σ) do sistema é igual a 20 dynas/cm. Para valores diferentes, a capacidade dada pela Figura 2.3.2.4.1 deve se modificada pela seguinte equação:

$$\frac{U_{VN}}{U_{VN_{\sigma=20 dynas/cm}}} = \left(\frac{\sigma}{20}\right)^{0,2} \qquad (2.3.2.4.1)$$

Embora as metodologias descritas nos itens 2.3.2.3 e 2.3.2.4 tenham sido desenvolvidas para processos da indústria química, este trabalho buscou avaliar a viabilidade de sua utilização em processos da indústria de óleos vegetais, como a desacidificação por via física e a desodorização.

2.3.3 Equilíbrio de fases

Para o desenvolvimento e o planejamento de um processamento de óleos vegetais, envolvendo processos de contato líquido-vapor, é essencial o conhecimento do equilíbrio de fases do sistema de interesse e a escolha de métodos e/ou equações de predição das propriedades físicas das misturas envolvidas.

O equilíbrio de fases é definido em um sistema no qual duas fases homogêneas diferentes estão em equilíbrio. No equilíbrio líquido-vapor (ELV) a temperatura, pressão e fugacidades dos componentes das fases são iguais (REID et al., 1987). Rigorosamente, é definido pela equação a seguir:

$$y_i \cdot P = \gamma_i(T, x) \cdot x_i \cdot P_i^{vp}(T) \cdot \frac{\phi_i^{sat}}{\phi_i} \cdot \int_{P_i^{vp}}^{P} \frac{V_i^L}{R \cdot T} dP \qquad (2.3.3.1)$$

A constante de equilíbrio K_i é um parâmetro chave na análise do equilíbrio e pode ser definida de acordo com a Equação 2.3.3.2 abaixo:

$$K_i = \frac{y_i}{x_i} = \frac{\gamma_i(T, x) \cdot P_i^{vp}(T) \cdot \phi_i^{sat} \cdot POY}{\phi_i \cdot P} \qquad (2.3.3.2)$$

Nas Equações 2.3.3.1 e 2.3.3.2, os coeficientes de fugacidade, ϕ_i e ϕ_i^{sat} podem ser facilmente calculados através da equação virial truncada no segundo termo (Equação 2.3.3.3), combinada com regras de mistura (REID et al., 1987).

$$\ln \phi_i = \frac{P}{R \cdot T}\left(2\sum_j y_i \cdot B_{ij} - B\right) \qquad (2.3.3.3)$$

onde: $B = \sum\sum y_i \cdot y_j \cdot B_{ij}$. Para o cálculo de ϕ_i^{sat}, substitui-se, na equação anterior, P por P_i^{vp} (pressão de vapor do componente i). Propriedades críticas e fatores acêntricos dos componentes puros são necessários no cálculo dos coeficientes viriais. REID et al. (1987) apresentam métodos tradicionais para a estimativa de volumes, pressões e temperaturas críticas. O parâmetro V_i^L pode ser estimado a partir do método de Rackett (REID et al., 1987), citado por HALVORSEN et al. (1993). Os coeficientes de atividade, γ_i, podem ser determinados utilizando-se métodos de contribuição de grupos, como os modelos ASOG (KOJIMA & TOCHIGI, 1979) e UNIFAC (FREDENSLUND et al., 1977), e as pressões de vapor devem ser estimadas por equações empíricas ou modelos teóricos.

2.3.3.1 Ponto de bolha

O termo ponto de bolha é definido como a temperatura na qual a primeira bolha de gás se forma a partir do líquido, para um certo composto ou mistura. Conhecidas a pressão do sistema (P) e a composição da fase líquida, é possível se calcular a temperatura (ponto de bolha) e a composição do vapor, que satisfaçam a condição abaixo:

$$\sum_i (y_i) - 1 \leq \varepsilon \qquad (2.3.3.1.1)$$

O método de Newton-Raphson minimiza o erro, de forma a garantir que ele seja menor que ε.

Em termos de dados experimentais de equilíbrio líquido-vapor de compostos graxos, a literatura é limitada. Apresenta dados, que em sua maioria são antigos, obtidos quando as técnicas experimentais em geral, e analíticas em particular, eram menos desenvolvidas. TORRES & MEIRELLES (1997) e TORRES (1996) trabalharam com a predição do ELV de misturas binárias de AG saturados e insaturados e ésteres graxos para pressões entre 10 e 100 mmHg. Dados de

equilíbrio líquido-vapor de misturas binárias de TAG são fornecidos por GOODRUM et al. (1998).

A literatura apresenta alguns artigos que discutem o desempenho de miscelas de diferentes óleos vegetais e solventes, sob uma faixa extensa de temperatura e pressão. LEBERT & RICHON (1984) mediram o coeficiente de atividade à infinita diluição de miscelas de óleo de oliva com hidrocarbonetos (C_5 a C_{10}) e álcoois (C_1 a C_6) à pressão atmosférica. SMITH (1951), SMITH & FLORENCE (1951) e SMITH & WECHTER (1950) apresentam dados isotérmicos de equilíbrio líquido-vapor para miscelas de hexana e óleo de soja. POLLARD et al. (1945) reportam pontos de ebulição para sistemas constituídos por óleo de algodão e óleo de amendoim diluídos em hexana para pressões entre 160 e 760mmHg.

Fontes de dados do equilíbrio líquido-vapor de misturas binárias de compostos graxos estão colocados na Tabela 2.3.3.1.1. Estes dados de equilíbrio líquido-vapor foram utilizados neste trabalho de tese para avaliar a capacidade preditiva da ferramenta desenvolvida para predizer a pressão de vapor de compostos graxos em conjunto com diferentes versões do UNIFAC.

Tabela 2.3.3.1.1. Banco de dados de equilíbrio

Classe dos compostos	Nº de misturas	N º de pontos experimentais	Referências
AG saturados	6 b(S-S)	158 b (S-S)	TORRES (1996)
AG insaturados	1 b(S-IS)	8 b (S-IS)	TORRES (1996)
Ésteres graxos	6 b(S-S)	133 b (S-S)	TORRES (1996)
TAG	3 b(S-S)	21 b (S-S)	GOODRUM et al. (1998)

b = sistema binário, S = saturado, IS = insaturado.

2.3.4 Propriedades termodinâmicas

O conhecimento de diversas propriedades termodinâmicas é necessário para um correto equacionamento de sistemas químicos. No caso de óleos vegetais, a complexidade e a diversidade dos compostos presentes na mistura fazem com que seja bastante interessante a utilização de métodos preditivos de propriedades físicas baseados no conceito de contribuição de grupos, cuja idéia básica consiste em se considerar uma mistura ou substância qualquer como um agregado de grupos funcionais presentes nas moléculas que a constituem. Desta forma, suas

propriedades são resultantes do somatório de cada uma destas contribuições, representadas através de parâmetros de contribuição de grupos, ajustados com base nos dados experimentais das substâncias de interesse. Esta generalização do método, no entanto, nem sempre consegue predizer com boa precisão a propriedade do composto, pois considera a influência de um determinado grupo sempre igual, em qualquer molécula (TORRES, 1996). Na ausência de equações empíricas é, sem dúvida, uma alternativa a ser considerada.

2.3.4.1 Pressão de vapor

A pressão de vapor é definida como a pressão exercida pelo vapor quando está em equilíbrio com o líquido que lhe deu origem. É uma propriedade dependente da temperatura do sistema.

Trabalhos experimentais de desacidificação por via física e desodorização de óleos vegetais (VERLEYEN et al., 2001, PETRAUSKAITÈ et al., 2000) apontam para o fato de a volatilidade de MAG, DAG e TAG não ser desprezível, representando um fator importante na perda de óleo neutro nestes processos. Óleos láuricos, em especial, são formados por componentes graxos de cadeia carbônica mais curta e, portanto mais volátil do que em outros óleos, sendo sua vaporização ainda mais evidente. VERLEYEN et al. (2001) mostram que a fração de acilgliceróis nos destilados da desodorização varia consideravelmente de acordo com o óleo: 0,72% para o óleo de milho e 13,67% para o óleo de soja. Tendo uma ferramenta para a predição da pressão de vapor de acilgliceróis, seria possível verificar se a perda de óleo neutro no refino físico e/ou desodorização ocorre apenas pelo arraste mecânico ou também por destilação.

Em vista do vasto banco de dados de pressão de vapor dos mais variados compostos graxos, este trabalho teve como etapa inicial o ajuste de uma equação preditiva para esta propriedade. No total, mais de 1300 dados foram agrupados. Por se tratar de dados de diferentes autores, alguns deles muito antigos, constatou-se, em certos casos, conflito expressivo dos valores experimentais

medidos. Mais detalhes sobre este assunto está colocado no Capítulo 3 e no Apêndice II desta tese.

2.3.4.2 Método UNIFAC para o cálculo do coeficiente de atividade

No modelo UNIFAC, o coeficiente de atividade é calculado considerando-se uma contribuição entrópica, relacionada à diferença de tamanho e forma das moléculas e uma contribuição residual, devido à interações intermoleculares. A partir da versão de FREDENSLUND et al., (1977), novos grupos e pequenas modificações nas equações originais foram sendo propostas. No modelo UNIFAC modificado (Dortmund) de GMEHLING et al. (1993), por exemplo, a porção combinatorial foi modificada de uma forma empírica, com o objetivo de se trabalhar com misturas de compostos com tamanhos bem diferentes. Além disso, os parâmetros de Van der Waals sofreram uma leve modificação e foram introduzidas também dependências com a temperatura no termo residual. Outras versões sugeriram modificações apenas no termo combinatorial (FORNARI et al., 1994; KIKIC et al., 1980).

2.3.4.3 Calor específico do líquido e vapor

Calor específico é uma propriedade envolvida diretamente no cálculo de balanços de energia, no projeto e controle de processos químicos, estando, portanto relacionada ao consumo energético do processo. O cálculo do calor específico do líquido não é muito dependente da temperatura, exceto para valores de T_r (T/T_c) acima de 0,7 a 0,8. Métodos de predição podem ser divididos em quatro categorias: teórico, contribuição de grupos, lei dos estados correspondentes e ciclo termodinâmico de Watson (REID et al., 1987). Pode-se encontrar ainda equações, onde se evidencia a dependência linear desta propriedade com a temperatura, como no caso de alguns AG e óleos vegetais (CEDEÑO et al., 2000; COUPLAND & MCCLEMENTS, 1997).

O método de Rowlinson-Bondi (REID et al., 1987) baseia-se no princípio dos estados correspondentes e foi empregado tanto por MORAD et al. (2000)

quanto por CEDEÑO et al. (2000), na estimativa do calor específico do líquido de AG, TAG e óleos vegetais. A equação do método de Rowlinson-Bondi, de acordo com REID et al. (1987) é como se segue:

$$\frac{C_p - C_p^o}{R} = 1{,}45 + 0{,}45 \cdot (1 - T_r)^{-1} + 0{,}25 \cdot w \cdot [17{,}11 + 25{,}2 \cdot (1 - T_r)^{1/3} \cdot T_r^{-1} + 1{,}742 \cdot (1 - T_r)^{-1}] \quad (2.3.4.3.1)$$

onde: C_p é o calor específico do líquido, C_p^o é o calor específico do gás ideal, R é a constante universal dos gases, T_r é a temperatura reduzida (razão entre a temperatura do sistema e a temperatura crítica), w é o fator acêntrico.

Este método, portanto, necessita de valores de C_p^o, T_r e w, que podem ser calculados por métodos preditivos de contribuição de grupos, sugeridos pelos autores citados acima.

Todos os métodos para a estimativa de propriedades no estado de gás ideal envolvem algum tipo de divisão dos compostos em grupo, isto porque a lei dos estados correspondentes não se aplica neste caso. REID et al. (1987) apresenta quatro métodos capazes de predizer esta propriedade. Segundo os autores, o método proposto por JOBACK & REID (1987) é mais fácil de ser empregado e tem uma grande aplicabilidade. Este método utiliza o conceito de contribuição de grupos, de acordo com a equação a seguir:

$$C_p^o = \sum(a) - 37{,}93 + [\sum(b) + 0{,}210] \cdot T + [\sum(c) - 3{,}91 \cdot 10^{-4}] \cdot T^2 + [\sum(d) + 2{,}06 \cdot 10^{-7}] \cdot T^3 \quad (2.3.4.3.2)$$

onde: *a, b, c* e, *d* são parâmetros ajustados para cada grupo que compõe a molécula; T é a temperatura em Kelvin

Para o cálculo da temperatura crítica de compostos, o método por contribuição de grupos de Fedor (REID et al., 1987) é menos preciso que o método de JOBACK & REID (1987), mas tem a grande vantagem de não precisar da temperatura normal de ebulição como entrada. Sua equação pode ser escrita como:

$$T_c = 535 \cdot \log\left(\sum \Delta_T\right) \qquad (2.3.4.3.3)$$

onde: T_c é a temperatura crítica em Kelvin e Δ_T são valores fornecidos para cada grupo.

O fator acêntrico é definido como a acentricidade ou a não esfericidade de uma molécula, sendo proporcional à polaridade e ao tamanho da cadeia do composto. Pode ser obtido pela seguinte relação, de acordo com REID et al., (1987):

$$w = 12{,}5 \cdot \left(0{,}291 - \frac{P_c \cdot V_c}{R \cdot T_c}\right) \qquad (2.3.4.3.4)$$

onde: P_c V_c e T_c são, respectivamente a pressão, volume e temperatura críticos e R é a constante universal dos gases.

Da mesma forma que T_c , a pressão e volume críticos podem ser calculados por métodos de contribuição de grupos, neste caso, os propostos por JOBACK & REID (1987), de acordo com as equações abaixo:

$$P_c = (0{,}113 + 0{,}0032 \cdot n_A - \sum)^{-2} \qquad (2.3.4.3.5)$$

onde: n_A é o número total de átomos da molécula e $\sum$ é a somatória dos valores de cada grupo.

$$V_c = (17{,}5 + \sum) \qquad (2.3.4.3.6)$$

onde: V_c é o volume crítico e $\sum$ é a somatória dos valores de cada grupo.

Para a água, os calores específicos do líquido $\left(C_{p\text{água}}\right)$ e do gás ideal $\left(C^{o}_{p\text{água}}\right)$ podem ser calculados, respectivamente, por (DIPPR, 2005):

$$C^{o}_{p\text{água}}(\text{J/kmol.K}) = 33363 + 26790 \cdot \left[\frac{2610{,}5/T(\text{K})}{\text{senh}\left(2610{,}5/T(\text{K})\right)}\right] + 8896{,}0 \cdot \left[\frac{1169{,}0/T(\text{K})}{\text{senh}\left(1169{,}0/T(\text{K})\right)}\right] \qquad (2.3.4.3.7)$$

$$C_{p\text{água}}(\text{J/kmol.K}) = 276370 - 2090{,}1 \cdot T(\text{K}) + 8{,}1250 \cdot T^2(\text{K}) - 0{,}014116 \cdot T^3(\text{K}) + 9{,}3701 \cdot 10^{-6} \cdot T^4(\text{K}) \qquad (2.3.4.3.8)$$

2.3.4.4 Entalpia de vaporização

A entalpia de vaporização representa a diferença entre a entalpia do vapor saturado e a entalpia do líquido saturado na mesma temperatura. Dados experimentais de entalpias de vaporização podem ser medidos diretamente em um calorímetro ou indiretamente pela dependência da pressão de vapor com a temperatura.

Em geral, dados experimentais de entalpia de vaporização são escassos para compostos graxos. Muitos métodos de predição, baseados na lei dos estados correspondentes, utilizam propriedades críticas como parâmetros de equações envolvendo propriedades reduzidas (REID et al., 1987).

Como já comentado anteriormente, métodos de contribuição de grupos são mais interessantes neste trabalho. Dos métodos sugeridos por TU & LIU (1996) e KLÜPPEL et al. (1994), o primeiro é mais conveniente por se tratar de uma equação simples, onde são necessários os parâmetros de grupo do modelo e a temperatura reduzida. Já o método sugerido por KLÜPPEL et al. (1994), denominado UNIVAP (UNIversal heats of VAPorization), está baseado no UNIFAC e se utiliza da parte residual do mesmo para descrever esta propriedade, modificando todos os parâmetros de interação energética.

O modelo por contribuição de grupos para a estimativa da entalpia de vaporização do trabalho proposto por TU & LIU (1996) é dado como se segue:

$$\Delta H_{vap} = \sum N_i \cdot \left[a_i \cdot \left(1 - \frac{T}{T_c}\right)^{1/3} + b_i \cdot \left(1 - \frac{T}{T_c}\right)^{2/3} + c_i \cdot \left(1 - \frac{T}{T_c}\right) \right] \qquad (2.3.4.4.1)$$

onde: ΔH_{vap} é a entalpia de vaporização calculada em kJ/mol, T_c é a temperatura crítica em Kelvin e a_i, b_i e c_i são constantes preditas para cada grupo *i*. A temperatura crítica pode ser estimada pelo método de Fedor, de acordo com REID et al. (1987).

Para a água, ΔH_{vap} pode ser calculado pela equação a seguir (DIPPR, 2005):

$$\Delta H_{vap}^{água}\,(\mathrm{J/kmol}) = 5{,}2053\ \mathrm{E7} \cdot \left[1 - \frac{T(\mathrm{K})}{647{,}13}\right]^{0{,}3199 - 0{,}212 \cdot \frac{T(\mathrm{K})}{647{,}13} + 0{,}25795 \cdot \left(\frac{T(\mathrm{K})}{647{,}13}\right)^2}$$

(2.3.4.4.2)

O valor 647,13K na Equação 2.3.4.4.2 representa a temperatura crítica experimental para água.

2.3.5 Estimativa da composição de óleos vegetais

A partir da composição mássica em AG de óleos vegetais e seus respectivos pesos moleculares, é possível determinar sua composição provável em TAG, baseando-se no método estatístico sugerido por ANTONIOSI FILHO et al. (1995). Este método estatístico se baseia nas teorias da distribuição "casual" e "1,3-casual 2-casual" (ANTONIOSI FILHO et al., 1995). A teoria da distribuição "casual" estabelece que os AG se encontram distribuídos ao acaso, estatisticamente, entre as três posições da molécula do glicerol.

Este método, frente a outros métodos estatísticos e a métodos cromatrográficos para a determinação da composição em TAG, mostrou-se eficiente, proporcionando resultados bastante satisfatórios, sendo largamente empregado em trabalhos deste grupo de pesquisa. Para a utilização do método, é necessário se conhecer o teor de TAG trisaturados. Esta informação está disponível na literatura para alguns óleos. Como exemplo, o teor de TAG trisaturados do óleo de soja é considerado nulo; do óleo de palma igual a 7,9% (CHUAN HO, 1976) e do óleo de coco 84% (THEME, 1968).

Já a composição em DAG pode ser obtida, partindo-se da composição em TAG do óleo vegetal da seguinte forma: Cada TAG pode ser quebrado em 1,2- e 1,3- DAG; cada DAG, por sua vez, pode ser dividido em MAG, de acordo com a relação estequiométrica entre os compostos. Alguns trabalhos da literatura informam também a concentração de DAG e MAG em alguns óleos vegetais. De acordo com LONCIN (1962), o óleo de coco apresenta 3% de DAG e 1% de MAG;

já o óleo de palma (CHUAN HO, 1976) possui de 5,3 a 7,8% de DAG e 0,44 a 0,51% de MAG.

As concentrações de componentes minoritários e de AGL (acidez) nos óleos vegetais pode ser facilmente obtida na literatura (BASIRON, 1996; CANAPI et al., 1996; DAVIDSON et al., 1996; FIRESTONE, 1999; JONES & KING, 1996; O'BRIEN, 1998; MICHAEL ESKIN et al., 1996; SALUNKHE et al, 1992; SIPOS & SZUHAJ, 1996; YOUNG, 1996).

Referências

ABIOVE. Referência bibliográfica de documento eletrônico. Disponível na Internet: http://www.abiove.com.br. Acesso em fevereiro de 2005.

ABEQ. Referência bibliográfica de documento eletrônico. Disponível na Internet: http://www.abeq.org.br/view.php?id=259. Acesso em agosto de 2005.

AHRENS, D. Comparison of tray, thin-film deodorization. *Inform.* v.9, no. 6, p. 566-576, 1998.

AHRENS, D. Industrial thin-film deodorization of seed oils with SoftColumn technology. *Fett/Lipid.* v.101, no. 7, p. 230-234, 1999.

ALFA LAVAL. Packed Column for Edible Oil Refining. ALFA LAVAL AB, Fats and Oils Division S147-80, Tumba, Sweden

ANDERSON, D. A Primer on Oils Processing Technology. In: HUI, Y.H. *Bailey's Industrial Oil and Fat Products*. 5 ed., v. 4, New York: John Wiley & Sons, p.1-61, 1996.

ANTONIASSI, R., ESTEVES, W., MEIRELLES, A.J.A. Pretreatment of corn oil for physical refining. *J. Am.Oil.Chem.Soc*., v.75, no.10, p.1411-1415, 1998.

ANTONIOSI FILHO, N.R., MENDES, O.L., LANÇAS, F.M. Computer prediction of triacilglicerol composition of vegetable oils by HRGC. *J. Chromatographia*, v.40, no.9-10, p.557-562, 1995.

ANVISA, Referência bibliográfica de documento eletrônico. Disponível na Internet: http://www.anvisa.gov.br/faqdinamica. Acesso em fevereiro de 2005.

ANVISA. Resolução RDC nº 482, de 23 de setembro de 1999. Agência Nacional de Vigilância Sanitária aprova o "Regulamento Técnico para Fixação de Identidade e Qualidade de Óleos e Gorduras Vegetais". Diário Oficial da União, Brasília, 13 out. 1999.

ARO, A., VAN AMELSVOORT, J., BECKER, W., VAN ERP-BAART, M.A., KAFATOS, A., LETH, T., VAN POPPELS, G. Trans Fatty Acids in Dietary Fats and Oils from 14 European Countries: The TRANSFAIR Study. *J. Food Compos. Anal.*, v.11, p. 150-160, 1998.

BALCHEN, S., GANI, R., ADLER-NISSEN, J. Deodorization Principles, *Inform.* v.10, no.3, p.245-262, 1999.

BASIRON, Y. Palm Oil. In: HUI, Y.H. *Bailey's Industrial Oil and Fat Products*. 5 ed., v.2, New York: John Wiley & Sons, p.271-377, 1996.

BAILEY, A.E. Steam Deodorization of Edible Fats and Oils, *Ind. Eng. Chem.,* v.33, no.3, p.404-408, 1941.

BENSON, S.W., *The Foundations of Chemical Kinetics*, New York: McGraw-Hill, 1960

BROCKMANN, R., DEMMERING, G., KREUTZER, U. Fatty acids. In: KAUDY, L., ROUNSAVILLE, J.F., SCHULZ, A. *Ullmann's Encyclopedia of Industrial Chemistry,* Weinheim: Verlog Chemie, v. A10, p.245-275, 1987.

CAMACHO, M.L., RUIZ-MÉNDEZ, M.V., GRACIANI-CONSTANTE, M., GRACIANI-CONSTANTE, E. Kinetics of the Cis-Trans Isomerization of Linoleic Acid in the Deodorization and/or Physical Refining of Edible Oils. Prediction of trans Polyunsaturated Fatty Acid Content. *Eur. J. Lipid Sci. Technol.*, v.103, p. 85-92, 2001.

CANAPI, E.C., AGUSTIN, Y.T.V., MORO, E.A., PEDROSA, E., BENDAÑO, M.L.J. Coconut Oil. In: HUI, Y.H. *Bailey's Industrial Oil and Fat Products.* 5 ed., v.2, New York: John Wiley & Sons, p.97-125, 1996.

CARLSON, K.F. Deodorization. In: HUI, Y.H. *Bailey's Industrial Oil and Fat Products.* 5 ed., v.4, New York: John Wiley & Sons, p.339-391, 1996.

CEDEÑO, F.A., PRIETO, M.M., XIBERTA, J. Measurements and Estimate Heat Capacity for some pure fatty acids and their binary and ternary mixtures. *J.Chem. Eng. Data*, v.45, p. 64-69, 2000.

COELHO PINHEIRO, M.N., GUEDES DE CARVALHO, J.R.F. Stripping in a Bubbling Pool under Vacuum. *Chem. Eng. Sci.,* v.49, no.16, p. 2689-2698, 1994.

CHUAN HO, O. Studies in Palm Oil Crystallization. *J. Am.Oil.Chem.Soc*. v.53, no.10, p.609-617, 1976.

CONSTANTE, E.G., BERBEL, F.R., TORRONTERAS, A.P., LOPE, J.H. Deacidification by distillation using Nitrogen as Stripper. Possible Application to the Refining of Edible. *Grasas y Aceites*. v.42, no.4, p. 286-292, 1991.

COUPLAND, J.N., MCCLEMENTS, D.J. Physical Properties of Liquid Edible Oils. *J. Am.Oil.Chem.Soc*. v.74, no.12, p.1559-1564, 1997.

DAVIDSON, H., CAMPBELL, E.J., BELL, R.J., PRITCHARD, R.J. Sunflower Oil. In: HUI, Y.H. *Bailey's Industrial Oil and Fat Products*. 5 ed., v.2, New York: John Wiley & Sons, p.603-690, 1996.

DECAP, P., BRAIPSON-DANTHINE, S., VANBRABANT, B., DE GREYT, W., DEROANNE, C. Comparison of Steam and Nitrogen in the Physical Deacidification of Soybean Oil. *J. Am.Oil.Chem.Soc.*, v.81, no.6, p.611-617, 2004.

DIPPR. Referência bibliográfica de documento eletrônico. Disponível na Internet: http://www.dippr.byu.edu/students. Acesso em abril de 2005.

FAIR, J.R., MATTHEWS, R.L. *Petrol. Refiner,* v.37, no.4, p.153, 1958.

FIRESTONE, D. *Physical and Chemical Characteristics of Oils, Fats and Waxes*. Washington: AOCS Press, 151p, 1999.

FORNARI, T., BOTTINI, S., BRIGNOLE, E.A. Applications of UNIFAC to Vegetable Oils – Alkanes Mixtures. *J. Am.Oil.Chem.Soc*., v.71, no.4, p.391-395, 1994.

FREDENSLUND, A., GMEHLING, J., RASMUSSEN, P*. Vapor-liquid equilibria using UNIFAC.,* Amsterdam: Elsevier, 1977.

GAVIN, A.M. Edible Oil Deodorization. *J. Am.Oil.Chem.Soc.,* v.55, no.11, p.783-791, 1978.

GEAR, G.W. Simultaneous Numerical Solution of Ordinary Differential-Algebraic Equations. *IEEE Trans. On Circuit Theory*, v.18, no.1, p.89-95, 1971

GMEHLING, J., LI, J., SCHILLER, M. A Modified UNIFAC Model. 2. Present Parameter Matriz and Results for Different Thermodynamic Properties. *Ind. Eng. Chem. Res*., v.32, p.178-193, 1993.

GOODRUM, J.W., GELLER, D.P., LEE, S.A. Rapid Measurement of Boiling Points and Vapor Pressure of Binary Mixtures of Short-Chain Triglycerides by TGA Methods. *Thermochim. Acta*. v.311, p. 71-79, 1998.

HALVORSEN, J.D., MAMMEL, W.C., CLEMENTS, L.D. Density Estimation for Fatty Acids and Vegetable Oils based on their Fatty Acid Composition, *J. Amer. Oil Chem. Soc*., v.70, no.9, p.875-880, 1993.

HÉNON, G., VIGNERON, P.Y., STOCLIN, B., CAIGNIEZ, J. Rapeseed Oil Deodorization Study using the Response Surface Methodology. *Eur. J. Lipid Sci. Technol*., v.103, p.467-477, 2001

HÉNON, G., KEMÉNY, Zs., RECSEG, K., ZWOBADA, F., KOVARI, K. Deodorization of Vegetable Oils. Part I: Modelling the Geometrical Isomerization of Polyunsaturated Fatty Acids. *J. Am.Oil.Chem.Soc*., v.76, no.1, p.73-81, 1999

HÉNON, G., KEMÉNY, Zs., RECSEG, K., ZWOBADA, F., KOVARI, K. Degradation of α-Linolenic Acid During Heating. *J. Am.Oil.Chem.Soc*., v.74, no.12, p.1615-1617, 1997

INGHAM, J., DUNN, I.J., HEINZLE, E., PRENOSIL, J.E. *Chemical Engineering Dynamics*, Winheim: VCH Publishers, 1994.

JOBACK, K.G., REID, R.C. Estimation of Pure-Component Properties form Group-Contributions*. Chem. Eng. Comm*., v.57, p.233-243, 1987.

JONES, L.A., KING, C.C. Cottonseed Oil. In: HUI, Y.H. *Bailey's Industrial Oil and Fat Products*. 5 ed., v. 2, New York: John Wiley & Sons, p.159-241, 1996.

KARLESKIND, A. In: KARLESKIND, A. *Oils and Fats Manual: a Comprehensive Treatise*, v. 2, Paris: Lavoisier, 1996.

KEMÉNY, Zs., RECSEG, K., HÉNON, G., KOVARI, K., ZWOBADA, F. Deodorization of Vegetable Oils. Prediction of trans Polyunsaturated Fatty Acid Content. *J. Am.Oil.Chem.Soc*., v.78, no.9, p.973-979, 2001

KIKIC, I., ALESSI, P., RASMUSSEN, P., REDENSLUND, A. On the Combinatorial Part of the UNIFAC and UNIQUAC Models, *Can. J. Chem. Eng*.. v.58, p.253-258, 1980

KOJIMA, K., TOCHIGI, K. Prediction of Vapor-Liquid Equilibria by the ASOG Method, Tokio: Elsevier, 1979.

KLÜPPEL, M., SCHULZ, S., ULBIG, P. UNIVAP – A Group-contribution method for prediction of enthalpy of vaporization of pure substances. *Fluid Phase Equilibr.,* v.102, no.1, p.1-15, 1994.

LEBERT, A.; RICHON, D. Study of the Influence of Solute (n-Alcohols and n-Alkanes) Chain Length on their Retention by Purified Olive Oil. *J. Food Sci.,* v.49, p. 1301-1304, 1984.

LONCIN, M. L'Hydrolyze Spontanée des Huiles Glycéridiques et en Particulier de l'Huile de Palme, Couillet: Maison-D'Edition, 1962

LUDWIG, E.E. Applied Process Design for Chemical and Petrochemical Plants, v.2, Houston: GPC, 1995.

MACFARLAND, S.A., SIGMUND, P.M. VAN WINKLE, M. Predict Distillation Efficiency. *Hydrocarbon Proc.,* v.51, p.111-114, 1972.

MAZA, A., ORMSBEE, R.A., STRECKER, L.R. Effects of Deodorization and Steam-Refining Parameters on Finished Oil Quality*. J.Am.Oil.Chem.Soc*., v.69, no.10, p.1003-1008, 1992.

MATTIL, K.F. Deodorization. In: MATTIL, K.F., NORRIS, F.A., STIRTON, A.J. *Bailey's Industrial Oil and Fat Products*. 3 ed., New York: John Wiley & Sons, p. 897-930, 1964.

MICHAEL ESKIN, N.A., MCDONALD, B.E., PRZYBYLSKI, R., MALCOLMSON, L.J., SCARTH, R., MAG. T., WARD, K., ADOLPH, D. Canola Oil. In: HUI, Y.H. *Bailey's Industrial Oil and Fat Products*. 5 ed., v.2, New York: John Wiley & Sons, p.1-95, 1996.

MILLIGAN, E.D., TANDY, D.C. Distillation and Solvent Recovery, *J. Am.Oil.Chem.Soc*. v.51, no.8, p. 347-350, 1974

MORAD, N.A., KAMAL, A.A.M., PANAU, F., YEM, T.W. Liquid specific heat capacity for fatty acids, triacylglycerols, and vegetable oils based on their fatty acids composition*. J. Am.Oil.Chem.Soc.* v.77, no.9, p.1001-1005, 2000.

NAPHTALI, L.M., SANDHOLM, D.P. Multicomponent separation calculations by linearization, *AIChe Journal*., v.17. no.1, p.148-153, 1971.

O'BRIEN, R.D. Fats and Oils: Formulating and Processing for Applications, 2 ed., New York: CRC Press, 2004.

O'BRIEN, R.D. Fats and Oils: Formulating and Processing for Applications. Lancaster: Technomic, 1998.

O'KEEFE, S.F, WILEY, V.A.,WRIGHT, D. Effect of Temperature on Linolenic Acid Loss and 18:3 ∆9-*cis*, ∆12-*cis*, ∆15-*trans* Formation in Soybean Oil. *J.Am.Oil.Chem.Soc*., v.70, no.9, p.915-917, 1993.

ORTHOEFER, F.T. Vegetable Oils. In: HUI, Y.H. *Bailey's Industrial Oil and Fat Products*. 5 ed., v. 1, New York: John Wiley & Sons, p.19-43, 1996.

PETRAUSKAITÈ, V., DE GREYT, W.F., KELLENS, M.J. Physical Refining of Coconut Oil: Effect of Crude Oil Quality and Deodorization Conditions on Neutral Oil Loss. *J.Am.Oil.Chem.Soc*., v.77, no.6, p.581-586, 2000.

POLLARD, E.F., VIX, H.L., GASTROCK, E.A. Solvent Extraction of Cottonseed and Peanut Oils. *Ind. Eng. Chem.,* v.37, no.10, p.1022-1026, 1945.

PRYDE, E.H. Composition of Soybean Oil. In: ERICKSON, D.R., *Practical Handbook of Soybean Processing and Utilization*, Champaign: AOCS Books, p.13-31, 1995.

RAMIREZ, W.F. *Computational Methods for Process Simulation.* 2th ed., Oxford: Butterworth, 1997.

REID, R.C., PRAUSNITZ, J.M., POLING, B.E. *The properties of gases & liquids*, New York: McGraw-Hill, 1987.

ROSSI, M., GIANAZZA, M., ALMPRESE, C., STANGA, F. The Effect of Bleaching and Physical Refining on Color and Minor Components of Palm Oil. *J. Am.Oil.Chem.Soc*., v.78, no.10, p.1051-1055, 2001.

RUIZ-MÉNDEZ, M.V., MÁRQUEZ-RUIZ, G., DOBARGANES, M.C. Comparative Performance of Steam and Nitrogen as Stripping Gas in Physical Refining of Edible Oils. *J. Am.Oil.Chem.Soc*., v.73, no. 12, p.1641-1645, 1996.

SALUNKHE, D.K., CHAVAN, J.K., ADSULE, R.N., KADAM, S.S. World Oilseeds: Chemistry, Technology, and Utilization. New York: Van Nostrand Reinhold, 1992.

SCHWARZ, W. Trans Unsaturated Fatty Acids in European Nutrition. *Eur. J. Lipid Sci. Technol*., v.102, p.633-635, 2000a

SCHWARZ, W. Formation of Trans Polyalkenoic Fatty Acids During Vegetable Oil Refining. *Eur. J. Lipid Sci. Technol*., v.102, p.648-649, 2000b

SINGH, L., RICE, W.K. Method for Producing Wheat Germ Lipid Products, U.S. Patent 4.298.622 (1979).

SIPOS, E.F., SZUHAJ, B.F. Soybean Oil. In: HUI, Y.H. *Bailey's Industrial Oil and Fat Products*. 5 ed., v. 2, New York: John Wiley & Sons, p.497-603, 1996.

SMITH, A.S. Correlation of Vegetable Oil-Hexane Solution Vapor Pressures. *J. Am.Oil.Chem.Soc*., v.28, p.356-359, 1951.

SMITH, A.S., FLORENCE, B. Vapor Pressure of Hexane- Soybean Oil Solution at High Solvent Concentrations, *J. Am.Oil.Chem.Soc*., v.28, p.360-361, 1951.

SMITH, A.S., WECHTER, F.J. Vapor Pressure of Hexane- Soybean Oil Solution at Low Solvent Concentrations. *J. Am.Oil.Chem.Soc*., v.27, p.381-383, 1950.

SWERN, D. Composition and Characteristics of Individual Fats and Oils. In: MATTIL, K.F.; NORRIS, F.A.; STIRTON, A.J. *Bailey's Industrial Oil and Fat Products.* 3 ed., New York: John Wiley & Sons, p.165-247, 1964.

SZABO SARKADI, D. Hydrolysis during Deodorization of Fatty Oils. Catalytic Action of Fatty Acids. *J. Am.Oil.Chem.Soc*., v.36, p.143-145, 1959.

THEME, J.G. Coconut Oil Processing, Rome: FAO 1997, 1968

TORRES, M.B.R. Predição da pressão de vapor e equilíbrio líquido-vapor de ácidos e ésteres graxos usando UNIFAC. Campinas, 1996. 93p. Dissertação de mestrado – FEA UNICAMP.

TORRES, M.B., MEIRELLES, A.J. Prediction of fatty acids and fatty esters vapor pressure and of vapor-liquid equilibrium using UNIFAC. *Engineering and Food at ICEF 7 Supplement*, Academic Press, p.SA35-SA38, 1997.

TU, C.H., LIU, C.P. Group-contribution estimation of the enthalpy of vaporization of organic compounds. *Fluid Phase Equilibr.*, v.121, no. 1-2, p.45-65, 1996.

VERLEYEN, T., VERHE, R., GARCIA, L., DEWETTINCK, K., HUYGHEBAERT, A., DE GREYT, W. Gas Chromatographic characterization of vegetable oil deodorization distillate. *J. of Chromatography A,* v.921, p.277-285, 2001.

WALSH, L., WINTERS, R.L., GONZALEZ, R.G. Optimizing deodorizer distillate tocopherol yields*. Inform*, v.9, no.1, p. 78-83, 1998.

WANG, T., JOHNSON, L.A. Refining High-Free Fatty Acid Wheat Germ Oil. *J.Am.Oil.Chem.Soc*., v.78, no.1, p.71-76, 2001.

WHITE, F.B. Deodorization*. J. Am.Oil.Chem.Soc.*, v.29, no.11, p. 515-526, 1953.

WILLIANS, M.A., HRON, R.J. Obtaining Oils and Fats from Source Materials. In: HUI, Y.H. *Bailey's Industrial Oil and Fat Products*. 5 ed., v. 4, New York: John Wiley & Sons, p.61-157, 1996.

WOERFEL, J.B. Soybean Oil Processing Byproducts and their Utilization. In: ERICKSON, D.R., *Practical Handbook of Soybean Processing and Utilization*, Champaign: AOCS Books, p.306-313, 1995.

WOLFF, R.L. Heat-Induced Geometrical Isomerization of α-Linolenic Acid: Effect of Temperature and Heating Time on the Appearance of Individual Isomers. *J. Am. Oil. Chem. Soc*., v.70, no.4, p.425-430, 1993.

YOUNG, C.T. Peanut Oil. In: HUI, Y.H. *Bailey's Industrial Oil and Fat Products*. 5 ed., v. 2, New York: John Wiley & Sons, p.377-393, 1996.

ZEHNDER, C.T. Deodorization. In: ERICKSON, D.R., *Practical Handbook of Soybean Processing and Utilization*, Champaign: AOCS Books, p.239-257, 1995.

CAPÍTULO 3. PREDICTING VAPOR-LIQUID EQUILIBRIA OF FATTY SYSTEMS

Roberta Ceriani and Antonio J. A. Meirelles

Trabalho publicado na revista **Fluid Phase Equilibria, v. 215, p. 227-236 (2004).**

Key words

Vapor pressure model; UNIFAC; Vapor-liquid equilibria; Fatty mixtures; Oil-hexane mixtures; Deodorization; Physical refining; Edible oils.

Abstract

In the present work a group contribution method is proposed for the estimation of the vapor pressure of fatty compounds. For the major components involved in the vegetable oil industry, such as fatty acids, esters and alcohols, triacylglycerols and partial acylglycerols, the optimized parameters are reported. The method is shown to be accurate when it is used together with the UNIFAC model for estimating vapor-liquid equilibria of binary and multicomponent fatty mixtures comprised in industrial processes such as stripping of hexane, deodorization and physical refining. The results achieved show that the group contribution approach is a valuable tool for the design of distillation and stripping units since it permits to take into account all the complexity of the mixtures involved. This is particularly important for the evaluation of the loss of distillative neutral oil that occurs during the processing of edible oils.

The combination of the vapor pressure model suggested in the present work with the UNIFAC equation gives results similar to those already reported in the literature for fatty acid mixtures and oil-hexane mixtures. However it is a better tool for predicting vapor-liquid equilibria of a large range of fatty systems, also involving unsaturated compounds, fatty esters and acylglycerols, not contemplated by other methodologies. The approach suggested in this work generates more realistic results concerning vapor-liquid equilibria of systems encountered in the edible oil industry.

3.1 Introduction

Equilibrium relationships are of great importance in the edible oil and related compounds industry as a consequence of separation processes such as

fatty acids distillation, fatty alcohols fractionation, physical refining and deodorization of vegetable oils and solvent recovery after extraction [1-5].

Information about vapor-liquid equilibria (VLE) is essential for the design and operation of equipments, especially for processes that usually involve multicomponent mixtures with minor constituents that have to be distilled. The related properties have to be precisely predicted by empirical or theoretical models.

Physical refining and deodorization are processes in the oil industry that intend to strip off odoriferous compounds and fatty acids. Some works in the literature show, however, that the high temperatures applied also generate the vaporization of a fraction with high acylglycerol content, known as neutral oil loss [6-8]. In order to evaluate the volatility of acylglycerols it would be necessary to have a tool to estimate their vapor pressures.

Much work has been done on estimating physicochemical properties [9-11] and phase equilibria [12-18] of fatty mixtures with success. In most approaches the widely known concept of group contributions is used.

In the present work we have developed a new model to estimate the vapor pressure of fatty compounds, such as acids, alcohols, esters, mono-, di- and triacylglycerols, based on the concept of group contributions, and employed this equation for predicting the vapor-liquid equilibria of binary and multicomponent mixtures of these compounds using UNIFAC as a tool to estimate activity coefficients. Four versions of UNIFAC were tested, including different entropic [12, 19, 20] and enthalpic [21] expressions.

Nowadays the design of equipments for vapor-liquid contact is largely based on simulation results obtained using commercial softwares, such as Aspen Plus®, HYSYS® and PRO/II® [22], or using softwares developed by research groups [23, 24]. Even equipments for processing complex multicomponent mixtures, as orange essential oil and orange aqueous essence, can be adequately simulated by them [22]. However the simulation requires an appropriate estimation of the vapor pressures and VLE involved. For this reason, this paper

proposes a procedure for calculating vapor pressures and VLE of fatty mixtures, which could be used to evaluate physical refining and deodorization of vegetable oils.

3.2 Vapor pressure model development

Mixtures involved in separation processes of the edible oil industry are very complex and are formed mainly by triacylglycerols (TAG), free fatty acids (FFA), partial acylglycerols, tocopherols and sterols. Works on the areas of physical refining and deodorization of vegetable oils [6-8] have shown that the volatility of mono-, di- and triacylglycerols is of importance when evaluating their neutral oil loss. For lauric oils as coconut oil, the chain length of the acylglycerol fraction is shorter and this fraction is more volatile than for other oils and its vaporization is even more evident. Verleyen et al. [6] have found that the acylglycerolic portion of deodorizer distillates can vary considerably depending on the oil: 0.72% for corn oil and 13.67% for soybean oils. In the case of soybean oil Ruiz-Mendez et al. [8] have encountered a value of 17.2% for the triacylglycerolic portion of the distillate.

In addition to the lack of experimental data for monoacylglycerols (MAG) and absence for diacylglycerols (DAG), the literature does not provide a feasible tool to estimate the vapor pressure of acylglycerol compounds. This gap has encouraged us to develop a new predictive model for vapor pressures of the whole class of fatty compounds based on the concept of group contributions.

On the development of this idea, it was first necessary to collect a representative data bank for the whole class of fatty compounds, including acids, alcohols, esters, MAG and TAG. The last classes of components are of major interest in analyzing the causes of neutral oil loss in oil industry. Having an equation to predict the vapor pressure of such compounds, it could be stated whether the neutral oil loss occurs just by liquid entrainment in the refining equipment or also by vaporization.

More than 1300 experimental values on vapor pressure were gathered and after a critical elimination of some conflicting data[⊗], we have obtained a data bank of 1220 points, distributed as given in Table 3.2.1. All the experimental data were taken from references 25 to 35. Some papers report an experimental temperature range for each value of vapor pressure. For example, in the case of elaidic acid a vapor pressure of 1330 Pa is reported for the temperature range of 226-228°C [27]. In such cases, we have assumed that each integer value of temperature (for example 226, 227, 228 °C, in the case of elaidic acid) was an equally probable experimental value and all these values were included in the parameter adjustment procedure. This situation occurs only for 11 experimental points, including *trans*-unsaturated fatty acids and triacylglycerols [27, 34].

Table 3.2.1. Experimental vapor pressure data bank of fatty compounds

Class of compounds	Saturated fatty acids	Unsaturated fatty acids	Fatty esters	Fatty alcohols	TAG	MAG	References
Data bank	490	89	344	342	47	6	25-35
Data utilized	443	85	307	332	47	6	25-35

TAG: triacylglycerols; and MAG: monoacylglycerols.

Some analyses of the data bank have shown that special considerations should be done on the development of the model. As discussed above, the data bank for the whole class of acylglycerolic compounds is small and to overcome this limitation it would be necessary to describe MAG and DAG behavior based also on TAG data. On the other hand, isomeric esters have dissimilar boiling points. As an example the isomers metil-laureate and propil-caprate, both with $C_{13}H_{26}O_2$ chemical formulas, have an average difference of 5.9 °C in their boiling points over a large range of pressure data. Differences also occur between the experimental vapor pressure values of conformational isomers (*cis* and *trans*). Literature does provide some data for isomeric unsaturated fatty acids [27, 32] and emphasize the

[⊗] A seleção do banco de dados foi feita com base na observação dos valores experimentais de cada composto plotados na forma ln (P^{vp}) versus ($T^{-1,5}$). Como se trata de dados de diferentes autores, alguns deles muito antigos, constatou-se, em certos casos, conflito expressivo dos valores experimentais medidos. Assim, foram excluídos do banco de dados pontos que se mostraram muito distantes da tendência predominante do conjunto. Vale ressaltar que nenhuma das referências traziam valores de desvio nas medidas experimentais.

presence of isomerization reactions at deodorizing temperatures [36]. The model must have the capacity to differentiate these cases and similar ones.

There are some group contribution methods available that are applicable for estimating the vapor pressure of some fatty compounds. Most of them are based on the Clausius-Clapeyron equation as those proposed by Bokis et al. [11] and Tu [37]. Bokis et al. [11] have shown that the best exponent to correlate the logarithm of the vapor pressure as a function of the inverse temperature is 1.5 instead of one, as traditionally used. Another interesting idea from their work is the inclusion of a "perturbation term" to describe the influence of the compound chain length on its vapor pressure.

Tu [37] has proposed that some molecular structures (double bounds, side chain) and functional groups (-OH, -COOH) may have a significant effect on the vapor pressure and has grouped then in a correction term.

Following these interesting ideas we have developed a model to correlate vapor pressure P_i^{vp} in Pa and temperature T in K of component i expressed as:

$$\ln P_i^{vp} = \sum_k N_k \cdot \left(A_{1k} + \frac{B_{1k}}{T^{1.5}} - C_{1k} \cdot \ln T - D_{1k} \cdot T \right) + \left[M_i \cdot \sum_k N_k \cdot \left(A_{2k} + \frac{B_{2k}}{T^{1.5}} - C_{2k} \cdot \ln T - D_{2k} \cdot T \right) \right] + Q \tag{3.2.1}$$

where N_k is the number of groups k in the molecule, M_i is the component molecular weight that multiplies the "perturbation term", A_{1k}, B_{1k}, C_{1k}, D_{1k}, A_{2k}, B_{2k}, C_{2k} and D_{2k} are parameters obtained from the regression of the experimental data, k represents the groups of component i, Q is a correction term expressed as

$$Q = \xi_1 \cdot q + \xi_2 \tag{3.2.2}$$

where ξ_1 and ξ_2 are related to each class of compounds.

In Equation 3.2.2, q is a function of the temperature, as expressed by

$$q = \alpha + \frac{\beta}{T^{1.5}} - \gamma \cdot \ln(T) - \delta \cdot T \tag{3.2.3}$$

where α, β, γ and δ are optimized parameters obtained by regression of the data bank as a whole.

The effect of functional groups on the vapor pressure is corrected by the term Q according to the total number of carbon atoms N_c in the molecules, as in Equation 3.2.4. ξ_1 is a function of N_c applicable to all compounds and stated as follows:

$$\xi_1 = f_o + N_c \cdot f_1 \tag{3.2.4}$$

where f_o and f_1 are optimized constants.

The term ξ_2 describes the differences between the vapor pressures of isomer esters at the same temperature, and is related to the number of carbons of the substitute fraction (N_{cs}) as follows:

$$\xi_2 = s_o + N_{cs} \cdot s_1 \tag{3.2.5}$$

where s_o and s_1 are optimized constants. Equation 3.2.5 is mainly used to account for the effect of the alcoholic portion of fatty esters. Since they are obtained from the reaction of fatty acids and short chain alcohols (C_1 to C_4) [38], the molecule can be split in two parts; N_{cs} represents the number of carbons of the alcoholic part.

All the fatty compounds found in the separation processes discussed here were split into eight functional groups: CH_3, CH_2, COOH, CH=*cis*, CH=*trans*, COO, OH and CH_2-CH-CH_2. This last group describes the glycerol portion of acylglycerols. The *cis-trans* isomerism is intrinsic to the molecular conformation of the compounds and directly related to the double bond. This is the reason to define two different CH= groups and not include this type of isomerism in the term Q, as was done for isomer esters. It should be noted that each double bond corresponds to two CH= groups.

Table 3.2.2 shows the adjusted values of the parameters cited above.

They were fitted using the Statistical Analysis System (SAS, Cary, NC) package with the regression method suggested by Marquardt [39] with the following objective function:

$$f = \sum_{i=1}^{n} \left[\frac{\left| \ln(P_{exp}^{vp}) - \ln(P_{calc}^{vp}) \right|}{\ln(P_{exp}^{vp})} \right]_i \qquad (3.2.6)$$

where n is the number of experimental data considered, $\ln(P_{exp}^{vp})$ and $\ln(P_{calc}^{vp})$ are, respectively, the logarithm of the experimental and calculated vapor pressures. We have started adjusting A_{1k}, B_{1k}, C_{1k}, D_{1k}, A_{2k}, B_{2k}, C_{2k} and D_{2k} for fatty acids and their groups, followed by the addition of other classes and their representative groups. The Q term was adjusted as a final trial[⊗].

Table 3.2.2. Adjusted parameters for Equations 3.2.1 to 3.2.5

Group	A_{1k}	B_{1k}	C_{1k}	D_{1k}	A_{2k}	B_{2k}	C_{2k}	D_{2k}
CH_3	-117.5	7232.3	-22.7939	0.0361	0.00338	-63.3963	-0.00106	0.000015
CH_2	8.4816	-10987.8	1.4067	-0.00167	-0.00091	6.7157	0.000041	-0.00000126
COOH	8.0734	-20478.3	0.0359	-0.00207	0.00399	-63.9929	-0.00132	0.00001
$CH=_{cis}$	2.4317	1410.3	0.7868	-0.004	0	0	0	0
$CH=_{trans}$	1.843	526.5	0.6584	-0.00368	0	0	0	0
COO	7.116	49152.6	2.337	-0.00848	0.00279	10.0396	-0.00034	0.00000295
OH	28.4723	-16694	3.257	0	0.00485	0	0	0
CH_2-CH-CH_2	688.3	-349293	122.5	-0.1814	-0.00145	0	0	0
Compound	f_o		f_1		s_0		s_1	
Esters	0.2773		-0.00444		-0.4476		0.0751	
Acylglycerols	0		0		0		0	
Fatty acids	0.001		0		0		0	
Alcohols	0.7522		-0.0203		0		0	
q	α		β		γ		δ	
	3.4443		-499.3		0.6136		-0.00517	

3.3 Thermodynamic of fatty mixtures

Fornari et al. [12] have predicted the VLE of vegetable oil-hexane miscellas usually found as a result of the oil extraction step. In their work the miscella was considered as a binary system, since the oil was taken as a pseudo nonvolatile

[⊗] No Apêndice II desta tese estão colocados o banco de dados completo utilizado neste trabalho e um gráfico do resíduo entre os valores experimental e calculado da pressão de vapor de todos os compostos considerados.

component. Considering that hexane is about seven orders of magnitude more volatile than the oil [12] and that the process occurs at moderate temperature and pressure, this assumption is appropriate. However, for the deodorization and physical refining processes, that occur at very high temperature and very low pressures, the glyceridic volatility is considerable, as discussed elsewhere [6-8], and should not be neglected.

Equation 3.3.1 gives a rigorous relation for VLE for every component *i* in a mixture [40], neglecting the variation of the liquid molar volume with the pressure:

$$y_i \cdot P = \gamma_i \cdot x_i \cdot P_i^{vp} \cdot \Im_i \qquad \text{where} \quad \Im_i = \frac{\phi_i^{sat}}{\phi_i} \cdot \exp\left(\frac{V_i^L \cdot \left(P - P_i^{vp}\right)}{R \cdot T}\right) \quad (3.3.1)$$

where $\Im_i$ is the non-ideality factor of the vapor phase, x_i and y_i are the molar fractions of component *i* in the liquid and vapor phases, respectively, P is the total pressure, R is the gas constant, T is the system temperature, P_i^{vp} and ϕ_i^{sat} are, respectively, the vapor pressure and the fugacity coefficient of the pure component, γ_i is the activity coefficient, ϕ_i is the fugacity coefficient and V_i^L is the liquid molar volume of component *i*. The exponential term in Equation 3.3.1 is called the Poynting factor (POY).

On the equation above, the fugacity coefficients can be calculated using the virial equation truncated at the second term in combination with mixing rules. Critical properties and acentric factors of the pure components are needed to calculate second virial coefficients. Well-known estimation methods as Joback's technique for critical volumes and pressures, and Fedor's group contributions for critical temperatures can be used [40]. The V_i^L values for all components can be obtained with the modified Rackett technique [40]. The activity coefficients can be determined using group contribution methods such as the ASOG or UNIFAC models, and the vapor pressure has to be estimated by an empirical equation or a theoretical model.

At low pressures, some simplifications in the VLE relation (Equation 3.3.1) may be applied [40]. The correction factor $\Im_i$ is often set equal to unit and all the non-idealities of the system are assumed to reside only in the liquid phase. In this work, almost all the VLE calculations were done taking the vapor phase as ideal, since the range of pressures prevailing in stripping and distillation units of the vegetable oil industry is usually low, going from vacuum to subatmospherical conditions. However, for oil-hexane miscellas, Fornari et al. [12] have included the fugacity coefficient ϕ_i^{sat} for hexane in their VLE calculations. In fact, if P_i^{vp} is sufficiently high at the equilibrium temperature, as occurs for hexane in the prior mentioned case, ϕ_i^{sat} deviates considerably from unity and is normally used to represent the vapor phase non-idealities. For this reason, in the case of oil-hexane miscellas, the VLE was further predicted in two different forms to account for vapor phase non-idealities. In the first form, Equation 3.3.1 was applied integrally. In the second way, ϕ_i^{sat} has denoted the non-ideal vapor phase. $\Im_i$ and ϕ_i^{sat} were estimated using the methodology described above [40] for all components, including fatty compounds.

In the present work, to account the non-idealities of the liquid phase, four different versions of the UNIFAC model were tested. The activity coefficient for each component *i* is calculated by:

$$\ln\gamma_i = \ln\gamma_i^C + \ln\gamma_i^R \tag{3.3.2}$$

where γ_i^C is the entropic contribution to the non-ideality of the mixture (related to size and shape differences between molecules) and γ_i^R is the residual or energy-related contribution. The combinatorial part is obtained by the following relations:

$$\ln\gamma_i^C = \ln\frac{\tau_i}{x_i} + 1 - \frac{\tau_i}{x_i} - 5\cdot q_i\cdot\left(\ln\frac{\Phi_i}{\theta_i} + 1 - \frac{\Phi_i}{\theta_i}\right) \tag{3.3.3}$$

$$\tau_i = \frac{x_i \cdot r_i^{pi}}{\sum_j x_j \cdot r_j^{pi}} \tag{3.3.4}$$

$$\Phi_i = \frac{x_i \cdot r_i}{\sum_j x_j \cdot r_j} \tag{3.3.5}$$

$$\theta_i = \frac{x_i \cdot q_i}{\sum_j x_j \cdot q_j} \tag{3.3.6}$$

$$r_i = \sum_k \upsilon_k^{(i)} \cdot R_k \tag{3.3.7}$$

$$q_i = \sum_k \upsilon_k^{(i)} \cdot Q_k \tag{3.3.8}$$

where x_i, r_i, q_i, $\upsilon_k^{(i)}$, R_k, Q_k are the molar fraction of component *i*, the volume parameter for molecule *i*, the area parameter for molecule *i*, the number of groups of type *k* in molecule *i*, the volume parameter for group *k*, the area parameter for group *k*, and *pi* is an exponent suggested by Kikic et al. [20].

For the residual term, the equation is:

$$\ln \gamma_i^R = \sum_k \upsilon_k^{(i)} \left(\ln \Gamma_k - \ln \Gamma_k^{(i)} \right) \tag{3.3.9}$$

where Γ_k and $\Gamma_k^{(i)}$ are the group residual activity coefficient and the residual activity coefficient of group *k* in a reference solution containing only molecules of type *i*. The group activity coefficient Γ_k is found from

$$\ln \Gamma_k = Q_k \left[1 - \ln\left(\sum_m \theta_m \psi_{mk} \right) - \sum_m \frac{\theta_m \psi_{km}}{\sum_n \theta_n \psi_{nm}} \right] \tag{3.3.10}$$

which also holds for $\ln \Gamma_k^{(i)}$. In Equation 3.3.10, θ_m is the area fraction of group *m*, and the sums are over all different groups

$$\theta_m = \frac{X_m \cdot Q_m}{\sum_n X_n \cdot Q_n} \tag{3.3.11}$$

where X_m is the mole fraction of group *m* in the mixture. The group interaction parameter ψ_{mn} is given by

$$\Psi_{mn} = \exp\left(-\frac{a_{mn} + b_{mn} \cdot T + c_{mn} \cdot T^2}{T}\right) \tag{3.3.12}$$

where a_{mn}, b_{mn}, c_{mn} and T are, respectively, group interaction parameters and the system temperature, in K. Note that there are six parameters a_{mn}, b_{mn}, c_{mn} for each pair of groups ($a_{mn} \neq a_{nm}$, $b_{mn} \neq b_{nm}$, $c_{mn} \neq c_{nm}$). Table 3.3.1 shows the differences in some parameters of the combinatorial and residual expressions studied in the present case. All the van der Waals group volume R_k and area Q_k parameters, and group interactions parameters were obtained from Fredenslund et al. [19], for UNIFAC original, UNIFAC $r^{2/3}$, UNIFAC $r^{3/4}$, and from Gmehling et al. [21], for UNIFAC Dortmund.

Table 3.3.1. Differences between the versions of UNIFAC used

Source	*pi*	Ψ_{mn}
Fredenslund et al. [19], UNIFAC original	1	$a_{mn} \neq 0$; b_{mn} and $c_{mn} = 0$
Kikic et al. [20], UNIFAC $r^{2/3}$	2/3	$a_{mn} \neq 0$; b_{mn} and $c_{mn} = 0$
Fornari et al. [12], UNIFAC $r^{3/4}$	3/4	$a_{mn} \neq 0$; b_{mn} and $c_{mn} = 0$
Gmehling et al. [21], UNIFAC Dortmund	3/4	a_{mn}, b_{mn} and $c_{mn} \neq 0$

3.4 Results and discussion

After the optimization of the adjusted parameters a sensibility analysis of the vapor pressure model was performed. Even though most of the data was extracted from different and, in some cases, old data banks, our model behaved stable, generating oscillations between one to four percent under application of ± 1°C variations on the experimental temperature values. The final results are presented in Table 3.4.1.

As can be seen, a good representation of the vapor pressure of fatty compounds was achieved. In comparison with some models from the literature [11, 37], the proposed equation guarantees lower deviations as well as allows the vapor pressure prediction of an extended range of compounds.

Table 3.4.1. Average Relative Deviation (ARD) for vapor pressure of fatty compounds

Class of compounds	$ARD = \sum_{i=1}^{n} \frac{1}{n} \cdot \left[100 \cdot \left\lvert P_{exp}^{vp} - P_{cal}^{vp} \right\rvert / P_{exp}^{vp} \right]_i$		
	This work	Bokis et al. [11]	Tu [37]
Saturated fatty acids	4.74	15.07	17.26
Unsaturated fatty acids	18.66	25.68	40.29
cis	21.57	23.68	36.30
trans	13.54	28.03	45.71
Fatty esters	6.40	N.A	47.28
Methyl-	5.04	N.A	44.67
Ethyl-	8.60	N.A	6.25
Propyl-	12.37	N.A	61.55
Butyl-	8.80	N.A	63.70
Fatty alcohols	8.04	9.35	8.73
Triacylglycerols	18.16	N.A	N.A
Monoacylglycerols	9.05	N.A	N.A
Total	6.82	13.96	29.50

N.A = not applicable.

Figure 3.4.1 shows a comparison of the experimental and predicted vapor pressure data for some fatty acids, esters and alcohols, while Figure 3.4.2 shows the agreement achieved for short chain triacylglycerols.

Petrauskaitè et al. [7] have suggested that short chain monoacylglycerols of coconut oil have a volatility similar to that of long chain fatty acids. Figure 3.4.3 shows a comparative plot with predicted and experimental boiling points for two fatty acids (C18-C20) and monoacylglycerols (C10-C14). As can be seen the model confirms the above-mentioned statement.

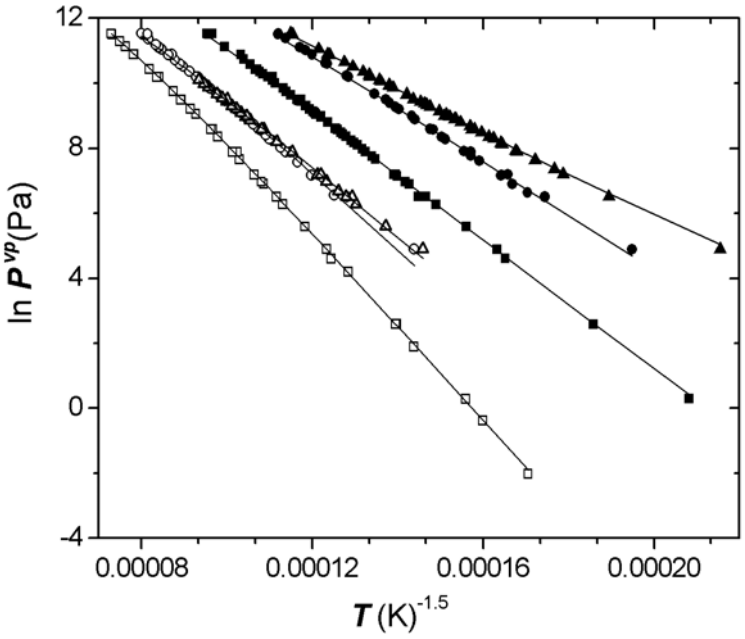

Figure 3.4.1. Comparative vapor pressure of linear fatty compounds. Code for experimental data: caproic acid (■); lauric acid (□); caproic alcohol (●); lauryl alcohol (○); caproic methyl ester (▲), lauryl methyl ester (Δ).

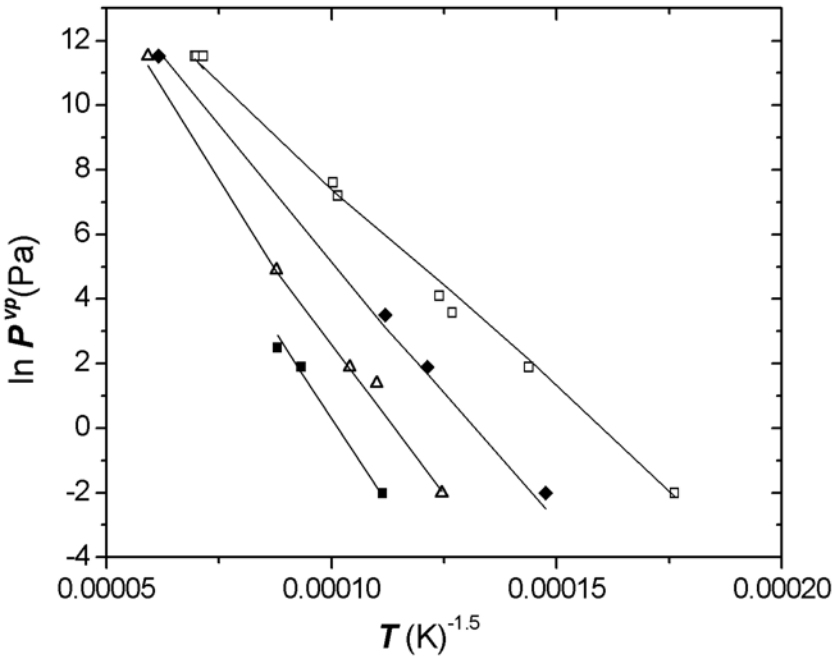

Figure 3.4.2. Experimental and predicted values of short chain triacylglycerols vapor pressure. Code for experimental data: tributirin (□); tricaproin (◆); tricaprilin (Δ) and tricaprin (■).

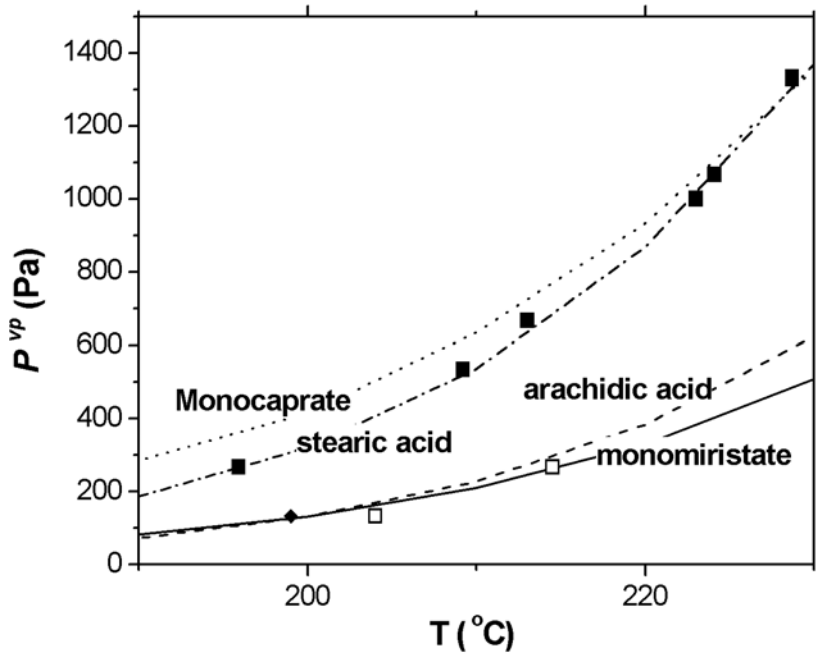

Figure 3.4.3. Comparative vapor pressure of short-chain monoacylglycerols and long-chain fatty acids. Code for experimental data: stearic acid (■); arachidic acid (□) and monomiristate (◆).

There are a few experimental works on VLE of fatty systems, which gather binary mixtures of fatty acids, fatty esters, triacylglycerols and oil/solvent systems [29, 34, 41]. In particular, Goodrum et al. [34] have done experimental measurements of the VLE for binary mixtures of three triacylglycerols (tributirin, tricaproin and tricaprilin) at different temperatures and concentrations.

Some works [12-14] have focused their attention on the prediction of VLE for these mixtures. Ralev and Dobrudjaliev [13] have used ASOG to predict the activity coefficient and an empirical equation (applicable only for saturated fatty acids) to determine the vapor pressure, being able to estimate the VLE of saturated fatty acid binary mixtures. These systems and similar ones were predicted by Torres and Meirelles [14], using UNIFAC, with new adjusted parameters, as the tool to estimate both properties.

In this work, the same systems have their VLE estimated using our proposed vapor pressure model (Equation 3.2.1) and different versions of UNIFAC [12, 19-21], considering the vapor phase as ideal $(\Im_i = 1)$. As can be seen (Table

3.4.2), when compared with other pairs of predictive tools (for activity coefficient and vapor pressure) our methodology have produced results, at least, similar to those reported in the literature. Although the responses are almost independent of the UNIFAC version used, the one proposed by Fredenslund et al. [19] have generated slightly lower deviations.

Table 3.4.2. Calculation of the equilibrium vapor composition (Δy^{abs}(mole%))[a] for fatty acids and fatty esters binary mixtures[b]

Binary Mixture	Ralev & Dobrudjaliev [13] ASOG	Torres & Meirelles [14] UNIFAC	This work UNIFAC version sources			
			Ref.19	Ref 20	Ref.12	Ref.21
C6:0/C8:0	1.14	2.10	1.32	1.40	1.39	1.37
C8:0/C10:0	1.22	1.12	1.26	1.31	1.30	1.30
C10:0/C12:0	1.07	1.22	1.74	1.78	1.77	1.77
C12:0/C14:0	1.21	1.15	1.63	1.65	1.64	1.65
C14:0/C16:0	1.26	0.44	0.86	0.88	0.87	0.88
C16:0/C18:1	--	4.26	1.85	1.84	1.84	1.82
MC6:0/MC8:0	--	1.52	1.34	1.34	1.34	1.35
MC8:0/MC10:0	--	1.10	0.99	1.02	1.01	1.08
MC10:0/MC12:0	--	0.66	0.77	0.77	0.77	0.76
MC12:0/MC14:0	--	2.42	2.41	2.39	2.39	2.35
MC14:0/MC16:0	--	1.79	1.50	1.50	1.50	1.48
MC16:0/MC18:0	--	2.64	2.63	2.63	2.63	2.62
Average deviation	0.97	2.28	2.09	2.12	2.12	2.15

[a] $\Delta y^{abs}(mole\%) = (1/n)\cdot\sum_{j=1}^{n}\left|y(mole\%)_{calc} - y(mole\%)_{\exp}\right|_j$; [b] All the experimental data for fatty esters mixtures were taken from reference 44. For fatty acid mixtures, the references are 29, 42 and 43.

The proposed equation is advantageous compared with Ralev and Dobrudjaliev [13] work due to its capacity of predicting the VLE of unsaturated fatty acids; in relation to the results of Torres and Meirelles [14], our methodology is much better for the only mixture with an unsaturated fatty acid and comparable for fatty esters. It is also capable of predicting with a good precision the VLE of triacylglycerols, whose activity coefficients were close to one (Table 3.4.3). The tributirin (TC4:0)/tricaprilin (TC8:0) mixture has molecules with greater difference

of size and, as a consequence, a more evident non-ideal behavior, which was better predicted by the UNIFAC models.

Table 3.4.3. Average Relative Deviation (ARD) for boiling point of triacylglycerols mixtures ($\Delta T(\%)$)[a]

Mixtures	This work (UNIFAC version sources)				Goodrum et al. [34] $\gamma_i = 1$
	Reference 19	Reference 20	Reference 12	Reference 21	
TC4:0/TC6:0	0.68	0.68	0.68	0.65	0.71
TC6:0/TC8:0	0.62	0.62	0.62	0.59	0.64
TC4:0/TC8:0	1.51	1.58	1.57	2.30	2.01

[a] $\Delta T(\%) = \frac{1}{n} \cdot \sum_{j=1}^{n} \left(\frac{\left| T_{calc} - T_{\exp} \right|}{T_{\exp}} \right)_j$

As a final comparison we have estimated the VLE of miscellas, mixtures of oil/solvent, usually found as a product of solvent oil extraction, to determine the performance of the methodology proposed above.

Pollard et al. [41] have investigated the boiling points of mixtures of crude cottonseed and peanut oils with commercial hexane over a large range of pressures from 160 to 760 mmHg. Cottonseed oil had a FFA-content of 3.5%, expressed as oleic acid, and an iodine value (IV) of 105.5, while peanut oil had a FFA-content of 0.85%, expressed as oleic acid, and an IV of 103.8. With this information and the fatty acid compositions of cottonseed and peanut oils given by Firestone [45], it was possible to estimate the TAG composition for both oils, following the procedure of Antoniosi Filho et al. [46]. The estimated cottonseed oil had an average molecular weight of 849.4 g/gmol and the same FFA-content and IV reported by Pollard et al. [41]. It was composed by 13 FFAs (Table 3.4.4) and 24 TAGs (Table 3.4.5).

Table 3.4.4. Fatty acid composition of cottonseed oil

Fatty acid	Trivial name (abbreviation)	Mass (%)	Mole (%)
C12:0	Lauric (L)	0.20	0.27
C14:0	Miristic (M)	1.00	1.20
C16:0	Palmitic (P)	26.40	28.13
C16:1	Palmitoleic (Po)	1.20	1.29
C18:0	Stearic (S)	2.10	2.02
C18:1	Oleic (O)	18.00	17.41
C18:2	Linoleic (Li)	50.00	48.71
C18:3	Linolenic (Ln)	0.40	0.39
C20:0	Arachidic (A)	0.20	0.17
C20:1	Gadoleic (G)	0.05	0.04
C20:2	Gadolenic (Gn)	0.10	0.09
C22:1	Erucic (E)	0.25	0.20
C22:2	Docosadienoic (D)	0.10	0.08

Table 3.4.5. Estimated composition of cottonseed oil

Group[b]	Major Triacylglycerol	M [a] (g/gmol)	Mass (%)	Mole (%)
46:1	LOP	776	0.09	0.11
48:1	PPoP	804	0.62	0.66
50:1	POP	832	3.67	3.77
52:1	POS	860	0.54	0.54
54:1	POA	888	0.07	0.06
46:2	LLiP	774	0.26	0.29
48:2	MLiP	802	1.16	1.23
50:2	PLiP	830	13.74	14.16
52:2	PLiS	858	3.91	3.90
54:2	PLiA	886	0.39	0.37
48:3	LOLi	800	0.19	0.20
50:3	PPoLi	828	1.93	1.99
52:3	POLi	856	14.30	14.29
54:3	SOLi	884	1.31	1.27
56:3	OLiA	912	0.09	0.09
48:4	LLiLi	798	0.23	0.25
50:4	MLiLi	826	1.11	1.15
52:4	PLiLi	854	26.58	26.62
54:4	SLiLi	882	4.75	4.60
56:4	LiLiA	910	0.17	0.16
52:5	PoLiLi	852	1.30	1.31
54:5	OLiLi	880	10.43	10.14
54:6	LiLiLi	878	12.88	12.56
54:7	LiLiLn	876	0.28	0.28

[a] M, molecular weight (g/gmol). For other abbreviations see Table 3.4.4.

[b] Isomer set including different triacylglycerols, but all with the same number of fatty acid carbons and double bounds. For example, Group 48:1 means the isomer set of triacylglycerols with 48 fatty acid carbons and one double bound.

Note that the oil acidity was composed by all fatty acids shown in Table 3.4.4. The concentration values given in Table 3.4.4 and 3.4.5 correspond to percentages within each considered fatty compound class (TAG and FFA). For peanut oil the average molecular weight was 859.9 g/gmol and it contained 14 FFAs and 35 TAGs. Using the oil compositions it was possible to calculate the VLE for these systems and analyze the effects of different combinatorial [12,19, 20] and residual [21] expressions on the prediction of these VLE. We have also worked with three different hypotheses to describe the vapor phase: (option 1) Equation 3.3.1 was applied integrally, (option 2) ϕ_i^{sat} was used to characterize the vapor non-ideality $\left(\frac{\text{POY}}{\phi_i}=1\right)$ and (option 3) $\Im_i$ was set equal to unity (ideal vapor phase).

Figure 3.4.4 compares the experimental boiling temperatures of commercial hexane-cottonseed oil mixtures [41] at 310 mmHg with the predicted values obtained using different UNIFAC versions (Table 3.3.1) and option 1 for the vapor phase behavior. It is also included the ideal-solution boiling curve, given by Raoult's law. As can be seen, the hexane-oil miscella has a negative deviation of ideality throughout the composition range, i.e. the miscella vapor pressure is lower than would be expected for an ideal mixture (and therefore the boiling point is higher). The results also show that the predictions are not so much affected by the exponent value of Equation 3.3.4, but as suggested by Fornari et al. [12], the exponent *pi* =3/4 gives intermediate values, compared with original UNIFAC and UNIFAC $r^{2/3}$, and such results are closer to the experimental data. The unique curve with positive deviation from Raoult's law was obtained using UNIFAC Dortmund [21], which activity coefficient values for hexane (γ_{hexane}) vary in the range of 1.05 and 1.42. Such behavior was not observed for other UNIFAC versions used in this work. Our results indicate that the use of UNIFAC Dortmund [21] for VLE calculations of vegetable/oil miscellas could lead to a mistaken interpretation of their behavior, i.e., a positive deviation of ideality (lower boiling

point). To be assured of this statement, we have compared these results with the other two hypotheses for vapor phase behavior (options 2 and 3). In both cases, it is possible to confirm that there is no significant qualitative influence in the profiles of the UNIFAC curves shown in Figure 3.4.4.

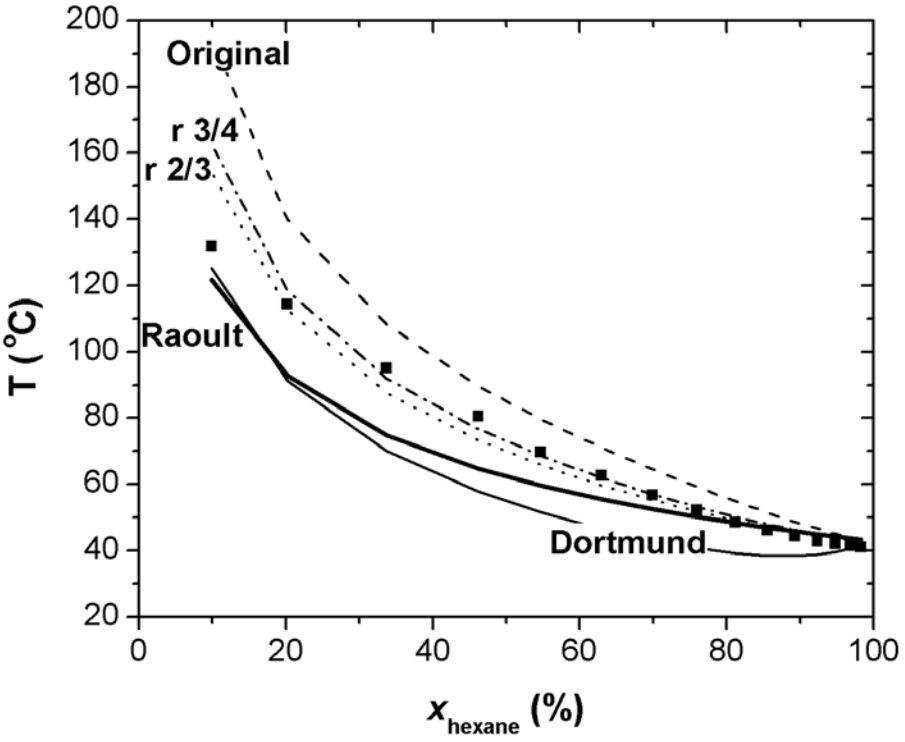

Figure 3.4.4. Comparison between experimental boiling temperatures of commercial hexane-cottonseed oil miscellas and predicted values by different UNIFAC versions at 310 mmHg (option 1 for the vapor phase behavior). Code for experimental data (■).

We have also compared the average relative deviations (ARD) and the absolute errors (T_{calc}–T_{exp},°C) from the prediction of peanut and cottonseed miscellas from 160 to 760 mmHg, using UNIFAC r $^{3/4}$ for the activity coefficient estimations. As shown in Figure 3.4.5, the (T_{calc} –T_{exp},°C) values found were lower than 33.7°C for cottonseed oil miscellas and 30.5°C for peanut oil miscellas, while ARD values were, respectively, 0.91% and 0.98%. Fornari et al. [12] have also reported (T_{calc} –T_{exp},°C) values for the same systems, assuming the oil as a nonvolatile component, and a non-ideal vapor phase composed only by hexane. In their work, the vapor phase non-ideality was described by ϕ_i^{sat} and their maximum

absolute error was 31 °C. Using the three different options already discussed, to describe vapor phase behavior, the ARD values encountered were 0.95% for option 1, 1.06% for option 2 and 1.08% for option 3, indicating that the inclusion of vapor phase non-ideality slightly reduces the observed deviations. Nevertheless, the maximum absolute deviation (T_{calc} –T_{exp},°C) shows the opposite behavior: the maximum (T_{calc} –T_{exp},°C) value was 33.7°C for option 1, 32.0°C for option 2 and 24.0°C for option 3. As indicated in Figure 3.4.5, higher deviations were observed for diluted miscellas (high oil/ low solvent concentrations).

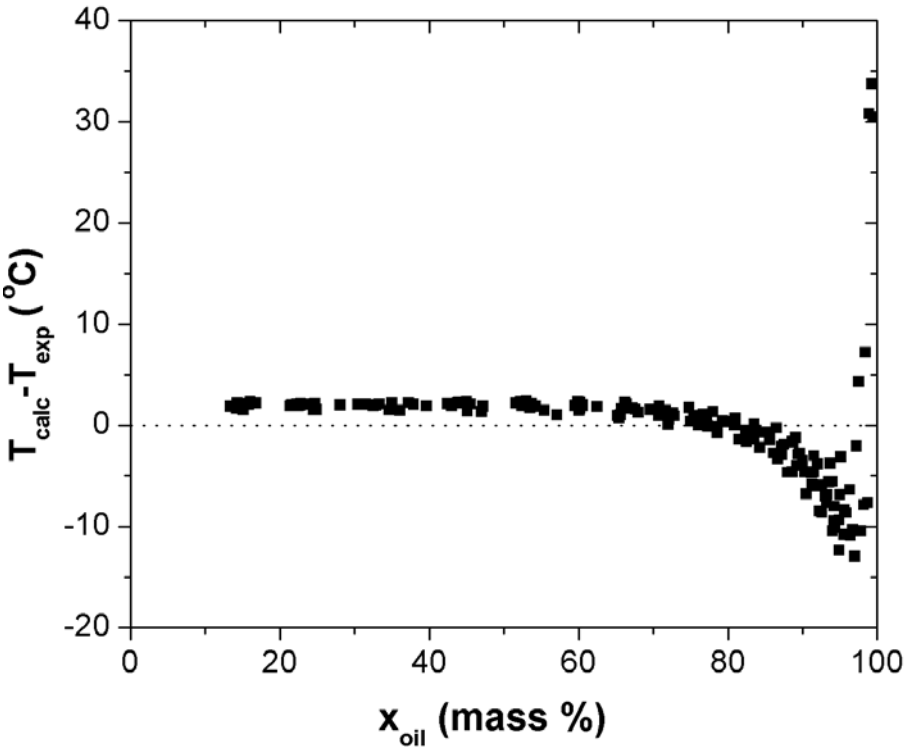

Figure 3.4.5. Absolute errors in the boiling temperatures as predicted by the methodology proposed in this work using UNIFAC $r^{3/4}$ for mixtures of commercial hexane with cottonseed and peanut oils (option 1 for the vapor phase behavior). Code for predicted values (■).

Perhaps the activity coefficients for hexane in this concentration range were poorly predicted by the UNIFAC models, and this behavior is more evident when the vapor phase non-ideality was considered in the prediction. It should also be noted that, for all predictions, the fatty compound concentration in the vapor

phase was negligible and hexane was almost pure in this phase. At the temperature range prevailing in hexane stripping equipment, the fatty compound volatilities have no relevant influence on the VLE prediction, as already observed by Fornari et al. [12].

To further test the methodology proposed in this work, the simulation of a laboratory-scale batch deodorizer [7] of coconut oil was performed to evaluate neutral oil losses, which are composed mainly by partial acylglycerols (MAG and DAG). The batch deodorizer modeling was based in a differential distillation [47] with stripping steam injection after a heating period. In a case study (230 °C, 160 Pa, 0.7% of stripping steam and 3.18% of initial acidity, expressed as percentage of lauric acid), the neutral oil losses calculated for the batch process was 1.26% and the final oil acidity was 0.010%. The experimental value reported by Petrauskaitè et al. [7] was 1.28% for neutral oil loss and 0.019% for final oil acidity. The simulation of further five experiments reported by Petrauskaitè et al. [7] has also generated results similar to the experimental ones. At the temperature conditions prevailing in deodorization and physical refining units, the fatty compound volatilities are significant, requiring its inclusion in the evaluation of such processes.

3.5 Conclusion

We present a group contribution method for the vapor pressure prediction of major fatty compounds encountered in the edible oil industry, as a function of temperature. The simultaneous use of this equation and the UNIFAC models, gives good agreement with experimental data of binary and multicomponent fatty mixtures equilibria. Its major advantage is the prediction of the VLE for unsaturated compounds, fatty esters and acylglycerols, not contemplated by other methodologies. The results reported in the present work have indicated that the methodology suggested can be a valuable tool to deeply investigate common processes of the vegetable oil industry.

List of symbols

ARD	Average Relative Deviation
a_{mn}, b_{mn}, c_{mn}	Group interaction parameters
A_{1k},..., D_{1k}, A_{2k},..., D_{2k}, Q	Constants of Eq. (3.2.1)
DAG	Diacylglycerol
exp	Exponential
$\Im_i$	Non-ideality factor defined by Eq. (3.3.1)
f_o, f_1	Constants of Eq. (3.2.4)
FFA	Free fatty acid
ln	Natural logarithm ($\log_e$)
M_i	Molecular weight of component *i*
MAG	Monoacylglycerol
N_c	Total number of carbon atoms in the molecules
N_{cs}	Number of carbons of the alcoholic part in fatty esters
N_k	Number of groups *k* in the molecule
P	Total pressure in Pa
P_i^{vp}	Vapor pressure of component *i* in Pa
POY	Poynting factor
r_i	Volume parameter for molecule *i*
q_i	Area parameter for molecule *i*
q	Constant of Eq. (3.2.2)
R	Gas constant
R_k, Q_k, Q_m, Q_n	Van der Waals constants for group *k* or *m* or *n*
s_o, s_1	Constants of Eq. (3.2.5)
T	Temperature in K
T	Temperature in ^oC
TAG	Triacylglycerol
VLE	Vapor-liquid equilibria

V_i^L	Liquid molar volume of component *i*
X, x	Liquid molar fraction
y	Vapor molar fraction

Greek Symbols

$\alpha, \beta, \gamma, \delta$	Constants of Eq. (3.2.3)
ϕ_i	Fugacity coefficient of component *i*
γ_i	Activity coefficient of component *i*
$\upsilon_k^{(i)}$	Number of groups *k* in molecule *i*
τ_i, Φ_i	Volume fractions of group *i*
$\theta_i, \theta_m, \theta_n$	Area fraction of group *i* or *m* or *n*
$\Psi_{mk}, \Psi_{km}, \Psi_{nm}$	Group interaction parameters
ξ_1, ξ_2	Constants of Eq. (3.2.2)
$\Gamma_k, \Gamma_k^{(i)}$	Residual activity coefficient for group *k*

Subscripts

calc	Calculated
exp	Experimental
i	Component
k	Group of component *i*
m, n	Group in the mixture

Supercripts

C	Combinatorial
L	Liquid
pi	Exponent of Eq. (3.3.4)
R	Residual
vp	Vapor pressure
(i)	Reference solution containing only molecules of type *i*
sat	Saturation (pure component)

Acknowledgements

The authors wish to acknowledge FAPESP (Fundação de Amparo à Pesquisa do Estado de São Paulo - 01/06798-7) and CNPq (Conselho Nacional de Desenvolvimento Científico e Tecnológico - 46668/00-7 and 521011/95-7) for the financial support.

Appendix: Calculation of vapor pressure of propil-laureate ester at 396.85K.

Propil-laureate ester has the following structure

CH_3-$(CH_2)_{10}$-COO-**$(CH_2)_2$-CH_3**

where the underlined chain comes from the alcohol. Thus according to the group contribution method described above, the group count is:

CH_3	2
CH_2	12
COO	1

N_c = 15; N_{cs} = 3; M_i =242 g/ gmol

From Eq. (3.2.1), using the adjusted parameters from Table 3.2.2.

$\ln P^{vp}$ (Pa)= {[2(-117.5)+12(8.4816)+1(7.116)]+242[2(0.00338)+12(-0.00091)+1(0.00279)]}+ {[2(7232.3)+12(-10987.8)+1(49152.6)]+242[2(-63.3963)+12(6.7157)+1(10.0396)]}/ $T^{1.5}$ - {[2(-22.7939)+12(1.4067)+1(2.337)]+242[2(-0.00106)+12(0.000041)+1(-0.00034)]}ln(T)- {[2(0.0361)+12(-0.00167)+1(-0.00848)]+242[2(0.000015)+12(-0.00000126)+1(2.95E-6)]}T+ (0.2773-0.00444(15))(3.4443-499.3/ $T^{1.5}$-0.6136ln(T)+0.00517T)+(-0.4476+3(0.0751))

P^{vp} (T=396.85K) =261.4 Pa. The experimental value is 267 Pa, corresponding to an error of 2.11%.

References

[1] H. Stage, J. Am. Oil Chem. Soc., 61 (1984) 204-214.

[2] U.R. Kreutzer, J. Am. Oil Chem. Soc., 61 (1984) 343-348.

[3] K.F. Carlson, in Y.H. Hui (Ed.), Bailey's Industrial Oil and Fat Products: Edible Oil and Fat Products Processing Technology, Volume 4, John Wiley and Sons, New York, 1996, pp. 339-391.

[4] R.P. Hutchins, J. Am. Oil Chem. Soc., 33 (1956) 457-462.

[5] D.C. Tandy and W.J. McPherson, J. Am. Oil Chem. Soc., 61 (1984) 1253-1258.

[6] T. Verleyen, R. Verhe, L. Garcia, K. Dewettinck, A. Huyghebaert and W. De Greyt, J. Chromatogr. A, 921 (2001) 277-285.

[7] V. Petrauskaitè, W.F. De Greyt and M.J. Kellens, J. Am. Oil Chem. Soc., 77 (2000) 581-586.

[8] M.V. Ruiz-Mendez, G. Marquez-Ruiz, and M.C. Dobarganes, Grasas y aceites, 40 (1995) 22-25.

[9] J. Rabelo, E. Batista, F.W. Cavalieri and A.J.A. Meirelles, J. Am. Oil Chem. Soc., 77 (2000) 1255-1261.

[10] J.D. Halvorsen, W.C. Mammel and L.D. Clements, J. Am. Oil Chem. Soc., 70 (1993) 875-880.

[11] C.P. Bokis, C.C. Chen and H. Orbey, Fluid Phase Equilib., 155 (1999) 193-203.

[12] T. Fornari, S. Bottini and E. A. Brignole, J. Am. Oil Chem. Soc., 71 (1994) 391-395.

[13] N. Ralev and D. Dobrudjaliev, Fluid Phase Equilib., 65 (1991) 159-165.

[14] M.B. Torres and A.J.A. Meirelles, Proc. 7nd Int. Congr. on Engineering and Food, Brighton, United Kingdom, April 13-14, 1997, Sheffield Academic Press, London, 1997, Supplement, pp. SA 35-SA 38.

[15] E. Batista, S. Monnerat, K. Katio, L. Stragevitch and A.J.A. Meirelles, J. Chem. Eng. Data, 44 (1999) 1360-1364.

[16] E. Batista, S. Monnerat, L. Stragevitch, C.G. Pina, C.B. Gonçalves and A.J.A. Meirelles, J. Chem. Eng. Data, 44 (1999) 1365-1369.

[17] C.B. Gonçalves, E. Batista and A.J.A. Meirelles, J. Chem. Eng. Data, 47 (2002) 416-420.

[18] C.E. Rodrigues, R. Antoniassi and A.J.A. Meirelles, J. Chem. Eng. Data, 48 (2003) 367-373.

[19] A. Fredenslund, J. Gmehling and P. Rasmussen, Vapor-liquid equilibria using UNIFAC, Elsevier, Amsterdan, 1977.

[20] I. Kikic, P. Alessi, P. Rasmussen and A. Fredenslund, Can. J. Chem. Eng., 58 (1980) 253-258.

[21] J. Gmehling, J. Li and M. Schiller, Ind. Eng. Chem. Res., 32 (1993) 178-193.

[22] E. Haypek, L.H.M. Silva, E. Batista, D.S. Marques, M.A.A. Meireles and A.J.A. Meirelles, Braz. J. Chem. Eng. 17 (2000) 705-712.

[23] E. Batista and A.J.A. Meirelles, J. Chem. Eng. Jpn. 30 (1997) 45-51.

[24] E. Batista, R. Antoniassi, M.R.W. Maciel and A.J.A. Meirelles, Proc. Int. Solvent Extraction Conference, Johannesburg, South Africa, March 17-21, 2002, Chris van Rensburg Publications, Johannesburg, 2002, pp. 638-643.

[25] D. Ambrose, J.H. Ellender, H.A. Gundry, D.A. Lee and R. Townsend, J. Chem. Thermodyn., 13 (1981) 795-802.

[26] T. Boublík, in T. Boublík, V. Fried and E. Hála (Eds.), The Vapour Pressure of Pure Substances: Selected Values of the Temperature Dependence of the Vapour Pressures of Some Pure Substances, Elsevier, Amsterdan, 1984.

[27] R. Brockmann, G. Demmering, and U. Kreutzer, in L. Kaudy, J.F. Rounsaville and A. Schulz (Eds.), Ullmann's Encyclopedia of Industrial Chemistry, Verlag Chemie, Weinheim, 1987, pp. 245-275.

[28] D.R. Lide (Ed.), CRC Handbook of Chemistry and Physics, 79th ed., CRC Press, Boca Raton, 1998.

[29] E. Müller and H. Stage, Experimental Measurement of Vapor-liquid Equilibria of Fatty Acids (in German, Experimentelle Vermessung von Dampf-Flüssigkeits-Phasengleichgewichten Dargestellt am Beispiel des Siedeverhaltens von Fettsäuren), Springer-Verlag, Berlin, 1961

[30] W.O. Pool and A.W. Ralston, Ind. Eng. Chem., 34 (1942) 1104-1105.

[31] A. Rose, J.A. Acciari, R.C. Johnson and W.W. Sanders, Ind. Eng. Chem., 49 (1957) 104-109.

[32] D.R. Stull, Ind. Eng. Chem., 39 (1947) 517-535.

[33] Unichema International, Fatty Acid Data Book, Emmerich, 1987.

[34] J.W. Goodrum, D.P. Geller and S.A. Lee, Thermochim. Acta, 311 (1998) 71-79.

[35] D. Swern, in K.F. Mattil, F.A. Norris and A.J. Stirton, Bailey's Industrial Oil and Fat Products, John Wiley & Sons, New York, 1964, pp. 97-144.

[36] W. Schwarz, Eur. J. Lipid Sci. Tech., 102 (2000) 648-649.

[37] C.H. Tu, Fluid Phase Equilib., 121 (1996) 45-65.

[38] K. Noweck and H. Ridder, in L. Kaudy, J.F. Rounsaville and A. Schulz (Eds.), Ullmann's Encyclopedia of Industrial Chemistry, Verlag Chemie, Weinheim, 1987, pp. 277-297.

[39] D.W. Marquardt, J. Soc. Ind. Appl. Math, 11 (1963) 431-436.

[40] R. C. Reid, J.M. Prausnitz and B.E. Poling, The Properties of Gases and Liquids, fourth Ed., McGraw-Hill, New York, 1987.

[41] E.F. Pollard, H.L. Vix and E.A. Gastrock, Ind. Eng. Chem., 37 (1945) 1022-1026.

[42] J. Gmehling and U. Onken, Vapor-Liquid Equilibrium Data Collection, Dechema, Frankfurt, 1977.

[43] J. Hollo and T Lengyel, Fette, Seifen, Anstrichm., 62 (1960) 913.

[44] A. Rose and W. R. Supina, J. Chem. Eng. Data, 6 (1961) 173-179.

[45] D. Firestone, Physical and Chemical Characteristics of Oils, Fats and Waxes, AOCS Press, Champaign, 1999.

[46] N.R. Antoniosi Filho, O.L. Mendes and F.M. Lanças, J. Chromatogr., 40 (1995) 557-562.

[47] J. Ingham, I.J. Dunn, E. Heinzle and J.E. Prenosil, in J. Inghan (Ed.), Chemical Engineering Dynamic: Modeling with PC Simulation, VCH Publishers, Weinheim, 1995, pp. 589-593.

CAPÍTULO 4. SIMULATION OF BATCH PHYSICAL REFINING AND DEODORIZATION PROCESSES

Roberta Ceriani and Antonio J. A. Meirelles

Trabalho publicado na revista **The Journal of the American Oil Chemists Society, v. 81(3), p. 305-312 (2004).**

Key words

Coconut oil, deodorization, differential distillation, edible oils, neutral oil loss, physical refining and vapor-liquid equilibria.

Abstract

This work presents an application of a differential distillation model for the simulation of batch physical refining and/or deodorization processes in the vegetable oil industry. The vapor-liquid equilibria of these fat systems are described by group contribution equations for vapor pressures and activity coefficients. The full complexity of the oil, expressed as its total composition of TAG, DAG, MAG, and FFA, is considered within the simulation. This approach permitted us to quantify and characterize distillative neutral oil losses during physical refining. Three different models of differential distillation were tested to develop a good representation of the batch process to be applied to the physical refining and/or deodorization of complex mixtures such as vegetable oils. To evaluate the recommended approach, a case study was performed, namely, a batch deodorizer was simulated for coconut oil refining, and the results were compared with those reported in the literature.

4.1 Introduction

The physical refining and deodorization are processes of the oil industry that are intended to vaporize odoriferous compounds and fatty acids (FA) from the oil. They are based on the large difference in volatility between the oil and the majority of its unwanted substances, and are accomplished by applying high temperatures and low pressures. However, some works in the literature have shown that these conditions also allow the vaporization of an acylglycerol fraction from the oil, known as neutral oil loss NOL (1-3). Ordinarily, NOL can be divided in two types: (i) a distillative loss and (ii) a loss due to mechanical carry-over (or entrainment), which is usually low, 0.1% approximately (2, 4).

The experimental work of Petrauskaitè *et al.* (2) has quantified NOL during the physical refining of coconut oil and confirmed that the distillation of volatile acylglycerolic components (mainly monoacylglycerols and diacylglycerols) is its major cause. Petrauskaitè *et al.* (2) have also highlighted the similarity between the volatilities of long-chain FA and short-chain monoacylglycerols (MAG), indicating the reason for the occurrence of distillative neutral oil loss in their study.

Coconut oil is classified as a lauric oil, characterized by a high level of short-chain and saturated FA (5). Its high free fatty acid (FFA) content (between 1 and 6%) denotes the presence of a considerable amount of MAG and diacylglycerols (DAG) (2). For oils with high acidity, the physical refining method is highly recommended, because it reduces NOL (6).

This work presents an application of a differential distillation model for the simulation of batch physical refining and/or deodorization processes for vegetable oils. The vapor-liquid equilibria (VLE) of these fat systems are described by group contribution equations for vapor pressures (7) and activity coefficients (7, 8) published elsewhere. The full complexity of the oil, expressed at its total composition in TAG, DAG, MAG and FFA, is considered within the simulation in order to quantify and characterize NOL during physical refining. Chemical reactions, vaporization efficiencies and entrainment are not considered.

Nowadays, simulation results are largely used to design of equipments for vapor-liquid contact. Commercial software, such as Aspen Plus®, HYSYS® and PRO/II® (9), or software developed by research groups (10, 11) is usually used, even for complex multicomponent mixtures, as orange essential oil and orange aqueous essence (9). The procedure proposed by Ceriani and Meirelles (7) for calculating vapor pressures and VLE of multicomponent fatty mixtures allows the simulation of different processes within the vegetable oil industry. In the present work this procedure is used to simulate a batch deodorizer for coconut oil refining.

4.2 Modeling a batch deodorizer

To quantify NOL during physical refining, Petrauskaitè et al. (2) performed experiments in a laboratory-scale batch deodorizer initially containing 250 g of bleached coconut oil. The experiments were conducted for 60 min under temperatures and pressures between 190 and 230 °C and 1.6 to 3.0 mbar, respectively, and with the addition of 0.6 to 1.2% of sparge steam. Their results showed that partial acylglycerols (MAG and DAG) were the major cause of NOL in lauric oils.

To simulate the experiments carried out by Petrauskaitè et al. (2), the vapor pressure equation and the thermodynamic approach suggested by Ceriani and Meirelles (7) were applied to predict the VLE of the fatty compounds involved in these experiments. The VLE model is described below (7)

$$y_i \cdot P = \gamma_i \cdot x_i \cdot P_i^{vp} \cdot \Im_i \qquad [4.2.1]$$

$$\Im_i = \frac{\phi_i^{sat}}{\phi_i} \cdot \exp\left(\frac{V_i^L \cdot \left(P - P_i^{vp}\right)}{R \cdot T}\right) \qquad [4.2.2]$$

where $\Im_i$ is the nonideality factor of the vapor phase, x_i and y_i are the molar fractions of component *i* in the liquid and vapor phases, respectively, P is the total pressure, R is the gas constant, T is the system temperature, P_i^{vp} and ϕ_i^{sat} are, respectively, the vapor pressure and the fugacity coefficient of the pure component, γ_i is the activity coefficient, ϕ_i is the fugacity coefficient and V_i^L is the liquid molar volume of component *i*. The exponential term in Equation 4.2.2 is called the Poynting factor (POY).

Because of the high temperatures used in deodorizing units, the vapor pressures of some components, such as water and short-chain FA (6:0 to 12:0) are high enough to generate ϕ_i^{sat} values notably different from unity. For this reason, and despite the low pressures prevailing in such units, Equations 4.2.1 and 4.2.2 are more suitable to describe the VLE observed in this kind of process (7).

In a multicomponent differential distillation process, a tank (still) is charged with feed and then heated. Vapor flows overhead, is condensed, and is collected in a receiver. Since the still composition is changing continuously, this process is inherently dynamic, i.e., it cannot be modeled in steady state. The composition of the material collected in the receiver also varies with time, so the composition of the distillate is an average of all the material collected. It is possible to look at the differential distillation as a sequence of numerous and successive vaporizations.

Batch deodorization is similar to multicomponent differential distillation, for which the total and component balances are given by Equation 4.2.3 and 4.2.4 (12):

$$\frac{dL}{dt} = -v \qquad [4.2.3]$$

$$\frac{d(L \cdot x_i)}{dt} = -v \cdot y_i \qquad [4.2.4]$$

where L is the total moles of liquid in the still, v is the molar vaporization rate in moles/time, and x_i and y_i are the liquid and vapor mole fractions of component i in the liquid and vapor phases, respectively.

Assuming that the liquid and vapor phases are in equilibrium at each instant, i.e., that the still acts as a theoretical stage, the equilibrium relationship can be stated as Equations 4.2.1 and 4.2.2. This assumption considers a vaporization efficiency factor equal to unity, which means that the steam becomes totally saturated with the volatiles as it passes through the oil in the still.

For the receiver distillate tank, the total and component balances are (12):

$$\frac{dD}{dt} = v \qquad [4.2.5]$$

$$\frac{dD_i}{dt} = v \cdot y_i \qquad [4.2.6]$$

where D is the total moles of distillate and D_i corresponds to the moles of component i in the tank.

Combining Equations 4.2.3-4.2.6 with the equilibrium relationship (Eqs. 4.2.1 and 4.2.2) we have a system that is easily solvable by direct integration (12).

Three different alternatives for simulating a batch deodorization (differential distillation) were considered in this work. The simplest one, named Model 1, does not take into account the injection of sparge steam. In this case, the boiling temperature at each instant should be determined by solving Equation 4.2.7 (objective function) below: The sum of the partial pressures of the fatty compounds must be equal to the system total pressure.

$$f = P - \sum_{i=1}^{n} \left[\gamma_i \cdot x_i \cdot P_i^{vp} \cdot \Im_i \right] \qquad [4.2.7]$$

where n is the total number of fatty compounds.

Model 2 considers the injection of sparge steam, but it assumes that the steam is an inert component that only decreases the system total pressure by its partial pressure in the vapor phase. In this case, steam (water) is believed to be totally immiscible with the oil, and the sum of the fatty component partial pressures $\sum_{i=1}^{n} P_i$ should be equal to the total pressure less the sparge steam partial pressure P_w. The objective function, f, was appropriately changed, as shown in Equation 4.2.8:

$$f = P - \sum_{i=1}^{n} \left[\gamma_i \cdot x_i \cdot P_i^{vp} \cdot \Im_i \right] \cdot \left[1 + \frac{\dot{m}_w \left({}^{g}/_{s} \right)}{\dot{m}_{vol} \left({}^{g}/_{s} \right)} \cdot \frac{\sum_{i=1}^{n} y_i \cdot M_i}{18} \right] \qquad [4.2.8]$$

where n is the total number of fatty compounds, $\dot{m}_w$ and $\dot{m}_{vol}$ are, respectively, the mass rate of water and volatile fatty compounds in the vapor phase in grams per second (g/s), M_i is the molar weight of each fatty component i, y_i is its molar fraction in the vapor phase, the number 18 refers to the molar

weight (m.w.) of water (g/gmol), and $\dot{m}_w(g/s)/\dot{m}_{vol}(g/s)$ gives the ratio of sparge steam to vaporized fatty components used in the batch deodorizer.

Model 3 takes into account the effect of steam upon the liquid (oil) phase. In fact, one should consider that very small amounts of steam (water), which condense and dissolve in the oil, are able to enhance the volatility of the fatty compounds and decrease the necessary boiling temperature. As such, the simulation performed was similar to the operation of an industrial batch deodorizer. Anderson (13) indicates that in a batch deodorizer, the oil is first slowly heated under vacuum conditions until the desired temperature is reached; when this temperature is attained, the injection of sparge steam begins and the process is performed until the required oil acidity (OA) is obtained. For this reason the process simulation was divided in two parts: (i) *heating* (in absence of water) and (ii) *stripping* with sparge steam at constant temperature, which was allowed by the presence of water in the liquid phase. The simulation of the first part (heating) was conducted as in Model 1, in which the boiling temperature determined by Equation 4.2.7. When the desired temperature was achieved (the start of stripping), water was included as the (n+1)th component in the liquid phase. Equation 4.2.9 below was then solved to determine the water concentration in the liquid at the chosen temperature and pressure conditions:

$$f = P - \sum_{i=1}^{n+1}\left[\gamma_i \cdot x_i \cdot P_i^{vp} \cdot \Im_i\right] \qquad [4.2.9]$$

All the models just depicted above use an iterative procedure for convergence, as Newton-Raphson model (14). P_i^{vp}, γ_i and $\Im_i$ are calculated for each component, including water when suitable, in every iteration.

Model 3 is probably the alternative that better simulates the experiments conducted by Petrauskaitè *et al.* (2). But one should observe that the authors (2) reported only the system pressure, the oil initial load and final acidity, the amount and temperature of sparge steam, and the amount and acidity of the distillate; but the still (oil) temperature was apparently not measured. The temperature reported

in the work is the oven temperature, so the oil temperature during the experiments should probably be a little bit lower than that value to allow heat transfer. As a consequence of the lack of information concerning the oil temperature, the value chosen for the second part of Model 3 simulation was the available oven temperature less 5 °C. This difference was justified by supposing that heat transfer occurred throughout the 60 min of each experiment.

The simulation results were appropriately transformed to mass fraction unities and expressed as percentage of NOL, OA and distillate acidity (DA). Such results were compared with those reported by Petrauskaitè *et al.* (2).

4.3 Results and discussion

Models 1 to 3 were used to simulate the batch deodorization experiments conducted by Petrauskaitè *et al.* (2). All the property calculations were performed using the procedure of Ceriani and Meirelles (7), with γ_i calculated with UNIFAC r¾, as suggested by Fornari *et al*. (15). The same FA composition (Table 4.3.1) and acidity (3.18%, expressed as percentage of lauric acid) reported by Petrauskaitè *et al.* (2) were used. Since Petrauskaitè *et al.* (2) did not give the partial acylglycerol composition of their samples, three different magnitudes were considered for the simulation: (i) composition 1 (OC1), with 3% mass concentration of DAG and 1% of MAG (16), (ii) composition 2 (OC2), with 0.89% mass concentration of DAG and 0.27% of MAG, and (iii) composition 3 (OC3) with no partial acylglycerols (no DAG and MAG). From the data in Table 4.3.1, the composition in TAG of the coconut oil (*M*, molecular weight of 601.0 g/gmol and 9.31 of iodine value) was estimated using the procedure of Antoniosi Filho *et al.* (17), considering 84% of TAG as trisaturated (18). The estimated TAG composition is shown in Table 4.3.2. Even though the partial acylglycerol composition was obtained intuitively[⊗] from the estimated TAG composition (see Table 4.3.2), it is in accordance with Petrauskaitè *et al.* (2) observation about the MAG composition of

[⊗] A composição em DAG e MAG foi obtida seguindo a estequiometria da reação de hidrólise . Desta forma, cada TAG gerou 1,2 e 1,3 DAG; cada DAG gerou MAG.

coconut oil (up to 50% of short-chain-length, ranging from C_6 to C_{12}). As a whole, the coconut oil was divided into 72 components, i.e., 9 FA (Table 4.3.1), 36 TAG (Table 4.3.2), and 27 partial acylglycerols (Table 4.3.2). Note that the OA was composed of all FA shown in Table 4.3.1. The MAG and DAG considered are listed in Table 4.3.2. The concentration given in Tables 4.3.1 and 4.3.2 add to 100% within each fatty compound class. To calculate the total oil compositions, all three different partial acylglycerol levels should be taken into account.

Table 4.3.1. FA composition of coconut oils

FA	Trivial name (abbreviation)	Petrauskaitè *et al* (2) [a]		Firestone (20)			
				More Volatile		Less Volatile	
		Mass (%)	Mole (%)	Mass (%)	Mole (%)	Mass (%)	Mole (%)
C6:0	Caproic (Co)	0.60	1.07	0.60	1.04		
C8:0	Caprilic (Cp)	7.29	10.49	9.40	13.17	4.6	6.84
C10:0	Capric (C)	5.89	7.10	7.80	9.15	5.5	6.84
C12:0	Lauric (L)	46.55	48.24	49.20	49.63	45.1	48.25
C14:0	Miristic (M)	18.58	16.89	16.80	14.87	18.5	17.36
C16:0	Palmitic (P)	9.49	7.68	7.70	6.07	10.2	8.53
C18:0	Stearic (S)	2.70	1.97	2.30	1.63	3.5	2.64
C18:1	Oleic (O)	7.00	5.15	5.40	3.86	9.9	7.51
C18:2	Linoleic (Li)	1.90	1.41	0.80	0.58	2.1	1.6
C18:3	Linolenic (Ln)					0.2	0.15
C20:0	Arachidic (A)					0.2	0.14
C20:1	Gadoleic (G)					0.2	0.14

[a] FA compositions for oil compositions OC1,OC2 and OC3.

Using the simulation tools developed in the present work, we simulated the first six experiments reported by Petrauskaitè *et al.* (2). A total of 54 simulations were performed, corresponding to the three different models (Models 1, 2 and 3) and to the three different partial acylglycerol levels in the bleached coconut oil (OC1, OC2 and OC3).

Table 4.3.2. Estimated composition of coconut oil

		TAG				DAG		
Group[a]	Major TAG	M[b] (g/gmol)	Mass (%)	Mole (%)	Acylglycerol compound	M[b] (g/gmol)	Mass (%)	Mole (%)
24:0	CpCpCp	470	0.13	0.18	CoCp-	316	0.23	0.33
26:0	CoCpL	498	0.43	0.57	CpCp-	344	1.15	1.53
28:0	CpCpL	526	1.64	2.05	CpC-	372	1.91	2.36
30:0	CpCL	554	2.99	3.57	CpL-	400	16.11	18.49
32:0	CpLL	582	8.36	9.49	CL-	428	1.2	1.29
34:0	CpLM	610	10.09	10.93	LL-	456	38.61	38.86
36:0	LLL	638	17.39	18.02	LM-	484	16.62	15.76
38:0	LLM	666	15.34	15.23	LP-	512	12.64	11.33
40:0	LLP	694	11.22	10.69	LS-	540	2.29	1.95
42:0	LMP	722	6.41	5.87	MS-	568	0.33	0.26
44:0	LMS	750	2.84	2.50	CpO-	482	1.52	1.44
46:0	LPS	778	1.05	0.89	CO-	510	1.15	1.03
48:0	MPS	806	0.30	0.25	LO-	538	4.01	3.43
50:0	PPS	834	0.07	0.05	MO-	566	1.05	0.85
34:1	CpCpO	608	0.20	0.21	CpLi-	452	0.35	0.36
36:1	CpCO	636	0.41	0.43	CLi-	508	0.28	0.26
38:1	CpLO	664	1.89	1.88	LLi-	536	0.49	0.42
40:1	CLO	692	1.89	1.80	MLi-	564	0.06	0.05
42:1	LLO	720	5.09	4.67		MAG		
44:1	LMO	748	3.44	3.04	Co--	190	0.11	0.16
46:1	LPO	776	2.11	1.80	Cp--	218	10.30	13.02
48:1	MPO	804	0.93	0.77	C--	246	2.20	2.47
50:1	MSO	832	0.27	0.21	L--	274	64.83	65.19
52:1	PSO	860	0.07	0.05	M--	302	9.27	8.46
34:2	CpLiCp	606	0.05	0.05	P--	330	6.79	5.67
36:2	CpCLi	634	0.10	0.11	S--	358	1.44	1.11
38:2	CpLiL	662	0.46	0.46	O--	356	4.36	3.38
40:2	CLiL	690	0.46	0.45	Li--	354	0.70	0.54
42:2	LLLi	718	1.26	1.16				
44:2	LMLi	746	0.96	0.85				
46:2	LPLi	774	0.60	0.51				
48:2	LOO	802	0.79	0.65				
50:2	MOO	830	0.27	0.21				
52:2	POO	858	0.11	0.09				
48:3	LOLi	800	0.28	0.23				
50:3	MOLi	828	0.10	0.08				

[a] Isomer set including different TAG, but all with the same number of FA carbons and double bounds. For example, Group 26:0 means the isomer set of TAG with 26 FA carbons and none double bound. For other abbreviations see Table 4.3.1.
[b] M, molecular weight (g/gmol).

An important concept used to quantify the facility of the compounds in a mixture to be distillated under certain conditions is the relative volatility $(\alpha_{i,j})$,

which relates the distribution coefficient, *k,* of one compound or one class of compounds with another less-volatile compound or class of compounds. In our simulations this parameter gives an idea about the range of volatilities of each class of compounds (FFA, MAG, DAG, TAG) considered in relation to the volatility of TAG. It is defined by Equation 4.3.1 as given below:

$$\alpha_{i,TAG} = \frac{(y/x)_i}{(y/x)_{TAG}} \qquad [4.3.1]$$

where *i* refers to TAG, DAG, MAG or FFA classes.

Figure 4.3.1 gives the relative volatility $(\alpha_{i,TAG})$ of the FFA, MAG and DAG classes for coconut oil (OC2) at 300 Pa. Note that the $(\alpha_{i,TAG})$ values are inversely proportional to the m.w. of the compound class. The results show that even with a considerable difference between the volatility of FFA and partial acylglycerols, the loss of neutral oil can increase considerably, mainly when the amount of FFA in the still is close to the desired final acidity (in the last 20 min, approximately).

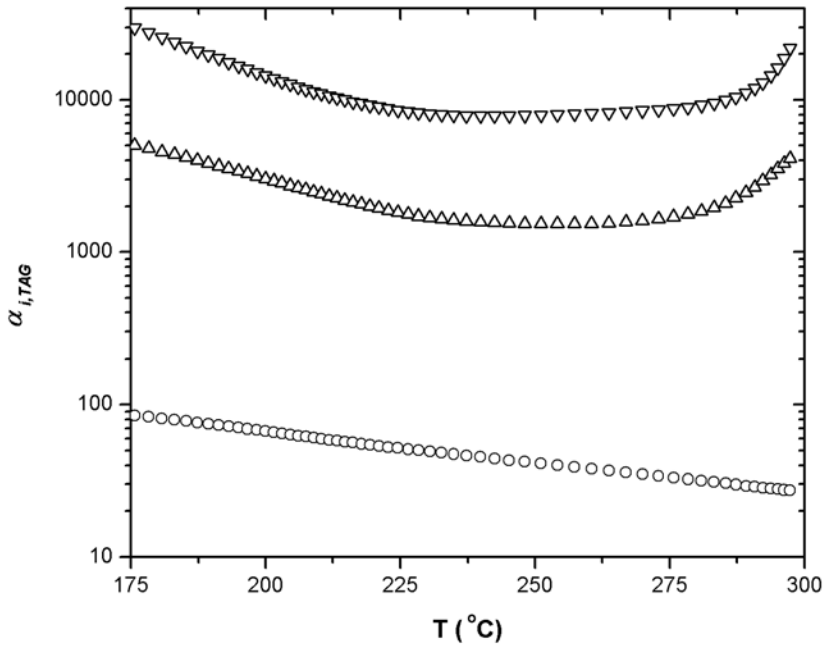

Figure 4.3.1. Relative volatility $(\alpha_{i,TAG})$ of the FFA, MAG and DAG classes for coconut oil (OC2) calculated during Experiment 6 simulation (Model 1). Code: FFA (∇); MAG (∆) and DAG (○). OC2 oil composition.

Table 4.3.3 shows a comparison of NOL as calculated by Petrauskaitè *et al*. (2) and in this work using Model 3 to illustrate that the oil composition used in their experiments might have a value between OC1 and OC3. Although there is some uncertainty in the partial acylglycerol concentration, its precise value should be not far from our estimations. Our results show that as MAG and DAG concentrations increase (from OC3 to OC1), the NOL also becomes higher, independent of the process conditions selected.

The NOL calculated using Model 3 for OC3, a coconut oil without any partial acylglycerol, is always lower than the experimental results. A possible explanation is that the similar volatility of short-chain MAG and long-chain FA can play no role in this case. Once the crude oil has a larger partial acylglycerol fraction, a portion of these components is evaporated instead of FFA, decreasing the FFA content in the distillate, and increasing NOL values.

Table 4.3.3. Comparison of calculated neutral oil loss and refined oil acidity by Petrauskaitè et al. (2) and this work using Model 3 as the simulation tool [a,b]

	Refined Oil Acidity (%)							Neutral Oil Loss (%)			
Exp. no.	P (Pa)	T (°C)	% steam	Petrauskaitè et al. (2)	This work Oil compositions			Petrauskaitè et al. (2)	This work Oil compositions		
					OC1	OC2	OC3		OC1	OC2	OC3
1	160	190	0.6	0.240	0.670	0.364	0.170	0.28	0.59	0.30	0.10
2	160	210	0.8	0.070	0.466	0.161	0.030	0.57	0.76	0.47	0.34
3	160	230	0.7	0.019	0.165	0.008	0.001	1.28	1.29	1.15	1.13
4	230	230	0.6	0.033	0.266	0.036	0.003	1.21	1.06	0.85	0.81
5	230	230	0.6	0.035	0.295	0.051	0.001	0.89	1.01	0.78	0.73
6	300	230	1.2	0.017	0.280	0.043	0.004	0.93	1.04	0.82	0.77

[a] All simulations have a 60 min period of time
[b] The experiment numbers correspond exactly to those reported by Petrauskaitè et al. (2).

The literature establishes that the FFA content cannot be reduced indefinitely but reaches a minimum value of 0.005% due to hydrolysis of the oil caused by the steam (4). The final OA calculated using Model 3 for OC3 (see Table 4.3.3) was lower than this limit for the last four experiments (Experiments 3 to 6), whereas the experimental values from Petrauskaitè *et al*. (2) were consistently higher. In fact, our simulations did not consider reactions that might occur during

vegetable oil deodorization, as hydrolysis of acylglycerols, which generates partial acylglycerols and FFA.

As shown in Figure 4.3.2A, Model 1 gives higher temperatures compared with the other two models all along the sparging steam period, behavior that occurred for all process conditions and oil compositions studied. It happens that one effect of the sparge steam is to decrease the required partial pressure of volatiles and, as a consequence, the boiling temperature of the mixture. For the heating period, Models 1 and 3 have the same objective function (Eq. 4.2.7) and, as a consequence, the same boiling temperatures.

Figures 4.3.2B and 4.3.2C show the profile per time of two variables studied (DA and OA) for the three models. For the last 20 min of the process the OA curves for Model 1 became considerably different from the others (Figure 4.3.2C), which can be seen as a consequence of the absence of the water effects in the liquid and vapor phases. The same behavior can be observed for the DA curves (Figure 4.3.2B), even though it starts earlier (after 30 min of processing). It is important to highlight the correspondence between the OA and DA curves regarding the component mass balance.

For Model 1, as an example, the OA curve is on top of the others, which means that less FFA were withdrawn from the crude oil. On the other hand, DA curve shows a smaller amount of that FFA in the distillate, as expected. However, the experimental points in the two graphics behave in a slightly different way, which is a probable consequence of small errors inherent to experimentation.

The simulation results for Model 3, especially those with oil compositions OC1 and OC2, are more compatible with those reported by Petrauskaitè *et al.* (2). In fact, this model seems better able to reproduce the experimental conditions observed in the operation of batch deodorizers.

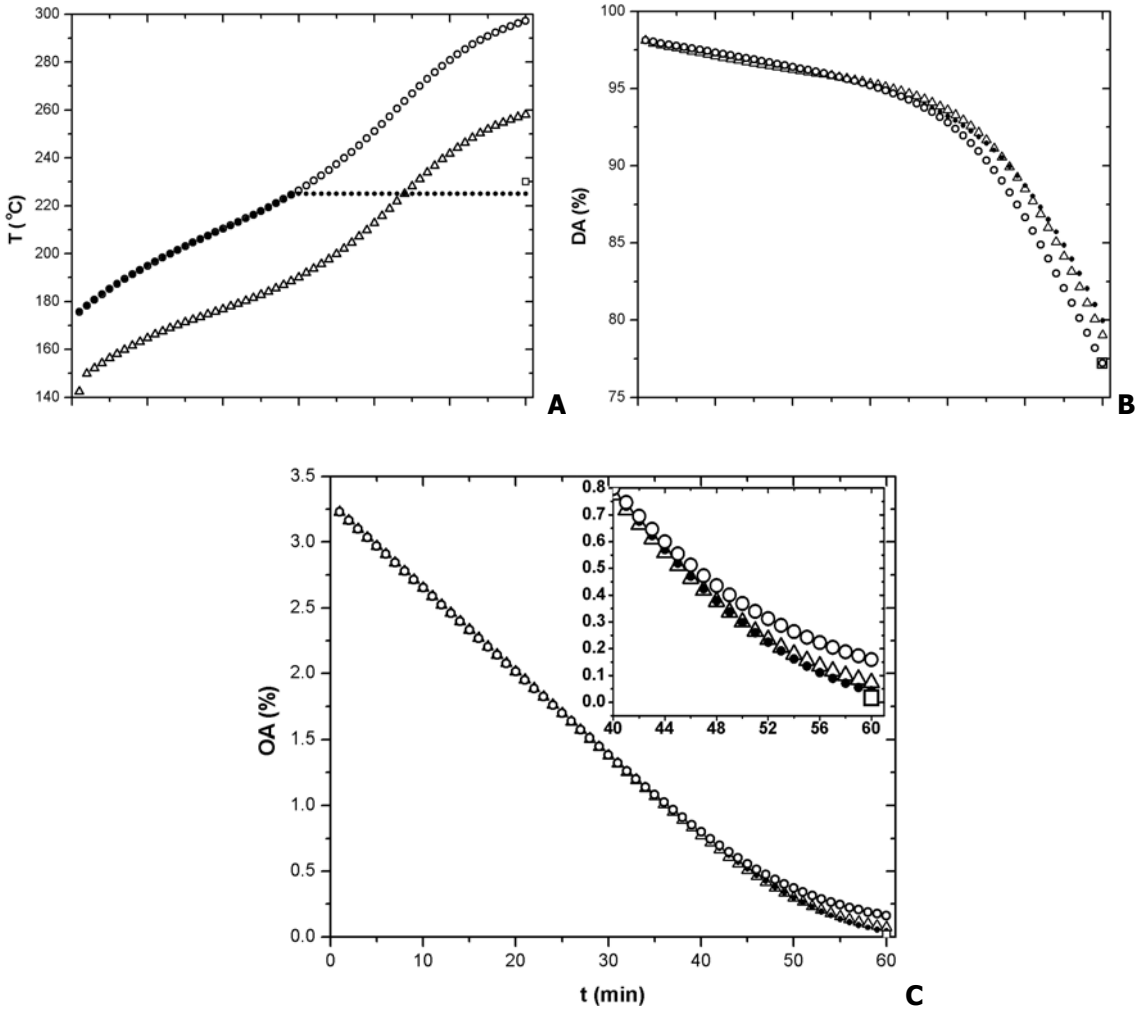

Figure 4.3.2. Variation of (A) the boiling temperatures, (B) FFA content of the distillate (DA), and (C) FFA content of the oil (OA) with time for the physical refining of coconut oil (OC2, 1.16% of partial acylglycerols) for Experiment 6 (see Table 4.3.3). Code: Model 1 (○); Model 2 (∆); Model 3 (●) and experimental points (□). The experimental temperature shown is the oven temperature. OA, oil acidity; DA distillate acidity; for other abbreviation see Figure 4.3.1

It should be noted that in all 18 simulations corresponding to Model 3, the calculated water concentration in the oil was consistently less than 0.00003 wt%. Despite this very low level, water had such a strong influence on the VLE that it possibly allows the industrial deodorization process without a further temperature increase. Note that the literature reports a water concentration in refined coconut oil of 0.09 wt% at room conditions (19). Furthermore, as can be seen in Figure 4.3.2A, without this water effect on the volatility of fatty components, the

temperature at the final part of the deodorization process would be higher, even higher than the temperature of the heat source used by Petrauskaitè *et al.* (2).

From our simulations, it is also possible to extract important information about the composition of the products throughout the distillation process. We have explored our results to show the usefulness of a simulation program in projecting and evaluating physical refining and deodorization units. Figure 4.3.3 illustrates the main FFA and acylglycerol classes found in coconut oil and their behavior under processing conditions (Experiment 6 in Table 4.3.3).

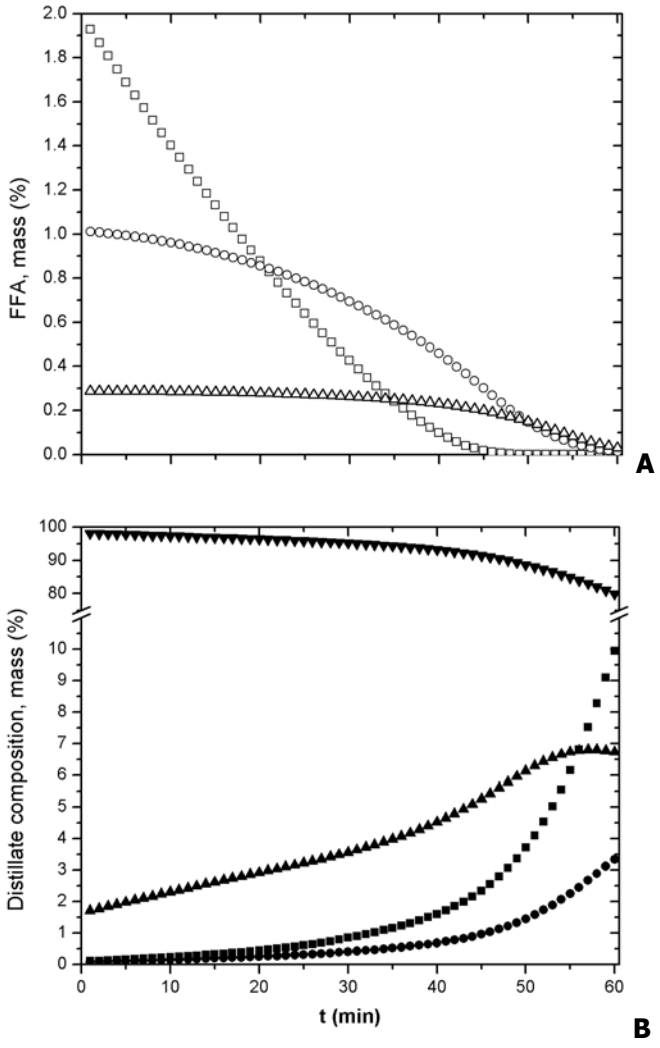

Figure 4.3.3. Main classes of (A) FFA in the oil acidity and (B) acidity and acylglycerols in the distillate for Experiment 6 (see Table 4.3.3). Code: (A) C6:0 to C12:0 (□); C14:0 to C18:0 (○); C18:1 and C18:2 (∆); (B) DA (▼); TAG (■); DAG (●) and MAG (▲). For other abbreviations see Figure 4.3.2.

As show in Figure 4.3.3A, for the first 20 min, short-chain FFA are the key fraction distilled from the oil, and completely removed after 49 min. At this time, the coconut oil has an OA of 0.337%, formed mainly by long-chain and unsaturated FFA, as oleic and linoleic. FFA are undoubtedly the main fraction of the distillate (see Figure 4.3.3B). However, it is possible to observe that its acylglycerol portion - and, as a consequence, the NOL – became important at the last 20 min of processing, when it starts to increase exponentially. Note also that after this point, considerable amounts of TAG and DAG are distilled, since the MAG concentration in the still is lower than 0.17 (wt/wt).

We have given a special attention to the calculated values of ϕ_i^{sat}, ϕ_i and POY for all components, including water and short-chain FA, to explain the use of vapor-phase nonidealities, even at the very low pressures found in this work. ϕ_i^{sat} values have differentiated considerably from unity $0.89 < \phi_i^{sat} < 0.96$ for those components, whereas ϕ_i and POY values were close to one (>0.978) for all components in the system. It is a consequence of the high values calculated along for vapor pressure, with the high temperatures observed, for water and short-chain FA. Vapor pressure is a parameter that is used in the calculation of ϕ_i^{sat}.

For further analyses of our methodology, we also studied the influence of the FFA concentration itself (initial OA) on NOL, OA and DA values. Following the composition ranges given by Firestone (20), we estimated two different compositions for coconut oil: one more volatile (MVO), rich in lauric and short-chain FA, and other less volatile (LVO), poor in lauric acid and rich in long-chain FA, as shown in Table 4.3.1. Their compositions of TAG, DAG and MAG were estimated following the same procedure as described earlier in this section.

To evaluate the impact of the initial FFA content in the final results, we simulated the deodorization of the more volatile coconut oil, varying its initial acidity from 1 to 6% (expressed as percentage of oleic acid) while maintaining 1% of MAG and 3% of DAG and using the conditions of Experiment 3. Model 3 was used as the simulation tool to reach at least 0.03% of final acidity for all cases. As

expected, the increase of the initial OA generated more significant values for DA and NOL as a consequence of the increased time of processing. The NOL values ranged from 1.60% (1% acidity) to 2.40% (6% acidity). The final acidity (0.03%) was achieved after 31 and 91 minutes, respectively.

To finalize this work, we have studied the influence of the oil composition, expressed in terms of the more and less volatile coconut oils (Table 4.3.1). The simulations were conducted to compare NOL, DA and OA at the same processing conditions stated in the above paragraph. The major differences between the two estimated oils were in their m.w. (574.7 and 631.8 g/gmol for MVO and LVO, respectively), chain lengths, and unsaturation of the fatty compounds (6.03 and 12.83 iodine values of MVO and LVO, respectively). Both oils had 1% of MAG, 3% of DAG and 2.13% of acidity, expressed as lauric acid. As a result, their partial acylglycerols had also different volatilities, having been distilled differently. These results are shown in Figure 4.3.4.

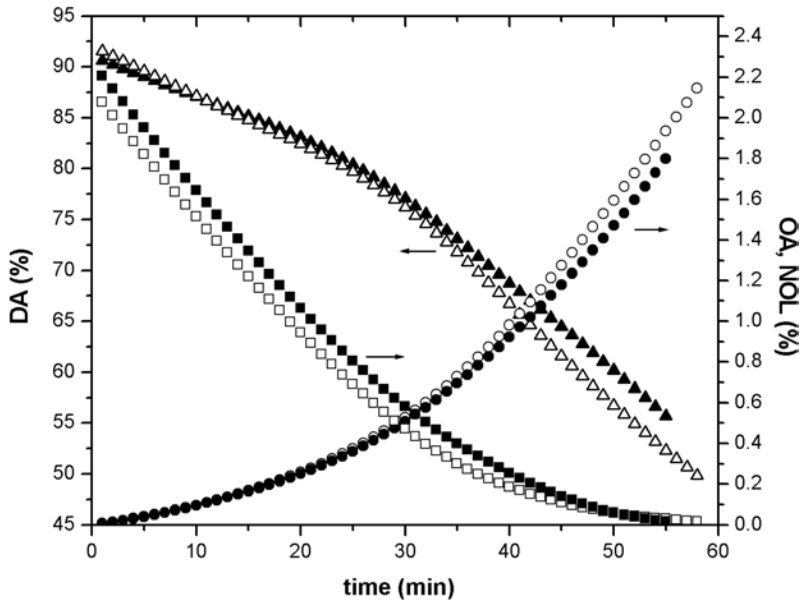

Figure 4.3.4. Variation in DA, NOL and OA as a function of the FA composition of the coconut oil and its volatility. Code: More-volatile DA (∆); OA (□) and NOL (○) ; less-volatile DA (▲); OA (■) and NOL (●). NOL, neutral oil loss; for other abbreviations see Figure 4.3.2.

Note that the OA of the LVO, although composed of long chain-length FFA, was evaporated more easily because its partial acylglycerols were less volatile and, for this reason, there was less competition among them in the vaporization process. As a consequence, the DA was also higher. The total NOL for the MVO was notably higher (2.14%) than the value found for the LVO (1.80%). The processing times were almost equivalent (only 3 min different).

The concordance of our simulation results with the experimental data from Petrauskaitè *et al.* (2) shows the possibility of applying our methodology to simulate edible-oil refining plants and to evaluate NOL in presence of MAG and DAG. To scale up our approach and design a real plant, it may be necessary to consider vaporization efficiency factors in the equilibrium equations, degradation reactions (as hydrolysis) and losses due to mechanical entrainment. Nevertheless, our model is a valuable tool for a first estimation of NOL, especially in presence of considerable amounts of MAG and DAG, as occurs for oils with high acidity.

Acknowledgements

The authors wish to acknowledge FAPESP (Fundação de Amparo à Pesquisa do Estado de São Paulo - 01/06798-7, 03/04949-3) and CNPq (Conselho Nacional de Desenvolvimento Científico e Tecnológico - 521011/95-7) for the financial support.

References

[1] Verleyen, T., R. Verhe, L. Garcia, K. Dewettinck, A. Huyghebaert, and W. De Greyt, Gas Chromatographic Characterization of Vegetable Oil Deodorization Distillate, *J. Chromatogr. A*. 921: 277-285 (2001).

[2] Petrauskaité, V., W.F. De Greyt and M.J. Kellens, Physical Refining of Coconut Oil: Effect of Crude Oil Quality and Deodorization Conditions on Neutral Oil Loss, *J. Am. Oil Chem. Soc*. 77: 581-586 (2000).

[3] Ruiz-Mendez, M.V., G. Marquez-Ruiz, and M.C. Dobarganes, Quantitative Determination of Major Compounds Present in Deodorizer Distillated from Fats and Oils. *Grasas y aceites* 46: 21-25 (1995).

[4] Carlson, K.F., Deodorization, in *Bailey's Industrial Oil and Fat Products*, 5th edn., edited by Y.H. Hui, Wiley-Interscience, New York, 1996, Vol.4, pp. 339-390.

[5] Canapi, E.C., Y.T.V. Agustin, E.A. Moro, E. Pedrosa, J.M. Luz and J. Bendano, Coconut Oil, in *Bailey´s Industrial Oil and Fat Products*, 5th edn., edited by Y.H. Hui, Wiley-Interscience, New York, 1996, Vol.2, pp. 97-124.

[6] Tandy, D.C. and W.J. McPherson, Physical Refining of Edible Oil, *J. Am. Oil Chem. Soc*., 61: 1253-1258 (1984).

[7] Ceriani, R. and A.J.A. Meirelles, Predicting Vapor-Liquid Equilibria of Fatty Systems, *Fluid Phase Equilib.,* 215: 227-236 (2004).

[8] Fredenslund, A., J. Gmehling., and P. Rasmussen, *Vapor-liquid equilibria using UNIFAC*, Elsevier Scientific Publishing Company, Amsterdan, 1977.

[9] Haypek, E., L.H.M. Silva, E. Batista, D.S. Marques, M.A.A. Meireles, and A.J.A. Meirelles, Recovery of aroma compounds from orange essential oil, *Braz. J. Chem. Eng*. 17: 705-712 (2000).

[10] Batista, E. and A.J.A. Meirelles, Simulation and thermal integration SRV in an extractive distillation column, *J. Chem. Eng. Japan* 30: 45-51 (1997).

[11] Batista, E., R. Antoniassi, M.R.W. Maciel, and A.J.A. Meirelles, Liquid-Liquid Extraction for Deacidification of Vegetable Oils, in ISEC 2002 (Proceedings of the International Solvent Extraction Conference, edited by Sole, K.C., P.M. Cole, J.S. Preston, and D.J. Robinson, Chris van Rensburg Publications, Johannesburg, South Africa, 2002, pp. 638-643.

[12] Ingham, J., I.J. Dunn, E. Heinzle, and J.E. Prenosil, in *Chemical Engineering Dynamic: Modeling with PC Simulation*, edited by J. Inghan, VCH Publishers, Weihneim, 1995, pp. 589-593.

[13] Anderson, D., A Primer on Oils Processing Technology, in *Bailey's Industrial Oil and Fat Products*, 5th edn., edited by Y.H. Hui, Wiley-Interscience, New York, 1996, Vol.4, pp. 1-60.

[14] Ramirez, W.F., *Computational Methods for Process Simulation*, 2th edn., Butterworth-Heinemann, Oxford, 1997, pp. 82-83.

[15] Fornari, T., S. Bottini, and E. A. Brignole, Application of UNIFAC to Vegetable Oil-Alkane Mixtures, *J. Am. Oil Chem. Soc*. 71: 391-395 (1994).

[16] Loncin, M., *L'Hydrolyze Spontanée des Huiles Glycéridiques et en Particulier de l'Huile de Palme*. Maison D'Editon, Couillet, 1962, 62 p.

[17] Antoniosi Filho, N.R., O.L. Mendes, F.M. Lanças, Computer prediction of triacilglicerol composition of vegetable oils by HRGC, *J. Chromatogr*., 40: 557-562 (1995).

[18] Theme, J.G., *Coconut Oil Processing,* FAO, Rome, 1968.

[19] Hands, E.S., Lipid Composition of Selected Foods, in *Bailey's Industrial Oil and Fat Products*, 5th edn., edited by Y.H. Hui, Wiley-Interscience, New York, 1996, Vol.1, pp. 441-506.

[20] Firestone D., Physical and Chemical Characteristics of Oils, Fats and Waxes, AOCS Press, Champaign, 1999, 152p.

CAPÍTULO 5. SIMULATION OF CONTINUOUS DEODORIZERS: EFFECTS ON PRODUCT STREAMS

Roberta Ceriani and Antonio J. A. Meirelles

Trabalho publicado na revista **The Journal of the American Oil Chemists Society, v. 81(11), p. 1059-1069 (2004).**

Key words

Countercurrent flow, cross-flow, deodorization, entrainment, multicomponent stripping, Murphree efficiency, neutral oil loss, simulation, tocopherol retention, and vegetable oils.

Abstract

This work deals with the simulation of deodorization, one important process of the edible oil industry related to the removal of odoriferous compounds. The deodorizer was modeled as a multicomponent stripping-column in cross-flow and countercurrent flow. The impact of processing parameters on the quality of the product streams was analyzed. The deodorization of soybean oil and canola oils (plant scale) and wheat germ oil (lab-scale) was studied under typical ranges of temperature, stripping steam rate and pressure. Their entire compositions were considered within the simulations, including acylglycerols, free fatty acids (FFA) and other key components such as tocopherols and sterols. The deodorization results were analyzed in terms of retention of tocopherol and sitosterol and neutral oil loss to the distillate. The deodorizer modeling considered Murphree efficiencies and entrainment for each plate. A case study, i.e. the deodorization of soybean oil, illustrated the applicability of our modeling.

5.1 Introduction

Deodorization is a steam-stripping process responsible for vaporizing odoriferous compounds and FFA from the oil, carrying them to the distillate, and producing edible oil. Although it targets only these undesirable compounds, other components with comparable volatilities are also lost (1).

Since deodorizer operating conditions are based on oil quality rather than distillate concerns, a vaporization of tocopherols and sterols occurs in the course of deodorization, even though these components are less volatile than FFA (2). The economical importance of these compounds is related to their value to food and chemical industries: Tocopherols are natural antioxidants and are considered as a

quencher of free radicals (3), whereas sterols are used in the manufacture of pharmaceuticals, such as hormones and corticoids (2). As pointed out by Ahrens (3), different markets pose different quality demands. Although the economic value of the distillate depends on its composition and content of tocopherols and sterols (4), some markets, such as Europe, are concerned with the retention of tocopherols in the refined oil (3). In United States, the deodorization temperature is set up to 270 °C, since it is important to recover tocopherol in the distillate (3).

This work deals with the evaluation by process simulation of the impact of processing parameters on quality and composition of finished oil and, as a consequence, of the deodorization distillate. We selected three different vegetable oils for this study: soybean oil, because it is widespread; genetically modified canola oil rich in oleic acid; and the wheat germ oil, because of its unique composition that is rich in polyunsaturated fatty acids (PUFA) and tocopherols (5).

The continuous deodorizers (plant and lab-scale) were modeled as a multicomponent stripping column, following the method described by Naphtali and Sandholm (6). Group contribution methods were selected to calculate all the physical properties needed in the equilibrium relationships and energy balances.

Soybean oil was presumed to contain triacylglycerols (TAG), diacylglycerols (DAG) and monoacylglycerols (MAG); FFA; δ-tocopherol; squalene; and β-sitosterol (7). Wheat germ oil was assumed to have TAG, DAG and MAG; FFA; and α-tocopherol (5). Canola oil was characterized by TAG, DAG, MAG; FFA; and γ-tocopherol (8). Note that we considered a representative tocopherol and sitosterol to identify the whole class of these compounds. Pryde (7) and Woerfel (2) found that the main sitosterol and the main tocopherol of soybean oil are, respectively, β-sitosterol and δ-tocopherol. For wheat germ oil, α-tocopherol is the representative tocopherol (5). In canola oil, γ-tocopherol is the main tocopherol (8).

5.2 Modeling continuous deodorizers: plant and lab-scale

In commercial deodorization, two relevant flow patterns are used: cross-flow (Figure 5.2.1A), which implies that the flow directions of the phases cross each other, and countercurrent flow, in which the inlet of the gas is at the outlet of the oil, and the outlet of the gas is at the inlet of the oil (9). Thin-film deodorizers are based in the countercurrent contact between gas and oil (9). Lab-scale continuous tray deodorizers, such as the one used by Wang and Johnson (5) for wheat germ oil, also use a countercurrent flow (Figure 5.2.1B).

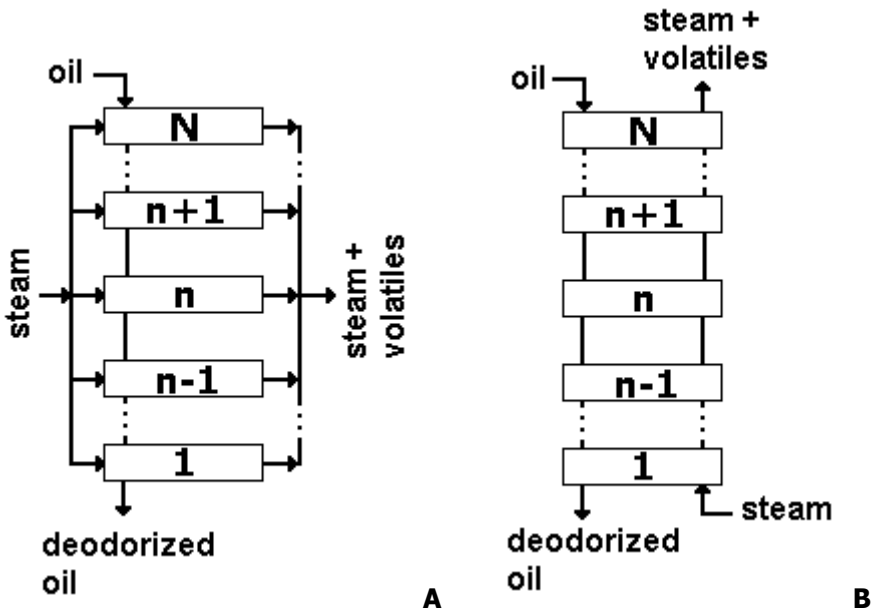

Figure 5.2.1. Continuous tray design: (A) cross-flow, and (B) countercurrent flow.

Modeling of the multicomponent stripping column steady-state was based on the method described by Naphtali and Sandholm (6). The general equations, which include material and energy balances and Murphree efficiencies coupled with vapor-liquid equilibrium relationships, are described briefly in Appendixes I and II. An iterative procedure (Newton-Raphson) is used for simultaneous convergence until the true values of $l_{n,i}$ (the component liquid molar flow), $v_{n,i}$ (the component vapor molar flow) and T (the temperature), corresponding to each stage are found. Input data to the calculations were as follows: (i) identification and division

of the mixture components in usual groups and the respective parameters, according to each group contribution method selected; (ii) specification of the processing variables: number of stages, Murphree efficiencies, feed location and composition, flow pattern (cross-flow or countercurrent), feed flow rates and thermal states, and column pressure; and (iii) initial estimation for the total molar flow rates for each stage and for the temperature profile.

To express the vapor-liquid equilibria (VLE) found in each tray, the thermodynamic approach of Ceriani and Meirelles (10), which considers the nonideality of the vapor and liquid phases, was applied. Their VLE approach is shown below:

$$k_i = \frac{y_i}{x_i} = \frac{\gamma_i \cdot f_i^o}{P \cdot \phi_i} \qquad [5.2.1]$$

where

$$f_i^o = P_i^{vp} \cdot \phi_i^{sat} \cdot \exp\left(\frac{V_i^L \cdot \left(P - P_i^{vp}\right)}{R \cdot T}\right) \qquad [5.2.2]$$

where f_i^o is the standard-state fugacity; x_i and y_i are the molar fractions of component *i* in the liquid and vapor phases, respectively; *P* is the total pressure; *R* is the gas constant; *T* is the system absolute temperature; P_i^{vp} and ϕ_i^{sat} are, respectively, the vapor pressure and the fugacity coefficient of the pure component *i;* γ_i is the liquid-phase activity coefficient; ϕ_i is the vapor-phase fugacity coefficient; and V_i^L is the liquid molar volume of component *i*. The exponential term corresponds to the Poynting factor (POY). As shown in Appendixes I and II, this correlation is valid for each stage *n*, corrected by the Murphree efficiency. The vapor pressure P_i^{vp} and the activity coefficient γ_i are calculated for each fatty compound using, respectively, the group-contribution approach developed by Ceriani and Meirelles (10) and the UNIFAC r ¾ (11). Various works in the area of

VLE of fatty mixtures (10, 11) have confirmed that UNIFAC r ¾ better suits the prediction of the liquid-phase behavior.

Equations 5.2.1 and 5.2.2 describe the VLE rigorously. Previous works (10, 11) have demonstrated that some simplifications may be applied in the analysis of oil-solvent mixtures. POY and ϕ_i are nearly one, whereas ϕ_i^{sat} deviates notably from unity for compounds whose vapor pressures are very high at the system temperature, such as water, short-chain FA and *n*-hexane. A good investigation of the nonidealities of fatty mixtures can be found in Ceriani and Meirelles (10).

5.3 Estimation of oil composition, physical properties, Murphree efficiencies and entrainment

Soybean, canola and wheat germ oils are formed by TAG, DAG and MAG in addition to a variety of other minor compounds. This work, in particular, is concerned with the behavior of fatty components (FA and acylglycerols), tocopherols and sterols within the deodorization process. To estimate their entire composition in terms of TAG, we used the methodology suggested by Antoniosi Filho et al. (12), which is based in a statistical procedure that considers lipase hydrolysis characteristics. In this way, the TAG compositions were estimated from the FA compositions given by Firestone (8) for soybean oil, by Rabelo et al. (13) for canola oil, and by Wang and Johnson (5) for wheat germ oil. The composition in DAG and MAG was obtained from the estimated TAG composition in the following way: Each TAG was split into 1,2 and 1,3 DAG; each DAG was split into MAG following the stoichiometric relations of the prior compounds (TAG in the case of DAG, and DAG in the case of MAG). The same considerations were previously applied successfully by Ceriani and Meirelles (14) to estimate coconut oil composition (15) in the evaluation of batch physical refining by simulation, and by Rabelo et al. (13) to predict kinematic viscosities. The tocopherol, squalene and β-sitosterol concentrations in soybean oil were taken from Pryde (7) and Maza et al. (16). The tocopherol concentration in canola oil was taken from Firestone (8). The tocopherol concentration in wheat germ oil was given by Wang and Johnson (5).

Compounds responsible for odors and flavors were not included in the oil composition, given that the residual FFA content can be used as an indicator of the odor elimination (1).

Pertinent information on the general composition of soybean, canola and wheat germ oils is shown in Table 5.3.1.

As a whole, the wheat germ oil had 7 FFA (Table 5.3.1), 22 TAG, 11 DAG and 5 MAG. The main TAG were PLiLi (18.0%, w/w), POLi (10.3%, w/w), LiLiLi (22.8%, w/w) and OLiLi (18.2%, w/w). PLi-, LiLi- and OLi- were the key DAG (27.7%, 27.0% and 22.1%, respectively). The MAG class was formed mainly by O-- (19.1%), P-- (20.4%) and Li-- (55.7%). The complete composition of acylglycerols for the soybean oil is shown in Table 5.3.2. The complete TAG composition for canola oil can be found by referring to Rabelo et al. (13). Its key TAG were OOLi (24.3%, w/w), OOO (24.0%, w/w) and OOLn (17.8%, w/w). OO- (44.7%, w/w) and O-- (69.4%, w/w), were the main DAG and MAG, respectively.

Because of the high number and large diversity of compounds found in the deodorizer, predictive group contribution methods were selected to estimate all the physical properties required for the enthalpy balances and equilibrium conditions. To calculate activity coefficients, UNIFAC r ¾ (UNIquac Functional group Activity Coefficients) was used (11). Fugacity coefficients were calculated using the virial equation (19). Critical properties and acentric factors of the pure components, needed to calculate second virial coefficients, were estimated using the well-known Joback's technique for critical volumes and pressures, and Fedor's group contributions for critical temperatures (19). For the energy balances, vapor and liquid heat capacities and enthalpies of vaporization are required. We selected Joback's technique for ideal vapor heat capacities, Rowlinson-Bondi's method for liquid heat capacities (19), and the method of Tu and Liu (20) to estimate the enthalpy of vaporization of each compound involved. The physical properties of water (stripping steam) were calculated using the equations from the Design Institute for Physical Properties (DIPPR) Chemical Database (21).

Table 5.3.1. General composition of soybean, wheat germ and canola oils.

FA	Trivial name (abbreviation)	Soybean Oil Mass (%) [a]		Wheat Germ Oil Mass (%) [b]		Canola Oil Mass (%) [c]	
C14:0	Miristic (M)	---		---		0.10	
C16:0	Palmitic (P)	9.7		16.3		6.79	
C16:1	Palmitoleic (Po)	---		---		0.33	
C18:0	Stearic (S)	5.4		0.9		1.83	
C18:1	Oleic (O)	25.0		18.2		60.99	
C18:2	Linoleic (Li)	52.4		56.5		21.01	
C18:3	Linolenic (Ln)	5.5		6.0		8.48	
C20:0	Arachidic (A)	0.6		0.2		0.32	
C20:1	Gadoleic (G)	0.2		1.9		---	
C20:2	Gadolenic (Gn)	0.1		---		---	
C22:0	Behenic (Be)	0.7		---		---	
C22:1	Erucic (E)	0.2		---		0.15	
C24:0	Lignoceric (Lg)	0.2		---		---	
Class of compounds		Mass (%)	*M* g/gmol	Mass (%)	*M* g/gmol	Mass (%)	*M* g/gmol
TAG		99.300	875.27	96.6831	869.07	99.376	875.68
DAG		0.146	612.05	2.6000 [d]	606.60	0.200	612.98
MAG		0.004	352.03	0.3000 [d]	349.58	0.005	352.43
FFA		0.070 [e]	279.37	0.1700 [b]	277.07	0.100 [f]	279.80
Squalene		0.014 [g]	410.72	---	---	---	---
β-sitosterol		0.330 [g]	414.72	---	---	0.250 [a]	414.72
Tocopherol		0.136 [e]	414.00	0.2469 [b]	414.00	0.070 [a]	414.00
Molecular weight		864.61		848.26		867.18	
Iodine Value (IV)		126.34		128.98		110.99	
IV ranges [a]		118-139		115-128		110-126	

[a] From Firestone (8).
[b] Same composition of the bleached wheat germ oil, from Wang and Johnson (5).
[c] From Rabelo et al. (13).
[d] From Barnes (17).
[e] From Maza et al (16).
[f] From Eskin et al. (18).
[g] From Pryde (7).

Table 5.3.2. Estimated composition of soybean oil

	TAG			DAG		
Group[a]	Major Triacylglycerol	M [b] (g/gmol)	Mass (%)	Acylglycerol compound	M [b] (g/gmol)	Mass (%)
50:1	POP	832	0.78	PP-	568	1.25
52:1	POS	860	0.82	PS -	596	0.44
54:1	SOS	888	0.31	SS-	624	0.17
56:1	POBe	916	0.15	PLg-	680	0.06
58:1	POLg	944	0.10	PO-	594	5.91
50:2	PLiP	830	1.44	SO-	622	5.86
52:2	POO	858	3.94	OA -	650	0.73
54:2	SOO	886	1.86	OBe-	678	0.57
56:2	PLiBe	914	0.46	OLg -	706	0.08
58:2	OOBe	942	0.36	PLi -	592	16.85
60:2	OOLg	970	0.14	OO-	620	8.63
50:3	PLnP	828	0.16	LiA-	648	0.43
52:3	POLi	856	9.16	LiBe -	676	0.43
54:3	SOLi	884	6.75	LiLg -	704	0.20
56:3	OLiA	912	0.72	PLn -	590	1.18
58:3	OLiBe	940	0.66	OLi -	618	32.62
60:3	OLiLg	968	0.31	LiG-	646	0.22
52:4	PLiLi	854	9.28	LiE-	674	0.18
54:4	OOLi	882	15.41	LiLi -	616	21.33
56:4	LiLiA	910	0.77	LiGn-	644	0.07
58:4	LiLiBe	938	0.77	LiLn -	614	2.79
60:4	LiLiLg	966	0.30	MAG		
52:5	PLiLn	852	1.84	P--	330	13.10
54:5	OLiLi	880	21.56	S--	358	3.33
56:5	LiLiG	908	0.40	O--	356	31.59
58:5	LiLiE	936	0.32	Li--	354	48.42
60:5	LiLnLg	964	0.06	Ln--	352	2.00
52:6	PLnLn	850	0.10	A--	386	0.60
54:6	LiLiLi	878	16.29	G--	384	0.11
56:6	LiLiGn	906	0.13	Gn--	382	0.03
54:7	LiLiLn	876	4.21	Be--	414	0.53
54:8	LiLnLn	874	0.44	E--	412	0.10
				Lg--	442	0.19

[a] Isomer set including different TAG, but all with the same number of FA carbons and double bounds. For example, Group 50:1 means the isomer set of TAG with 50 fatty acid carbons and one double bound.
[b] M, molecular weight (g/gmol). For other abbreviations see Table 5.3.1.

To predict the vapor pressure of squalene we selected the method of Voutsas et al. (22). Required inputs are the normal boiling temperature and the respective liquid density, which were calculated using the methods of Retzekas et

al. (23) and Elbro et al. (24), respectively. Equation 5.3.1 was obtained from the direct use of these methods on squalene. For β-sitosterol, the empirical equation suggested by Bokis et al. (25) was applied. For tocopherol, we have adjusted an equation for the curve of vapor pressure versus temperature shown by Woerfel (2). This last step was taken to overcome the inadequacy of group contribution methods (22) in predicting the vapor pressure of tocopherols. It is important to highlight that, in this way, we were capable of describing the existing relation among the volatilities of the minor compounds considered: squalene > tocopherol > sitosterol (2, 4). In this way, Equation 5.3.2 was developed to predict the vapor pressure of tocopherol. Note that Equation 5.3.2 has the same form for the dependence between the logarithm of the vapor pressure and temperature as Bokis et al. (25) suggested for sitosterol (Equation 5.3.3).

$$\ln P^{vp}_{squalene}(\text{Pa}) = 101325 \cdot \frac{T(\text{K}) - 733.14}{T(\text{K}) - 121.2966} \qquad [5.3.1]$$

$$\ln P^{vp}_{tocopherol}(\text{Pa}) = 21.44191 - \frac{191754.2}{T^{1.5}(\text{K})} \qquad [5.3.2]$$

$$\ln P^{vp}_{sitosterol}(\text{Pa}) = 20.75045 - \frac{199959.3}{T^{1.5}(\text{K})} \qquad [5.3.3]$$

Other properties of these compounds were calculated using the aforementioned methods.

For vapor-liquid separation process, considering that both liquid and vapor phases are mixed perfectly, a measure of the efficiency of mass transfer for a component *i* on n^{th} stage, is the Murphree efficiency (26). As suggested by Ludwig (26), the Murphree efficiency (η) can be estimated with the user-friendly equations of MacFarland et al. (27) as a function of dimensionless groups: the surface tension number N_{Dg}, the liquid Schmidt number N_{Sc}, and the modified Reynolds number N_{Re}. The two models developed by the authors for traditional hydrocarbon and chemical industries are given below:

$$\eta = 7.0 \cdot \left(N_{Dg}\right)^{0.14} \cdot \left(N_{Sc}\right)^{0.25} \cdot \left(N_{\mathrm{Re}}\right)^{0.08} \quad [5.3.4]$$

$$\eta = 6.8 \cdot \left(N_{\mathrm{Re}} \cdot N_{Sc}\right)^{0.1} \cdot \left(N_{Dg} \cdot N_{Sc}\right)^{0.115} \quad [5.3.5]$$

$$N_{Dg} = \sigma_L / \left(\mu_L \cdot U_{VN}\right);\ N_{Sc} = \mu_L / \left(\rho_L \cdot D_{LK}\right);\ N_{\mathrm{Re}} = \rho_V \cdot U_{VN} \cdot h_w / \left(\mu_L \cdot FA\right) \quad [5.3.6]$$

where: σ_L is the surface tension of the liquid (lb/h^2), μ_L is the liquid viscosity (lb/h.ft*)*, U_{VN} is the vapor superficial velocity (ft/h), ρ_L and ρ_V are the liquid and vapor densities (lb/ft^3), respectively, h_w is the weir height (ft), *FA* is the fractional free area (the ratio of the fractional area of the holes to the column free cross-sectional area), and D_{LK} is the liquid diffusivity (ft^2/h) at infinite dilution from Wilke-Chang equation (19). Surface tensions and diffusivities were calculated using well-known methods from Reid et al. (19). Viscosities and densities were calculated according to Rabelo et al. (13) and Halvorsen et al. (28), respectively. As pointed out by Carlson (1), for properly designed deodorizers, U_{VN} is usually less than 2 m/s.

All $\eta_{n,i}$ values (Murphree efficiencies for each component at each tray; see Appendixes I and II) were considered equal to η (Equations 5.3.4 – 5.3.6), which is a simplifying approximation. To calculate η, we have considered a typical load of soybean oil (4,425 kg/h) at 3 mmHg, 260 ºC and 1% of stripping steam. The mixture involved in this calculation was characterized by pseudo-compounds: an equivalent TAG (same molecular weight and unsaturations of the oil), an equivalent FFA (same molecular weight and unsaturations of the oil acidity), and water. The calculated values of η for soybean oil were 57.15% using Equation 5.3.4 and 46.91% using Equation 5.3.5. For wheat germ oil η was 53.65% using Equation 5.3.4 and 44.64% using Equation 5.3.5. For comparison purpose we also calculated η for palm oil (752 g/gmol). The values obtained were 61.68% and 49.99%, respectively, for Equations 5.3.4 and 5.3.5. As one can see, η ranged from 54% to 62% for Equation 5.3.4, and from 45% to 50% (more conservative) for Equation 5.3.5. For simplicity, $\eta_{n,i}$ =0.50 was chosen to represent the Murphree efficiency in our work. The approximation of the whole multicomponent mixture by

an equivalent ternary one, containing pseudo-compounds, was used only in the case of efficiency estimation.

Mechanical entrainment of oil is defined as the carrying of oil droplets in the vapor upward from the free surface to the outlet of the equipment (1). In industrial deodorizers, losses of neutral oil by entrainment are believed to be around 0.1-0.2%, with an additional loss of about 10% of the FFA amount in the feed (1). To account for the mechanical entrainment in our simulations, we used the graphical method of Fair and Mathews (see Ref. 26) for bubble-cap and perforated plates. This correlation was developed on the basis of a flow parameter $\left(L_n/V_n \cdot (\rho_V/\rho_L)^{0.5}\right)$ and a capacity parameter $\left(U_{VN} \cdot (\rho_V/\rho_L - \rho_V)^{0.5}\right)$. It relates percent of flood, the fractional entrainment ψ (moles of liquid entrained/ moles of liquid downflow), liquid and vapor flow rate, and the densities of the vapor and liquid. The ψ value from our calculations was 0.024 moles of liquid entrained/ moles of liquid downflow. The entrainment term, e_n (moles of liquid entrained/ moles of vapor), of Equations A1 and A2 and of Equations A6 and A7 is related to ψ by the following equation (26):

$$e_n = \frac{\psi}{1-\psi} \cdot \frac{L_n}{V_n} \qquad [5.3.7]$$

In particular, for countercurrent flow tray deodorizers, part of the liquid of lower concentration of the plate below (*n-1*) is entrained and carried by the vapor to the plate above (*n*), reducing its liquid concentration with respect to the more volatile compounds. As a consequence, the vapor rising from this plate (*n*) will be of lower concentration, reducing the net amount of mass transfer and the efficiency as well. The Murphree efficiency must be corrected to take this effect into account (26). The wet Murphree efficiency, η_w, can be easily calculated as a function of ψ (26):

$$\eta_w = \eta \Big/ \left(1 + \eta \cdot \frac{\psi}{1-\psi}\right) \qquad [5.3.8]$$

All $\eta_{n,i}$ values in the equilibrium relationships of countercurrent deodorizer (see Appendix I) were considered equal to η_w. For cross-flow deodorizers $\eta_{n,i}$ values (see Appendix II) were set as equal to η.

For countercurrent deodorizer (lab-scale), the pressure drops[⊗] of the trays are added so that the pressure at the bottom of the column is two to three times the top pressure (29). For cross-flow deodorizers, the pressure drop was negligible.

5.4 Results and discussion

We now present the results obtained in our deodorization simulations following processing parameters ranges found in the literature: oil load (kg/h), percentage of stripping steam, temperature, and pressure. To evaluate the industrial deodorization of soybean and canola oil, we followed the directions given by Maza et al. (16), Ahrens (3), Eskin et al. (18), and Brekke (30). In the case of the lab-scale deodorization of wheat germ oil, we were guided by the work of Wang and Johnson (5), in which a laboratory-scale continuous countercurrent deodorizer of 15 trays (as Fig. 5.2.1B) was used. Murphree efficiencies and entrainment were also inputs for the program simulations. Table 5.4.1 shows the processing parameters studied in this work. As one can see, the combination of these parameters led to a considerable number of possibilities for simulation. In the case of soybean oil, two sets of simulation conditions were studied; the first one was related to the work of Maza et al. (16). The most significant results are discussed below.

From the parameters given in Table 5.4.1, we selected a typical condition for the deodorization of soybean oil from Ahrens (3) (2.775 mmHg, 1.3% of stripping steam and 250 °C) to explore and discuss some of the results given by the simulation program.

[⊗] Para que a pressão no estágio 1 fosse igual a 2 vezes a pressão do estágio 15 (topo), calculou-se uma perda de carga de 0,36 mmHg por estágio. Desta forma: $P_1=P_{15}+0,36*14=10,0$ mmHg. Note (Tabela 5.4.1) que $P_{15}=5,0$ mmHg.

Table 5.4.1. Operating conditions for the continuous deodorizer simulations.

Parameter	Soybean Oil (plant scale, cross-flow)		Canola Oil (plant scale, cross-flow)	Wheat Germ Oil [a] (lab-scale, counter-current)
Stripping steam	880 lb/h (399.2 kg/h) [b, c]	1.0, 1.3 and 2.0 % [c, d, e]	1.3 and 2.0% [c, d, e, f]	0.25 cm^3 of water/min [g] (0.015 kg/h)
Temperature (°C)	246, 253 and 260 [b] (475, 488 and 500 °F)	242, 250 and 258 [e]	240, 250 and 260 [f]	200 and 250
Oil load	40,000, 45,000 and 50,000 lb/h [b] (18,144, 20,412 and 22,680 kg/h)	4,425 kg/h [e]	4,425 kg/h [e]	10 and 25 mL/min (0.5 and 1.2 kg/h)
Top Pressure (mmHg)	4 [b]	1, 2.775 (3.7 mbar) and 6 [e]	1, 2.5 and 4 [f]	5
Pressure drop	Negligible	Negligible	Negligible	0.36 mmHg per tray [h]
Number of trays	3 [e]	3 [e]	3 [e]	15
Murphree efficiency ($\eta_{n,i}$)	0.50	0.50	0.50	0.494[i]
Entrainment (e_n) [j]	0.4324	0.4324	0.4324	0.4324

[a] From Wang and Johnson (5)
[b] From Maza et al. (16).
[c] The stripping steam is distributed equally in each stage of the column (Fig. 5.2.1A).
[d] Calculated as percentage of total oil load.
[e] From Ahrens (3) and Brekke (30). The oil feed is introduced into the column at the top stage (3^{th})
[f] From Eskin et al.(18)
[g] The stripping steam is fed at the bottom, as a single stream (Fig. 5.2.1B).
[h] Following the directions of Stage (29).
[i] Murphree efficiency corrected for entrainment for stage *n* and component *i*.
[j] Entrainment for each stage *n* (moles of liquid entrained/ moles of vapor).

Figure 5.4.1 shows the profiles of the mass fraction of FFA, acylglycerol, squalene, tocopherol, and sterol curves in the liquid and vapor phases within the column. As expected, the FFA concentration in the liquid phase (Fig. 5.4.1A) dropped off from the feed third stage to the first stage. The total acylglycerol concentration (including TAG, DAG and MAG) did not change significantly, since TAG concentration prevailed over DAG and MAG in the liquid oil. The squalene, tocopherol and sterol curves had slight variations, but as is shown later, these changes were significant when compared with the feed concentration of each compound. As shown in Figure 5.4.1B, the vapor phase formed at the top stage

was richer in acylglycerols, FFA and squalene than the vapor phase formed at the bottom. Given that the steam fed at the third stage was in contact with the oil feed, there was a stronger driving force for mass transfer. Figure 5.4.1C shows the profiles of liquid and vapor flows (mol/h) and enthalpies (kJ/h) for each stage. Since the difference between temperatures at the top and the bottom of the column was less than 0.1 °C (249.96 and 249.91, respectively), and stripping steam was injected at each stage, the enthalpies did not change considerably.

To analyze the results of our methodology, we also studied the influence of the processing conditions on the quality of product streams, i.e., the deodorized oil and the distillate. As already discussed, the optimized conditions for operating a deodorizer depend on the composition of the oil at the inlet of the deodorizer (neutralized or bleached oil) and the desired compositions of products. Table 5.4.2 shows selected values of the deodorizer distillate as a function of temperature and pressure, obtained with 1.3% of stripping steam. As expected, the distillate flow increased with temperature and decreased with system pressure. Neutral oil loss (NOL) followed the same statement, since the volatility of acylglycerols rose at higher temperatures. Because of entrainment, acylglycerols became the main fraction of the distillate.

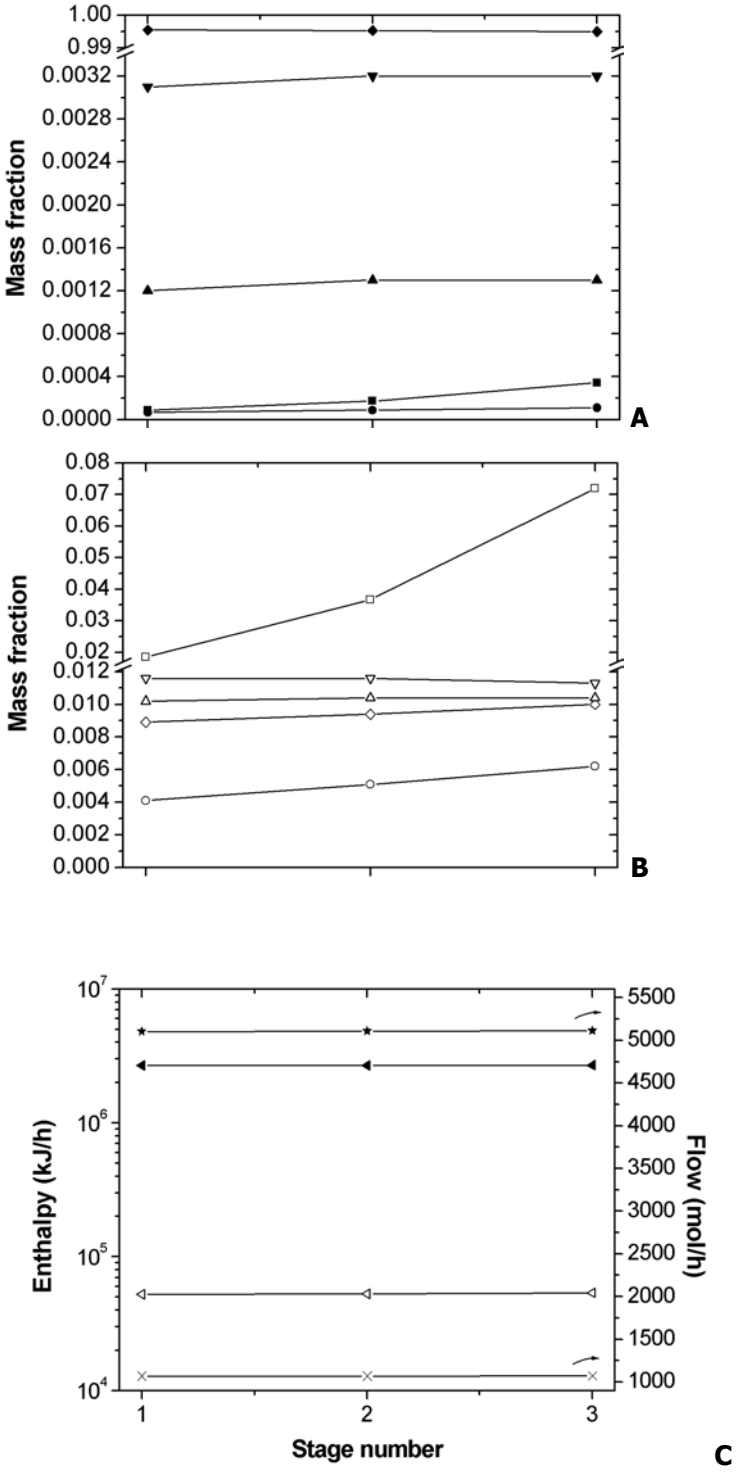

Figure 5.4.1. Profiles for the mass fractions of acylglycerols, FFA, squalene, β-sitosterol and δ-tocopherol (A) in the liquid phase and (B) in the vapor phase; (C) enthalpies and flows for a typical deodorizing condition (3). Code: (♦) Liquid phase acylglycerols, (■) FFA, (▼) β-sitosterol, (▲) δ-tocopherol and (●) squalene. (◇) Vapor phase acylglycerols, (□) FFA, (▽) β-sitosterol, (△) δ-tocopherol (○) and squalene. Liquid (◀) and vapor (◁) enthalpies. Liquid (★) and vapor (×) flows.

Table 5.4.2. Composition of the deodorizer distillate (%) of soybean oil and the corresponding final oil acidity for different temperatures and pressures [a, b].

Class of compounds	1 mmHg			2.775 mmHg				6 mmHg		
				250 °C						
	242 °C	250 °C	258 °C	242 °C	With entrainment	Without entrainment	258 °C	242 °C	250 °C	258 °C
TAG	7.40	11.62	17.57	4.45	85.08	7.14	11.25	3.24	5.08	7.96
DAG	2.68	3.63	4.68	1.63	0.47	2.27	3.11	1.19	1.62	2.22
MAG	2.27	1.93	1.56	2.55	0.39	2.48	2.28	2.44	2.50	2.49
Squalene	6.91 (74.8%) [c]	6.02 (82.0%)	4.97 (87.7%)	6.68 (43.4%)	1.01 (52.1%)	6.47 (51.8%)	6.04 (60.2%)	5.84 (24.1%)	5.77 (30.1%)	5.64 (36.9%)
β-sitosterol	19.65 (9.0%)	22.33 (12.9%)	24.03 (18.0%)	12.26 (3.4%)	2.52 (5.5%)	14.50 (4.9%)	16.65 (7.0%)	9.03 (1.6%)	10.46 (2.3%)	12.05 (3.3%)
δ-tocopherol	17.12 (19.1%)	18.84 (26.4%)	19.43 (35.3%)	11.20 (7.5%)	2.14 (11.3%)	13.08 (10.8%)	14.76 (15.1%)	8.38 (3.6%)	9.65 (5.2%)	11.02 (7.4%)
FFA	43.96	35.62	27.77	61.22	8.39	54.06	45.90	69.88	64.90	58.62
Distillate (kg/h)	6.70	8.44	10.94	4.02	31.97	4.96	6.17	2.56	3.23	4.04
NOL (%) [d]	0.02	0.03	0.06	0.01	0.06	0.01	0.02	0.004	0.007	0.01
Tocopherol (mg/kg) [e]	1,104	1,004	884	1,260	1,215	1,216	1,157	1,313	1,291	1,261
Oil acidity (%) [f]	0.0029	0.0015	0.0008	0.0137	0.0089	0.0089	0.0055	0.0288	0.0219	0.0158
Ratio AV/SV [g]	0.79	0.69	0.55	0.89	0.09	0.83	0.75	0.92	0.89	0.83

[a] 1.3% of stripping steam. Murphree efficiencies were considered.
[b] Concentration expressed as g/ 100g of distillate, in free basis of water.
[c] The number in parenthesis is the compound recovery in the distillate, expressed in percentage (%).
[d] Neutral oil loss (NOL) calculated in relation to the total oil feed (4,425 kg/h).
[e] Tocopherol content in the deodorized oil.
[f] Expressed as percentage of oleic acid (% C18:1) in the deodorized oil.
[g] Ratio of acid value (AV) to saponification value (SV) (31).

Simulation results (250 °C and 2.775 mmHg, as an example in Table 5.4.2) including entrainment effects led to a considerable increase of NOL values (0.01% to 0.06%), especially of TAG content in the distillate (7.14% to 85.08%, in free basis of water). Walsh et al. (31) explain that a good indication of excess neutral oil in the distillate is the ratio of acid value to saponification value. According to the authors, this parameter should be ≥0.67. Looking at Table 5.4.2, we can see that, in the simulation that considers entrainment, this value is equal to 0.09. As pointed out by Carlson (1), entrainment separators are capable of preventing the mechanical carryover of oil droplets, thereby reducing entrainment losses to less than 0.1%-0.2%. An additional loss by distillation also occurs and is usually lower than 0.1% for non-lauric oils (1). The distillate composition in terms of minor compounds (squalene, tocopherol and β-sitosterol) and their recovery are also expressed in Table 5.4.2. Depending on temperature and pressure conditions, important quantities of tocopherol and β-sitosterol were present in the distillate. As an example, for temperatures greater than 250°C, our simulations showed that, depending on the system pressure, it was possible to recover between 7% and 35% of the initial tocopherol in the distillate. At 242 °C, this value was lower than 20% even at 1 mmHg. For a typical deodorization condition (250 °C and 2.775 mmHg), the tocopherol and sitosterol retentions were 89.2% and 95.1%, respectively. Ahrens (3) reported a tocopherol retention of 76% for soybean oil for the same condition, although the initial content of FFA and tocopherol were different (0.06% and 1,120 mg/kg, respectively). For this simulation, the initial FFA content was 0.07%, and the initial tocopherol content was 1,360 mg/kg, which can explain the relatively higher tocopherol retention.

In general, as the system temperature increased, the deodorizer distillate became richer in TAG, DAG, tocopherol and β-sitosterol. On the other hand, an increase in the system pressure led to a reduction in the fractions of TAG, DAG, tocopherol, and β-sitosterol. A high degree of tocopherol recovery (>20%), which enhances the economical value of the distillate (3), is possible to attain by controlling the deodorization conditions. In general, lowering the system pressure

allowed the recovery of higher concentrations of tocopherol and β-sitosterol in the distillate. Walsh et al (30) indicated that, for optimal tocopherol recovery, temperatures should be above 260°C. To exemplify this statement, we simulated a condition of 2.775 mmHg and 274 °C, with 1.3% of stripping steam. In this case, 27.6% of tocopherol could be recovered in the distillate.

Most of the results presented in Table 5.4.2 do not include losses due to entrainment (or mechanical carryover), but only losses due to distillation. For a better understanding of these two effects, we separated then in Figure 5.4.2. At 250 °C and 2.775 mmHg, vaporization was the main cause of squalene, tocopherol and β-sitosterol losses. On the other hand, almost all NOL was due to entrainment.

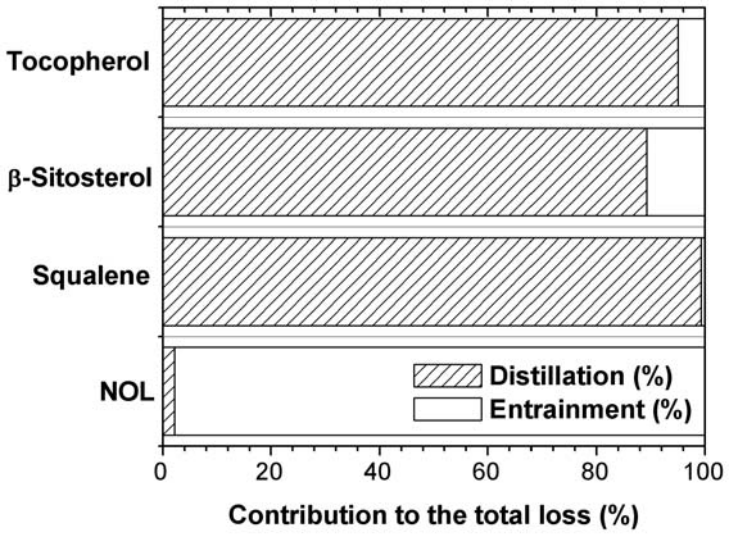

Figure 5.4.2. Contribution of distillative and entrainment effects to the total loss of neutral oil (NOL), squalene, β-sitosterol and tocopherol at 2.775 mmHg, 250 °C and 1.3% of stripping steam.

In relation to deodorizer distillate composition, our simulations showed that, apart from the temperature and pressure effects, TAG, DAG, MAG and FFA contents ranged from 3.2% to 17.6%, from 1.2% to 4.7%, from 1.6 to 2.6%, and from 27.8 to 69.9%, respectively. For squalene, β-sitosterol and tocopherol contents, the ranges within the distillate were from 5.0% to 6.9%, from 9.0% to 24.0%, and from 8.4% to 19.4%, in that order. In the GC analysis of two different deodorizer distillate samples of soybean oil, Verleyen et al. (4) found the following

composition: 5.1% and 5.9% of TAG, 2.7% and 3.8% of DAG, 1.2% and 1.9% of MAG, 32% and 33% of FFA, 1.3% and 2.1% of squalene, 7.9% and 8.3% of sitosterol, and 16.5% and 18.0% of tocopherols. Roughly, these results fit between the ranges obtained from our simulations, except for squalene. Even though the conditions selected for our work (see Table 5.4.1) covered a common range of operating pressures and temperatures, some combinations might be not usual (258 °C and 1 mmHg, or 242°C and 6 mmHg). For example, in our simulations the highest concentration of acylglycerols (TAG, DAG and MAG) in the distillate was obtained at the condition of 258 °C and 1 mmHg, but in industrial practice this temperature would be combined with a pressure nearer to 5 mmHg (31). Note also that, in this case, the ratio of acid value to saponification value is equal to 0.55, which indicates excess neutral oil in the distillate (31). However, this first comparison permits one to observe that our deodorizer modeling gave satisfactory results. In particular, in the case of tocopherol content in the deodorized oil, a very good comparison can be made with the work of Maza et al. (16).

Maza et al. (16) studied the effect of deodorization parameters (temperature and oil flow rate) on tocopherol retention using response surface methodology (RSM), which allowed the development of a equation (Eq. 5.4.1) correlating this important quality factor to process conditions (oil flow rate and temperature). In their work, a plant continuous deodorizer was used. Table 5.4.3 shows the values reported by Maza et al. (16) and the results of our simulations. The estimated values using their equation are also shown. It is important to highlight that Equation 5.4.1 is valid for any combination in the range of temperatures and oil flow rates studied.

$$TOCO_r(\%) = 821.255 - 12.840 \cdot r - 1.569 \cdot t + 0.028 \cdot t \cdot r \quad R^2 = 0.997 \qquad [5.4.1]$$

where: $TOCO_r$ (%) is the tocopherol retention, r is the oil throughput rate (1,000 lb/h) and t is the deodorization temperature (°F).

Table 5.4.3. Effects of deodorization conditions on final oil acidity and tocopherol retention in soybean oil

	Experimental results from Maza et al. (16)					
Temperature	475 °F (246.1 °C)		488 °F (253.3°C)		500 °F (260°C)	
Oil flow rate	40,000 lb/h (18,144 kg/h)	50,000 lb/h (22,680 kg/h)	45,000 lb/h (20,411 kg/h)	45,000 lb/h	40,000 lb/h	50,000 lb/h
Tocopherol (mg/kg)	1,150	1,190	1,110	1,120	1,000	1,130
Tocopherol retention (%)	84.6	87.5	81.6	82.4	73.5	83.1
Tocopherol retention (%) [b]	94.4	99.0	92.8	92.8	83.2	94.8
Oil acidity [c](%)	0.020	0.024	0.018	0.018	0.014	0.017

	Simulation results from this work [a]								
Temperature	475			488			500		
Oil flow rate (1,000 lb/h)	40	45	50	40	45	50	40	45	50
Tocopherol (mg/kg)	1,220	1,235	1,247	1,169	1,188	1,204	1,108	1,133	1,153
Tocopherol retention (%)	89.7	90.8	91.7	86.0	87.3	88.5	81.5	83.3	84.8
Tocopherol retention (%) [b]	94.4	96.7	99.0	88.8	92.8	96.9	83.2	89.0	94.8
Oil acidity [c](%)	0.009	0.011	0.012	0.006	0.007	0.008	0.004	0.004	0.005

[a] Murphree efficiencies were considered.
[b] Estimated using the equation of Maza et al. (16), see Equation 5.4.1. Initial tocopherol content of 1,360 mg/kg.
[c] Expressed as percentage of oleic acid (% C18:1) in the deodorized oil.

As one can see in Table 5.4.3, there is a very good agreement between the experimental values for tocopherol content from Maza et al. (16) and our work. The greatest difference was equal to 108 mg/kg (40,000 lb/h and 500 °F) whereas the lowest difference was of only 23 mg/kg (50,000 lb/h and 500 °F), corresponding to 10.1% and 2.0% of deviation, respectively. In general, very good tocopherol retention values were achieved by Maza et al. (16).

Our simulations always gave higher values than the experimental ones, although they were not so high as the ones calculated using Equation 5.4.1 suggested by Maza et al. (16). Since Equation 5.4.1 was obtained from a statistical procedure (RSM), it is possible to say that there was no significant difference between our tocopherol levels and theirs. We should highlight that, for the simulation results of Table 5.4.3, all processing conditions (P, T and %steam) and

initial concentrations of tocopherol in the oil to be deodorized were given by Maza *et al.* (16). In this way, our simulation program was capable of reproducing them faithfully and generating agreeable results. In case of final FFA content, our work has generated lower values. One possible explanation is the absence of hydrolytic reactions. Nevertheless, it is noteworthy that only one value (500°F and 40,000 lb/h) was lower than 0.005%, which was taken as the minimum final FFA level when steam was used for stripping (1). In general, both tocopherol and FFA content decreased with temperature (became more volatile) and increased with oil flow rate. From a statistical analysis of the results of Table 5.4.3, it was possible to conclude that temperature had the main effect on tocopherol retention in the oil, which is in accordance with the work of Walsh et al. (31).

To further show the applicability of our methodology, we investigated the deodorization of canola oil, which differs from soybean and wheat germ oil due to its high content of oleic acid (61%, see Table 5.3.1). The simulation results for the deodorizer distillate composition were compared with the work of Verleyen et al. (4). The authors reported two different results for the composition of deodorizer distillates from canola oil (shown in parenthesis in the next sentence). At 240 °C and 4 mmHg with 1.3% of stripping steam, the distillate (in free basis of water) contained 6.5% of β-sitosterol (4.0% and 6.2%), 4.1% of tocopherol (3.7% and 4.2%), 2.1% of MAG (1.4% and 2.1%), 2.2% of DAG (3.8% and 3.9%) and 2.8% of TAG (3.0% and 7.5%). Verleyen et al. (4) called attention to the strong relation linking tocopherol and sterol contents in the deodorizer distillate, the initial FFA content in the oil, and the deodorization process conditions applied (including temperature, steam rate and pressure). We explored our simulation tool to investigate these relations. Reducing the initial FFA content, from 0.1% to 0.05% while maintaining the concentrations of other minor compounds (see Table 5.3.1) and the aforementioned processing conditions (240 °C, 4 mmHg, and 1.3% of stripping steam) increased the content of β-sitosterol and tocopherol, in the distillate, to 11.0% and 7%, respectively. The same behavior occurred when increasing the steam rate to 2% (4 mmHg and 240 °C, initial concentrations as in

Table 5.3.1). In this case, the content of β-sitosterol and tocopherol in the distillate rose to 8.0% and 5.1%, respectively.

Because our simulation program permitted the investigation of different flow patterns, we studied the effect of countercurrent (Figure 5.2.1B) and cross-flow (Figure 5.2.1A) configurations on the composition of the product streams. At 250 °C, 1.3% of stripping steam and 2.775 mmHg, the main differences encountered were in the final oil acidity and tocopherol content. In comparison with the values found for the cross-flow deodorizer (see Table 5.4.2), the countercurrent deodorizer generated a lower level of FFA (0.0028%), which was three times less, and a superior tocopherol content (1,361 mg/kg), which was 12% higher. Even with the bottom pressure almost twice the top pressure (due to the pressure drop), irrelevant changes were generated in the distillate composition. These differences could be due to column configuration (cross-flow and countercurrent) and/or pressure drop. However, as shown in Table 5.4.4, when the pressure drop in the countercurrent pattern was not considered, an even lower final acidity was generated whereas NOL and tocopherol values were not affected.

On the subject of the VLE approach adopted in this work, a careful analysis of the calculated values of ϕ_i^{sat}, ϕ_i and POY for all components, including water, was done to explain the use of vapor phase nonidealities even at very low pressures. ϕ_i^{sat} values differentiated considerably from unity $\left(\phi_i^{sat} < 0.89\right)$ for water, whereas ϕ_i and POY values were virtually one (>0.997) for all components in the system. This was a consequence of the high values of water vapor pressures calculated at the high temperatures observed in the deodorizer. The vapor pressure was a parameter that was used in the calculation of ϕ_i^{sat}. For simplification, it is possible to consider ϕ_i and POY as equal to one, and ϕ_i^{sat} only for water in the calculation of the VLE.

Table 5.4.4. Comparison between cross-flow and countercurrent flow in multitray deodorizers.

	2.775 mmHg and 250 °C		
Quality	Cross-flow (Figure 5.2.1A)	Countercurrent flow (Figure 5.2.1B)	
		With pressure drop [a]	Without pressure drop
Oil acidity (%)	0.0088	0.0028	0.0017
Tocopherol in the oil (mg/kg)	1,216	1,361	1,361
NOL (%)	0.01	0.02	0.02
Distillate (kg/h)	4.96	3.97	4.17

[a] Bottom pressure of 4.775 mmHg. For other abbreviations, see Table 5.4.2.

The main effect related to the inclusion of Murphree efficiencies within the deodorizer was the increase in the final oil acidity. In this case, more stages would have been necessary to achieve the same final content. This is in accordance with the definition of Murphree efficiency, i.e. that as it approaches unity, the mass transfer of the oil components (FFA, for example) from the liquid to the vapor phase is more efficient, depleting their concentration in the oil.

For wheat germ oil deodorization, we were able to make a qualitative comparison with the experimental work of Wang and Johnson (5), using the configuration from Figure 5.2.1B and the processing conditions given at Table 5.4.1. The simulation results indicate that at 200 °C, there were 2,454 mg/kg and 2,431 mg/kg of tocopherol in the oil deodorized at 25 and 10 mL/min of oil flow rate, respectively. At 250°C, these values were 2,230mg/kg and 1,874 mg/kg, in that order. The oil flow rate (related with residence time) did not affect tocopherol content considerably for lower temperatures but had an important effect at higher ones. Both temperature and oil flow rate had an impact on the final oil acidity. At 25 mL/min, the increase in temperature, from 200 to 250 °C, changed the final FFA content from 0.120% to 0.001%. At 10 mL/min, this change was even greater. For the conditions studied, the tocopherol reduction varied from 0.6% (200 °C and 25 mL/min) to 24.1% (250 °C and 10 mL/min). NOL values increased with temperature and decreased with oil flow rate (2.05% for 10 mL/min and 250°C, and 0.62% for 25 mL/min and 200 °C). Because the complete oil

composition used as feed stream in some of the deodorization experiments performed by Wang and Johnson (5) was not available, a quantitative comparison was not possible. But from a qualitative point of view, they also found that to reduce FFA efficiently while maintaining the tocopherol in the oil, it is better to use lower temperatures and oil flow rates.

The multicomponent stripping column modeling proposed in this work permitted the simulation of oil-refining processes performed under vacuum at high temperatures, as deodorization and deacidification by steam refining. Despite the good agreement with experimental results, some limitations should be considered. Our modeling needs several physical properties to describe enthalpy balances and equilibrium relationships, in combination with methods to estimate entrainment and Murphree efficiencies. Some of the required properties are often difficult to determine experimentally because of the complexity of the mixture, diversity of compounds and range of operating conditions (high temperatures, for example). To overcome this limitation, we adopted shortcuts, such as the use of predictive methods for the cases where empirical equations were not available, and the application of methods developed for other kind of industry equipments to deodorizers (entrainment and Murphree efficiency, for example). We should highlight that the procedures and methods selected for estimating physical properties and other process parameters play an important role in the calculations i.e., there is a direct relation between the predictive capacity of the selected methods and the results given by the simulation program. Further improvements, specially concerning the estimation methods for entrainment and Murphree efficiencies for deodorizers, might enhance the applicability of this simulation tool in the edible oil industry. Also, chemical reaction effects, as FA generation (from hydrolysis of acylglycerols) and FA isomerization, were not considered and have an impact in the final results (oil acidity, for example). Such aspects should be included in a future work.

With the tools provided by Ceriani and Meirelles (10), phase equilibria can be rigorously calculated. The software developed in the present work takes into

account the detailed oil composition and includes Murphree efficiencies and entrainment effects, so it can be used to analyze the effect of possible operating conditions, and help guiding industrial and experimental works. Despite the necessary shortcuts that must be done, process simulation, together with experimental work and industrial knowledge, can lead to an efficient process development and optimization.

Acknowledgements

The authors wish to acknowledge FAPESP (Fundação de Amparo à Pesquisa do Estado de São Paulo – 03/04949-3) and CNPq (Conselho Nacional de Desenvolvimento Científico e Tecnológico – 521011/95-7) for the financial support. The authors also thank Prof. Dr. Tong Wang who contributed with important information about her work.

Appendix I: Equations for the continuous multitray countercurrent flow design

For an arbitrary stage *n* of a stripping column, the related nomenclature can be set as follows.

Subscript *n*: flow from stage *n, n* =1, 2, …, *NS*; subscript *i*: component *i, i* =1, 2, …, *NC; H* = vapor phase enthalpy (J/h); *h* = liquid phase enthalpy (J/h); h_f = liquid feed enthalpy (J/h); H_f = vapor feed enthalpy (J/h); *V* = total vapor flow (mol/h); *v* = component vapor flow (mol/h); *L* = total liquid flow (mol/h); *l* = component liquid flow (mol/h); *f* = component feed flow as liquid (mol/h); *F* = component feed flow as vapor (mol/h).

For each stage *n*, a set of dependent relationships (test functions $F_{k(n,i)}$) must be satisfied. In the equations below, the entrainment term (e_n) is already introduced.

Component Balances (Total: *NS* x *NC* relations)

$$F_{1(n,i)} = l_{n,i} + v_{n,i} + V_n \cdot e_n \cdot \frac{l_{n,i}}{L_n} - v_{n-1,i} - V_{n-1} \cdot e_{n-1} \cdot \frac{l_{n-1,i}}{L_{n-1}} - l_{n+1,i} - f_{n,i} - F_{n,i} = 0 \qquad [A1]$$

Enthalpy Balances (Total: *NS* relations)

$$F_{2(n)} = h_n + H_n + e_n \cdot V_n \cdot \frac{h_n}{L_n} - H_{n-1} - e_{n-1} \cdot V_{n-1} \cdot \frac{h_{n-1}}{L_{n-1}} - h_{n+1} - h_{f,n} - H_{f,n} = 0 \qquad [A2]$$

Equilibrium conditions derived from the definitions of the vapor-phase Murphree plate efficiency, $\eta_{n,i}$ (Total: *NS* x *NC* relations)

$$F_{3(n,i)} = \eta_{n,i} \cdot K_{n,i} \cdot V_n \cdot \frac{l_{n,i}}{L_n} - v_{n,i} + (1 - \eta_{n,i}) \cdot v_{n-1,i} \cdot \frac{V_n}{V_{n-1}} = 0 \qquad [A3]$$

The above relationships comprise a vector of test functions

$$\mathbf{F(x)} = \{\mathbf{F_1}; \mathbf{F_2}; \mathbf{F_3}\} = 0 \qquad [A4]$$

which contains *NS* (2*NC* + 1) elements, and which may be solved for equally many unknowns

$$\mathbf{x} = \{\mathbf{l}; \mathbf{v}; \mathbf{T}\} \qquad [A5]$$

where the vector **l** contains all the elements $l_{n,i}$, **v** all the elements $v_{n,i}$ and **T** all elements T_n.

Once $l_{n,i}$, $v_{n,i}$ and T_n are known, the product compositions, the product flow rates, the concentration, and temperature profiles in the column follow readily. The iterative Newton-Raphson method solves Equation A4 using the prior set of values of the independent variables (Eq. A5). A first estimative is necessary to initiate the calculations.

Appendix II: Equations for the continuous multitray cross-flow design

Component Balances (Total: *NS* x *NC* relations)

$$F_{1(n,i)} = l_{n,i} + v_{n,i} + V_n \cdot e_n \cdot \frac{l_{n,i}}{L_n} - l_{n+1,i} - f_{n,i} - F_{n,i} = 0 \qquad [A6]$$

Enthalpy Balances (Total: *NS* relations)

$$F_{2(n)} = h_n + H_n + e_n \cdot V_n \cdot \frac{h_n}{L_n} - h_{n+1} - h_{f,n} - H_{f,n} = 0 \qquad [A7]$$

Equilibrium conditions derived from the definitions of the vapor phase Murphree plate efficiency, $\eta_{n,i}$ (Total: *NS* x *NC* relations)

$$F_{3(n,i)} = \eta_{n,i} \cdot K_{n,i} \cdot V_n \cdot \frac{l_{n,i}}{L_n} - v_{n,i} + (1 - \eta_{n,i}) \cdot V_n \cdot \frac{F_{n,i}}{\sum_i F_{n,i}} = 0 \qquad [A8]$$

References

[1] Carlson, K.F., Deodorization, in *Bailey's Industrial Oil and Fat Products*, 5th edn., edited by Y.H. Hui, Wiley-Interscience, New York, 1996, Vol.4, pp. 339-390.

[2] Woerfel, J.B., Soybean Oil Processing Byproducts and their Utilization, in *Practical Handbook of Soybean Processing and Utilization,* edited by D.R. Erickson, AOCS, Champaign, 1995, pp. 306-313.

[3] Ahrens, D., Comparison of tray, thin-film deodorization, *Inform* 9: 566-576 (1998).

[4] Verleyen, T., R. Verhe, L. Garcia, K. Dewettinck, A. Huyghebaert, and W. De Greyt, Gas Chromatographic Characterization of Vegetable Oil Deodorization Distillate, *J. Chromatogr. A*. 921: 277-285 (2001).

[5] Wang, T., and L.A. Johnson, Refining High-Free Fatty Acid Wheat Germ Oil, *J. Amer. Oil Chem. Soc.* 78: 71-76 (2001).

[6] Naphtali, L.M., and D.P. Sandholm, Multicomponent separation calculations by linearization, *AIChe J.,*17: 148-153 (1971).

[7] Pryde, E.H. Composition of Soybean Oil in *Practical Handbook of Soybean Processing and Utilization,* edited by D.R. Erickson, AOCS, Champaign, 1995, pp. 13-31.

[8] Firestone D., *Physical and Chemical Characteristics of Oils, Fats and Waxes*, AOCS Press, Champaign, 1999, 152pp.

[9] Balchen, S., R. Gani, and J. Adler-Nissen, Deodorization Principles, *Inform.* 10: 245-262 (1999).

[10] Ceriani, R., and A.J.A. Meirelles, Predicting Vapor-Liquid Equilibria of Fatty Systems. *Fluid Phase Equilib.*, 215, 227-236 (2004).

[11] Fornari, T., S. Bottini, and E. A. Brignole, Application of UNIFAC to Vegetable Oil-Alkane Mixtures, *J. Am. Oil Chem. Soc*. 71: 391-395 (1994).

[12] Antoniosi Filho, N.R., O. L. Mendes, F.M. Lanças, Computer prediction of triacilglicerol composition of vegetable oils by HRGC, *J. Chromatogr.*, 40: 557-562 (1995).

[13] Rabelo, J., E. Batista, F.W. Cavaleri, and A.J.A. Meirelles, Viscosity Prediction for Fatty Systems. *J. Amer. Oil Chem. Soc.,* 77: 1255-1261 (2000).

[14] Ceriani, R., and A.J.A. Meirelles, Simulation of Batch Physical Refining and Deodorization Processes, *J. Amer. Oil Chem. Soc.* 81: 305-312 (2004).

[15] Petrauskaitè, V., W.F. De Greyt, and M.J. Kellens, Physical Refining of Coconut Oil: Effect of Crude Oil Quality and Deodorization Conditions on Neutral Oil Loss, *J. Am. Oil Chem. Soc*. 77: 581-586 (2000).

[16] Maza, A., R.A. Ormsbee, and L.R. Strecker, Effects of Deodorization and Steam-Refining Parameters on Finished Oil Quality, *J. Am. Oil Chem. Soc*. 69: 1003-1008 (1992).

[17] Barnes, P.J., Lipid Composition of Wheat Germ and Wheat Germ Oil, *Fette Seifen Anstrichmittel*, 84: 256-268 (1982).

[18] Eskin, N.A.M., B.E. McDonald, R. Przybylski, L.J. Malcolmson, R. Scarth, T. Mag, K. Ward, and D. Adolph, Canola Oil, in *Bailey's Industrial Oil and Fat Products*, 5th edn., edited by Y.H. Hui, Wiley-Interscience, New York, 1996, Vol.2, pp. 1-95.

[19] Reid R. C., J.M. Prausnitz., and B.E. Poling, *The Properties of Gases and Liquids*, McGraw-Hill, New York, 1987.

[20] Tu, C.H., and C.P. Liu, Group-contribution estimation of the enthalpy of vaporization of organic compounds, *Fluid Phase Equilib.*, 121:45-65 (1996).

[21] DIPPR Student Chemical Database Login, http://dippr.byu.edu/students/ chemsearch.asp (accessed April. 2003).

[22] Voutsas, E., M. Lampadariou, K. Magoulas, and D. Tassios, Prediction of Vapor Pressures of Pure Compounds from Knowledge of the Normal Boiling Point Temperature, *Fluid Phase Equilib.*, 198: 81-93 (2002).

[23] Retzekas, E. E. Voutsas, K. Magoulas, and D. Tassios, Prediction of Physical Properties of Hydrocarbons, Petroleum and Coal Liquid Fractions, *Ind. Eng. Chem. Res.*, 41: 1695-1702 (2002).

[24] Elbro, H.S., A. Fredenslund, P. Rasmussen, Group Contribution Method for the Prediction of Liquid Densities as a Function of Temperature for Solvents, Oligomers and Polymers, *Ind. Eng. Chem. Res.*, 30: 2576-2582 (1991).

[25] Bokis,C.P., C.C. Chen, and H. Orbey, A Segment Contribution Method for the Vapor Pressure of Tall-oil Chemicals, *Fluid Phase Equilib.*, 155: 193-203 (1999).

[26] Ludwig, E.E., *Applied Process Design for Chemical and Petrochemical Plants*, 3rd edn., GPC, Houston. 1995, Vol. 2, pp. 42-44.

[27] MacFarland, S.A., P.M. Sigmund, and M. Van Winkle, Predict Distillation Efficiency, *Hydrocarbon Process.* 51: 111-114, (1972).

[28] Halvorsen, J.D., W.C. Mammel, and L.D. Clements, Density Estimation for Fatty Acids and Vegetable Oils based on their Fatty Acid Composition, *J. Amer. Oil Chem. Soc.*, 70: 875-880 (1993).

[29] Stage, H., The Physical Refining Process, *J. Amer. Oil Chem. Soc.,* 62: 299-307 (1985).

[30] Brekke, O.L., Deodorization, in *Handbook of Soy Oil Processing and Utilization*, 4th edn., edited by D.R. Erickson, E.H. Pryde, O.L. Brekke, T.L. Mounts, and R.A. Falb, AOCS, Champaign, 1980, pp. 155-191.

[31] Walsh, L., R.L. Winters, and R.G. Gonzalez, Optimizing Deodorizer Distillate Tocopherol Yields, *Inform,* 9: 78-83 (1998).

CAPÍTULO 6. SIMULATION OF PHYSICAL REFINERS FOR EDIBLE OIL DEACIDIFICATION

Roberta Ceriani and Antonio J. A. Meirelles

Trabalho aceito para publicação na revista **Journal of Food Engineering.**

Abstract

Physical refining, also known as deacidification by steam distillation, is a process in which free fatty acids and other volatile compounds are distilled off from the oil, using an effective stripping agent (usually steam) and suitable processing conditions. In general, vegetable oils are formed by triacylglycerols, free fatty acids, partial acylglycerols and some minor compounds, constituting a complex mixture.

This work presents the implementation of a simulation program applied to the physical refining of edible oils, following a multicomponent stripping tray-column design. Two singular vegetable oils, from palm and coconut, were selected. Their entire compositions were considered within the simulations, including acylglycerols and free fatty acids. To describe the required physical properties, group contribution methods and empirical equations were selected. The results were analyzed and compared with the literature in terms of neutral oil loss and final oil acidity, as a function of the processing conditions. Murphree efficiencies and entrainment were considered for each plate.

Key words

Simulation, multicomponent-stripping column, physical refining, vegetable oils, vapor-liquid equilibria, distillative neutral oil loss, Murphree efficiency, and entrainment.

6.1. Introduction

The physical refining process has been under interest and research, as a suitable alternative for the caustic refining process (Hodgson, 1996; Stage, 1985; Tandy & McPherson, 1984). In the case of palm oil, it practically replaced the use of chemical refining (Hodgson, 1996), as a consequence of the high acidity of this oil. The effect of the processing parameters in the final products (refined oil and distillate) has also been widely studied by many authors (Verleyen, Verhe, Garcia,

Dewettinck, Huyghebaert & De Greyt, 2001; Petrauskaité, De Greyt & Kellens, 2000; Maza, Ormsbee & Strecker, 1992).

Physical refining of vegetable oils is based on the higher volatility of free fatty acids (FFA) compared with triacylglycerols (TAG) at the processing conditions (high temperatures and low pressures). Throughout the process, complex chemical and physical phenomena do occur, and their main physical effects are the vaporization of volatile compounds and the entrainment or mechanical carry-over of neutral oil droplets within the stripping steam (Maza et al., 1992). Hydrolysis of TAG is one of the chemical reactions, and its importance is related to the generation of FFA during the physical refining process. Nevertheless, the hydrolysis reaction has only a slight influence on the final product quality. According to Carlson (1996), the final FFA content can be reduced to a value not lower than 0.005% due to the hydrolysis effect, but such value is very low if compared with the limit required (0.3% w/w) by the Codex Alimentarius (1999).

Besides the loss of neutral oil due to entrainment, there is also a distillative loss, caused by the vaporization of an acylglycerol part from the oil, known as neutral oil loss (NOL) (Verleyen et al., 2001; Petrauskaitè et al., 2000). As highlighted by some authors (Ceriani & Meirelles, 2004a; Petrauskaitè et al., 2000), this loss is determined mainly by the distillation of monoacylglycerols (MAG) and diacylglycerols (DAG).

In addition to the high FFA content of coconut and palm oils, which is an indicative for the use of physical refining (Tandy & McPherson, 1984), both oils have singular compositions. Coconut oil typifies lauric oils, with its high level of short-chain fatty acids (FA) and low unsaturation (Petrauskaitè et al., 2000), while palm oil is rich in palmitic and monounsaturated FA (Firestone, 1999).

Computer simulation has been used in the investigation of some traditional processes of the food industry, as batch steam refining of coconut oil (Ceriani & Meirelles, 2004a), continuous deodorization of a selection of mono- and polyunsaturated vegetable oils (Ceriani & Meirelles, 2004c), and whisky manufacture (Gaiser, Bell, Lim, Roberts, Faraday, Schulz & Grob, 2002). The good

performance of the simulation programs developed in these works emphasizes the applicability of this kind of tool for complex systems. Ceriani & Meirelles (2004c) compared with success the tocopherol retention in soybean oil submitted to deodorization in industrial scale equipments (18,000 to 23,000 kg/h) following data from Maza et al. (1992). Unfortunately, we found few experimental data for continuous physical refining of coconut and palm oils. One of interest was given by Chu, Baharin, Quek & Man (2003) about the content of fatty compounds in the palm fatty acid distillate (PFAD): 85% of FFA and 13.7% of acylglycerols. Some feasible comparison with this work was done along the text.

This work presents the implementation of a simulation program, developed with MatLab®, for a multicomponent-stripping column applied to the physical refining of edible oils. The vapor-liquid equilibria (VLE) of these fatty systems were described by a group contribution equation for vapor pressures (Ceriani & Meirelles, 2004b) and the UNIFAC model for activity coefficients (Ceriani & Meirelles, 2004b; Fornari, Bottini & Brignole, 1994; Reid, Prausnitz & Poling, 1987). The entire oil composition in terms of fatty compounds (TAG, DAG, MAG and FFA) was considered within the simulations in order to analyze losses of neutral oil due to vaporization and entrainment during physical refining. Acidity generation (from hydrolysis of acylglycerols) was not considered at this time and should be included in a future work. According to Ruiz-Méndez, Márques-Ruiz & Dobarganes (1996), hydrolysis can be avoided using nitrogen as the stripping gas. Economics aspects would dictate this choice.

6.2. Modeling a continuous physical refiner

As described by Ahrens (1998), an industrial continuous physical refiner is based on a series of steam-agitated vertical trays stacked in a cylindrical shell. In this equipment, the oil is refined by flowing over a series of four to five trays (Stage, 1985), wherein the intimate contact with the stripping steam is achieved. The refined oil is collected at the bottom (first stage) of the equipment (Balchen, Gani & Adler-Nissen, 1999). It is interesting to note that two feasible flow patterns

are used industrially: countercurrent flow (CCF, Figure 6.2.1A) and cross-flow (CRF, Figure 6.2.1B). Tray physical refiners are usually designed in CRF while thin-film equipments are based in the countercurrent contact between gas and oil (Balchen, Gani & Adler-Nissen, 1999). In this work, we compared the performance of both column configurations. In a previous work, Ceriani & Meirelles (2004c) simulated the deodorization of soybean and canola oils in CRF tray deodorizers.

The multicomponent-stripping column modeling proposed in this work was based on the method described by Naphtali & Sandholm (1971) and the computational program was developed in MatLab®. The general equations, which include material- and energy balances and Murphree efficiencies coupled with vapor-liquid equilibrium relationships, are described separately for CRF and CCF configurations in the Appendixes I and II.

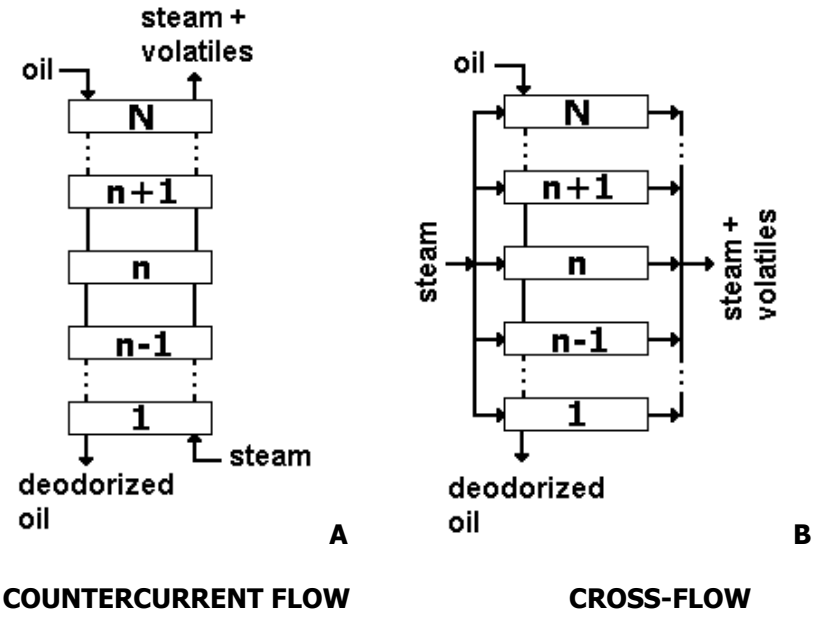

Figure 6.2.1. Schematic flow diagram of a continuous tray design: (a) in countercurrent flow, and (b) in cross-flow.

This method uses Newton-Raphson as the iterative procedure for simultaneous convergence until the true values of $l_{n,i}$ (the component liquid molar flow), $v_{n,i}$ (the component vapor molar flow) and the temperature T are found. Input data to the calculations were as follows:

- Identification and division of the mixture components in usual groups, according to each group contribution method selected.
- Data bank with parameters for model UNIFAC (Fornari et al., 1994; Reid et al., 1987) and for predictive equations for critical properties (Reid et al., 1987), second virial coefficients (Reid et al., 1987), vapor pressures (Ceriani & Meirelles, 2004b; DIPPR, 2003) and enthalpies (DIPPR, 2003; Tu & Liu, 1996; Reid et al., 1987).
- Specification of the processing variables: number of stages, Murphree efficiencies, feed location and composition, feed flow rates and thermal states, and column pressure.
- Initial estimation for the total molar flow rates for each stage and for the temperature profile.

6.2.1 Vapor-liquid equilibria

Physical refining is essentially a mass transfer process and therefore its VLE has to be described. To calculate the VLE, for each compound in each tray, the thermodynamic approach of Ceriani & Meirelles (2004b) was applied. The VLE model adopted in this work is shown below:

$$k_i = \frac{y_i}{x_i} = \frac{\gamma_i \cdot f_i^o}{P \cdot \phi_i} \tag{6.2.1.1}$$

where

$$f_i^o = P_i^{vp} \cdot \phi_i^{sat} \cdot \exp\left(\frac{V_i^L \cdot \left(P - P_i^{vp}\right)}{R \cdot T}\right) \tag{6.2.1.2}$$

where f_i^o is the standard-state fugacity, x_i and y_i are the molar fractions of component i in the liquid and vapor phases, respectively, P is the total pressure, R is the gas constant, T is the system absolute temperature, P_i^{vp} and ϕ_i^{sat} are, respectively, the vapor pressure and the fugacity coefficient of the pure component i, γ_i is the activity coefficient, ϕ_i is the fugacity coefficient and V_i^L is the liquid molar volume of component i. The exponential term in Equation 6.2.1.2

corresponds to the Poynting factor (POY). As explained in the Appendixes, these correlations are valid for each stage *n*, corrected by the Murphree efficiency. The vapor pressure P_i^{vp} and the activity coefficient γ_i are calculated for each fatty compound using, respectively, the group-contribution approach developed by Ceriani & Meirelles (2004b) and the UNIFAC model. As confirmed by previous works (Ceriani & Meirelles, 2004b; Fornari et al., 1994), UNIFAC r ¾ is more suitable in the prediction of VLE of fatty mixtures.

6.2.2 Estimation of oil composition and physical properties

Crude vegetable oils are formed by TAG, DAG and MAG, in addition to a variety of other minor compounds. This work is specifically concerned with the behavior of fatty components (FA and acylglycerols) within the physical refining process. To estimate the entire composition of palm and coconut oils in terms of TAG, the methodology suggested by Antoniosi Filho, Mendes & Lanças (1995), which is based in a statistical procedure, was used. The TAG compositions were estimated from the FA compositions, considering a percentage of trisaturated TAG: 7.9% for palm oil (Chuan Ho, 1976) and 84% for coconut oil (Theme, 1968) approximately. The compositions in DAG and MAG were obtained from the estimated TAG composition in the following way: each TAG was split into 1,2- and 1,3- DAG; each DAG was then split into MAG following the stoichiometric relations of the prior compounds. This procedure was already applied successfully by Ceriani & Meirelles (2004a and 2004c).

In order to enhance our analyses, two different compositions for each oil (one more volatile, MV, rich in short-chain fatty acids, and other less volatile, LV, rich in long-chain fatty acids), were selected using the concentration ranges given by Firestone (1999). Table 6.2.2.1 brings some relevant aspects on the composition of the oils selected. For the sake of simplicity, Table 6.2.2.2 gives the complete composition for each class of fatty compounds just for the more volatile palm oil (MVPO).

Table 6.2.2.1. Simplified composition of palm and coconut oils.

Fatty acid		Palm Oil				Coconut Oil			
Formula	Trivial name (abbreviation)	More Volatile (MVPO)		Less Volatile (LVPO)		More Volatile (MVCO)		Less Volatile (LVCO)	
		Mass (%)		Mass (%)		Mass (%)		Mass (%)	
C6:0	Caproic (Co)	---		---		0.60		---	
C8:0	Caprilic (Cp)	---		---		9.40		4.60	
C10:0	Capric (C)	---		---		7.80		5.50	
C12:0	Lauric (L)	1.00		0.10		48.20		43.00	
C14:0	Miristic (M)	1.50		0.90		16.80		20.60	
C16:0	Palmitic (P)	46.40		41.80		7.70		10.20	
C16:1	Palmitoleic (Po)	0.30		0.10		---		---	
C18:0	Stearic (S)	4.20		5.10		2.30		3.50	
C18:1	Oleic (O)	37.30		40.70		5.60		9.90	
C18:2	Linoleic (Li)	9.10		10.0		1.50		2.10	
C18:3	Linolenic (Ln)	---		0.60		0.05		0.20	
C20:0	Arachidic (A)	0.20		0.70		---		0.20	
C20:1	Gadoleic (G)	---		---		0.05		0.20	
Class of compounds		Mass (%)	*M* g/gmol	Mass (%)	*M* g/gmol	Mass (%)	*M* g/gmol	Mass (%)	*M* g/gmol
TAG		88.25	839.76	91.99	847.71	93.75	645.21	93.61	682.50
DAG		7.75 [a]	585.36	5.34 [a]	590.09	3.00 [b]	442.28	3.00 [b]	476.12
MAG		0.51 [a]	338.68	0.44 [a]	340.11	1.00 [b]	267.21	1.00 [b]	283.92
FFA		3.49	267.68	2.23	270.34	2.25	202.67	2.39	241.92
Molecular weight		752.33		786.41		596.55		630.91	
Iodine Value (IV)		48.12		53.99		7.58		12.83	
IV ranges [c]		49-55				5-13			

[a] From Chuan Ho (1976).; [b] From Loncin (1962).; [c] From Firestone (1999).

Table 6.2.2.2. Complete estimated composition of the more volatile palm oil (MVPO)

TAG					DAG			
Group [b]	Major TAG	*M* [a] (g/gmol)	Mass (%)	Mole (%)	Acylglycerol compound	*M* [a] (g/gmol)	Mass (%)	Mole (%)
44:0	LPP	750	0.41	0.46	LM-	484	0.04	0.04
46:0	MPP	778	0.59	0.64	LP-	512	1.33	1.52
48:0	PPP	806	5.11	5.32	MP-	540	2.28	2.47
50:0	PPS	834	1.28	1.29	PP-	568	23.43	24.15
52:0	PSS	862	0.16	0.16	PS -	596	3.75	3.68
44:1	LOM	748	0.08	0.08	PA-	624	0.35	0.33
46:1	LOP	776	1.79	1.94	LO-	538	1.10	1.20
48:1	MOP	804	2.78	2.91	MO-	566	1.68	1.74
50:1	POP	832	33.73	34.04	PO-	594	46.37	45.69
52:1	POS	860	5.66	5.52	SO-	622	1.73	1.63
54:1	POA	888	0.49	0.46	AO-	650	0.04	0.04
46:2	LLiP	774	0.44	0.48	LLi -	536	0.35	0.38
48:2	MLiP	802	1.09	1.14	MLi	564	0.78	0.81
50:2	PLiP	830	9.19	9.30	PLi -	592	10.77	10.65
52:2	POO	858	19.32	18.90	OO-	620	4.50	4.25
54:2	SOO	886	1.63	1.54	OLi -	618	1.50	1.42

Table 6.2.2.2. Continuação

56:2	OOA	914	0.07	0.07	MAG			
48:3	LOLi	800	0.23	0.24	L--	274	1.27	1.57
50:3	MOLi	828	0.38	0.39	M--	302	2.26	2.53
52:3	POLi	856	8.85	8.68	P--	330	54.83	56.28
54:3	OOO	884	3.23	3.08	S--	358	2.9	2.74
52:4	PLiLi	854	1.11	1.09	O--	356	31.65	30.11
54:4	OOLi	882	1.93	1.84	Li--	354	6.93	6.63
54:5	OLiLi	880	0.45	0.43	A--	386	0.16	0.14

[a] *M*, molecular weight (g/gmol). For other abbreviations see Table 6.2.2.1.
[b] Isomer set including different triacylglycerols, but all with the same number of fatty acid carbons and double bounds. For example, Group 50:3 means the isomer set of triacylglycerols with 50 fatty acid carbons and three double bounds. Moreover, groups with a total concentration of TAG lower than 0.05% were ignored.

Due to the high number and diversity of compounds found in the physical refiner, predictive group contribution methods were selected to describe the physical properties required for the enthalpy balances and equilibrium conditions. To calculate activity coefficients, UNIFAC r ¾ was used (Fornari et al., 1994). Fugacity coefficients were calculated using the virial equation truncated at the second term in combination with mixing rules (Reid et al., 1987). Critical properties and acentric factors of the pure components are needed to calculate second virial coefficients. Well-known estimation methods as Joback's technique for critical volumes and pressures, and Fedor's group contribution equation for critical temperatures were used (Reid et al., 1987). The V_i^L values for all components can be obtained with the modified Rackett technique (Reid et al., 1987). For the energy balances, vapor and liquid heat capacities, and enthalpies of vaporization were required. We selected Joback's technique for ideal vapor heat capacities, Rowlinson-Bondi's method for liquid heat capacities (Reid et al., 1987) and the method of Tu & Liu (1996) for estimation of the enthalpy of vaporization of each compound involved. The physical properties (V_i^L, vapor and liquid heat capacities, and enthalpies of vaporization) of water (stripping steam) were calculated using the equations from the Design Institute for Physical Properties Chemical Database (DIPPR, 2003).

6.2.3 Murphree efficiencies and entrainment (or mechanical carry-over)

For vapor-liquid separation process, considering that both liquid and vapor phases are mixed perfectly, a measure of the efficiency of mass transfer for a component *i* on n^{th} stage, is the Murphree efficiency (Ludwig, 1995). As suggested by Ludwig (1995), the Murphree efficiency (η) can be estimated using the equations of MacFarland, Sigmund & Van Winkle (1972), as a function of dimensionless groups: the surface tension number, N_{Dg}, the liquid Schmidt number, N_{Sc}, and the modified Reynolds number N_{Re}. The two models are given below:

$$\eta = 7.0 \cdot \left(N_{Dg}\right)^{0.14} \cdot \left(N_{Sc}\right)^{0.25} \cdot \left(N_{\mathrm{Re}}\right)^{0.08} \quad (6.2.3.1a)$$

$$\eta = 6.8 \cdot \left(N_{\mathrm{Re}} \cdot N_{Sc}\right)^{0.1} \cdot \left(N_{Dg} \cdot N_{Sc}\right)^{0.115} \quad (6.2.3.1b)$$

$$N_{Dg} = \sigma_L / \left(\mu_L \cdot U_{VN}\right);\ N_{Sc} = \mu_L / \left(\rho_L \cdot D_{LK}\right);\ N_{\mathrm{Re}} = \rho_V \cdot U_{VN} \cdot h_w / \left(\mu_L \cdot FA\right) \quad (6.2.3.1c)$$

where: σ_L is the surface tension of the liquid (kg/s^2), μ_L is the liquid viscosity ($\mathrm{Pa \cdot s}$), U_{VN} is the vapor superficial velocity (kg/s), ρ_L and ρ_V are the liquid and vapor densities (kg/m^3), respectively, h_w is the weir height (m), *FA* is the fractional free area (the ratio of the fractional area of the holes to the column free cross-sectional area) and D_{LK} is the liquid diffusivity (m^2/s) at infinite dilution from Wilke-Chang equation (Reid et al., 1987). All the physical properties mentioned above were calculated using well-known methods from Reid et al. (1987), except the oil viscosity, which was obtained using the method of Rabelo, Batista, Cavaleri & Meirelles (2000).

All $\eta_{n,i}$ values (Murphree efficiencies for each component at each tray; see Appendixes I and II) were considered equal to η, which is a simplifying approximation. Rigorous methods to estimate $\eta_{n,i}$ have already been developed (Rao, Goutami & Jain, 2001), but their implementation is very complicated and out of the scope of this work. To calculate η, we considered a typical load of palm oil

(4,425 kg/h) at 3 mmHg, 260 ºC and 1% of stripping steam. The mixture involved in this calculation was characterized by pseudo-compounds: an equivalent TAG (same molecular weight and unsaturations of the palm oil), an equivalent FFA (same molecular weight and unsaturations of the palm oil acidity) and water. The calculated values of η were 61.876% using Equation 6.2.3.1a and 49.986% ($\eta_{n,i}$ = 0.50) using Equation 6.2.3.1b. In this case, Equation 6.2.3.1b gives a more conservative design basis, and was chosen to represent the Murphree efficiency in our work. The approximation of the whole multicomponent mixture by an equivalent one, containing pseudo-compounds, was used only in the case of efficiency estimation.

Mechanical entrainment of oil is defined as the carry of oil droplets upward from the free surface by the vapor to the outlet of the equipment (Carlson, 1996). According to Carlson (1996), entrainment separators are capable of preventing the mechanical carry-over of oil droplets, thereby reducing entrainment losses to less than 0.1-0.2%, with an additional loss of about 10% of the FFA content in the feed. In order to evaluate the effects of mechanical entrainment in some of our simulations, we used the graphical method of Fair & Mathews (see Ludwig, 1995) for bubble-cap and perforated plates. This correlation was developed on the basis of a flow parameter $\left(L_n/V_n \cdot (\rho_V/\rho_L)^{0.5}\right)$ and a capacity parameter $\left(U_{VN} \cdot (\rho_V/(\rho_L - \rho_V))^{0.5}\right)$. It relates the fractional entrainment ψ (moles of liquid entrained/ moles of liquid downflow) to the liquid and vapor flow rates, to the densities of the vapor and liquid, and to the percentage of flood. The ψ value from our calculations was 0.024 moles of liquid entrained/ moles of liquid downflow. The entrainment term, e_n (moles of liquid entrained/ moles of vapor), of Equations A1, A2, A6 and A7 is related to ψ, by the following equation (Ludwig, 1995):

$$e_n = \frac{\psi}{1-\psi} \cdot \frac{L_n}{V_n} \qquad (6.2.3.2)$$

The calculated value for e_n, using Equation 6.2.3.2, was 0.4324 moles of liquid entrained/ moles of vapor. In particular, for CCF tray equipments, part of the

liquid of lower concentration of the plate below (*n-1*) is carried by the vapor to the plate above (*n*), reducing its liquid concentration with respect to the more volatile compounds. As a consequence, the vapor rising from this plate (*n*) will be also of lower concentration, reducing the net amount of mass transfer and the efficiency as well. The Murphree efficiency must be corrected to take this effect into account (Ludwig, 1995). The wet Murphree efficiency, η_w, can be easily calculated as a function of ψ (Ludwig, 1995):

$$\eta_w = \eta \Big/ \left(1 + \eta \cdot \frac{\psi}{1-\psi} \right) \qquad (6.2.3.3)$$

All $\eta_{n,i}$ values in the equilibrium relationships of countercurrent pattern (see Appendix I) were considered equal to η_w (0.494). For CRF deodorizers $\eta_{n,i}$ values (see Appendix II) were set as equal to η (0.50).

For CCF deodorizers, the pressure drops of the trays are added so that the pressure at the bottom of the column is greater than the top pressure[⊗]. For CRF deodorizers, the pressure drop is negligible.

6.3. Results and discussion

To evaluate the physical refining of palm and coconut oils, we selected from the literature (Rossi, Gianazza, Almprese, & Stanga, 2001; Petrauskaitè et al., 2000; Ahrens, 1998; Maza et al., 1992; Willems, 1985) usual processing conditions for oil load (kg/h), percentage of stripping steam, temperature and pressure. Two compositions were also considered for each type of oil: MVPO (more volatile palm oil), MVCO (more volatile coconut oil), LVPO (less volatile palm oil) and LVCO (less volatile coconut oil). The processing parameters studied in this work are shown in Table 6.3.1. As one can see, the combination of these parameters led to a considerable number of possibilities for simulation. The most interesting ones are discussed below.

[⊗] Foi considerada uma perda de carga de 1 mmHg por estágio, seguindo o trabalho de F.B White, (*Deodorization*, Journal of the American Oil Chemists Society, v. 29 (11), p. 515-526 (1953).

From the parameters given in Table 6.3.1, we selected a typical physical refining (267 Pa, 1% of stripping steam and 260°C) of the MVPO to show the profiles of temperature and of the vapor and liquid flow rates (kg/h) within the stripping column (see Figure 6.3.1). The simulations considered Murphree efficiencies, despising however entrainment effects. Because our simulation program permitted the investigation of different flow patterns, we studied the effect of CCF and CRF configurations on the results.

Table 6.3.1. Operating conditions for the continuous physical refiner simulations

Parameter	Palm Oil [b]	Coconut Oil [c]
% Stripping steam [a]	1.0, 2.0 and 3.0	0.5, 1.0 and 2.0
Temperature (°C)	240, 260 and 270	190, 210, 230 and 260
Top Pressure (Pa)	267, 400 and 667	133, 267 and 400
Oil load	4,425 kg/h [d]	
Number of trays	5 [e]	

[a] Calculated as percentage of total oil load. The stripping steam is distributed equally in the five stages of the column in the CRF design and as a single feed (1st stage) in the CCF design.
[b] From Rossi et al. (2001) and Willems (1995).
[c] From Petrauskaitè et al. (2000).
[d] Ahrens (1998). The oil feed is introduced into the column at the top stage (5th).
[e] Stage (1985).

Figures 6.3.1A and 6.3.1D show the profile of the mass flow rates of FFA, MAG, DAG and TAG in the liquid within the column, respectively for CCF and CRF equipments. As the oil flowed down into the column (from stage 5 to 1), the liquid mass flow rates of FFA, MAG and DAG decreased as a consequence of their vaporization. The mass flow rate of TAG changed slightly, increasing from the 1st to the 5th stage. In general, the CCF configuration generated lower liquid mass flow rates of FFA, MAG, DAG and TAG for all stages. Figures 6.3.1B and 6.3.1E give the profiles of the vapor mass flow rates of FFA, MAG, DAG and TAG, respectively for the CCF and the CRF columns. It is interesting to note that all mass flow rate curves of Figure 6.3.1B had higher values, indicating that this behavior was a consequence of the flow pattern, i.e., for the same operational conditions, more volatiles were carried by the vapor to the plate above in the case of the CCF configuration. For both flow patterns, there was a sharp increase in the values of the liquid mass flow rate of FFA and MAG from the 4th to the 5th stage,

but this enhance was even higher for the CCF column, because at the 5th stage the fresh oil contacted a higher mass flow rate of vapor (total feed of steam plus the volatiles of all stages below). Note that the DAG curve also had this increase only in the CCF configuration, due to the same reason.

As shown in Figures 6.3.1C and 6.3.1F, the difference between temperatures at the top and the bottom of the column was less than 0.9°C and 1.5°C, respectively for the CCF and the CRF patterns. As one can see, the differences between the temperatures of each stage of the CCF and the CRF configurations varied from 0.3°C to 0.9°C. Note that the temperatures of the CRF column were always higher. At a first insight, one might expect that the temperature profile in the CCF column would be higher than in the CRF column, due to the pressure drop effect that increases the pressure of each stage in the CCF column. It is important to observe that, besides this effect, the amount of the vapor stream that pass through each stage in the CCF column, and therefore the concentration of water dissolved in the liquid phase, are much higher than in the CRF configuration. According to Ceriani & Meirelles (2004a), very small amounts of steam (water), that condense and dissolve in the oil, decrease the boiling temperature of the mixture. Our simulations showed that this second effect (amount of steam) prevailed, i.e. the temperatures of each stage in the CCF column were lower than the ones in the CRF column. In fact, in the CCF column, the water was present in the liquid phase in mass fractions between 3.0E-8 to 1.1E-6 while in the CRF column this range was 1.7E-8 and 1.8E-7. To confirm this statement, we simulated the processing conditions of Figure 6.3.1 in CCF pattern but with 0.2% of stripping steam, in a way that the amount of steam passing through each stage was in the same range of the CRF with 1.0% of stripping steam (0.2% in each of the five stages). As expected, the temperatures of the CCF column were always higher, because now the pressure drop effect prevailed.

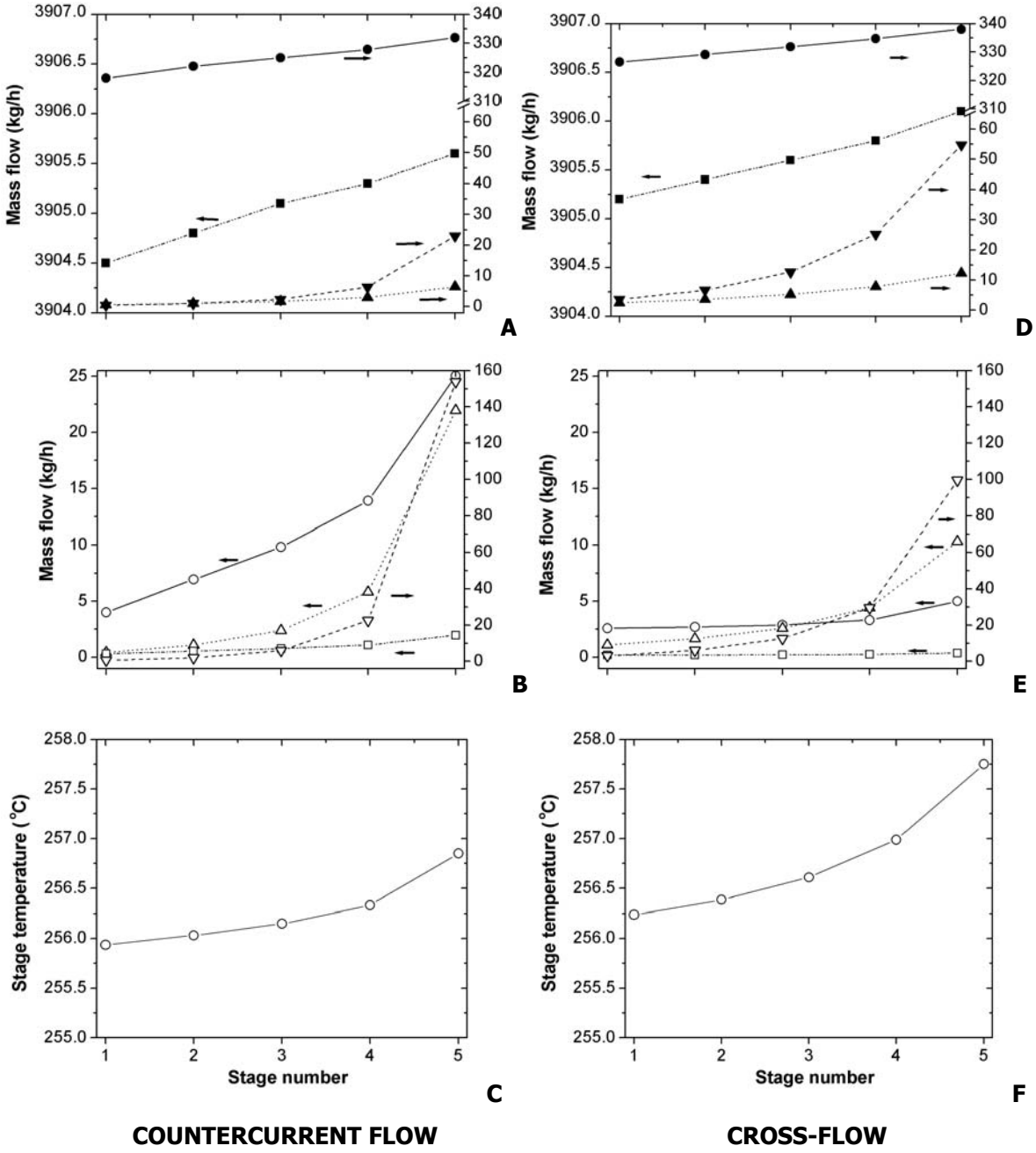

Figure 6.3.1. Profiles for the mass flow rates of FFA and acylglycerols in the liquid phase for the (a) CCF and (d) CRF design, in the vapor phase for the (b) CCF and (e) CRF design, and for the temperature in the (c) CCF and (f) CRF stripping column. Code: Vapor phase FFA (▽), TAG (□), DAG (○) and MAG (△); Liquid phase FFA (▼), TAG (■), DAG (●) and MAG (▲).

For the processing conditions of Figure 6.3.1 (CRF pattern), 188.49 kg/h of distillate was formed with 79.8% of FFA and 19.8% of acylglycerols, values not far from the observation of Chu et al. (2003). For comparison purposes, we report

that, at 240°C, the mass flow rate of distillate reduced to 155.37 kg/h, composed by 86.2% of FFA and 12.5% of acylglycerols. In general, the concentrations of acylglycerols and FFA in the distillate varied from 9.4% to 26.0%, and from 72.7% to 89.3%, respectively, for all the processing conditions studied for the MVPO.

In comparison with the values found for CRF design, the CCF always generated lower levels of final oil acidity (OA) and higher values of NOL for all the conditions studied for the physical refining of the MVPO (see Figure 6.3.2).

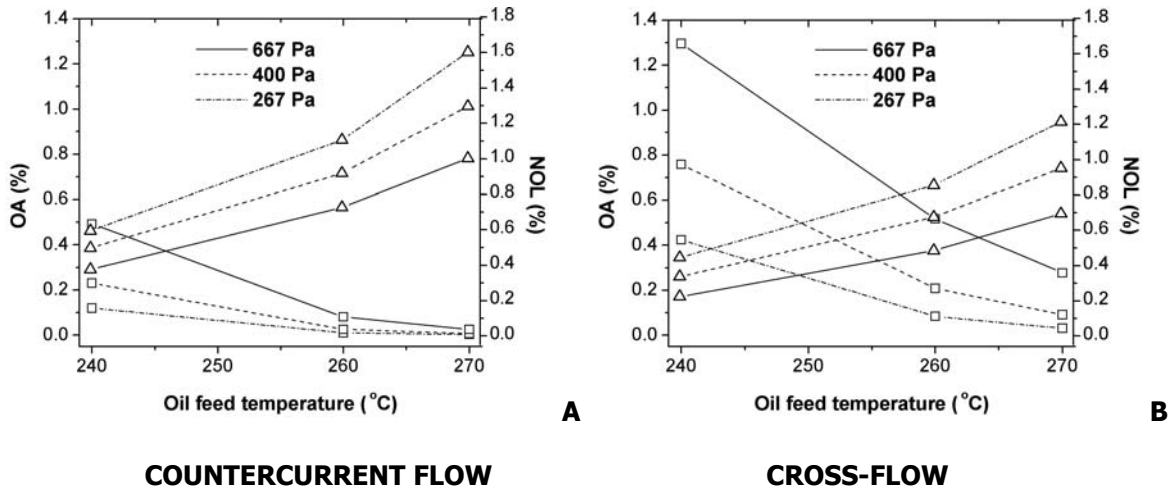

Figure 6.3.2. Final oil acidity (OA) and neutral oil loss (NOL) for physical refining of the MVPO with 1% of stripping steam for (a) CCF and (b) CRF patterns. Code: OA (□) and NOL (∆).

To elucidate this point, in the case of CCF, we simulated a condition with a reduced percentage of steam (0.5%, 50% less), while maintaining the other parameters fixed (260°C and 267 Pa). Similar values of NOL (0.86% for CRF and 0.83% for CCF) and OA (0.084% for CRF and 0.085% for CCF, in % of oleic acid) were achieved for both configurations, but in the case of CRF, the steam consumption must be kept at 1.0%. This result is very interesting since it indicates that with the CCF configuration, the same quality of the final product would be obtained, with half of the steam consumption. Ahrens (1999) informs that the steam consumption of thin-film deodorizers (also in CCF) is cut to a third of the amount required in conventional deodorizers.

To illustrate the feasible separation of the classes of fatty compounds (FFA, MAG, DAG, and TAG) within the column, we report the $K_{n,i}$ (distribution coefficient) values (see Equation 6.2.1.1) for stage number 5 at one of the processing conditions of Figure 6.3.2 (260°C, 267 Pa and 1% of stripping steam, CRF). The comparison of $K_{n,i}$ values gives an idea about the facility of the classes of compounds in a mixture to be distilled. The calculated values for the MVPO were as follows: $K_{5,\,TAG}$ = 0.002, $K_{5,\,DAG}$ = 0.27, $K_{5,\,MAG}$ = 13.11 and $K_{5,\,FFA}$ = 35.91. Note that the $K_{n,i}$ values were inversely proportional to the molecular weight of the compound class (see Table 6.2.2.1).

In general, the volatility of FFA increased with the temperature, vacuum magnitude and percentage of stripping steam. At higher temperatures, DAG and MAG volatility also reached important values and these compounds were stripped off from the oil, increasing NOL. The limiting factor for choosing processing conditions is the neutral oil loss (NOL), which was the object of our analysis. Table 6.3.2 gives the final OA and NOL values, for the MVCO and the LVCO. Note that the NOL values were more significant for the MVCO, even at lower temperatures, because its acylglycerol fractions were more volatile (see Table 6.2.2.1) in comparison to the LVCO fractions. As a consequence of the increase in the volatility of the acylglycerol fractions, 31-52% more losses of neutral oil were observed. The same association can be made comparing the NOL values found for the physical refining of the MVPO and LVPO.

The results discussed in the previous paragraphs evidence the important contribution of the vaporization of partial acylglycerols in the NOL values. Besides losses caused by distillation, there is also a loss due to entrainment. In fact, NOL is a consequence of two different contributions: the vaporization of acylglycerols (mainly DAG and MAG, which are more volatile than TAG) and the mechanical carry-over of liquid oil droplets, composed mostly by TAG.

Table 6.3.2. Effects of processing conditions on OA and NOL in the physical refining of coconut oil (MVCO and LVCO) with 1% of stripping steam.

	P (Pa)	T (°C)	NOL (%)	OA[a] (%)
LVCO	133	190	0.69	0.575
		210	1.09	0.231
		230	1.77	0.053
		260	4.52	0.002
	267	190	0.50	0.793
		210	0.86	0.384
		230	1.37	0.120
		260	3.24	0.006
	400	190	0.40	0.951
		210	0.72	0.501
		230	1.18	0.189
		260	2.66	0.013
MVCO	133	190	0.89	0.369
		210	1.47	0.141
		230	2.57	0.032
		260	6.95	0.001
	267	190	0.66	0.530
		210	1.13	0.238
		230	1.91	0.072
		260	4.92	0.004
	400	190	0.54	0.657
		210	0.95	0.317
		230	1.60	0.115
		260	3.98	0.008

[a] Expressed as percentage of lauric acid (% C12:0) in the refined oil.

For a better understanding of these two effects, we separated them in Figure 6.3.3 for the physical refining of the MVCO at different processing conditions. Because in the CCF design, the mechanical carry-over of the oil by the rising vapor stream affects the VLE and changes the phase compositions of each stage, we chose to report the results for the simulations considering entrainment just for the CCF configuration. Note, however, that similar conclusions would arise from the analysis of the results for the CRF column. As one can see, in Figure 6.3.3A, the contribution of distillation for the losses of neutral oil increased with temperature and percentage of stripping steam. At 230°C and 260°C, losses due to distillation were even more important than the mechanical carry-over (except

for the condition 230°C and 0.5% of steam), which was a direct consequence of the increase in the volatility of the acylglycerols at these temperatures.

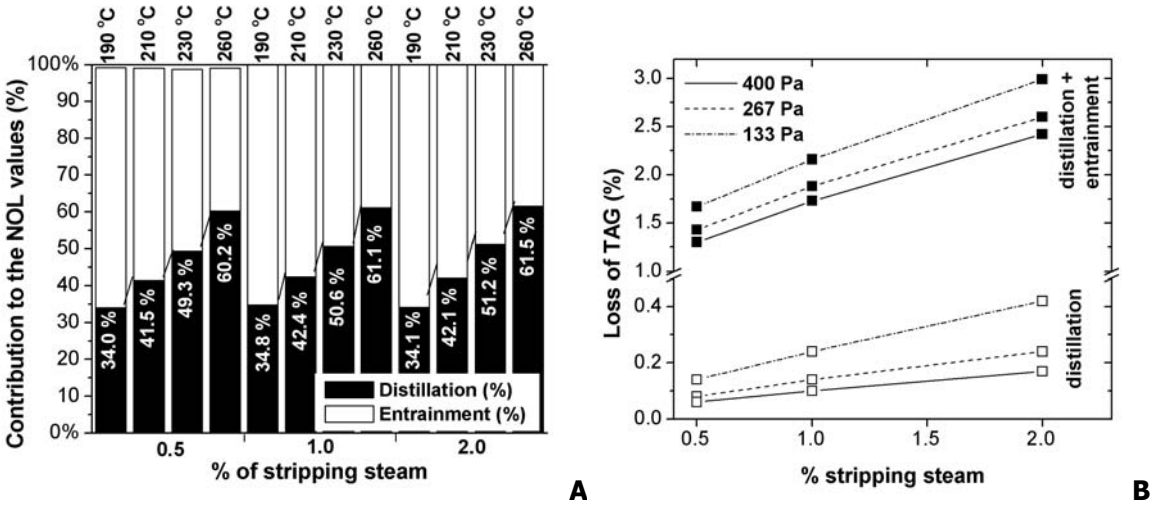

Figure 6.3.3. Contribution of distillation and entrainment to (a) the total loss of neutral oil (NOL) at 133 Pa and to (b) the loss of TAG at 210°C in the physical refining MVCO.

Figure 6.3.3B shows the values for TAG losses, as a function of the percentage of stripping steam and system pressure. As one can see, even at 210°C, the TAG fraction of coconut oil was vaporized. As expected, the entrainment increased TAG losses several times (minimum of 7 times at 133 Pa and 2% of steam; maximum of 23 times at 400 Pa and 0.5% of steam). It should be emphasized that physical refiners are usually equipped with entrainment separators to trap small oil droplets, reducing entrainment losses (Carlson, 1996). In our simulations, we considered entrainment for all stages, including the N^{th} stage, where this kind of apparatus acts. The NOL values reported may be over-estimated but they are an indicative of the necessity of using such improvements in physical refiners. It should be emphasized that this work did not consider losses of acylglycerols by hydrolysis during the process.

The main effect related to the inclusion of Murphree efficiencies within the equilibrium relationships was an increase in the final oil acidity. In this case, more stages would be required to achieve the same final content of FFA in the refined oil.

An important consideration about the VLE model adopted has to be discussed. As already highlighted by Ceriani & Meirelles (2004c), the calculated values of ϕ_i and POY for all components in the system (acylglycerols + FFA + water) were equal or very close to unity while the ϕ_i^{sat} values, specifically for water and short-chain fatty acids, deviated notably from unity, as a consequence of the high values of vapor pressures for these compounds at the operating conditions. This work showed however, that the results from the rigorous VLE model (Equation 6.2.1.1) produced no significant difference if compared with the results obtained considering the vapor phase as ideal. The differences in the mass fraction results were less than 0.001 in the vapor phase, and 0.00003 in the liquid phase. In general, the ϕ_i^{sat} values were not lower than 0.85 for water and 0.96 for the fatty compounds. In this way, it might be interesting to use, eventually, the ϕ_i^{sat} values only for water and some other selected fatty compounds of low molecular weight.

6.4. Conclusion

This work indicated that the tools developed by Ceriani & Meirelles (2004b) for calculating vapor pressures and evaluating the VLE of multicomponent fatty mixtures, coupled with the multicomponent stripping column program, allowed the simulation of different processes of the vegetable oil industry. As illustrated here, it is possible to build a computerized routine to design a multicomponent stripping column, including the rigorous estimation of the phase equilibria involved.

The software developed in the present work could be a suitable tool for the design of stripping columns, since it permits to investigate the composition (quality) of the refined oil and byproducts (as the distillate), as a function of processing variables (temperature, % stripping steam and pressure). Murphree efficiencies and entrainment had also important effects on the final products. The

combination of all these aspects could also lead to a better primary selection of the operating conditions of a real plant.

Acknowledgements

The authors wish to acknowledge FAPESP (Fundação de Amparo à Pesquisa do Estado de São Paulo – 03/04949-3) and CNPq (Conselho Nacional de Desenvolvimento Científico e Tecnológico - 521011/95-7) for the financial support.

Appendix I: Equations for the continuous multitray countercurrent flow design

For an arbitrary stage *n* of a stripping column, the related nomenclature can be set as follows.

Subscript *n*: flow from stage *n, n* =1, 2, …, *NS*; subscript *i*: component *i, i* =1, 2, …, *NC; H* = vapor phase enthalpy (J/h); *h* = liquid phase enthalpy (J/h); h_f = liquid feed enthalpy (J/h); H_f = vapor feed enthalpy (J/h); *V* = total vapor flow (mol/h); *v* = component vapor flow (mol/h); *L* = total liquid flow (mol/h); *l* = component liquid flow (mol/h); *f* = component feed flow as liquid (mol/h); *F* = component feed flow as vapor (mol/h).

For each stage *n*, a set of dependent relationships (test functions $F_{k(n,i)}$) must be satisfied. In the equations below, the entrainment term (e_n) is already introduced.

Component Balances (Total: *NS* x *NC* relations)

$$F_{1(n,i)} = l_{n,i} + v_{n,i} + V_n \cdot e_n \cdot \frac{l_{n,i}}{L_n} - v_{n-1,i} - V_{n-1} \cdot e_{n-1} \cdot \frac{l_{n-1,i}}{L_{n-1}} - l_{n+1,i} - f_{n,i} - F_{n,i} = 0 \qquad [A1]$$

Enthalpy Balances (Total: *NS* relations)

$$F_{2(n)} = h_n + H_n + e_n \cdot V_n \cdot \frac{h_n}{L_n} - H_{n-1} - e_{n-1} \cdot V_{n-1} \cdot \frac{h_{n-1}}{L_{n-1}} - h_{n+1} - h_{f,n} - H_{f,n} = 0 \qquad [A2]$$

Equilibrium conditions derived from the definitions of the vapor-phase Murphree plate efficiency, $\eta_{n,i}$ (Total: *NS* x *NC* relations)

$$F_{3(n,i)} = \eta_{n,i} \cdot K_{n,i} \cdot V_n \cdot \frac{l_{n,i}}{L_n} - v_{n,i} + (1 - \eta_{n,i}) \cdot v_{n-1,i} \cdot \frac{V_n}{V_{n-1}} = 0 \qquad [A3]$$

The above relationships comprise a vector of test functions

$$\mathbf{F(x)} = \{\mathbf{F_1}; \mathbf{F_2}; \mathbf{F_3}\} = 0 \qquad [A4]$$

which contains *NS* (2*NC* + 1) elements, and which may be solved for equally many unknowns

$$\mathbf{x} = \{\mathbf{l}; \mathbf{v}; \mathbf{T}\} \qquad [A5]$$

where the vector **l** contains all the elements $l_{n,i}$, **v** all the elements $v_{n,i}$ and **T** all elements T_n.

Once $l_{n,i}$, $v_{n,i}$ and T_n 's are known, the product compositions, the product flow rates, the concentration and temperature profiles in the column follow readily. The iterative Newton-Raphson method solves Equation A4 using the prior set of values of the independent variables (Equation A5). A first estimative is necessary to initiate the calculations. This estimative considers a linear profile for temperature, based on the oil and stripping steam feed temperature in each stage and for the vapor and liquid flows, based on an estimated value for L_n (total oil feed despising acidity) and for V_n, which is set as the total steam feed plus acidity. The derivatives of test functions (Jacobian matrix) with respect to temperature are found analytically, while those with respect to component flow rates are found numerically.

Appendix II: Equations for the continuous multitray cross-flow design

Component Balances (Total: *NS* x *NC* relations)

$$F_{1(n,i)} = l_{n,i} + v_{n,i} + V_n \cdot e_n \cdot \frac{l_{n,i}}{L_n} - l_{n+1,i} - f_{n,i} - F_{n,i} = 0 \qquad [A6]$$

Enthalpy Balances (Total: *NS* relations)

$$F_{2(n)} = h_n + H_n + e_n \cdot V_n \cdot \frac{h_n}{L_n} - h_{n+1} - h_{f,n} - H_{f,n} = 0 \qquad [A7]$$

Equilibrium conditions derived from the definitions of the vapor phase Murphree plate efficiency, $\eta_{n,i}$ (Total: *NS* x *NC* relations)

$$F_{3(n,i)} = \eta_{n,i} \cdot K_{n,i} \cdot V_n \cdot \frac{l_{n,i}}{L_n} - v_{n,i} + (1 - \eta_{n,i}) \cdot V_n \cdot \frac{F_{n,i}}{\sum_i F_{n,i}} = 0 \qquad [A8]$$

References

Ahrens, D. (1998). Comparison of tray, thin-film deodorization. *Inform,* 9 (6), 566-576.

Ahrens, D. (1999). Industrial thin-film deodorization of seed oils with SoftColumn technology. *Fett/Lipid,* 101 (7), 230-234.

Antoniosi Filho, N.R., Mendes, O.L., & Lanças, F.M. (1995). Computer prediction of triacilglicerol composition of vegetable oils by HRGC. *Journal of Chromatographia*, 40 (9-10), 557-562.

Balchen, S., Gani, R., & Adler-Nissen, J. (1999). Deodorization Principles, *Inform,* 10, 245-262.

Carlson, K.F. (1996). Deodorization. Y.H. Hui (Ed.), *Bailey's Industrial Oil and Fat Products*, (5th ed., vol. 4, pp. 339-390). Wiley-Interscience, New York.

Ceriani, R., & Meirelles, A.J.A. (2004a). Simulation of Batch Physical Refining and Deodorization Processes. *Journal of the American Oil Chemists Society*, 81(3), 305-312.

Ceriani, R., & Meirelles, A.J.A. (2004b). Predicting Vapor-Liquid Equilibria of Fatty Systems. *Fluid Phase Equilibria*, 215, 227-236.

Ceriani, R., & Meirelles, A.J.A. (2004c). Simulation of continuous deodorizers: effects on product streams. *Journal of the American Oil Chemists Society*, 81(11), 1059-1069.

Chu, B.S., Baharin, B.S., Quek, S.Y., & Man, Y.B.C. (2003). Separation of tocopherols and tocotrienols from palm fatty acid distillate using hydrolysis-neutralization-adsorption chromatography method. *Journal of Food Lipids*, 10(2), 141-152.

Chuan Ho, O. (1976). Studies in Palm Oil Crystallization. *Journal of the American Oil Chemists Society,* 53(10), 609-617.

Codex Alimentarius (1999). Codex Standard for Named Vegetable Oils (vol.8, pp. 1-16). Codex Stan 210-1999, Rome.

DIPPR Student Chemical Database Login, http://dippr.byu.edu/students/chemsearch.asp (accessed Nov. 2003)

Firestone D. (1999). *Physical and Chemical Characteristics of Oils, Fats and Waxes*. AOCS Press, Washington.

Fornari, T., Bottini, S. & Brignole, E.A. (1994) Application of UNIFAC to Vegetable Oil-Alkane Mixtures, *Journal of the American Oil Chemists Society,* 71 (4), 391-395.

Gaiser, M., Bell, G.M., Lim, A.W., Roberts, N.A., Faraday, D.B.F., Schulz, R.A. & Grob, R. (2002), Computer Simulation of a Continuous Wisky Still. *Journal of Food Engineering*, 51, 27-31.

Hodgson, A.L. (1996). Refining and Bleaching. In Y.H. Hui (Ed.), *Bailey's Industrial Oil and Fat Products*, (5th ed., vol. 4, pp. 157-212). Wiley-Interscience, New York.

Loncin, M. (1962). *L'Hydrolyze Spontanée des Huiles Glycéridiques et en Particulier de l'Huile de Palme*. Maison D'Editon, Couillet.

Ludwig, E.E. (1995). *Applied Process Design for Chemical and Petrochemical Plants*, (3rd ed., vol. 2, pp. 42-44). GPC, Houston.

MacFarland, S.A., Sigmund, P.M., & Van Winkle, M. (1972). Predict Distillation Efficiency, *Hydrocarbon Processing,* 51 (7), 111-114.

Maza, A., Ormsbee, R.A., & Strecker, L.R. (1992). Effects of Deodorization and Steam-Refining Parameters on Finished Oil Quality, *Journal of the American Oil Chemists Society,* 69 (10), 1003-1008.

Naphtali, L.M., & Sandholm, D.P. (1971) Multicomponent separation calculations by linearization. *AIChe Journal*, 17 (1), 148-153.

Petrauskaité, V., De Greyt, W.F., & Kellens, M.J. (2000). Physical Refining of Coconut Oil: Effect of Crude Oil Quality and Deodorization Conditions on Neutral Oil Loss. *Journal of the American Oil Chemists Society*, 77 (6), 581-586.

Rabelo, J., Batista, E., Cavaleri, F.W., & Meirelles, A.J.A. (2000). Viscosity prediction for fatty systems. *Journal of the American Oil Chemists Society,* 77(12), 1255-1261.

Rao, D.P., Goutami, C.V., & Jain, S. (2001). A direct method for incorporation of tray-efficiency matrix in simulation of multicomponent separation processes. *Computers and Chemical Engineering*, 25, 1141-1152.

Reid R. C., Prausnitz J.M., & Poling B.E. (1987). *The Properties of Gases and Liquids*, McGraw-Hill, New York.

Rossi, M., Gianazza, M., Almprese, C., & Stanga, F. (2001). The Effect of Bleaching and Physical Refining on Color and Minor Components of Palm Oil*. Journal of the American Oil Chemists Society,* 78 (10), 1051-1055.

Ruiz-Méndez, M.V., Márquez-Ruiz, G., & Dobarganes, M.C. (1996) Comparative Performance of Steam and Nitrogen as Stripping Gas in Physical Refining of Edible Oils. *Journal of the American Oil Chemists Society*, 73(12), 1641-1645.

Stage, H. (1985). The Physical Refining Process. *Journal of the American Oil Chemists Society*, 62 (2), 299-308.

Tandy, D.C., & McPherson, W.J. (1984). Physical Refining of Edible Oil, *Journal of the American Oil Chemists Society*, 61 (7), 1253-1258.

Theme, J.G. (1968). *Coconut Oil Processing,* FAO, Rome.

Tu, C.H., & Liu, C.P. (1996). Group-Contribution Estimation of the Enthalpy of Vaporization of Organic Compounds. *Fluid Phase Equilibria*, 121, 45-65.

Verleyen, T., Verhe, R., Garcia, L., Dewettinck, K., Huyghebaert, A., & De Greyt, W. (2001) Gas Chromatographic Characterization of Vegetable Oil Deodorization Distillate, *Journal of Chromatography A*, 921, 277-285.

Willems, M.G.A. (1985). Palm Oil; Quality Requirements from a Customer's Point of View, *Journal of the American Oil Chemists Society*, 62 (2), 454-459.

CAPÍTULO 7. MODELING VAPORIZATION EFFICIENCY FOR STEAM REFINING AND/OR DEODORIZATION

Roberta Ceriani and Antonio J. A. Meirelles

Trabalho aceito para publicação na revista **Industrial and Engineering Chemistry Research.**

Abstract

This work is primarily concerned with batch operations found in the oil industry, as steam deodorization and steam refining, in which sparging steam in injected into a bubbling pool of oil. The physical situation with some suitable simplifications is discussed and a theoretical model, which accounts for hydrostatic pressure and water solubility effects, is presented. The effects of some variables as temperature, working pressure, vapor flow and oil-layer height upon the vaporization efficiency values are analyzed. A good agreement was achieved for the prediction of vaporization efficiencies in comparison with few experimental data available. To estimate the required properties (densities, viscosities, diffusivities, activity coefficients and vapor pressures), group contribution methods and empirical equations were applied.

Key words

Steam refining, steam deodorization, edible oil, hydrostatic pressure, and vaporization efficiency.

7.1. Introduction

The edible oil industry involves some traditional processes that are accomplished by steam stripping at a low-pressure environment, such as steam refining and deodorization. Traditionally, live steam has been used as the stripping agent, although nitrogen was suggested recently as an alternative for physical deacidification and deodorization processes.[1] One advantage of nitrogen is the absence of hydrolysis in the oil, although thermolytic and oxidative reactions cannot be excluded.[2] Some authors[2] also verified a noteworthy higher stripping efficiency of nitrogen in relation to steam. Decap et al.[3], however, attributed this result to the inaccuracy in nitrogen dosage during the experiments. In their experimental work on physical deacidification, they measured nitrogen flow carefully, using a gas-flow meter, and concluded that one mole of nitrogen has almost the same stripping capacity as one mole of steam. From an ideal

thermodynamic point of view, the required amount of stripping gas is proportional to its molecular weight, which gives emphasis to the preference for steam.

The steam refining and/or deodorization are essentially a steam distillation in which volatiles, such as free fatty acids (FFA) and odor-causing substances, are stripped off from the oil under high temperatures and very low pressures (133 to 800 Pa and 190 to 270°C).[4] Both processes are very similar in execution (although different in purpose), since the odoriferous compounds and the FFA are comparable in volatility.[5]

One concept associated with steam distillation is the vaporization efficiency (ε), a measure of completeness with which the steam bubble becomes saturated with volatiles substances during its passage through the oil-layer.[5] In 1941, Bailey[5] proposed a mathematical model for vaporization efficiency applied to steam (batch) deodorization, which is still used nowadays. [2,3,4,6] In his work, Bailey[5] already discussed that a complete mathematical treatment should consider two effects of the hydraulic pressure on the rising bubble – for instance, continuously variation on its surface area (the bubble expands significantly) and its internal pressure.

A more recent work[7] dealt with this problem, describing a theoretical model of the mass transfer process and an experimental study of the stripping of pentane from both a mixture of heavier n-paraffins and of sunflower seed oil with nitrogen as the carrier gas. Although Coelho Pinheiro and Guedes de Carvalho[7] considered the two effects of hydraulic pressure in their model, their work suits better for stripping with inert (not condensable) gases (as nitrogen), since it did not take into account the solubility of the carrier agent. Coelho Pinheiro[8] also proposed a theoretical model for the stripping process, but at this time, it took into account the contribution of the interfacial tension to the pressure inside a gas bubble. According to the author, this consideration is important for the gas dispersed as very small bubbles (diameter lower than 0.1 mm).

This work is primarily concerned with the effects of processing parameters, such as temperature, working pressure, vapor flow and oil-layer height upon

vaporization efficiency. For this study, a detailed model was developed. It is based in stripping with live steam, in which water solubility effects cannot be despised. [4,9,10] As already shown by Ceriani and Meirelles,[10] very small amounts of steam (water), that condense and dissolve in the oil, decrease the necessary boiling temperature. In this way, deodorization can be accomplished at lower temperatures, maintained constant along the entire process. In fact, small amounts of water that dissolve in the oil can cause a water partial pressure high enough to keep the temperature constant most part of the process. This interesting aspect was indirectly confirmed by the computational simulation[10] of the experimental work of Petrauskaitè et al.[11] who have deacidified coconut oil with live steam. The use of an inert gas, such as nitrogen, that influences only the vapor phase, would require to increase steadily the heat source temperature to vaporize the less-volatile long-chain free fatty acids in the last part of the batch process. In fact, Ceriani and Meirelles[10] showed that the temperature using an inert gas should be higher than the corresponding one using live steam and, even higher than the heat source temperature used by Petrauskaitè et al.[11] at the last part of the process. Batch deodorizers equipped with nitrogen injection would require a significantly larger vacuum unit, because of special characteristics of the gas, i.e. being non-condensable and inert.[3]

To reinforce the presence of water in the liquid phase, some works[4,5,9] have shown that hydrolysis does occur during deodorization with live steam injection.

7.2. Developing a model for steam refining and/or deodorization

7.2.1 Physical Situation and Simplifying Hypothesis

In a batch deodorizer and/or steam refiner, live steam is blown through the liquid (oil), which contains a small amount of solute (fatty acids or odor-causing substances). In industrial equipments, a distributor is arranged for the stripping steam at the bottom of the equipment, consisting of a sparge line or an

arrangement with perforated pipes.[12,13] In this work, to simplify the mathematical model, we adopted a idealized situation of a single orifice through which the gas is injected.

Since the pressure above the free surface of the liquid (P^O) is sufficiently low, 133 to 800 Pa for steam deodorization,[4] the bubble formed at the orifice grow significantly as it ascends in a pressure field varying according to $P = P^O + \rho_L \cdot g \cdot (H - h)$, from $P = P^O + \rho_L \cdot g \cdot H$ (at the bottom) to P^O, where ρ_L is the liquid density, g is the acceleration by gravity, H is the total height of the oil-layer and h is the distance from the steam injection. As a consequence, the rising bubble expands with the decreasing external pressure, and the partial pressure of the solute (p_A), which is zero at the bottom, increases as the bubble moves toward the free surface. Figure 7.2.1.1 exemplifies the bubble expansion effect and the reference axis adopted in the model development.

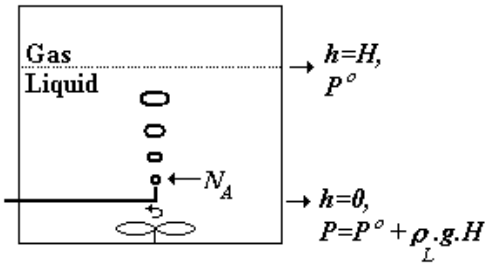

Figure 7.2.1.1. Diagram of continuous bubbling in a steam deodorization and/or steam refining under vacuum through a single orifice.

As shown in the literature, in batch deodorization processes, the oil is fed into the equipment and heated until the desired temperature. Afterwards the sparge steam is steadily blown through the liquid-layer to keep the temperature constant and strip off the more volatile fatty compounds.

The model developed in this work assumed that:

(i) The liquid is a pseudoternary mixture, formed by a volatile compound (*A*), the condensable steam (*B*) and a nonvolatile compound (*C*). The vapor phase is a pseudobinary mixture composed by *A* and *B*. In the case of deodorization and/or steam refining, *A* refers to a representative fatty acid, *B* is water, and *C* is a

representative triacylglycerol (TAG) of the oil, this last compound was assumed to be not volatile at the prevailing conditions.

(ii) The stripping steam is steadily blown through the liquid, keeping it saturated with compound *B*; *B* has a very low solubility in the liquid phase and its concentration, x_B, changes along the liquid-layer height since the local pressure changes as the liquid height increases. Bear in mind that $p_B = p_B^*$, hence $\left(P^O + \rho_L \cdot g \cdot (H - h)\right) \cdot y_B = \gamma_B \cdot x_B^* \cdot P_B^{vp}$, where y_B is the molar fraction of *B* in the vapor, γ_B and P_B^{vp} are, respectively, the activity coefficient and the vapor pressure of component *B*. This means that there is no mass-transfer of *B* during the deodorization process and along the liquid-layer height. Such a hypothesis seems to be very realistic, since the sparge steam is steadily blown and water has a very low solubility in the oil, indicating that small amounts of water, transferred to the liquid-phase at the beginning of the process, are enough to keep the oil-layer saturated along the whole batch period. A simple calculation using the experimental conditions of Decap et al.[3] showed that, considering the usual amount of steam used in deodorization and the water solubility in oil, the first set of bubbles that is blown into the oil layer is capable of saturating it with water.

(iii) Although x_B changes along the liquid-height, the liquid-phase is considered as a fully mixed one, in relation to the other liquid concentrations (x_A and x_C) and to the temperature. In fact, to keep the temperature constant, x_B changes along the liquid height. However, its value is always very small, so that x_A and x_C change less than 0.03% with *h*.

(iv) The vapor phase is ideal, since the process occurs at low pressures. The liquid phase, however, is considered as nonideal;[14]

(v) The individual bubbles forming at the injection orifice are all spherical and equal in size;[7]

(vi) The gas, free of solute, is injected at the bottom of the still (*h=0*, see Figure 7.2.1.1). As a consequence, the bubble contains only component *B* in *h=0*, and absorbs volatile solute (*A*) as it rises up toward the free surface (*h=H*);

(vii) There is no bubble coalescence;[7]

7.2.2 Mathematical Model Formulation

From the mass-transfer theory of gas absorption[15] it can be stated that the amount of solute transferred per unit of time $\left(dN_A = n_B \cdot dY_A/dt\right)$, from the oil into the steam bubble, is equal to the mass-transfer coefficient (K_{OG}) multiplied by the surface area of the bubble $\left(A_b = \pi \cdot d_b^2\right)$ and by the concentration difference available as a driving force $\left(\Delta Y_A = Y_A^* - Y_A\right)$. Mathematically,

$$n_B \cdot \frac{dY_A}{dt} = K_{OG} \cdot A_b \cdot \Delta Y_A \qquad (7.2.2.1)$$

where n_B is the number of moles of B in a bubble, d_b is the bubble diameter, t is the time of contact between a steam bubble and the oil, and Y_A is the vapor phase concentration of solute (A) in a solute-free basis. Taking into account the model assumptions, the formulation of Equation 7.2.2.1 in a solute-free basis is the most appropriate one. Just to clarify, remember that the bubble has n_B moles of compound B and n_A moles of compound A, i.e. $n_b = n_A + n_B$.

If u_b is the rising velocity of individual bubbles, for a differential time dt, the bubble rises a distance dh, according to the relation below:

$$dt = dh/u_b \qquad (7.2.2.2)$$

The relationship between bubble diameter (d_b) and the velocity of rise of large spherical bubbles can be expressed as:[16]

$$u_b = K \cdot \sqrt{g \cdot d_b} = C_1 \cdot d_b^{e_1} \otimes \qquad (7.2.2.3)$$

From the measured rates of gas bubbles in fluidized beds, it can be seen that the rates of rise can all be expressed with K varying in the range of 0.57 to

$^{\otimes}$ Na Equação 7.2.2.3, $e_1 = ½$.

0.85.[16] Following the work of Coelho Pinheiro and Guedes de Carvalho,[7] K was set as 0.71[∅].

From the theory of Davidson and Schüller[17] for bubble formation, cited by Coelho Pinheiro and Guedes de Carvalho,[7] the volume of bubbles formed during continuous gas injection through a single orifice (in low viscosity liquids) is given by:

$$V_b\left(\mathrm{m}^3\right) = 1.378 \cdot \frac{\nu_G^{6/5}\left(\mathrm{m}^3/\mathrm{s}\right)}{g^{3/5}\left(\mathrm{m}/\mathrm{s}^2\right)} \tag{7.2.2.4}$$

where ν_G is the volumetric flowrate of gas through the orifice.

Since we assumed that the gas obeys the ideal gas law, n_B is related to the bubble volume V_b as follows:

$$p_B \cdot V_b = n_B \cdot R \cdot T \;\Rightarrow n_B = 1.378 \cdot \frac{p_B(\mathrm{Pa})}{R\left(\mathrm{Pa}\cdot\mathrm{m}^3/\mathrm{kmol}\cdot\mathrm{K}\right)\cdot T(\mathrm{K})} \cdot \frac{\nu_G^{6/5}\left(\mathrm{m}^3/\mathrm{s}\right)}{g^{3/5}\left(\mathrm{m}/\mathrm{s}^2\right)} \tag{7.2.2.5}$$

Equation 7.2.2.5 allows to estimate n_B through the conditions observed at the orifice, being ν_G and p_B, the values calculated for that location.

The mass-transfer coefficient K_{OG}, considering both the liquid and the gas phase resistances, may be expressed as:

$$\frac{1}{K_{OG}} = \frac{m}{k_L \cdot c_L} + \frac{R \cdot T}{p_B \cdot k_G} \tag{7.2.2.6}$$

where k_L is the liquid side mass-transfer coefficient, $c_L = \rho_L / M_L$ is the molar density of the solute-free oil, m is the distribution coefficient of compound A in a solute-free basis and k_G is the gas side mass-transfer coefficient. In Equation 6, c_L corresponds to $c_L^{'} \cdot (1 - x_A)$, which indicates that, for diluted solutions $(x_A \to 0)$, $c_L \approx c_L^{'}$; $c_L^{'}$ is the molar density of the liquid.

The distribution coefficient m is the ratio of the A concentration in a solvent-free basis in the vapor and in the liquid phases:

[∅] A análise de sensibilidade dos modelos desenvolvidos em relação ao valor da constante K revelou que não há diferença significativa entre os valores calculados para a eficiência de vaporização.

$$m = \frac{Y_A^*}{X_A^*} = \frac{y_A^*/(1-y_A^*)}{x_A^*/(1-x_A^*)} = \frac{\gamma_A \cdot P_A^{vp}}{\gamma_B \cdot P_B^{vp}} \cdot \left(1 + \frac{x_C^*}{x_B^*}\right) \qquad (7.2.2.7)$$

where Y^* and X^* are, respectively, the concentration in free basis of the vapor and the liquid phases, y^* and x^* are equilibrium molar fractions, P^{vp} is the vapor pressure and γ is the activity coefficient. Given that x_B^* changes along the oil-layer, m is a function of h.

For a single bubble, the mass-transfer coefficients (k_L and k_G) are described by a constant (C_2) times a power of the bubble diameter and the square root of its respective diffusivity as in Equation 7.2.2.8 and 7.2.2.9, respectively:[7,18]

$$k_L = \left(\frac{4 \cdot D_L}{\pi \cdot t_C}\right)^{1/2} = \left(\frac{4 \cdot D_L}{\pi \cdot \frac{d_b}{u_b}}\right)^{1/2} = \left(\frac{4 \cdot C_1 \cdot D_L}{\pi}\right)^{1/2} \cdot d_b^{-1/4} = C_2 \cdot \sqrt{D_L} \cdot d_b^{e_2} \ ^{\otimes} \qquad (7.2.2.8)$$

$$k_G = \left(\frac{4 \cdot D_G}{\pi \cdot t_C}\right)^{1/2} = \left(\frac{4 \cdot D_G}{\pi \cdot \frac{d_b}{u_b}}\right)^{1/2} = \left(\frac{4 \cdot C_1 \cdot D_G}{\pi}\right)^{1/2} \cdot d_b^{-1/4} = C_2 \cdot \sqrt{D_G} \cdot d_b^{e_2} \ ^{\varnothing} \qquad (7.2.2.9)$$

where t_C is the contact time between elements of fluid at the bubble surface $(t_c = d_b/u_b)$.[18] The diffusivity of oleic acid in the liquid, D_L, was estimated combining the equation proposed by Siddiqi and Lucas[19] and the experimental values obtained by Smits[20] for diffusion of oleic acid in groundnut oil at 130°C (Equation 7.2.2.10).

$$D_L(\mathrm{m^2/s}) = 3.5135 \cdot 10^{-12} \cdot (1000 \cdot \mu_L(\mathrm{Pa \cdot s}))^{-0.907} \cdot T(\mathrm{K}) \qquad (7.2.2.10)$$

where μ_L is the viscosity of the liquid.

For D_G estimation, we used the equation of Wilke and Lee,[21] in which D_G is dependent on the system pressure P, as given below:

$^{\otimes}$ Na Equação 7.2.2.8, e_2= -¼.
$^{\varnothing}$ Na Equação 7.2.2.9, e_2= -¼.

$$D_G\left(\mathrm{m^2/s}\right) = 8.2265 \cdot 10^{-6} \cdot \frac{T^{3/2}(\mathrm{K})}{P(\mathrm{Pa})} \tag{7.2.2.11}$$

Substituting Equations 7.2.2.8 and 7.2.2.9 into Equation 7.2.2.6, leads to an expression for K_{OG}, which is:

$$K_{OG} = \frac{C_2 \cdot \sqrt{D_L \cdot D_G} \cdot d_b^{e_2} \cdot c_L \cdot p_B^*}{R \cdot T \cdot c_L \cdot \sqrt{D_L} + m \cdot p_B^* \cdot \sqrt{D_G}} \tag{7.2.2.12}$$

A simple manipulation of Equation 7.2.2.7 shows that $m \cdot p_B^*$ (in Equation 7.2.2.12) can be substituted by:

$$m \cdot p_B^* = \gamma_A \cdot P_A^{vp} \cdot \left(1 - x_A^*\right) \tag{7.2.2.13}$$

where $\gamma_A \cdot P_A^{vp} \cdot \left(1 - x_A^*\right)$ is constant (changes insignificantly); see simplifying hypothesis (iii). In this way, Equation 7.2.2.12 becomes:

$$K_{OG} = \frac{C_2 \cdot \sqrt{D_L \cdot D_G} \cdot d_b^{e_2} \cdot c_L \cdot p_B^*}{R \cdot T \cdot c_L \cdot \sqrt{D_L} + \gamma_A \cdot P_A^{vp} \cdot \left(1 - x_A^*\right) \cdot \sqrt{D_G}} \tag{7.2.2.14}$$

Equations 7.2.2.1 to 7.2.2.5, and 7.2.2.14 may be combined to give:

$$\frac{C_2 \cdot \sqrt{D_L \cdot D_G} \cdot c_L \cdot \pi^{\frac{(1+e_1-e_2)}{3}} \cdot \left(6 \cdot n_B \cdot R \cdot T\right)^{\frac{(2+e_2-e_1)}{3}}}{C_1 \cdot n_B \cdot \left(R \cdot T \cdot c_L \cdot \sqrt{D_L} + \gamma_A \cdot P_A^{vp} \cdot \left(1 - x_A^*\right) \cdot \sqrt{D_G}\right)} \cdot \frac{dh}{\left(p_B^*\right)^{\frac{(e_2-e_1-1)}{3}}} = \frac{1}{\left(Y_A^* - Y_A\right)} \cdot dY_A \tag{7.2.2.15}$$

In the right side of Equation 7.2.2.15, Y_A may be substituted by $\frac{p_A}{p_B^*}$ to yield:

$$\frac{1}{Y_A^* - Y_A} \cdot dY_A = \frac{1}{\frac{p_A^* - p_A}{p_B^*}} \cdot d\left(\frac{p_A}{p_B^*}\right) = \frac{p_B^*}{p_A^* - p_A} \cdot d\left(\frac{p_A}{p_B^*}\right) \tag{7.2.2.16}$$

However $p_B^* = P - p_A$. In this way, Equation 7.2.2.16 becomes:

$$\frac{p_B^*}{p_A^* - p_A} \cdot d\left(\frac{p_A}{P - p_A}\right) = \frac{p_B^*}{p_A^* - p_A} \cdot \left[\frac{dp_A}{P - p_A} + p_A \cdot \left(\frac{dp_A - dP}{(P - p_A)^2}\right)\right] = \frac{1}{p_A^* - p_A} \cdot \left[dp_A + \frac{p_A}{p_B^*} \cdot dp_A - \frac{p_A}{p_B^*} \cdot dP\right] \quad (7.2.2.17)$$

But $P = P^O + \rho_L \cdot g \cdot (H - h)$ and $dP = -\rho_L \cdot g \cdot dh$, then:

$$\frac{1}{Y_A^* - Y_A} \cdot dY_A = \frac{1}{p_A^* - p_A} \cdot \left(\frac{P}{p_B^*} \cdot dp_A + \rho_L \cdot g \cdot \frac{p_A}{p_B^*} \cdot dh\right) \quad (7.2.2.18)$$

p_B^* can be stated as:

$$p_B^* = C_3 \cdot P^{C_4} \ ^{\otimes} \quad (7.2.2.19)$$

Substituting Equations 7.2.2.18 and 7.2.2.19, and the constants C_1, C_2, e_1 and e_2 in Equation 7.2.2.15, we get the final equation

$$dp_A = \frac{dh}{P^o + \rho_L \cdot g \cdot (H - h)} \cdot \left\{ \frac{2 \cdot \sqrt{D_L \cdot D_G} \cdot c_L \cdot \pi^{1/12} \cdot (6 \cdot n_B \cdot R \cdot T)^{5/12} \cdot C_3^{19/12}}{\sqrt{0.71} \cdot g^{1/4} \cdot n_B \cdot \left(R \cdot T \cdot c_L \cdot \sqrt{D_L} + \gamma_A \cdot P_A^{vp} \cdot (1 - x_A^*) \cdot \sqrt{D_G}\right)} \cdot \right.$$
$$\left. \left(p_A^* - p_A\right) \cdot \left[P^o + \rho_L \cdot g \cdot (H - h)\right]^{19 \cdot C_4/12} - \rho_L \cdot g \cdot p_A \right\}$$

(7.2.2.20)

which numerical integration leads to the profile of p_A along the oil-layer for a given value of p_A^* (which is independent of h as a consequence of good mixing in the liquid). The value of p_A in the outgoing stream, $p_A^{h=H}$, can also be obtained. With this information, the vaporization efficiency, ε, can be finally estimated $\left(\varepsilon = p_A / p_A^*\right)$. For numerical integration, we used the subroutine ode15s$^{\varnothing}$ from MatLab®.[22]

Note that in Equation 7.2.2.20, D_G should be substituted by its expression in terms of the system pressure $P = P^O + \rho_L \cdot g \cdot (H - h)$ (Equation 7.2.2.11).

$^{\otimes}$ A dependência de p_B^* com P descrita na Equação 7.2.2.19 foi escolhida pela sua conveniência no desenvolvimento dos modelos para a eficiência de vaporização.

$^{\varnothing}$ Esta subrotina utliliza um método de integração de passo variável conhecido como método de GEAR (GEAR, G.W. Simultaneous Numerical Solution of Ordinary Differential-Algebraic Equations. IEEE Trans. On Circuit Theory, v.18, no.1, p.89-95, 1971).

It is interesting to observe that it is possible to obtain an analytical solution for Equation 7.2.2.15, if two simplifying assumptions are considered: the first one is to ignore the effect of dP in dY_A, which means that the effect of the reduction of the hydrostatic pressure in the evolution of p_A is ignored and, in this way, p_A increases steadily due to the transfer of solute caused by the available driving force $\left(p_A^* - p_A\right)$; the effect of hydrostatic pressure in bubble size is, however, maintained; the second supposition is that an average value for D_G could be used instead of the expression given in Equation 7.2.2.11. Thus,

$$\frac{1}{Y_A^* - Y_A} \cdot dY_A = \frac{1}{p_A^* - p_A} \cdot \left(dp_A + \frac{p_A}{p_B^*} \cdot dp_A \right) = \frac{1}{p_A^* - p_A} \cdot \left(\frac{P}{p_B^*} \cdot dp_A \right) \tag{7.2.2.21}$$

and

$$\overline{D}_G = \frac{\int_{P^o + \rho_L \cdot g \cdot H}^{P^o} D_G \cdot dP}{\int_{P^o + \rho_L \cdot g \cdot H}^{P^o} dP} = \frac{8.2265 \cdot 10^{-6} \cdot T^{3/2}(\mathrm{K})}{\rho_L\left(\mathrm{kg/m^3}\right) \cdot g\left(\mathrm{m/s^2}\right) \cdot H(\mathrm{m})} \cdot \log_e\left(1 + \frac{\rho_L\left(\mathrm{kg/m^3}\right) \cdot g\left(\mathrm{m/s^2}\right) \cdot H(\mathrm{m})}{P^o(\mathrm{Pa})}\right) \tag{7.2.2.22}$$

Substituting now Equation 7.2.2.21 in Equation 7.2.2.15 together with Equation 7.2.2.19 and the constants C_1, C_2, e_1 and e_2, a relation of dp_A with dh may be rewritten as:

$$\frac{2 \cdot \sqrt{D_L \cdot D_G} \cdot c_L \cdot \pi^{1/12} \cdot \left(6 \cdot n_B \cdot R \cdot T\right)^{5/12} \cdot C_3^{19/12}}{\sqrt{0.71} \cdot g^{1/4} \cdot n_B \cdot \left(R \cdot T \cdot c_L \cdot \sqrt{D_L} + \gamma_A \cdot P_A^{vp} \cdot \left(1 - x_A^*\right) \cdot \sqrt{D_G}\right)} \cdot P^{\frac{19 \cdot C_4}{12} - 1} \cdot dh = \frac{1}{\left(p_A^* - p_A\right)} \cdot dp_A \tag{7.2.2.23}$$

The analytical integration of Equation 7.2.2.23 generates an expression for the vaporization efficiency ε as a function of h. The value of ε at H (free surface), $\varepsilon^{h=H}$, can be calculated substituting $h=H$ in the equation below.

$$\varepsilon = \frac{p_A^h}{p_A^*} = f(h) = 1 - \exp\left[\frac{1.4991 \cdot \sqrt{D_L \cdot D_G} \cdot c_L \cdot \pi^{1/12} \cdot (6 \cdot n_B \cdot R \cdot T)^{5/12} \cdot C_3^{19/12}}{C_4 \cdot \rho_L \cdot g^{5/4} \cdot n_B \cdot \left(R \cdot T \cdot c_L \cdot \sqrt{D_L} + \gamma_A \cdot P_A^{vp} \cdot (1 - x_A^*) \cdot \sqrt{D_G}\right)} \cdot \left\{ \left(P^O + \rho_L \cdot g \cdot (H - h)\right)^{19 \cdot C_4/12} - \left(P^O + \rho_L \cdot g \cdot H\right)^{19 \cdot C_4/12} \right\} \right] \quad (7.2.2.24)$$

In Equation 7.2.2.24, D_G should be calculated with Equation 7.2.2.22.

7.2.3 Theory of Steam Stripping from Bailey[5]

For further discussion and comparison purposes, we explored the mathematical model, roughly described by Bailey, [5] for the mass transfer of volatile substances from the oil into a steam bubble. It is very similar to Equation 7.2.2.1, but it neglects any hydrostatic pressure effects on the rising bubble, and assumes that the gas-phase is a dilute solution of *A* (fatty acid) in *B*. In this way, dN_A is given by:

$$n_b \cdot \frac{dy_A}{dt} = K_{OG} \cdot A_b \cdot \left(y_A^* - y_A\right) \quad (7.2.3.1)$$

where the mass transfer coefficient, K_{OG}, is expressed as:

$$\frac{1}{K_{OG}} = \frac{m'}{k_L \cdot c_L} + \frac{R \cdot T}{P^o \cdot k_G} \quad (7.2.3.2)$$

In Equations 7.2.3.1 and 7.2.3.2, the vapor molar fraction is not on free basis. As a consequence m' is equal to y_A^*/x_A^* or $\left(\gamma_A \cdot P_A^{vp}/P^O\right)$, and is not a function of *P*. n_b should be appropriately changed i.e., $n_b = P^O \cdot V_b/R \cdot T$. Note that, in this case, $n_b \approx n_B$ throughout the oil layer, since $n_A << n_B$. Following a similar development, we found the equation below:

$$\varepsilon = \frac{p_A^h}{p_A^*} = f(h) = 1 - \exp\left(-5.008 \cdot \frac{c_L \cdot \sqrt{D_L \cdot D_G}}{R \cdot T \cdot c_L \cdot \sqrt{D_L} + P^O \cdot m' \cdot \sqrt{D_G}} \cdot \pi^{1/12} \cdot \left(\frac{P^O}{n_b}\right)^{7/12} \cdot \frac{(R \cdot T)^{5/12}}{g^{1/4}} \cdot h \right) \quad (7.2.3.3)$$

7.2.4 Steam or Gas Consumption in Stripping Processes

The required amount of stripping gas, either steam or nitrogen, is an important parameter in the evaluation of operational costs of stripping processes, and is directly related to vaporization efficiencies. Because of its importance it has being under study and use [3,5] since Bailey[5] proposed the first equation, in 1941. The original equation of Bailey[5] relates the total moles of stripping steam injected into the deodorizer (*S*) with the average vaporization efficiency ε_{1-2}. It is set below:

$$S = \frac{P^O \cdot F_{OIL}}{\varepsilon_{1-2} \cdot P_{FFA}^{vp}} \left(\ln \frac{x_{FFA_1}}{x_{FFA_2}} \right) \qquad (7.2.4.1)$$

where $\varepsilon_{1\text{-}2}$ is the average vaporization efficiency between times 1 and 2, F_{OIL} is moles of the oil feed, P_{FFA}^{vp} is the mean value of vapor pressure of the FFA, x_{FFA_1} and x_{FFA_2} are, respectively, the liquid molar fraction of FFA at times 1 and 2.

To obtain Equation 7.2.4.1, Bailey[5] has considered the following simplifications:

(i) The partial pressure of volatile (FFA) substances (p_{FFA}) is very small in relation to p_S (partial pressure of steam), so p_S approaches closely the total pressure *P*.

(ii) F_{FFA} (moles of volatile substances) is very small in relation to F_{OIL}, and therefore, $F_{FFA}+F_{OIL}$ approaches closely the value of F_{OIL}. If the initial concentration of FFA is sufficiently high, this simplification and also the previous one are not suitable to describe the deodorization process.

(iii) The liquid phase is ideal, and obeys Raoult's law.

Decap et al.[3] studied the effect of operating variables, such as temperature, pressure, amount of gas (steam or nitrogen) injected, in the overall vaporization efficiency values through a lab-scale apparatus. They developed a model similar to Bailey[5] to describe ε_{1-2}. Their main considerations were in relation

to the ideality of the liquid phase, and negligible neutral oil loss (NOL) by vaporization.

We followed the same steps of Bailey,[5] but without any of the simplifications i), ii), iii) depicted above, and obtained Equation 7.2.4.2 below:

$$S = F_{OIL} \cdot \left[\left(X_{FFA_2} - X_{FFA_1} \right) + \frac{P^O}{\varepsilon_{1-2} \cdot \gamma_{FFA} \cdot P_{FFA}^{vp}} \cdot \left(\ln \frac{X_{FFA_1}}{X_{FFA_2}} + \left(X_{FFA_1} - X_{FFA_2} \right) \right) \right] \quad (7.2.4.2)$$

where X_{FFA_1} and X_{FFA_2} are, respectively, the liquid molar ratio of FFA in solute-free basis at times 1 and 2, and γ_{FFA} is the activity coefficient for the FFA.

Note that γ_{FFA} does not change considerably with the normal range of initial and final oil acidities (variations are at the third decimal case), but its value is lower than one. F_{OIL} is the number of moles of neutral oil in the feed, excluding the oil acidity. Besides the non-ideality of the liquid phase, Equation 7.2.4.2 is analogous to the one developed by Decap et al.[3] This equation is capable of estimating the steam or gas consumption for stripping of oils with high acidity.

To investigate gas consumption in stripping processes, either with steam or nitrogen, we use the average vaporization efficiency, ε_{1-2}, which, as the name says, is the average value of $\varepsilon^{h=H}$. Note that $\varepsilon^{h=H}$ refers to the efficiency, at the free surface, of a bubble rising in a pool of liquid, an event that occurs several times, uninterruptedly, during a stripping process, as deodorization.

Equation 7.2.4.2 can also be used in the evaluation of the vaporization efficiency, ε_{1-2}, for given values of S.[2,3,23] In this way, it assumes a form similar to the equation given by Decap et al.:[3]

$$\varepsilon_{1-2} = \frac{P^O}{\gamma_{FFA} \cdot P_{FFA}^{vp}} \cdot \frac{\ln \frac{X_{FFA_1}}{X_{FFA_2}} + \left(X_{FFA_1} - X_{FFA_2} \right)}{\frac{S}{F_{OIL}} + \left(X_{FFA_1} - X_{FFA_2} \right)} \quad (7.2.4.3)$$

At this point, one important aspect to be discussed is the non-ideality of the liquid phase, not considered by Decap et al.[3] in the development of their

model. As we know, edible oils are multicomponent mixtures formed by a variety of compounds, including FFA and acylglycerols. Decap et al.[3] had it in mind, when they used a neutralized and bleached soybean oil with an added acidity (oleic acid) in their experiments, to approximate their mixture closely to a pseudo-binary one. However, even at this pseudobinary mixture, the γ_{FFA} value, calculated with UNIFAC (r ¾)[24], is in the range of 0.89 to 0.91. This is due to the differences between the size and polatirity of a FFA and a triacylglycerol. Looking at Equation 7.2.4.3, it is possible to note that γ_{FFA} can influence importantly the value of ε_{1-2}, raising it as γ_{FFA} deviates negatively from unity. We explore this topic in view of our results in other parts of this article. It is important to highlight that our previous works[10,14] have shown that UNIFAC (r ¾)[24] better suits in the VLE evaluation of fatty mixtures.

7.2.5 Estimation of Physical Properties of the Oil

To estimate the required properties (ρ_L, μ_L, D_L, γ, P^{vp}), we selected group contribution and empirical equations available in the literature. To calculate activity coefficients for components *A, B* and *C*, UNIFAC (r ¾)[24] was used. For vapor pressure of compound *B* (water), an equation from Design Institute of Physical Properties (DIPPR)[25] was chosen; for compound *A* (oleic acid), we used the empirical Lederer's equation[26] as suggested by Decap et al.[3]; for compound *C* (triacylglycerol), the equation suggested by Ceriani and Meirelles[14] was applied.

For viscosities and densities of vegetable oils, we followed, respectively, the methods of Rabelo et al.[27] and of Halvorsen et al.[28] Based on these methods, the following equations were obtained:

$$\rho_L\left(\mathrm{kg/m^3}\right) = \frac{52.904}{0.2230^{1+\left(1-\frac{T(\mathrm{K})}{819.41}\right)^{2/7}}} + 24.625 \qquad (7.2.5.1)$$

$$\mu_L(\mathrm{Pa\cdot s}) = 0.001 \cdot \exp\left(-2.9939 + \frac{1156}{T(\mathrm{K}) - 138.359}\right) \qquad (7.2.5.2)$$

For all calculations the oil was considered as containing a representative triacylglycerol (same molecular weight and insaturation of the oil) and a FFA (oleic acid).

7.3. Results and discussion

We concentrated our efforts to investigate the developed equations in the view of the work of Decap et al.,[3] which is the most recent on the study of vaporization efficiency. Besides, Decap et al.[3] were also careful in the conduction of their experiments, mainly in the added acidity and in the prevention of reflux of volatile compounds: (i) they used neutralized and bleached soybean oil with a low content of initial acidity (0.1%, w/w) to minimize the presence of other fatty acids than oleic acid (added before each stripping experiment); (ii) the top part of the batch deodorizer was heated 20-35°C above the deodorization temperature.

We selected soybean oil (M = 870 kg/kmol) with 1.1% of oleic acid, as the initial acidity,[3] for our investigation. The following step was to obtain the respective constants C_3 and C_4 of Equations 7.2.2.19, 7.2.2.20 and 7.2.2.24 by solving the vapor liquid equilibrium (VLE) relation $\left(\sum_i y_i = 1 = \gamma_i \cdot x_i \cdot P_i^{vp} / P\right)$ for some operating conditions (Table 7.3.1). Their values are brought in Table 7.3.2.

To confirm the validity of our previous consideration about the irrelevant variation of the molar concentrations of components A and C, we put some of their values, found from isothermal VLE calculations, in Table 7.3.1. As one can see, more water dissolves for higher pressures and lower temperatures. Note that, for a given temperature, x_A and x_C are practically independent of pressure, as already mentioned.

Table 7.3.1. VLE for components A, B and C at selected conditions of temperature and pressure for soybean oil with 1.1% of acidity.

T (°C)	P (Pa)	m	x_A	$10^3 x_B$ [a]	x_C
210	267	2.7309	0.03312	0.0150	0.9669
	667	1.0343	0.03312	0.0395	0.9668
	1333	0.5082	0.03312	0.0804	0.9668
	4000	0.1674	0.03311	0.2439	0.9666
	6666	0.1002	0.03311	0.4074	0.9665
230	267	7.3996	0.03312	0.0096	0.9669
	667	2.5690	0.03312	0.0276	0.9669
	1333	1.2304	0.03311	0.0576	0.9668
	4000	0.3989	0.03311	0.1775	0.9667
	6666	0.2381	0.03311	0.2975	0.9666

[a] The vapor liquid equilibrium relation was solved to determine the water concentration in the liquid at the chosen temperature and pressure conditions.

Table 7.3.2. VLE constants for Equations 7.2.2.19, 7.2.2.20 and 7.2.2.24 for soybean oil with 1.1% of acidity.

T (°C)	C_3	C_4
210	0.8026	1.0252
230	0.5613	1.0663
250	0.1528	1.2209

To achieve a general idea about the equations developed in this work (Equations 7.2.2.20, which includes hydrostatic pressure and water solubility effects, 7.2.2.24, which includes the water solubility effect and partially the effect of the hydrostatic pressure, and Equation 7.2.3.3, which does not include these effects), we selected an experimental condition of Decap et al.[3] (250°C, 1.5% of stripping steam and 300 Pa) to calculate the profile of vaporization efficiency within the stripping process. Instead of 3 cm, as used by Decap et al.,[3] we considered a pool of oil of 80 cm in this study. Just to notify, in industrial batch deodorizers, the liquid height is around 1.3 m,[12] and in industrial continuous deodorizers, this value ranges between 0.3 and 0.8 m on each plate.[29] Figure 7.3.1 shows the calculated values of p_A as a function of h for a given value of p_A^* calculated using Equations 7.2.2.20, 7.2.2.24, 7.2.3.3 and the one from Coelho Pinheiro and Guedes de Carvalho.[7]

As one can see in Figure 7.3.1A, p_A increases gradually with h as foreseen from the qualitative study of the problem. However, the initial trend of the curve

changed, after it reaches a maximum value (at $H/4$ approximately), and starts to decrease as the free surface is approached. Note that p_A decreases abruptly after the bubble passed through $h=3H/4$ approximately. At this point, $\varepsilon^{h=3\cdot H/4}$ was around 97%.

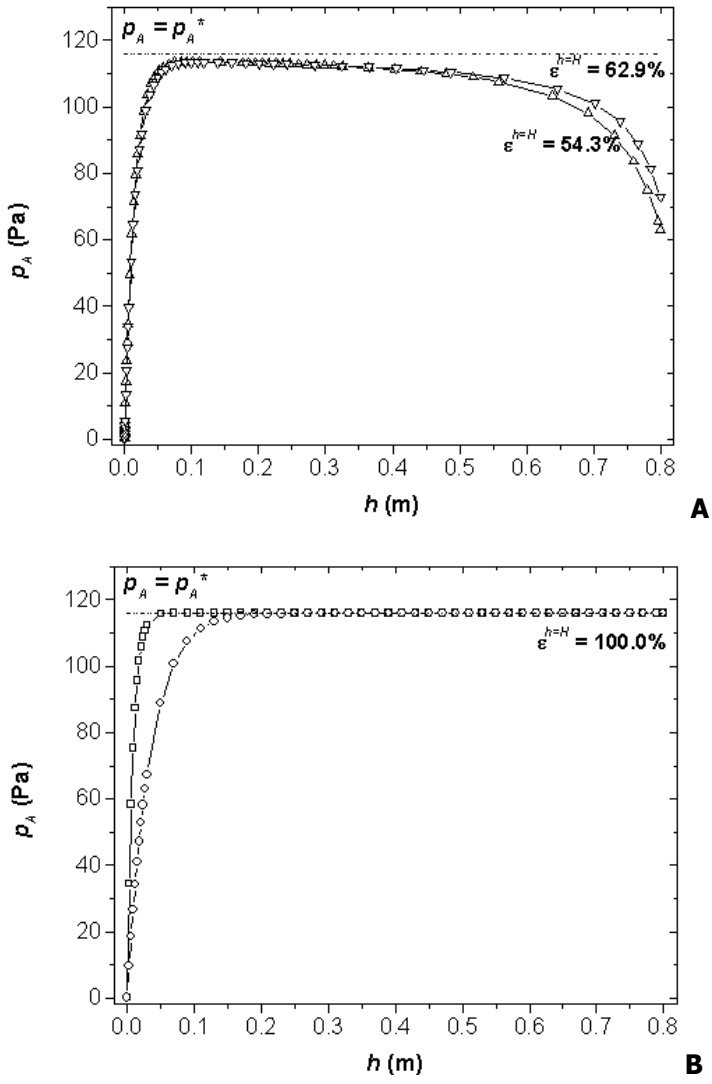

Figure 7.3.1. Predicted profiles of p_A as a function of h. Conditions: 260g of soybean oil, P^O = 300 Pa, T= 250°C, $\dot{m}_G$ = 0.016g/min (1.5%) and H = 0.8 m. (a) Equation 7.2.2.20 (∆) and Coelho Pinheiro and Guedes de Carvalho[7] (▽); (b) Equation 7.2.2.24 (□) and Equation 7.2.3.3 (○).

This behavior, as pointed out by Coelho Pinheiro and Guedes de Carvalho,[7] is a consequence of bubble expansion. As the free surface is approached, the

reduction in hydrostatic pressure over a short distance is large in comparison with the local pressure, and the gas bubble expands greatly.

For a better understanding of this fact, we plotted in Figure 7.3.2 the values of D_G and d_b corresponding to the p_A profile of Equation 7.2.2.20 (in Figure 7.3.1A).

Looking at Figure 7.3.2, it is possible to note that there is a considerable increase in values of D_G and d_b as the bubble ascends in a varying pressure field (from $P = P^O + \rho_L \cdot g \cdot H$ to P^O), but their effects in the mass-transfer are opposite. The bubble expansion causes a reduction in the surface area per unit of bubble volume, reducing mass-transfer. In contrast, as D_G increases, the mass-transfer resistance in the gas-phase reduces, improving mass-transfer of compound *A* to the bubble.

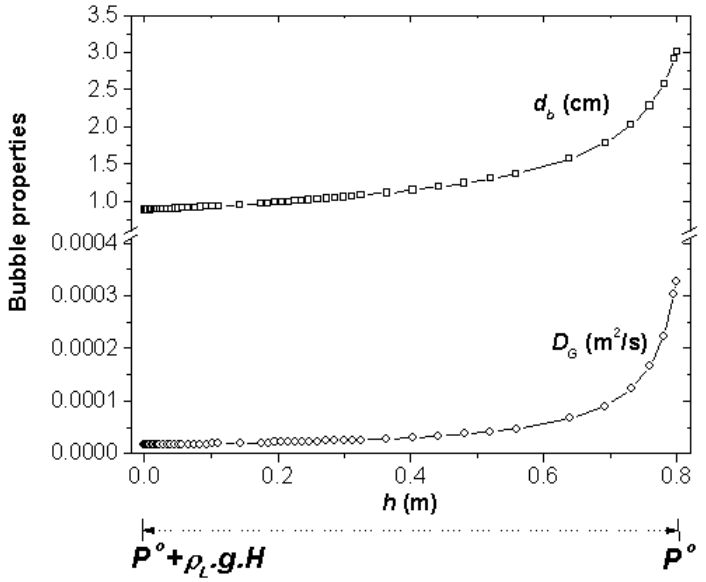

Figure 7.3.2. Bubble properties as a function *h*. Conditions: 260g of soybean oil, P^O = 300 Pa, *T*= 250°C, $\dot{m}_G$ = 0.016g/min (1.5%) and *H* = 0.8 m. D_G (○) from Equation 7.2.2.11 and d_b (□) from Equation 7.2.2.5.

Note in Figure 7.3.1A that water solubility (Equation 7.2.2.20) yields a lower value for $\varepsilon^{h=H}$, but its curve is almost coincident with the other until *h*= 3*H*/4, approximately. After this point, there is a slight divergence between the

curves obtained using Equation 7.2.2.20 and the one from Coelho Pinheiro and Guedes de Carvalho.[7] This difference is caused by the smaller local driving force found in our case, although the local mass transfer coefficient and also the bubble area were higher than in the case studied by Coelho Pinheiro and Guedes de Carvalho.[7] As a result, the effect of a decrease in the hydrostatic pressure in the evolution of p_A with h is more markedly.

Figure 7.3.1B gives the predicted profiles of $p_A(h)$ using Equations 7.2.2.24 and 7.2.3.3. As the hydrostatic pressure effect in the value of p_A was ignored in both equations, higher values of $\varepsilon^{h=H}$ (100.0%) were obtained. Although Equation 24 takes into account water solubility and hydrostatic pressure effects in the bubble size, our calculation shows that this equation is not able to describe a behavior similar to that obtained with the most complete formulation, given by Equation 7.2.2.20. The necessary simplifications assumed to obtain an analytical solution are responsible for the changes in the solute partial pressure profile. The difference in the curves obtained with Equations 7.2.2.24 and 7.2.3.3 in the region close to the injection point is the result of the greater interfacial area per unit of gas volume observed for smaller bubbles formed at the orifice; remember that with Equation 7.2.3.3 the bubble size is evaluated at P^O and considered constant during its rise. Furthermore, Equation 7.2.2.24 does not consider the variation of D_G with P.

As already discussed by Coelho Pinheiro and Guedes de Carvalho,[7] and also corroborated by our results (with Equation 7.2.2.20), stripping in low pressures can lead to an interesting situation in which the increase in the liquid-height may not lead to an increase in vaporization efficiency.

After this phenomenological overview about the profiles of p_A during the bubble growth, which can not be measured experimentally, we are interested in investigate the performance of Equations 7.2.2.20, 7.2.2.24, 7.2.3.3 and the one from Coelho Pinheiro and Guedes de Carvalho[7] in the view of the experimental data of Decap et al.[3] and check if these equations can be used in the prediction of

real problems. Decap et al.[3] used an lab-scale deodorizer to investigate the influence of processing variables such as temperature, working pressure and amount of steam or gas, in vaporization efficiency $\varepsilon^{h=H}$, calculated with a simplified version of Equation 7.2.4.3 (without γ_{FFA}).

At present, it is necessary to establish a relation between ε_{1-2} (in Equation 7.2.4.3) and $\varepsilon^{h=H}$ to start with this discussion. As mentioned above $\varepsilon^{h=H}$ is the vaporization efficiency at the free surface for a single rising bubble, whereas ε_{1-2} is the average vaporization efficiency relative to the entire stripping time (60 min in the case of Decap et al.[3]). As a bubble rises, it absorbs compound *A*, depleting the oil acidity and changing x_{FFA}. This phenomenon occurs several times successively. Mathematically, ε_{1-2} would be equal to:

$$\varepsilon_{1\text{-}2} = \frac{\int_{x_{FFA\,1}}^{x_{FFA\,2}} \varepsilon^{h=H} \cdot dx_{FFA}}{\int_{x_{FFA\,1}}^{x_{FFA\,2}} dx_{FFA}} \qquad (7.3.1.1)$$

Remember, however, that the VLE, and then p_B^*, depends on x_{FFA}, and the constants C_3 and C_4, in Equations 7.2.2.20 and 7.2.2.24, have to be reevaluated for each x_{FFA} considered. Table 7.3.3 shows the calculated values of ε_{1-2} for all nine experiments of Decap et al.[3] taken steps of 0.1% in w_{FFA}, and considering H=3cm. Decap et al.[3] emphasized, however, in their illustration of the oil flask and in the text, that the oil-layer height was not so accurately measured during their experiments, being around of 3 cm in the middle of the batch deodorizer flask. In this way, one should expect that it would be very difficult to get $\varepsilon^{h=H}$ precisely from an experimental task.

As a general rule, the ε_{1-2} values calculated using our version of Bailey equation (Equation 7.2.4.3) were always greater than the reported values of Decap et al.[3] This is a direct consequence of the inclusion of γ_{FFA}, since its values are

always lower than 1.0. Just one value of ε_{1-2} was greater than 100%, and this fact occurred also for Decap et al.[3] calculation. Considering that our previous works[10,14] indicated that fatty mixtures are better described as nonideal, we recommend to include γ_{FFA} in the estimation of ε_{1-2} for given values of steam amounts (*S*).

Looking at Table 7.3.3, it is noteworthy that all the equations studied in this work are capable of describing ε_{1-2}, either by the direct substitution of *H* (Equation 7.2.3.3) or in combination with Equation 7.3.1 (Equation 7.2.2.20, 7.2.2.24 and the one from Coelho Pinheiro and Guedes de Carvalho).[7] Despite the complexity of Equation 7.2.2.20, that has considered all the important effects on mass-transfer, its performance in the prediction of the experimental work of Decap et al.[3] was not better than Equation 7.2.2.24. Remember that two simplifications were assumed in the development of Equation 7.2.2.24 i.e., the effect of d*P* in dp_A is ignored and $\overline{D_G}$ is used as an average value. In relation to Equation 7.2.3.3, one can see that bubble expansion (Equation 7.2.2.24) leads to better results, mainly if P^O is higher (400 Pa and 500 Pa).

The equation from Coelho Pinheiro and Guedes de Carvalho[7] may be used in the prediction of p_A profiles for deodorization with nitrogen, which is an alternative for the traditional process.[1] In the present case (steam stripping) the prediction of ε_{1-2} with their equation gave a slightly higher ARD value.

We were surprised about the accuracy achieved, in this investigation, by the simpler equations (Equation 7.2.2.24 and 7.2.3.3). In Equation 7.2.3.3, the variation of x_{FFA} is not included, since m' is equal to $\gamma_A \cdot P_A^{vp}/P^O$, and the variation of γ_A with x_A and x_C was detected to be unimportant for the studied conditions. In this way, it is the easiest equation to use. Equation 7.2.2.24, even though VLE information is necessary, is also user-friendly because it is a result of an analytical integration. Taking into account the performance shown in Table 7.3.3, we recommend, for practical purposes, Equations 7.2.2.24 and 7.2.3.3. But, further experimental work, including the investigation of the influence of the oil-layer

height upon efficiency, is necessary to take a definitive decision concerning the performance of the equations developed in the present work.

In order to achieve some sensibility about the ARD values shown in Table 7.3.3, it can be mentioned the results reported by Coelho Pinheiro and Guedes de Carvalho.[7] These authors, for mixtures of pentane in n-paraffins and sunflower oil, compared experimental and theoretical vaporization efficiencies, from which we obtained an average deviation of 21% for the whole set of data, and 42% for the experiments with the edible oil.

It is very important to highlight that the good agreement found in the prediction of ε_{1-2} with all the developed equations is a direct consequence of the inclusion of the gas-phase mass-transfer resistance in the K_{OG} (see Equation 7.2.2.6). To not include this term leaded to ARD values in the range of 35 to 40%.

Table 7.3.3. Average Vaporization Efficiencies for steam refining, ε_{1-2}, at Experimental Conditions of Decap et al.[3] $\left(w_{FFA_1} = 1.1\%\right)$.

T (°C)	% of steam	P^{O} (Pa)	$w_{FFA\ 2}$ (%)	ε_{1-2} Decap et al.[3]	Eq. 7.2.4.3	Eq. 7.2.2.20	Eq. from Ref. 7	Eq. 7.2.2.24	Eq. 7.2.3.3
210	0.5	500	0.803	84	95	81.0	81.9	92.0	90.1
210	0.5	300	0.554	106	120	73.4	74.2	90.2	87.3
210	1.5	500	0.452	81	90	58.9	60.4	69.4	65.7
210	1.5	300	0.262	77	86	51.3	52.6	66.5	61.5
230	1.0	400	0.170±0.017	81 ± 4	92	60.1	63.1	72.8	71.2
250	0.5	500	0.262	70	78	66.7	75.7	77.5	85.0
250	0.5	300	0.062	81	91	57.9	66.3	73.6	80.7
250	1.5	500	0.060	49	56	44.5	53.4	52.8	58.6
250	1.5	300	0.040	34	38	35.7	44.6	47.0	53.3
ARD (Average Relative Deviation)						**18.7**	**19.8**	**14.3**	**19.4**

$\text{ARD}(\%) = \sum_{i=1}^{9} \frac{1}{9} \cdot \left[100 \cdot \frac{\left| \varepsilon_{1-2exp} - \varepsilon_{1-2calc} \right|}{\varepsilon_{1-2exp}} \right]_i$, where $\varepsilon_{1-2\,exp}$ is the value reported by Decap et al.[3] for each experiment.

Figure 7.3.3 shows that $\varepsilon^{h=H}$ varied unimportantly with x_{FFA}(%) for experiment 4 of Decap et al.[3] (in Table 7.3.3).

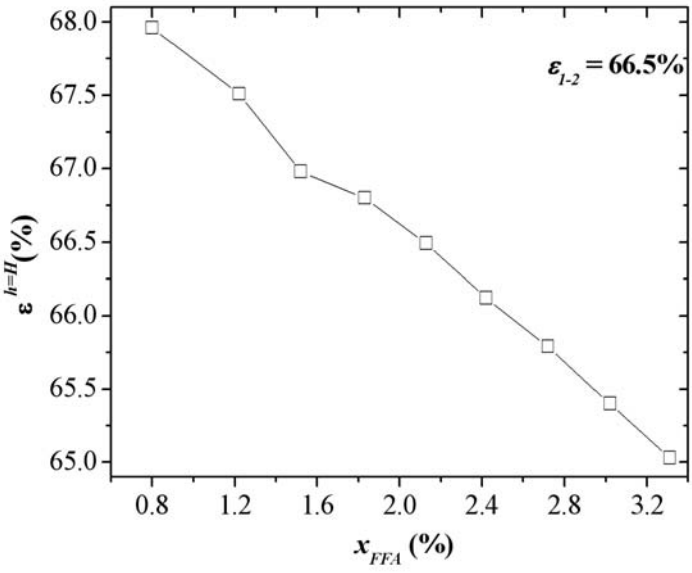

Figure 7.3.3. Vaporization efficiency $\varepsilon^{h=H}$ as a function of $x_{FFA}(\%)$. Conditions: 260 g of soybean oil, T= 210°C, P^{O}=300 Pa, 1.5% of steam and *H*= 0.03 m.

The calculated value of ε_{1-2} would be 66.5% with Equation 7.2.2.24, and the value reported by Decap et al.[3] was 77%.

Some conclusions about the dependence of vaporization efficiency with working temperature and amount of gas injected can be obtained looking at Table 7.3.3. As the % of steam increases, ε_{1-2} reduces, due to the decrease in the contact time between a bubble and the liquid layer. The same effect is get with an increase in the working temperature. A higher temperature increases the gas-phase mass transfer resistance directly (see Equation 7.2.2.6), and also the liquid-phase mass transfer resistance via an enhancement in the *m*-value (see Table 7.3.1), reducing K_{OG} (see Equation 7.2.2.6). The relation of vaporization efficiency with pressure is more complex, because bubble expansion and therefore, the decrease of p_A near the free surface, is more pronounced at lower operating pressure. Note, in Table 7.3.3, that from the results of Equations 7.2.2.20, 7.2.2.24, 7.2.3.3 and the one from Coelho Pinheiro and Guedes de Carvalho,[7] as pressure decrease, ε_{1-2} also diminishes.

7.4. Conclusion

For stripping processes conducted at low pressures, as deodorization and/or physical refining, the hydrostatic pressure effect is important in the bubble expansion and reduces the partial pressure of solute inside it. As already shown in previous works, water solubility cannot be despised, despite the low pressures used in these processes. The equation proposed in this work takes both factors into account. Simple physical and mathematical models were developed for vaporization efficiency, using fatty acid as the volatile substance. With the equations proposed in this work it is possible to estimate vaporization efficiency, and the required amount of steam to FFA removal. The phenomenon of a bubble rising in a pool of liquid was well described. The experience achieved in the development of this work showed that the gas-phase resistance of mass-transfer should not be despised in the physical situation described here.

Nomenclature

A_b	Surface area of the bubble, m^2
C_1, C_2, C_3, C_4	Constants
c_L	Molar density of the solute-free oil, $kmol/m^3$
d_b	Bubble diameter, m
D_L	Diffusivity of solute *A* in the liquid, m^2/s
F_{OIL}	Moles of the oil feed (kmol)
FFA	Free fatty acid
g	Acceleration of gravity, m/s^2
h	Height of the oil-layer, m
H	Total liquid height, m
k_G	Vapor phase mass-transfer coefficient, m/s
k_L	Liquid phase mass-transfer coefficient, m/s
K_{OG}	Mass-transfer coefficient, $\frac{\text{kmol A}}{\text{m}^2\text{s}\,(\text{kmol A/kmol B})}$ or $\frac{\text{kmol A}}{\text{m}^2\text{s}}$ (in Equation 7.2.3.1).

m Distribution coefficient of compound *A* in free basis, $\frac{\text{kmol A/kmol B}}{\text{kmol A/kmol (B + C)}}$

m' Distribution coefficient of compound *A*

$\dot{m}_G$ Mass flowrate of gas through an orifice, g/min

M_L Average molecular weight of the solute-free oil, kg/kmol

n Number of moles, kmol

N_A Number of moles of component A transferred from the oil to a bubble, kmol A

p Partial pressure, Pa

P^O Pressure above the free surface of the liquid, Pa

P^{vp} Vapor pressure, Pa

R Gas constant, $8314.4\ \text{Pa} \cdot \text{m}^3/\text{kmol} \cdot \text{K}$

S Total moles of stripping steam, kmol

t_C Contact time between elements of fluid at the bubble surface, s

T Temperature,°C or K

TAG Triacylglycerol

u_b Rising velocity of a bubble in the liquid, m/s

w Liquid mass fractions

x, y Liquid and vapor molar fractions

X, Y Liquid and vapor molar ratio in solute-free basis

X_A Liquid molar ratio of *A* in the liquid, $\frac{\text{kmol A}}{\text{kmol B + C}}$

Y_A Vapor molar ratio of *A* in a bubble, $\frac{\text{kmol A}}{\text{kmol B}}$

$\Delta Y_A = Y_A^* - Y_A$ Driving force for mass transfer, in free basis of *A*, $\frac{\text{kmol A}}{\text{kmol B}}$

Greek Symbols

ε Vaporization efficiency

γ	Activity coefficient
μ_L	Viscosity of the liquid, $Pa \cdot s$
v_G	Volumetric flowrate of gas through an orifice calculated at $P^o + \rho_L \cdot g \cdot H$, m^3/s
ρ_L	Density of the solute-free oil, kg/m^3
Subscripts	
A	Related to the volatile compound (*A*)
b	Related to a bubble
B	Related to the steam (compound *B*)
C	Related to the nonvolatile compound (*C*)
FFA	Free fatty acids
i	Related to component *i*
L	Liquid
OIL	Related to the oil
S	Related to the stripping steam
1	Related to free fatty acids in the crude oil (initial state)
2	Related to free fatty acids in refined oil (final state)
Supercripts	
*	Equilibrium condition
vp	Vapor pressure

Acknowledgments

The authors thank FAPESP (Fundação de Amparo à Pesquisa do Estado de São Paulo – 03/04949-3) and CNPq (Conselho Nacional de Desenvolvimento Científico e Tecnológico - 521011/95-7) for the financial support.

Literature cited

(1) Graciani, E.; Rodriguez-Berbel, F.; Paredes, A.; Huesa, J. Deacidification by Distillation using Nitrogen as Stripper. Possible Application to the Refining of Edible Fats. *Grasas y Aceites*. **1991**, *42*, 286.

(2) Ruiz-Méndez, M.V.; Márquez-Ruiz, G.; Dobarganes, M.C. Comparative Performance of Steam and Nitrogen as Stripping Gas in Physical Refining of Edible Oils. *J. Amer. Oil Chem. Soc.* **1996**, *73*, 1641.

(3) Decap, P.; Braipson-Danthine, S.; Vanbrabant, B.; De Greyt, W.; Deroanne, C.; Comparison of Steam and Nitrogen in the Physical Deacidification of Soybean Oil. *J. Amer. Oil Chem. Soc.* **2004**, *81*, 611.

(4) Carlson, K.F. Deodorization. In *Bailey's Industrial Oil and Fat Products*; Hui, Y.H., Ed.; Wiley-Interscience: New York, 1996: Vol. 4, pp. 339-390.

(5) Bailey, A.E. Steam Deodorization of Edible Fats and Oils, *Ind. Eng. Chem.* **1941**, *33*, 404.

(6) Ruiz-Méndez, M.V.; Garrido-Fernández, A.; Rodriguez-Berbel, F.C.; Graciani-Constante, E. Relationships among the Variables Involved in the Physical Refining of Olive Oil using Nitrogen as Stripping Gas. *Lipids.* **1996**, *98*, 121.

(7) Coelho Pinheiro, M.N.; Guedes de Carvalho, J.R.F. Stripping in a Bubbling Pool under Vacuum. *Chem. Eng. Sci.* **1994**, *49*, 2689.

(8) Coelho Pinheiro, M.N. Stripping in a Bubbling Pool under Vacuum-Contribution of the Interfacial Tension to the Pressure Inside the Bubbles. *Int. Comm. Heat Mass Transfer* **2001**, *28*, 1053.

(9) Szabo Sarkadi, D.; Hydrolysis during Deodorization of Fatty Oils. Catalytic Action of Fatty Acids. *J. Amer. Oil Chem. Soc.* **1959**, *36*, 143.

(10) Ceriani, R.; Meirelles, A.J.A.; Simulation of Batch Physical Refining and Deodorization Processes. *J. Amer. Oil Chem. Soc.* **2004**, *81*, 305.

(11) Petrauskaité, V.; De Greyt, W.F; Kellens, M.J. Physical Refining of Coconut Oil: Effect of Crude Oil Quality and Deodorization Conditions on Neutral Oil Loss. *J. Am. Oil Chem. Soc*. **2000**, *77*, 581.

(12) Theme, J.G., *Coconut Oil Processing;* FAO: Rome, 1968.

(13) Davidson, H.F.; Campbell, E.J.; Pritchard, R.A. Sunflower Oil. In *Bailey's Industrial Oil and Fat Products*; Hui, Y.H., Ed.; Wiley-Interscience: New York, 1996: Vol. 2, pp. 603-691.

(14) Ceriani, R.; Meirelles, A.J.A. Predicting Vapor-Liquid Equilibria of Fatty Systems. *Fluid Phase Equilib.* **2004**, *215*, 227.

(15) Lewis, W.K.; Whitman, W.G. Principles of Gas Absorption, *Ind. Eng. Chem.* **1924**, *16*, 1215.

(16) Kunii, D.; Levenspiel, O. *Fluidization Engineering;* John Wiley and Sons: New York, 1977.

(17) Davidson, J.F.; Schüller, B.O.G.; Bubble Formation at an Orifice in an Inviscid Liquid, *Trans. Inst. Chem. Eng.* **1960**, *38*, 335.

(18) Bird, R.B.; Stewart, W.E.; Lightfoot, E.N. *Transport Phenomena*; Wiley: New York, 1960.

(19) Siddiqi, M.A.; Lucas, K. Correlations for Prediction of Diffusion in Liquids. *J. Chem. Eng.* **1986**, *64*, 839.

(20) Smits, G. Measurement of the Diffusion Coefficient of Free Fatty Acid in Groundnut Oil by the Capillary-Cell Method. *J. Am. Oil Chem. Soc.* **1976**, *53*, 122.

(21) Wilke, C.R.; Lee, C.Y. Estimation of Diffusion Coefficients for Gases and Vapor. *Ind. Eng. Chem.* **1955**, *47*, 1253.

(22) Shampine, L.F.; Reichelt, M.W.; Kierzenka, J.A. Solving Index-1 DAEs in MatLab and Simulink. *Siam Review.* **1999**, *41*, 538.

(23) Szabo Sarkadi, D. Laboratory Deodorizer with a Vaporization Efficiency of Unity. *J. Am. Oil Chem. Soc.* **1958**, *35*, 472.

(24) Fornari, T.; Bottini, S.; Brignole, E.A. Application of UNIFAC to Vegetable Oil-Alkane Mixtures, *J. Am. Oil Chem. Soc.* **1994**, *71*, 391.

(25) DIPPR Student Chemical Database Login, http://dippr.byu.edu/students/chemsearch.asp (accessed May. 2004)

(26) Markley, K.S. *Fatty Acids: Their Chemistry and Chemical Properties*; Interscience: New York, 1947, pp.161-162.

(27) Rabelo, J.; Batista, E.; Cavaleri, F.W.; Meirelles, A.J.A. Viscosity prediction for fatty systems. *J. Amer. Oil Chem. Soc.* **2000**, *77*, 1255.

(28) Halvorsen, J.D.; Mammel, W.C.; Clements, L.D. Density-Estimation for Fatty-Acids and Vegetable-Oils based on their Fatty-Acid Composition. *J. Am. Oil Chem. Soc.* **1993**, *70*, 875.

(29) Ahrens, D. Comparison of tray, thin-film deodorization, *Inform* **1998**, 9, 566.

CAPÍTULO 8. STUDY OF CANOLA OIL DEODORIZATION COMBINING COMPUTATIONAL SIMULATION WITH RESPONSE SURFACE METHODOLOGY

Trabalho submetido à revista **European Journal of Lipid Science and Technology.**

Key words

Canola oil, deodorization, isomerization, response surface methodology, simulation.

Summary

This work presents the application of a differential distillation model for the simulation of canola oil deodorization. The response surface methodology (RSM) was selected to study the optimization of the process in terms of *cis-trans* isomerization of polyunsaturated fatty acids and final oil acidity. The simulations were performed considering a pilot-scale deodorizer (100 kg of oil). Temperature, duration of the batch (residence time), steam flow and pressure were the factors chosen for this study. Following a previous work, the vapor-liquid equilibria of the fatty compounds were described by group contribution equations for vapor pressures and activity coefficients. Energy balances and kinetics of the isomerization reactions were included. The RSM showed to be efficient in determining good ranges for the operation of batch deodorization, in terms of final oil acidity and total content of *trans* fatty acids, in the processing conditions selected for this work.

8.1. Introduction

Deodorization is a mass transfer purification process of the oil industry that aims to vaporize odoriferous compounds and fatty acids from the oil. It is based on the substantial difference between the vapor pressure of the oil and the volatile undesirable materials, and is carried out under high temperatures and low pressures. Because of this unique combination of the processing conditions, important chemical reactions, such as isomerization of polyunsaturated fatty acids (PUFA), and distillative losses of nutritional compounds (as tocopherols and sitosterols), do occur during deodorization [1]. The main factor influencing the speed of isomerization reaction is the deodorization temperature. The initial content of *trans* PUFA (0.1 to 0.3%) in crude oils may rise up to 5% in refined oils,

exclusively due to deodorization, since this reaction does not occur during preceding steps of the refining process [2]. According to Carlson [3], depending on oil type and deodorization temperature, up to 60% of the initial amounts of sterols and tocopherols can be distilled. Usually, most flavors and odors have been eliminated when the FFA content is below 0.03% [3].

PUFA are essential fatty acids, vitally important in human metabolism. *Trans* PUFA, on the other hand, are similar to saturated fatty acids in terms of their effects on cholesterol [4]. Tocopherols are natural antioxidants [5], whereas sterols are used in the manufacture of pharmaceuticals, such as hormones and corticoids [6].

Bearing in mind all these aspects, it is straightforward to realize that the quality of the deodorized oil depends on a large number of variables and their possible interactions. In such cases, response surface methodology (RSM) has come as a useful tool for determining the effect of operating variables, requiring a shorter number of trials in the investigation. On the other hand, computer simulation permits the study of a wide range of processing parameters without the difficulties inherent to experimentation. The good agreement obtained by our previous works dealing also with simulation [7,8,9], indicates the applicability of such tool in the study of complex systems. Batista *et al.* [10] optimized a complex distillation process, using in a successful way RSM in combination with computer simulation.

This work applied RSM in the investigation and performance improvement of the pilot-scale batch deodorization of canola oil under typical processing conditions. The effect of selected variables i.e., temperature, pressure, batch duration and percentage of stripping steam, upon the responses, *trans* PUFA isomer generation and final oil acidity was studied, and corresponding response surface equations obtained. Canola oil was chosen because of its high level of PUFA and natural antioxidants, being suitable for our investigation goals. We compared our final results for the contents of *trans* PUFA isomers with the experimental works of Hénon *et al.* [11,12].

8.2. Materials and methods

8.2.1 Response surface methodology (RSM)

This study was carried out by RSM, based on the results from factorial design and regression analysis [13,14]. To evaluate the batch deodorization of canola oil by RSM, we selected from the literature [5,11] usual ranges of processing conditions: deodorization temperature (X_1), duration (X_2), percentage of stripping steam (X_3) and pressure (X_4). The factorial design (Tab. 1), which requires the use of coded variables, was used as a tool for evaluating the influence of the main process variables on the isomerization degrees of linoleic and linolenic acids, and on the final oil acidity (OA) in the deodorized oil. This study was arranged to get a quadratic model, being necessary 25 simulations (2^4 trials plus a star configuration and one central point).

The complete RSM equation describes the contributions of each factor on the response. The coefficient b_o is the outcome at the central point and the other coefficients measure the main effects and the interactions of the coded variables X_i on the response Y:

$$Y = b_o + \sum b_i \cdot X_i + \sum b_{ii} \cdot X_i^2 + \sum b_{ij} \cdot X_i \cdot X_j \quad (with\ i \neq j) \qquad (8.2.1.1)$$

Note that only the significant coefficients shall be in the final RSM equation.

Table 8.2.1.1 Factorial design and coded variables of the deodorization of canola oil using RSM.

		Coded variables			
	Trial	X_1	X_2	X_3	X_4
Factorial design (16 trials)	1	-1	-1	-1	-1
	2	+1	-1	-1	-1
	3	-1	+1	-1	-1
	4	+1	+1	-1	-1
	5	-1	-1	+1	-1
	6	+1	-1	+1	-1
	7	-1	+1	+1	-1
	8	+1	+1	+1	-1
	9	-1	-1	-1	+1
	10	+1	-1	-1	+1
	11	-1	+1	-1	+1
	12	+1	+1	-1	+1
	13	-1	-1	+1	+1
	14	+1	-1	+1	+1
	15	-1	+1	+1	+1
	16	+1	+1	+1	+1
Star points $\alpha=\pm2$ (8 trials)	17	-2	0	0	0
	18	+2	0	0	0
	19	0	-2	0	0
	20	0	+2	0	0
	21	0	0	-2	0
	22	0	0	+2	0
	23	0	0	0	-2
	24	0	0	0	+2
Central point [a]	25	0	0	0	0
	Level				
	-2	-1	0	1	+2
T (°C)	210	225	240	255	270
t (h)	1	2	3	4	5
% steam	1	2	3	4	5
P (Pa)	267	400	533	667	800

[a] There is no trial error evaluation in simulation.

8.2.2 Modeling a batch deodorizer

Ceriani and Meirelles [7] simulated the laboratory-scale batch physical refining of coconut oil following the experiments of Petrauskaitè et al. [15] to characterize and quantify distillative neutral oil losses. The authors tested with success the application of a differential distillation model in this study, using the vapor pressure equation and the thermodynamic approach suggested by Ceriani

and Meirelles [16] to predict the vapor-liquid equilibria (VLE) of the fatty compounds involved. Their VLE model is shown below [16]:

$$k_i = \frac{y_i}{x_i} = \frac{\gamma_i \cdot f_i^o}{P \cdot \phi_i} \tag{8.2.2.1}$$

where

$$f_i^o = P_i^{vp} \cdot \phi_i^{sat} \cdot \exp\left(\frac{V_i^L \cdot \left(P - P_i^{vp}\right)}{R \cdot T}\right) \tag{8.2.2.2}$$

where f_i^o is the standard-state fugacity, x_i and y_i are the molar fractions of component *i* in the liquid and vapor phases, respectively, P is the total pressure, R is the gas constant, T is the system absolute temperature, P_i^{vp} and ϕ_i^{sat} are, respectively, the vapor pressure and the fugacity coefficient of the pure component *i*, γ_i is the liquid-phase activity coefficient, ϕ_i is the vapor-phase fugacity coefficient and V_i^L is the liquid molar volume of component *i*. The exponential term corresponds to the Poynting factor (POY).

In a multicomponent differential distillation, a tank (still) is charged with feed and then heated. Vapor flows overhead, is condensed and collected in a receiver (see Fig.8.2.2.1).

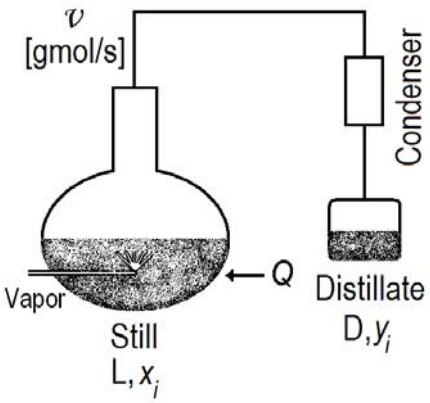

Figure 8.2.2.1. Scheme of a lab-scale batch deodorizer.

Since the still composition is changing continuously, this process is inherently dynamic, i.e., it cannot be modeled as a steady-state process. The composition of the material collected in the receiver also varies with time, so that the composition of the distillate is an average of all the material collected. It is possible to look at the differential distillation as a sequence of innumerous and successive vaporizations [7].

A reactive batch deodorization is similar to a multicomponent differential distillation, for which the total and component molar balances are given by [7,17]:

$$\frac{\mathrm{d}L}{\mathrm{d}t} = -\upsilon + \Delta R \tag{8.2.2.3}$$

and

$$\frac{\mathrm{d}(L \cdot x_i)}{\mathrm{d}t} = -\upsilon \cdot y_i + R_i \tag{8.2.2.4}$$

where L is the total moles of liquid in the still, υ is the molar vaporization rate in moles/time and x_i and y_i are the liquid and vapor molar fractions of component i in the liquid and vapor phases, respectively, ΔR is the total change of number of moles caused by reaction course (moles/time), and R_i is the number of moles of component i reacted (moles/time).

ΔR and R_i can be calculated using the relations below [17]:

$$\Delta R = \sum_i k_i \cdot (x_i \cdot L) \tag{8.2.2.5}$$

$$R_i = k_i \cdot (x_i \cdot L) \tag{8.2.2.6}$$

In this work, the k_i values were taken from Hénon *et al.* [12] for linoleic and linolenic acid isomerization. For linoleic acid:

$$k_{Li}(\mathrm{h}^{-1}) = 10^{-7921.95/T(\mathrm{K})+12.76} \tag{8.2.2.7}$$

and for linolenic acid:

$$k_{Ln}(\mathrm{h}^{-1}) = 10^{-6796.63/T(\mathrm{K})+11.78} \tag{8.2.2.8}$$

In our model, it is assumed that the liquid and vapor phases are in equilibrium at each instant, and that the steam becomes totally saturated with the volatiles as it passes through the oil in the still (vaporization efficiency factor equal to unity).

For the receiver distillate tank, the total and component molar balances are [7]:

$$\frac{\mathrm{d}D}{\mathrm{d}t} = \upsilon \tag{8.2.2.9}$$

and

$$\frac{\mathrm{d}D_i}{\mathrm{d}t} = \upsilon \cdot y_i \tag{8.2.2.10}$$

where D is the total moles of distillate and D_i represents the moles of component i in the tank.

To determine the molar vaporization rate, υ, at each time t, it is necessary to consider the energy balance of the still. It was set as shown below:

$$\upsilon = \frac{U \cdot A \cdot (T_{hs} - T) - L \cdot c_p \cdot \dfrac{dT}{dt}}{\Delta H_{vap}} \tag{8.2.2.11}$$

where U is the global coefficient of heat transfer $\left(\mathrm{J/s \cdot m^2 \cdot ^\circ C}\right)$, A is the total area of heat transfer $\left(\mathrm{m^2}\right)$, T_{hs} is the heat source temperature, c_p and ΔH_{vap} are, respectively, the liquid heat capacity $\left(\mathrm{J/gmol \cdot ^\circ C}\right)$ and the heat of vaporization of the oil $\left(\mathrm{J/gmol}\right)$. Reasonable values of U and A were taken from the literature. Perry and Chilton [18] inform that U ranges from 123.03 $\mathrm{J/s \cdot m^2 \cdot ^\circ C}$ to 227.13 $\mathrm{J/s \cdot m^2 \cdot ^\circ C}$ for the heat of edible oils with vapor. According to Theme [19], A varies from 0.5 $\mathrm{m^2/100\ kg\ of\ oil}$ to 0.75 $\mathrm{m^2/100\ kg\ of\ oil}$. For this study, it was set a value of 61.5 $\left(\mathrm{J/s \cdot ^\circ C}\right)$ for the product $U \cdot A$. The heat source temperature was supposed to be

equal to 280 °C for all the simulations performed. Note that, with this supposition, the heat flux (J/s) was a function of the temperature of the mixture during the heating period, and was constant during the stripping period (equal to the deodorization temperature). It is important to observe that the heat flux, provided by the heat source to the oil, depended of factor X_1, since it was calculated for each time t by $q(\text{J/s}) = U \cdot A \cdot (T_{hs} - T)$. The direct consequences are that the heat flux and the molar vaporization rate (v) were lower for higher values of X_1. For lab-scale and pilot plant scale batch deodorizers, a common situation is, in fact, that the generation of the steam used for heating has a small range of variation in terms of pressure and temperature.

In the simulations performed by Ceriani and Meirelles [7], based in the experimental work of Petrauskaitè et al. [15], the vaporization rate was set constant during the entire residence time of the oil in the deodorizer, for each deodorization temperature studied, because this information was available from the experimental trials.

Predictive group contribution methods were selected to estimate all the physical properties required for the energy balances. Following previous works [8,9], we selected Joback's technique for ideal vapor heat capacities, Rowlinson-Bondi's method for liquid heat capacities [20], and the method of Tu and Liu [21] to estimate the enthalpy of vaporization of each compound involved. The physical properties of water (stripping steam) were calculated using the equations from the Design Institute for Physical Properties (DIPPR) Chemical Database [22]. The property calculations required for the equilibrium relationships (Eq.8.2.2.1 and Eq.8.2.2.2) were performed using the well-set procedure of Ceriani and Meirelles [16]. For vapor pressures of tocopherol and β-sistosterol, we used the same equations shown in the work of Ceriani and Meirelles [8].

Combining Eq. 8.2.2.3 to 8.2.2.11 together with the equilibrium relationship (Eq. 8.2.2.1) we have a system that is easily solvable by direct numerical integration [7].

Following our previous work [7], the whole deodorization process was divided in two parts: (1) *heating* (in absence of water) and (2) *stripping* with sparge steam at constant temperature, which was allowed by the presence of very small amounts of water dissolved in the liquid phase [7]. The duration (coded variable X_2 in the RSM) was related to the residence time at the deodorization temperature, after the heating period.

All the models cited above use an iterative procedure for convergence, as Newton-Raphson [7]. All required physical properties of component *i* were calculated for each component, in each and every iteration.

The entire set of trials shown in Table 8.2.1.1 was simulated using the computational program developed with MatLab (Mathworks, v.5.0). The simulation results were expressed as percentage of *trans* linoleic and linolenic acids, and final OA (% of oleic acid). Such results were analysed using the software Statistica (Statsoft, v.5.0) following the central composite design, and compared with those reported by Hénon et al. [11]. The final concentrations of tocopherol and β-sistosterol in the deodorized oil were analyzed for the optimized conditions.

To test the predictive capacity of the statistical models developed in this work, comparing its values with the simulation results, the average relative deviations (ARD) were calculated according to the relation below:

$$\text{ARD } (\%) = 100 \cdot \frac{\sum_{i} \left(\frac{\left| Y_{simul} - Y_{est} \right|}{Y_{simul}} \right)_i}{n} \qquad (8.2.2.12)$$

where Y is the response, *n* is the number of trials, the subscripts *simul* and *est* are, respectively, the values obtained by simulation and the estimated ones. A further comparison was done based in the experimental results of Hénon et al. [11]. In this case, their statistical models were used and the results were compared with the values given by our simulations, whenever possible.

8.2.3 Composition of canola oil and reaction features

Table 8.2.3.1 shows the overall composition of canola oil considered in this work. We followed information from Firestone [23] and Kemény *et al.* [24] to set the values of the fatty acid composition of the oil, and γ-tocopherol and β-sitosterol levels.

Table 8.2.3.1. Overall composition of canola oil

Fatty acid		Mass (%)	M (g/gmol)
C16:0 (P)		6.0	256.43
C18:1 (O)		60.8	282.47
C18:2 (Li)		20.1	280.45
C18:3 (Ln)		13.1	278.44
Class of compounds		Mass (%)	M (g/gmol)
Triacylglycerol (TAG)	PLiO	7.56	857.39
	PLnO	10.84	855.38
	OLiO	51.00	883.43
	OLnO	27.28	881.42
Diacylglycerol (DAG)		1.00	621.00
Monoacylglycerol (MAG)		1.00	356.55
Free fatty acids (FFA)		1.00	282.47
β-sitosterol		0.25	414.72
Tocoferol		0.07	414.00

The composition in triacylglycerols (TAG) was simplified in a way that each TAG had only one kind of fatty acid accessible for isomerization. With this supposition, the constants of reaction given by Hénon *et al.* [12] (see Eq. 8.2.2.7 and 8.2.2.8) could be used straightforwardly. It is important to highlight that the initial content of TAG in the oil has a chief influence in the speed of the isomerization reaction, because it is a first order reaction, i.e. the rate of the reaction is proportional to the concentration of the reacting substance (*cis* TAG, in this case). Some hypotheses were adopted to simplify the mathematical model and make this study possible. Each of them is detailed below:

- The TAG PLi$_{cis}$O, OLi$_{cis}$O, PLn$_{cis}$O and OLn$_{cis}$O were isomerized, respectively, to PLi$_{trans}$O, OLi$_{trans}$O, PLn$_{trans}$O and OLn$_{trans}$O, where the *trans* linoleic acid was represented by the isomer C18:2 (9*c*,12*t*) while the *trans* linolenic acid was represented by the isomer C18:3 (9*c*,12*c*, 15*t*);

- The TAG PLi$_{trans}$O, OLi$_{trans}$O, PLn$_{trans}$O and OLn$_{trans}$O were not re-isomerized, since the concentrations, and consequently, the probability of isomerization of the *cis*-TAG were much higher. In fact, Wolff [24] shows that the concentrations of C18:2 (9*c*,12*t*) and C18:3 (9*c*,12*c*, 15*t*) are always much higher than the concentrations of C18:2 (9*t*,12*t*) e C18:3 (9*t*,12*c*,15*t*) respectively, even at long duration times and high temperatures (4h, 260°C);
- The isomerization reaction also occurs during the heating period, and its magnitude is determined by the system temperature;
- Only the TAG are accessible for isomerization. DAG, MAG and FFA did not react.
- The residence time was started when the oil reached the deodorization temperature.

8.3. Results and Discussion

To provide a better understanding of the simulation program developed in this work, the temperature (°C) and the vaporization rate (g/min) profiles for trial number 25 (central point, see Tab. 8.2.1.1) are shown in Fig. 8.3.1A. As one can see, during the heating period, there was no vaporization of volatiles, since the boiling point of the mixture was not achieved. In this way, the heat provided by the heating source was used just for heating the mixture. On the contrary, during the stripping period, the temperature did not change, as a direct consequence of the assumption of water dilution in the liquid phase. Thus, the vaporization of volatiles absorbed all the heat from the heating source. Note that the starting temperature was chosen to be 135 °C, following the work of Hénon et al. [11]. Fig. 8.3.1B gives the profiles per time of three of the responses studied, C18:2 *trans*, C18:3 *trans* and acidity (% mass). As expected, the rates of formation of the two isomers were proportional to temperature, increasing considerably in the stripping period. Observe also the parallelism of the curves, a consequence of the proximity of the linear coefficients of Eqs. 8.2.2.7 and 8.2.2.8 (12.76 and 11.78, respectively). The rate constants of C18:2 *trans* were lower than those of C18:3 *trans*, even though the initial concentration of TAG containing C18:2 *cis* was higher

than TAG containing C18:3 *cis* (see Tab. 8.2.3.1). The FFA of the OA were vaporized just in the stripping period, since the boiling point of the whole mixture was not achieved during the heating period.

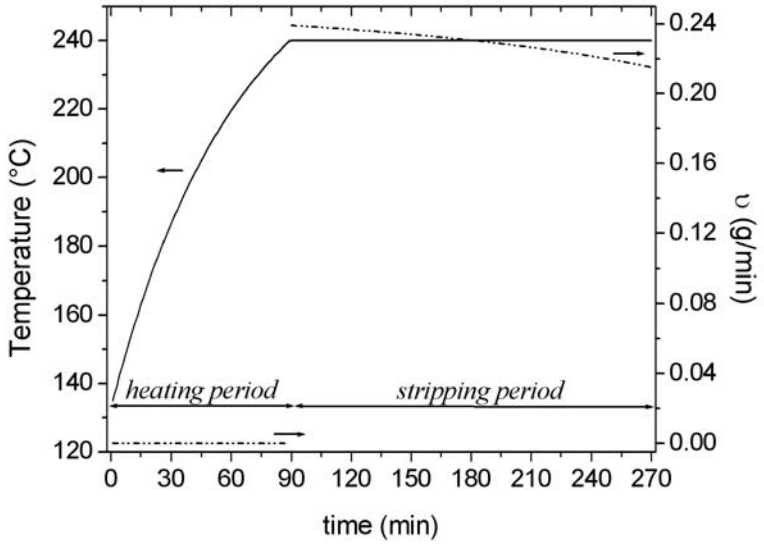

(A)

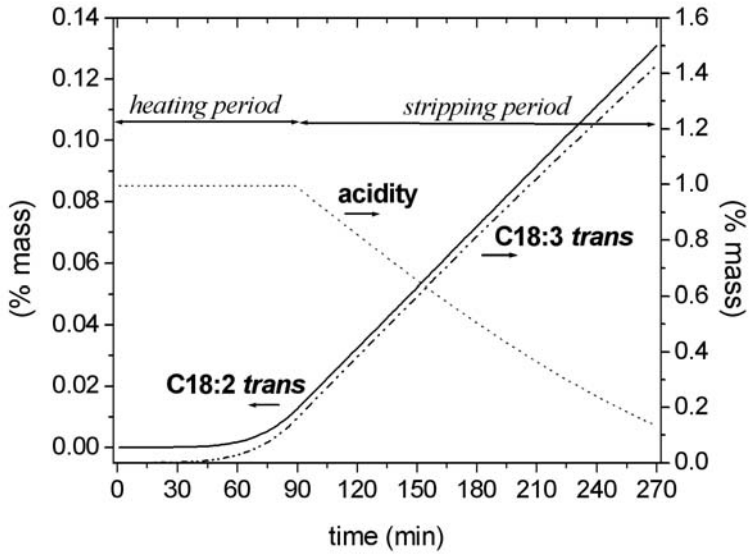

(B)

Figure 8.3.1. Variation of the (A) temperature and vaporization rate, and (B) C18:2 *trans*, C18:3 *trans* (% mass) and OA (%) with time for the deodorization of canola oil for trial number 25.

It is now presented the models obtained from the RSM, as a function of the coded variables for the four responses studied: C18:2 *trans* (%), C18:3 *trans* (%), total *trans* (%) and OA (expressed as % of oleic acid).

$$\log_{10}[\text{C18 : 2 } \textit{trans} \text{ (\%)}] = -0.891 + 0.470 \cdot X_1 + 0.139 \cdot X_2 - 0.022 \cdot X_2^2 \quad (8.3.1)$$

$$\log_{10}[\text{C18 : 3 } \textit{trans} \text{ (\%)}] = 0.158 + 0.381 \cdot X_1 - 0.017 \cdot X_1^2 + 0.128 \cdot X_2 - 0.024 \cdot X_2^2 - 0.013 \cdot X_1 \cdot X_2 \quad (8.3.2)$$

$$\log_{10}[\text{total } \textit{trans} \text{ (\%)}] = 0.195 + 0.388 \cdot X_1 - 0.015 \cdot X_1^2 + 0.129 \cdot X_2 - 0.024 \cdot X_2^2 - 0.012 \cdot X_1 \cdot X_2 \quad (8.3.3)$$

$$\text{final OA (\%)} = 0.142 + 0.177 \cdot X_1 + 0.062 \cdot X_1^2 - 0.139 \cdot X_2 + 0.049 \cdot X_2^2 - 0.040 \cdot X_1 \cdot X_2 \quad (8.3.4)$$

As one can see, for all responses, only the coefficients related to variables X_1 (temperature) and X_2 (duration), and b_o (content at the central point) were statistically significant at 99% of confidence. In fact, one should expect that the concentrations of C18:2 *trans* (%), C18:3 *trans* (%) and total *trans* (%) would increase with temperature since its effect is to increase the values of k_{Li} and k_{Ln} (Eq. 8.2.2.7 and 8.2.2.8). The residence time also increased the final concentrations of the isomerized compounds.

In the way the batch deodorizer was modeled, the temperature had two effects in the final OA. The first one was to increase the volatility of the FFA by increasing their vapor pressures. The other effect, much more important in this case, was to decrease the heat flux provided by the heating source and, consequently, decrease the vaporization of the FFA. Because this second effect was more important, the coefficient b_1 was positive in Eq. 8.3.4.

Fig. 8.3.2 shows the agreement between the *trans* contents obtained by the simulation program and the calculated values using Eqs. 8.3.1 and 8.3.2, and the comparison with the models developed by Hénon et al. [11] from their experimental trials.

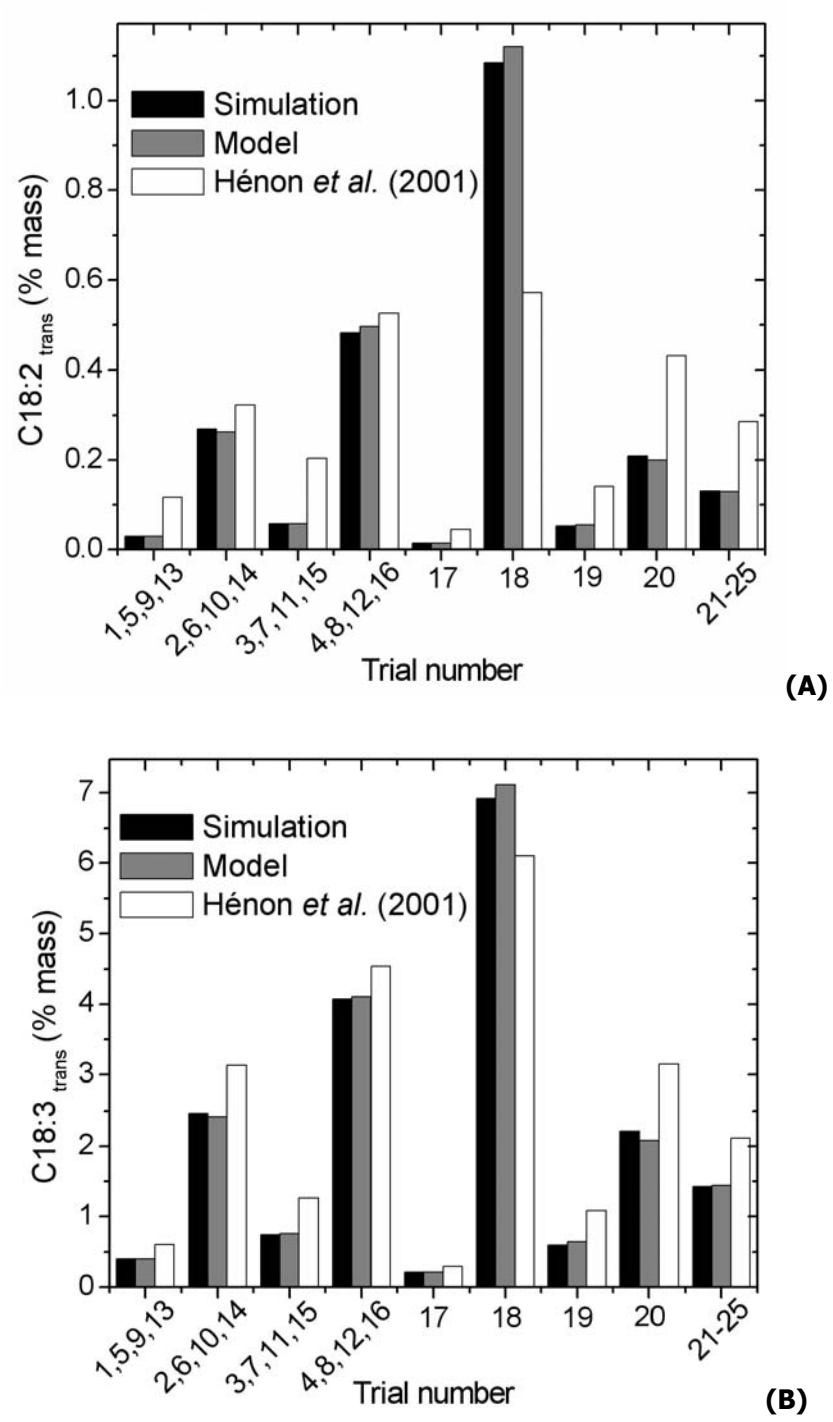

Figure 8.3.2. (A) C18:2 *trans* (% mass) and (B) C18:3 *trans* (% mass) as predicted, respectively, by Eqs. 8.3.1 and 8.3.2, and the models of Hénon *et al.* [8].

In general, our models described correctly the contents of both isomers considered. The ARD given by Eqs. 8.3.1 and 8.3.2, between the simulation results and the estimated values, were equal to 2.2% and 1.7% respectively. The highest

values of C18:2 *trans* (%) and C18:3 *trans* (%) were obtained in trial number 18 (1.08% and 6.92%, respectively) while the lowest values (0.03% and 0.40%, respectively) were obtained for the trials were X_1 and X_2 were at level –1 (see Tab. 8.3.1). For the values of C18:2 *trans* (%) and C18:3 *trans* (%), the simulation results followed the tendency of the model developed by Hénon et al. [11], but the absolute values were consistently different. This inaccuracy may be a consequence of differences in the deodorization processing time adopted by Hénon et al. [11] and the one considered in our simulations (heating plus stripping period), and also in the deodorizer heating system. Another possibility is the above-mentioned relation between the speed of the isomerization reactions and the concentrations of *cis* TAG throughout the residence time. Hénon et al. [11] did not inform in their article the initial composition of the oil used in their study. It is important to highlight that the temperature of trial number 18 (270°C) was out of the range studied by Hénon et al. [11], and, in this way, their models are not applicable to our situation. This estimation is shown in Fig. 8.3.2 just for illustration of the consequences of bad use of RSM models in the estimation of situations for which the processing conditions are different from the ones used in the achievement of the statistical models.

The final OA values given by the simulations ranged from 0.000% to 0.762%. Note that, according to Carlson [3], the final FFA content in deodorized oil will not be lower than 0.005%, when steam is used for stripping, due to the hydrolysis of the oil caused by the steam. Unfortunately, none information about the kinetics of hydrolysis during deodorization was found in the literature, and it was not possible to consider FFA generation in our simulation program. The ARD given by Eq. 8.3.4 was equal to 4.6%, despising the deviations on the trials for which the final OA was virtually zero. The total β-sitosterol and tocopherol contents of the finished oil ranged, respectively, from 44.93 to 248.73 mg/100g, and from 1.05 to 68.98 mg/100g for the simulations performed with the conditions shown in Tab. 8.2.3.1.

Table 8.3.1. Simulation results and estimated values for the deodorization of canola oil using RSM.

	Coded variables		Real variables		Responses C18:2 *trans* (%mass)		C18:3 *trans* (%mass)		Total *trans* (%mass)		Acidity (%)	
Trial	X_1	X_2	T(°C)	t(h)	Simul.	Eq. 8.3.1	Simul.	Eq. 8.3.2	Simul.	Eq. 8.3.3	Simul.	Eq. 8.3.4
1,5,9,13	-1	-1	225	2	0.030	0.030	0.399	0.394	0.429	0.424	0.180	0.175
2,6,10,14	+1	-1	255	2	0.269	0.262	2.466	2.415	2.734	2.673	0.600	0.609
3,7,11,15	-1	+1	225	4	0.057	0.057	0.743	0.753	0.800	0.811	0.000	-.023
4,8,12,16	+1	+1	255	4	0.482	0.497	4.071	4.102	4.553	4.581	0.267	0.251
17	-2	0	210	3	0.014	0.015	0.215	0.213	0.228	0.229	0.000	0.036
18	+2	0	270	3	1.084	1.119	6.919	7.112	8.003	8.147	0.762	0.744
19	0	-2	240	1	0.052	0.055	0.599	0.640	0.651	0.693	0.658	0.616
20	0	+2	240	5	0.209	0.199	2.205	2.080	2.415	2.275	0.000	0.06
21-25	0	0	240	3	0.131	0.129	1.430	1.439	1.560	1.567	0.134	0.142
ARD (%)					2.2%		1.7%		2.2%		4.6%	

Considering their initial concentrations (see Tab. 8.3.1), these values represents retention ranges of 18% to 99% for β-sitosterol and of 1% to 99% for tocopherol.

Tab. 8.3.2 provides the analysis of variance (ANOVA) for all responses studied at 99% of confidence. The four responses presented high correlation coefficients and the F-test showed that the models (Eqs. 13-16) are reliable, since the calculated F values were at least one hundred and eight times larger than the tabulated values from Box *et al.* [12].

Table 8.3.2. Analysis of variance (ANOVA)

Source of variation	C18:2 *trans* (% mass)				C18:3 *trans* (% mass)			
	SS[a]	DF[b]	MS[c]	F test[d]	SS[a]	DF[b]	MS[c]	F test[e]
Regression	5.786	3	1.929	9645	3.891	5	0.778	7780
Deviation	0.004	21	2E-3		0.002	19	1E-3	
Total variation	5.790	24	---		3.893	24	---	
R^2				0.999				0.999
Source of variation	Total *trans* (% mass)				Acidity (%)			
	SS[a]	DF[b]	MS[c]	F test[e]	SS[a]	DF[b]	MS[c]	F test[e]
Regression	4.042	5	0.808	8080	1.360	5	0.272	453
Deviation	0.002	19	1E-4		0.011	19	6E-4	
Total variation	4.044	24	---		1.371	24	---	
R^2				0.999				0.992

[a] Sum of squares; [b] Degrees of freedom; [c] Mean Squares; [d] $F_{0.99,\ 3,\ 21} = 4.87$; [e] $F_{0.99,\ 5,\ 19} = 4.17$

With the models presented in Eqs. 8.3.1-8.3.4, it was possible to generate surfaces, and the correspondent contour curves, that represent the influence of the coded variables (X_1 and X_2) in the responses C18:2 *trans* (%), C18:3 *trans* (%), total *trans* (%) and final OA (%).

In Fig. 8.3.3 it can be observed that the final content of C18:2 *trans* and C18:3 *trans* increased with temperature and duration. At lower temperatures, the final content of C18:2 *trans* were not relevant, independently of the duration. For higher temperatures (T> 255 °C), however, the duration of the deodorization exerted an important influence. Considerable values of C18:2 *trans* could be reached at extreme conditions (long duration and high temperatures). In the case of the final content of C18:3 *trans*, the effect of duration became relevant at temperatures above 225 °C. Very important values of C18:3 *trans* could also be obtained at extreme conditions. Note that both surfaces had a plateau of minimum.

Because the final OA is a very important quality factor [26] for refined edible oils, it was chosen to determine the good ranges of deodorization of canola oil, in conjunction with the total *trans* content for the deodorization system adopted in our simulations. According to Aro et al. [27], in European countries the quality parameters for refined edible oils also include low levels of *trans* fatty acids (<1.0%).

When the contour plots of total *trans* and final OA were superposed as in Fig. 8.3.4, it was possible to delineate a range of temperature and duration that minimize the total *trans* content in the deodorized oil, while respecting the maximum limit of acidity required by the Codex Alimentarius (0.3%, expressed as oleic acid).

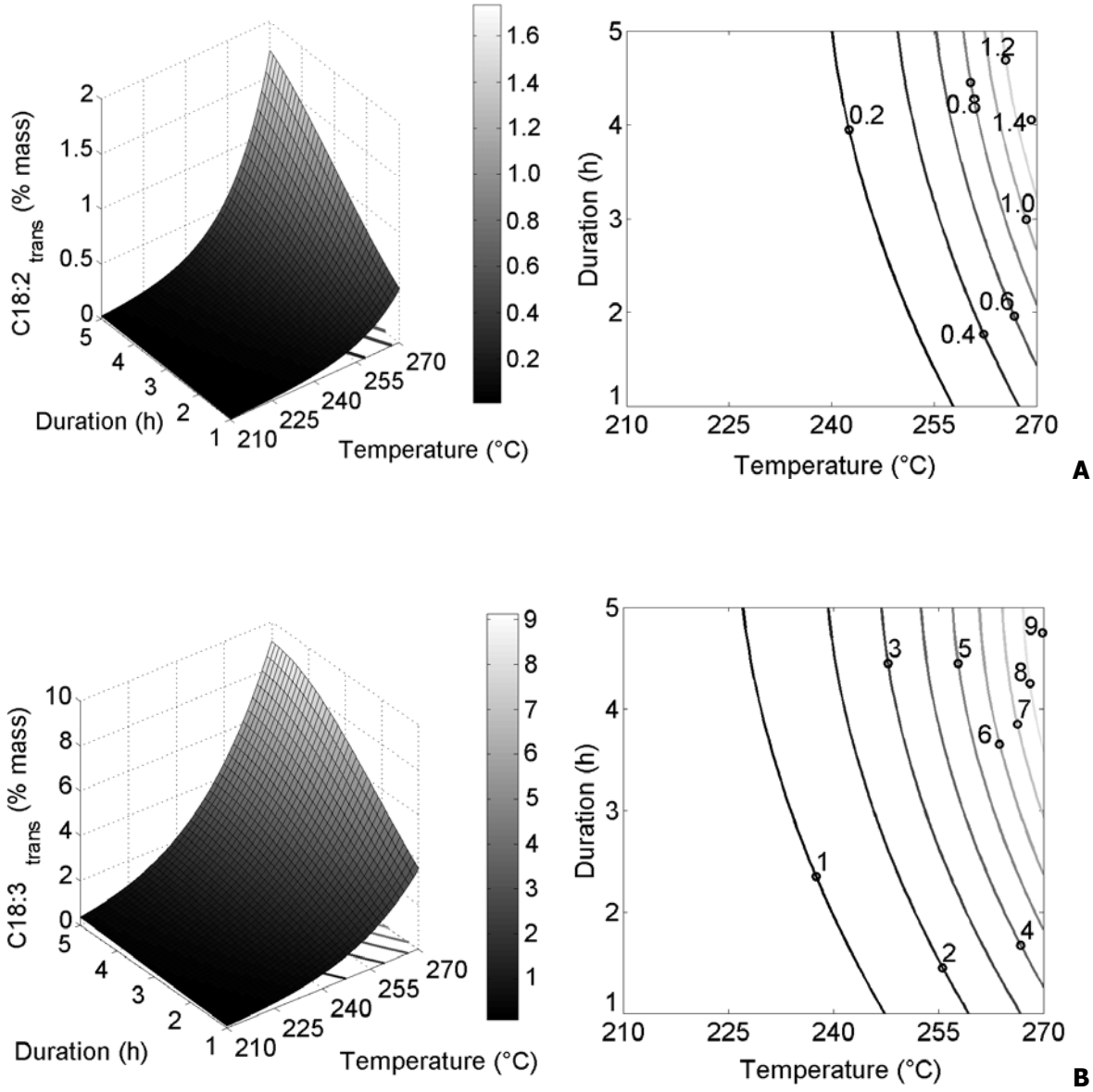

Figure 8.3.3. Response surface and contour curves of (A) C18:2 *trans* (% mass) and (B) C18:3 *trans* (% mass) as a function of T (°C) and duration (h).

The optimal values found were temperatures around 225 °C (X_1 = -1) and batch duration between 2 and 5 h ($-1 \leq X_2 \geq 2$). The results of the simulation performed with one of these optimized operating conditions (225 °C and 3 h) were compared to the values obtained by Eqs. 8.3.1 and 8.3.2. The values found for the simulation were 0.0437% of C18:2 *trans* and 0.5722% of C18:3 *trans*, and the deviations were equal to 0.23% and 0.56%, respectively.In this situation, the final

concentration of total *trans* given by the simulation program was equal to 0.6159% while the final OA was 0.004%. The β-sitosterol and γ-tocopherol contents were, respectively, 234.03 mg/100g and 58.41 mg/100g. These levels of nutraceutical compounds were very satisfactory, corresponding to retentions of 94% for the β-sitosterol and 83% for the γ-tocopherol. In Fig.8.3.4, it is also shown the region that would guarantee that most flavors and odoriferous compounds were eliminated (OA<0.03%).

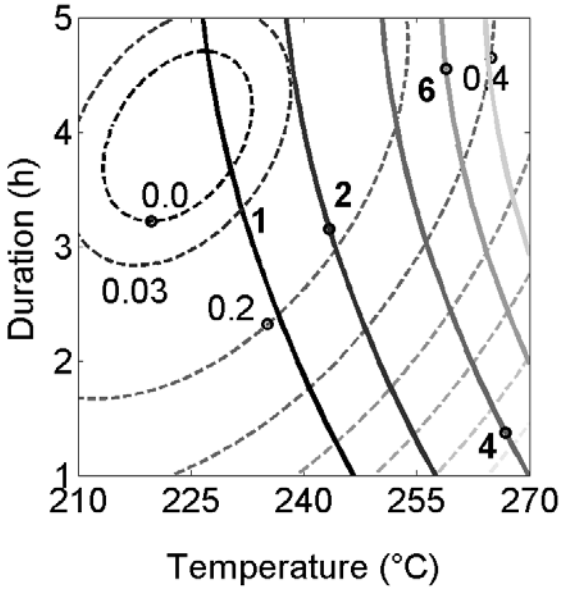

Fig. 8.3.4. Superposed contour curves of final OA (%) and total *trans* (% mass) as a function of T (°C) and duration (h).

Intuitively, one should expect that the effect of temperature in the final OA would be to decrease its value, because of the higher volatilities of FFA at higher temperatures. However, as shown in Fig.8.3.4, for a fixed residence time, the final OA increased with the deodorization temperature, because the vaporization rate, i.e., the amount of volatile compounds that are stripped of from the oil, decreased.

It is important to highlight that the results presented are highly dependent of the heat source features assumed in this work. It is possible that other results would be achieved if different values of the product $U \cdot A$ and of T_{hs} were considered.

Conclusion

Among the four parameters studied, temperature and duration were the most important factors during the deodorization of canola oil. These factors increased the formation of *trans* PUFA. The interaction of temperature and duration were also an important factor in the final levels of β-sitosterol and γ-tocopherol. In general, coupling the computer simulation and RSM, it was possible to simulate satisfactorily the deodorization of canola oil, and indicate good ranges of processing conditions. Without using the RSM, it would be necessary at least 625 simulation trials to achieve the same results (5 levels and 4 variables). The response surface equations generated good agreement with the simulation results. The importance of this work was to indicate that other degradative reactions, as hydrolysis and oxidation, could be evaluated by computer simulation once their kinetics are well established. The accuracy of the values of the simulation program were highly dependent of the heating system features supposed for the deodorizer.

Acknowledgements

The authors wish to acknowledge FAPESP (Fundação de Amparo à Pesquisa do Estado de São Paulo 03/04949-3) and CNPq (Conselho Nacional de Desenvolvimento Científico e Tecnológico - 46668/00-7 and 521011/95-7) for the financial support.

References

[1] A. Maza, R.A. Ormsbee, L.R. Strecker: Effects of deodorization and steam-refining Parameters on finished oil quality, *J. Amer. Oil Chem. Soc.* 1992, **69**, 1003-1008.

[2] W. Schwarz: Formation of trans polyalkenoic fatty acids during vegetable oil refining, *Eur. J. Lipid Sci. Technol.* 2000, **102**, 648-649.

[3] K.F. Carlson: Canola Oil. In *Bailey's Industrial Oil and Fat Products*. Ed. Y.H. Hui, Wiley-Interscience, New York, 1996, vol.4, 339-390.

[4] W. Schwarz: Trans unsaturated fatty acids in European nutrition, *Eur. J. Lipid Sci. Technol.* 2000, **102**, 633-635.

[5] N.A. Michael Eskin, B.E. McDonald, R. Przybylski, L.J. Malcolmson, R. Scarth, T. Mag, K. Ward, D. Adolph: Canola Oil. In *Bailey's Industrial Oil and Fat Products*. Ed. Y.H. Hui, Wiley-Interscience, New York, 1996, vol.2, 1-95.

[6] J.B. Woerfel: Soybean Oil Processing Byproducts and their Utilization, in *Practical Handbook of Soybean Processing and Utilization*. Ed. D.R. Erickson, AOCS, Champaign, 1995, 306-313.

[7] R. Ceriani, A.J.A. Meirelles: Simulation of batch physical refining and deodorization processes, *J. Amer. Oil Chem. Soc*. 2004, **81**, 305-312.

[8] R. Ceriani, A.J.A. Meirelles: Simulation of continuous deodorizers: effects on product streams, *J. Amer. Oil Chem. Soc.* 2004, **81**, 1059-1069.

[9] R. Ceriani, A.J.A. Meirelles: Simulation of physical refiners for edible oil deacidification, *J. Food Eng.* "in press".

[10] E. Batista, M.I. Rodrigues, A.J.A. Meirelles: Optimization of a secondary reflux and vaporization (SRV) distillation process using surface response analysis, *Comp. Chem. Eng.* 1998, **22**, S737-S740.

[11] G. Hénon, P.Y. Vigneron, B. Stoclin, J. Calgniez: Rapeseed oil deodorization study using the response surface methodology, *Eur. J. Lipid Sci. Technol.* 2001, **103**, 467-477.

[12] G. Hénon, Z. Zemény, K. Recseg, F.Zwobada, K. Kövári: Deodorization of vegetable oils. Part 1: modeling the geometrical isomerization of polyunsaturated fatty acids, *J. Am. Oil Chem. Soc.* 1999, **76**, 73-81.

[13] G.E.P. Box, J.S. Hunter: *Statistic for experimenters - an introduction to design, data analysis, and model building*, John Wiley & Sons, New York 1978.

[14] A.I. Khuri, J.A. Cornell: *Response surface - design and analysis*, ASQC Quality Press, New York 1987.

[15] V. Petrauskaitè, W.F. De Greyt, M.J. Kellens: Physical refining of coconut oil: effect of crude oil quality and deodorization conditions on neutral oil loss, *J. Am. Oil Chem. Soc.* 2000, **77**, 581-586.

[16] R. Ceriani, A.J.A. Meirelles: Predicting vapor-liquid equilibria of fatty systems, *Fluid Phase Equilib.* 2004, **215**, 227-236.

[17] K. Alejski, F. Duprat: Dynamic simulation of the multicomponent reactive distillation, *Chem. Eng.Sci.* 1996, **51**, 4237-4252.

[18] R.H. Perry, C.H. Chilton: *Chemical engineers' handbook*, McGraw-Hill, Tokyo, 1973.

[19] J.G. Theme: *Coconut oil processing*, FAO, Rome, 1968.

[20] R.C. Reid, J.M. Prausnitz, B.E. Poling: *The Properties of Gases and Liquids*, McGraw-Hill, New York, 1987.

[21] C.H. Tu, C.P. Liu, Group-contribution estimation of the enthalpy of vaporization of organic compounds, *Fluid Phase Equilib.* 1996, **121**, 45-65.

[22] DIPPR Student Chemical Database Login, http://dippr.byu.edu/students/chemsearch.asp (accessed Jan. 2005).

[23] D. Firestone: *Physical and chemical characteristics of oils, fats, and waxes*, AOCS Press, Washington, 1999.

[24] Z. Kemény, K. Recseg, G. Hénon, K. Kövari, F. Zwobada: Deodorization of Vegetable Oils. Prediction of trans Polyunsaturated Fatty Acid Content, *J. Am.Oil.Chem.Soc.* 2001, **78**, 973-979.

[25] R.L. Wolff: Heat-induced geometrical isomerization of alpha-linoleic acid - effect of temperature and heating time on the appearance of individual isomers *J. Am.Oil.Chem.Soc.* 1993, **70**, 425-430.

[26] Codex Alimentarius. Codex Standard for Named Vegetable Oils (vol.8, pp. 1-16). Codex Stan 210-1999, Rome, 1999.

[27] A. Aro, J. Van Ameslvoort, W. Becker, M.A. Van Erp-Baart, A. Kafatos, T. Leth, G. Van Poppels: Trans Fatty Acids in Dietary Fats and Oils from 14 European Countries: The TRANSFAIR Study, *J. Food Compos. Anal.* 1998, **11**, 137-149.

CAPÍTULO 9. CONCLUSÕES GERAIS

Este trabalho de tese foi elaborado de forma a cumprir cinco objetivos principais:

(i) Predição do equilíbrio líquido-vapor de misturas graxas;

(ii) Simulação da desodorização de óleos vegetais em batelada, considerando-se ou não reações químicas;

(iii) Simulação da desodorização contínua de óleos vegetais em regime permanente;

(iv) Modelagem da eficiência de vaporização associada à desodorização de óleos vegetais;

(v) Análise dinâmica da desodorização contínua de óleos vegetais.

A primeira etapa foi a obtenção de uma equação para predizer a pressão de vapor de compostos graxos. Em conjunto com as diferentes versões do UNIFAC, foi possível predizer o equilíbrio líquido-vapor de misturas graxas binárias e multicomponentes de forma efetiva. Os resultados obtidos pelas predições foram condizentes com os dados experimentais da literatura. As principais contribuições desta etapa do trabalho foram (a) tornar possível predizer a volatilidade de acilgliceróis em geral (TAG, DAG, MAG) e sua perda durante os processos de desacidificação por via física e/ou desodorização de óleos vegetais, (b) predizer a pressão de vapor de ésteres graxos, compostos bastante relevantes atualmente devido o interesse crescente no biodiesel, e finalmente, (c) permitir estimar a pressão de vapor de ácidos graxos insaturados *trans* , de grande importância na nutrição humana. A metodologia desenvolvida obteve desvios relativos menores que os métodos disponíveis na literatura para todas as classes de compostos graxos consideradas no trabalho. De uma maneira geral, a união entre a equação para predição da pressão de vapor desenvolvida neste trabalho e o UNIFAC gerou boas predições do equilíbrio líquido-vapor, sendo os desvios semelhantes à outros procedimentos relatados na literatura. Como sugerido por FORNARI et al. (1994),

o UNIFAC r ¾ foi aquele que permitiu os menores desvios em relação aos dados experimentais.

O trabalho experimental de PETRAUSKAITÈ et al. (2000) levantou o interesse em modelar o processo de desacidificação por via física em batelada para o óleo de coco como uma destilação diferencial e testar a viabilidade da metodologia desenvolvida na etapa anterior. Mesmo existindo algumas dúvidas em relação aos detalhes do experimento executado por PETRAUSKAITÈ et al (2000) e a composição do óleo de coco utilizado, bons resultados foram alcançados pelo programa computacional e, a capacidade exploratória da modelagem desenvolvida bem como sua aplicabilidade em problemas reais ficou evidente. Uma informação fundamental fornecida no trabalho de PETRAUSKAITÈ et al (2000) foi a quantidade de destilado obtida nos 60 minutos de processamento, o que permitiu uma estimativa da quantidade de vapor formada por minuto e, desta forma, excluiu a necessidade do balanço de energia no program. Pôde-se constatar que os valores obtidos por PETRAUSKAITÈ et al (2000) foram contidos dentro do conjunto de dados gerados pela ferramenta computacional aliada à algumas variações nos teores de acilgliceróis parciais do óleo de coco. O modelo 3 é aquele que melhor se aproxima do processo de desacidificação por via física em batelada em escala industrial.

Ainda em relação ao processo de desodorização em batelada, os trabalhos de HÉNON et al. (1997, 1999 e 2001), que investigaram as reações de isomerização dos ácidos linoléico e linolênico no óleo de canola, permitiram validar um equacionamento muito mais complexo do problema da destilação diferencial que o anterior, uma vez que os balanços de energia e a cinética das reações foram inclusos. A introdução do balanço de energia permitiu estimar a quantidade de vapor formada a cada tempo, variando ao longo de todo o processo. Foi interessante notar a viabilidade de unir duas ferramentas de análise de maneira satisfatória: simulação computacional e metodologia de superfície de resposta. Esta etapa do trabalho evidenciou que outras reações poderiam ser consideradas nas simulações, bastando apenas ter disponível sua cinética.

A revisão da literatura revelou a importância da eficiência de vaporização na desodorização em batelada de óleos vegetais. Percebeu-se que muitos trabalhos quantificavam esta variável tanto para sistemas com injeção de vapor como com injeção de nitrogênio, sem, no entanto, investigá-la. O trabalho de COELHO PINHEIRO & GUEDES DE CARVALHO (1994) modelou o fenômeno de forma rigorosa, considerando, entretanto, um aparato com injeção de nitrogênio e temperatura ambiente. O cuidadoso procedimento experimental descrito por DECAP et al. (2004), para quantificar a eficiência de vaporização durante a desacidificação de óleo de soja por via física, com vapor como agente de arraste, trouxe a possibilidade de validar uma nova modelagem. As equações desenvolvidas nesta etapa da pesquisa além de serem mais simples, quando comparadas ao trabalho de COELHO PINHEIRO & GUEDES DE CARVALHO (1994) e incluírem os efeitos da presença da água no líquido, foram capazes de predizer satisfatoriamente os valores reportados por DECAP et al. (2004), gerando desvios médios inferiores àqueles obtidos por COELHO PINHEIRO & GUEDES DE CARVALHO (1994) que trabalharam com condições de temperatura muito aquém daquelas encontradas no processo de desodorização. A grande dificuldade associada à predição do trabalho de DECAP et al. (2004) está na inexatidão da altura do leito de líquido, devido a grande turbulência gerada pelas baixas temperaturas e alto vácuo aplicados ao sistema, problema não encontrado por COELHO PINHEIRO & GUEDES DE CARVALHO (1994) em seu trabalho.

Em relação à simulação dos processos contínuos em regime estacionário, a ferramenta computacional desenvolvida foi bastante explorada tanto na avaliação da influência das variáveis de processo na qualidade dos produtos quanto na validação de trabalhos experimentais encontrados na literatura (MAZA et al., 1992; VERLEYEN et al., 2001). Estes últimos foram fundamentais para consolidar a viabilidade de toda a metodologia, incluindo as equações empíricas e/ou teóricas selecionadas. Em especial, destaca-se os resultados obtidos para o teor de tocoferóis no óleo de soja desodorizado nas condições de MAZA et al., (1992). Mesmo com algumas dúvidas a respeito da configuração do equipamento utilizado

pelos autores, o programa de simulação foi capaz de estimar com precisão a retenção deste antioxidante natural. Neste aspecto, esta parte do trabalho foi bastante inovadora na área de óleos vegetais, sendo base para outras investigações. Algumas dificuldades encontradas se devem ao fato da literatura aberta ser pouco elucidativa no que diz respeito à construção e ao funcionamento dos equipamentos industriais envolvidos.

Infelizmente, a análise dinâmica da desodorização contínua de óleos vegetais enfrentou problemas não imaginados na proposta deste trabalho e ficou limitada à uma modelagem bem mais simples do que a esperada. A presença da água como componente não-inerte na fase líquida dificultou a implementação do programa.

As ferramentas testadas e implementadas neste trabalho de tese são de uso corrente em processos da Engenharia Química. No entanto, sua aplicação nos processos de refino da indústria de óleos vegetais é original. É muito importante deixar claro que o sucesso deste trabalho foi conseqüência direta da busca constante de dados experimentais na literatura que pudessem validar os resultados das simulações. Muitas das dificuldades encontradas foram superadas com informações relevadas por revisores dos artigos e pelo contato com os autores. De uma maneira geral, esta tese abre caminho para outros trabalhos de investigação tanto experimental como computacional.

SUGESTÕES PARA TRABALHOS FUTUROS

(i) Simulação da desodorização e/ou desacidificação por dessorção contínua de óleos vegetais em regime permanente, introduzindo reações químicas relevantes para a qualidade do produto final;

(ii) Simulação de desodorizadores contínuos de contato diferencial (tipo *thin-fim* ou *Softcolumn*^{TM});

(iii) Análise dinâmica do processo de desodorização contínua em softwares comerciais da Engenharia Química (Aspen Plus®, Hysys®), utilizando sistemas modelos para a mistura;

(iv) Estudo experimental da desodorização de óleos vegetais em escala laboratorial, em equipamentos em batelada;

(v) Modelagem da eficiência de vaporização considerando população de bolhas;

(vi) Estudo experimental da eficiência de vaporização na desodorização de óleos vegetais em batelada.

(vii) Aplicação dos modelos desenvolvidos neste projeto em outros processos da indústria de alimentos, como a destilação de bebidas.

APÊNDICE I: DINÂMICA NA DESACIDIFICAÇÃO DE ÓLEOS VEGETAIS

A simulação dinâmica da desacidificação de óleos vegetais foi uma etapa adicional realizada neste trabalho, de caráter apenas investigativo e não conclusiva devido às dificuldades encontradas. Foi incluída no corpo da tese apenas como documentação de caráter informativo.

O modelo para a simulação dinâmica de uma coluna de destilação consiste de um grupo de equações diferenciais ordinárias (EDO), que correspondem aos balanços de massa e energia, e outro de equações algébricas, que descrevem o equilíbrio e a hidráulica do prato. Para cada estágio *n*, balanços molares global e por componentes, e o balanço de energia podem ser estabelecidos. O equacionamento do problema está colocado a seguir:

Estágio 1:
$$\begin{aligned} & h_2 \cdot L_2 - h_1 \cdot L_1 - H_1 \cdot V_1 \approx -H_F \\ & L_2 - L_1 - V_1 = -F_1 \end{aligned} \qquad \text{(A1)}$$

Estágio genérico *n:*
$$\begin{aligned} & h_{n+1} \cdot L_{n+1} - h_n \cdot L_n - H_n \cdot V_n \approx -H_F - h_f \\ & L_{n+1} - L_n - V_n = -F_n - f_n \end{aligned} \qquad \text{(A2)}$$

Estágio *N:*
$$\begin{aligned} & -h_N \cdot L_N - H_N \cdot V_N \approx -H_F - h_f \\ & -L_N - V_N = -F_N - f_N \end{aligned} \qquad \text{(A3)}$$

Os balanços molares por componente são:

Estágio 1:
$$\frac{dx_{i,1}}{dt} = \frac{1}{\mathrm{H}_1} \cdot \left[x_{i,2} \cdot L_2 - x_{i,1} \cdot L_1 - y_{i,1} \cdot V_1 + y_{i,F} \cdot F_1 \right] \qquad \text{(A4)}$$

Estágio genérico *n*:
$$\frac{dx_{i,n}}{dt} = \frac{1}{\mathrm{H}_n} \cdot \left[x_{i,n+1} \cdot L_{n+1} - x_{i,n} \cdot L_n - y_{i,n} \cdot V_n + x_{i,f} \cdot f_n + y_{i,F} \cdot F_n \right] \qquad \text{(A5)}$$

Estágio *N*:
$$\frac{dx_{i,N}}{dt} = \frac{1}{\mathrm{H}_N} \cdot \left[- x_{i,N} \cdot L_N - y_{i,N} \cdot V_N + y_{i,F} \cdot F_N + x_{i,f} \cdot f_N \right] \qquad \text{(A6)}$$

A nomenclatura utilizada nas Equações A1 a A6 foi estabelecida como segue: subscrito *n:* relativo ao estágio *n, n* =1, 2, …, *NS*; subscrito *i*: relativo ao componente *i, i* =1, 2, …, *NC; H* = entalpia da fase vapor (J/h); *h* = entalpia da fase líquida (J/h); h_f = entalpia da alimentação líquida (J/h); H_f = entalpia da alimentação vapor (J/h); *V* = vazão de vapor (mol/h); *L* = vazão de líquido (mol/h); *f* = vazão da alimentação como líquido (mol/h); *F* = vazão da alimentação como vapor (mol/h); *x* = composição do líquido; *F* = composição do vapor; H = hold-up molar de líquido.

Vale ressaltar que esta modelagem segue sugestões simplificadoras de RAMIREZ (1997): (1) o hold-up da fase vapor é desprezível; (2) o hold-up da fase líquida é constante; (3) a variação na entalpia de cada estágio é aproximadamente nula.

Por ter constituído apenas uma investigação preliminar, o óleo vegetal foi considerado como sendo uma mistura formada por pseudocomponentes representativos (trioleína+3% de ácido oléico).

A entrada de dados do programa desenvolvido, baseado no algoritmo da Figura 2.3.2.2.1 extraída do livro de RAMIREZ (1997), foi feita utilizando-se do resultado da simulação em regime estacionário na seguinte condição de processamento: 4425 kg/h de óleo (P.M. 830,92 g/gmol), 250 °C, 3 mmHg e 1% de vapor de arraste, distribuído igualmente nos três estágios da coluna (configuração em corrente cruzada). Segue:

ALIMENTAÇÃO: 4855,47 mols/h de trioleína (OOO), 469,96 mols/h de ácido oléico e 2458,3 mols/h de vapor (290 °C) divididos em 3 estágios.

COMPOSIÇÃO MOLAR DO LÍQUIDO EM CADA ESTÁGIO:

ESTÁGIO 1: 1,5E-5 DE ÁGUA+ 6,6E-3 DE ÁCIDO OLÉICO+0,993 DE TRIOLEÍNA

ESTÁGIO 2: 1,4E-5 DE ÁGUA+ 0,015 DE ÁCIDO OLÉICO+0,985 DE TRIOLEÍNA

ESTÁGIO 3: 1,1E-5 DE ÁGUA+ 0,035 DE ÁCIDO OLÉICO+0,965 DE TRIOLEÍNA

O cálculo do hold-up foi feito considerando-se um tempo de retenção de 30 minutos (AHRENS, 1998).

Partindo-se desta entrada de dados, esperava-se que o estado estacionário se mantivesse, com no máximo, pequenas modificações nas frações molares, devido ao cálculo do equilíbrio do sistema. No entanto, o programa apresentava valores negativos para as vazões molares do líquido e do vapor, mesmo utilizando um método de integração de passo variável, indicado para sistemas mal-comportados (rígidos). A avaliação criteriosa dos resultados revelou que a presença da água no sistema, como componente não inerte, foi a geradora deste comportamento.

Dos trabalhos anteriores (vide capítulo 4), é sabido que a presença da água na fase líquida (dissolvida no óleo) influencia sobremaneira o equilíbrio, reduzindo a temperatura de desodorização. Como pode ser observado no algoritmo de resolução do problema (Figura 2.3.2.2.1), a nova concentração de água (bem como dos demais componentes) é determinada pelo balanço molar por componente e não pelo equilíbrio. Desta forma, quando a quantidade de água no líquido é suficientemente grande, a temperatura de equilíbrio cai, reduzindo a entalpia do líquido, que se aquece condensando o vapor. A água, presente no líquido em baixíssimas concentrações, apresenta elevado coeficiente de atividade no sistema (ao redor de 7,0), além de uma elevada pressão de vapor. Desta forma, qualquer pequena variação na sua fração molar no líquido, acarreta variações importantes na temperatura de equilíbrio.

Os resultados revelaram que a derivada $dx_{água}/dt$ calculada pelo balanço de componentes é cerca de dez vezes maior que $dx_{oléico}/dt$. Isto significa que a água é um componente de dinâmica rápida em comparação com o ácido oléico, o que gera um problema de instabilidade numérica que não deve ser confundido com a resposta real/física do problema.

Da forma como o algoritmo de resolução do problema foi proposto, duas soluções poderiam resolver o problema: (a) considerar a derivada $dx_{água}/dt$ como

sendo nula, e neste caso supor que o componente de dinâmica rápida tem resposta instantânea, (b) considerar a água como componente inerte. Para considerar a derivada $dx_{água}/dt$ como sendo nula, admite-se que a quantidade de água presente no instante inicial (diferente de zero) não se altera com o tempo. Com esta hipótese, o programa gera resultados coerentes, ou seja, o estado estacionário permanece, como pode ser observado nas Figuras A1 e A2. As pequenas alterações são decorrentes da entrada de dados (frações molares ao invés de vazões).

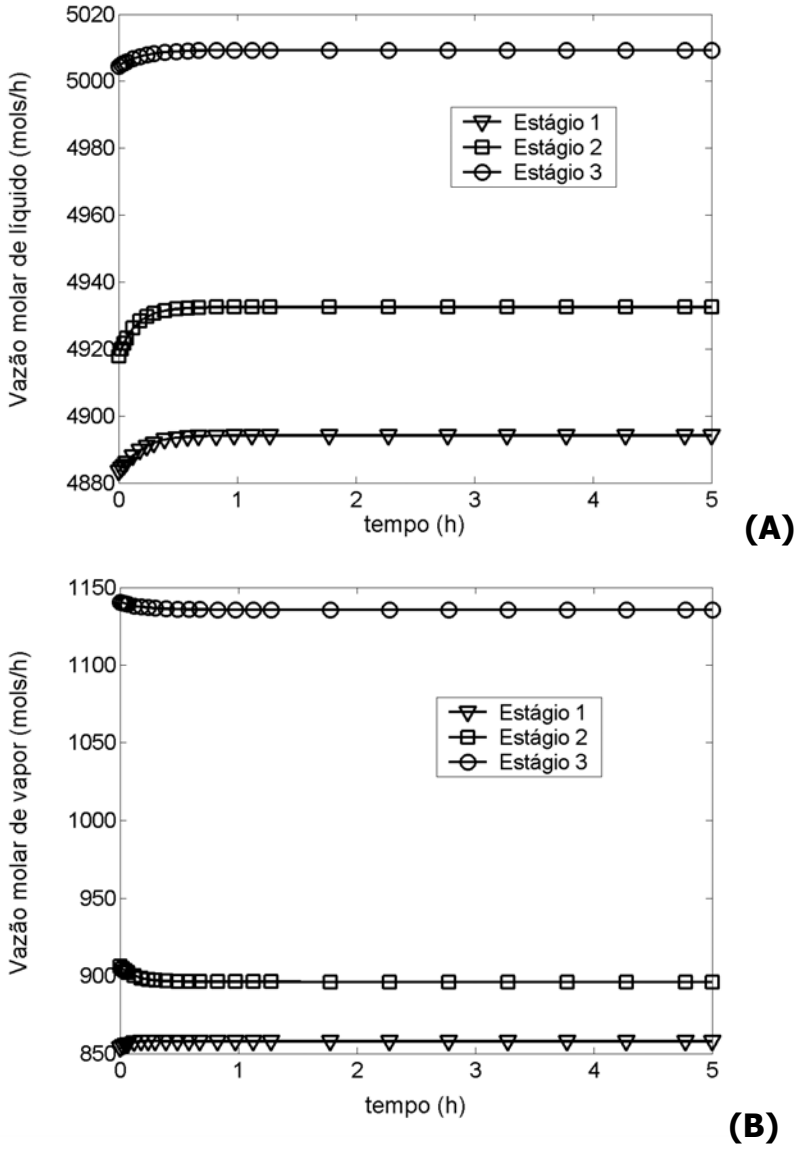

Figura A1. Vazões (a) de líquido e (b) de vapor no desodorizador.

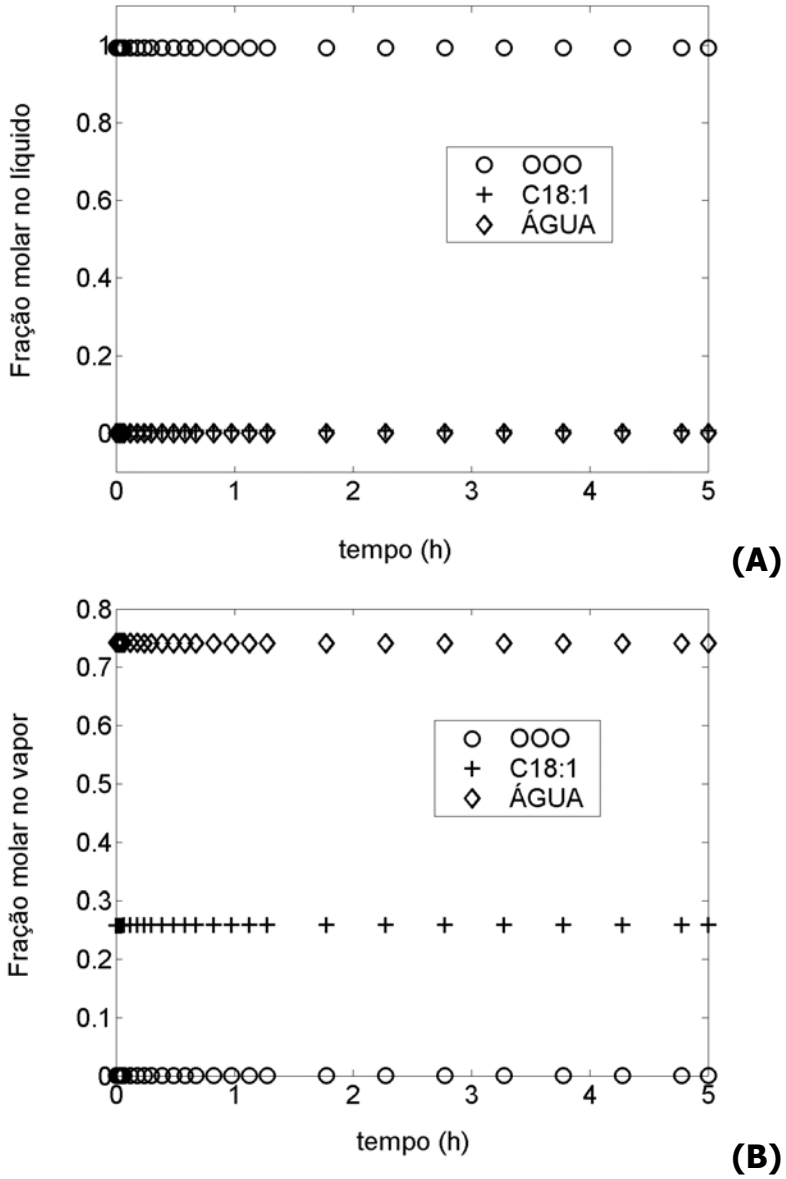

Figura A2. Frações molares (a) no líquido (Estágio 1) e (b) no vapor (Estágio N).

A segunda opção de considerar a água como inerte não foi implementada, uma vez que está em desacordo com os resultados indicados ao longo de todo o trabalho. Neste caso, a temperatura de equilíbrio do estágio seria maior, uma vez que a presença da água diminui o ponto de ebulição da mistura.

O objetivo então foi iniciar um busca na literatura de sugestões para a resolução deste problema da forma mais adequada. O artigo de revisão de TAYLOR & KRISHNA (2000) embora sobre destilação reativa, e de OSORIO et al.

(2004) sobre a simulação dinâmica da destilação de Pisco (bebida destilada chilena semelhante à cachaça) foram os pontos de partida.

No artigo de TAYLOR & KRISHNA (2000), está citado o trabalho de GROSSER et al. (1987), que modelaram uma coluna de destilação reativa para a produção de Nylon 6,6. Os autores levantaram algumas hipóteses simplificadoras, dentre elas (a) a solução é diluída e, portanto, as pequenas mudanças na temperatura foram desconsideradas; (b) o hold-up de líquido é constante em cada prato; (c) o hold-up do vapor é desprezível; (d) os calores latentes de vaporização dos componentes são bem próximos. Desta forma para cada mol de líquido vaporizado ocorre a condensação de um mol de vapor (*equimolar overflow*).

Excluindo a primeira hipótese, todas as outras foram implementadas no programa de simulação, agora com o cálculo das derivadas para a água e para o ácido oléico (trioleína por diferença). Com isso, apenas as composições das fases se alteram, mas não as suas vazões.

O teste feito neste caso foi considerar que, a partir do estado estacionário anterior, o óleo alimentado na coluna (Estágio 3) passou a ter 100 mols/h a mais em acidez livre. Os resultados estão apresentados nas Figuras A3 a A5.

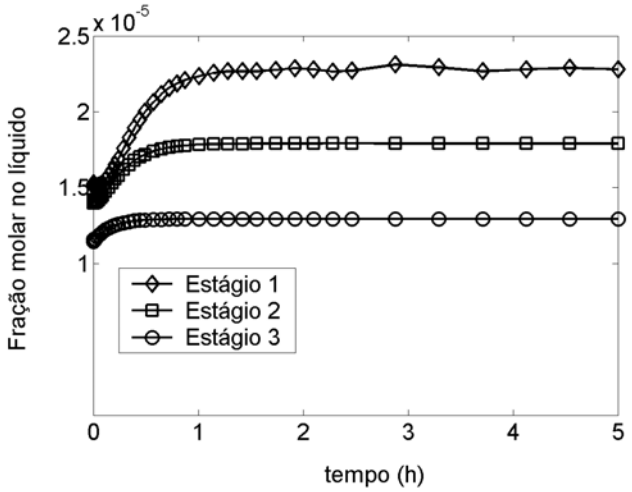

(A)

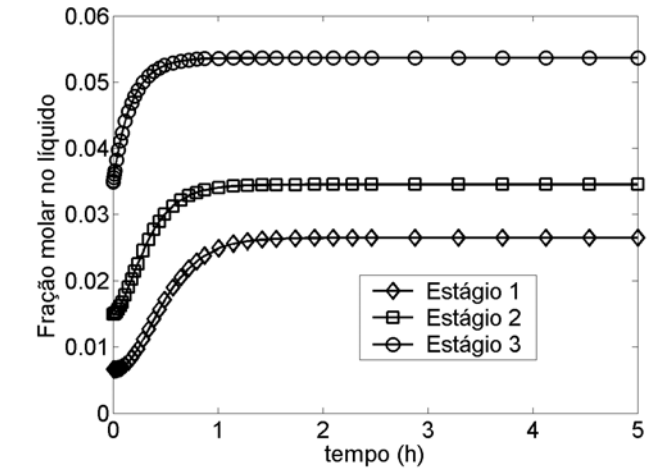

(B)

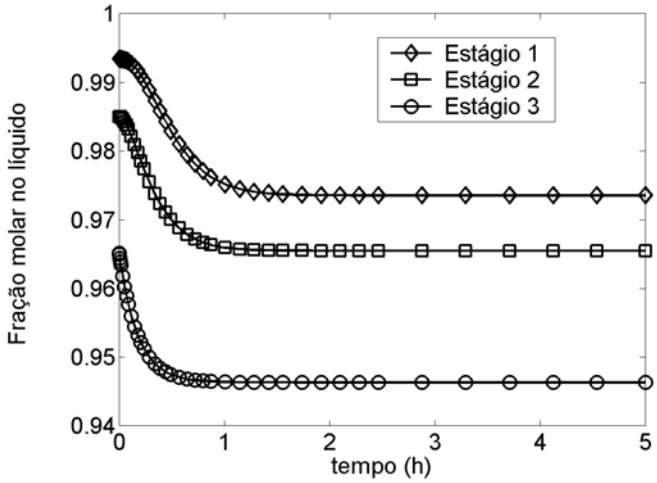

(C)

Figura A3. Frações molares no líquido para (a) água, (b) ácido oléico e (c) trioleína.

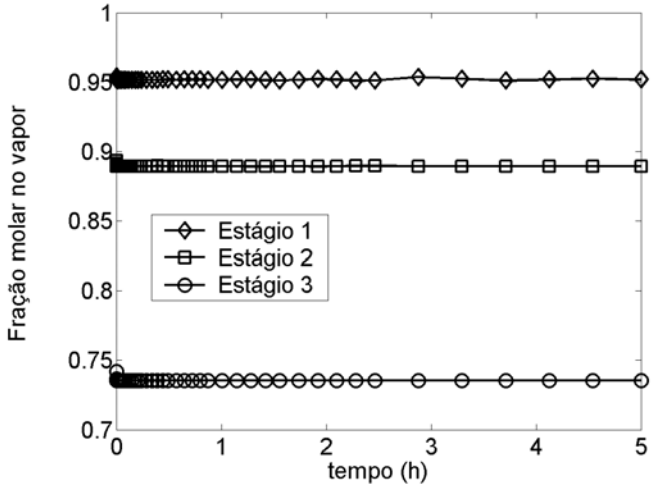

(A)

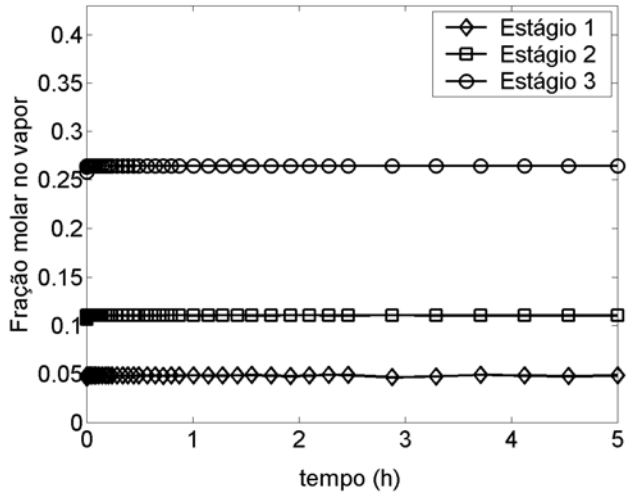

(B)

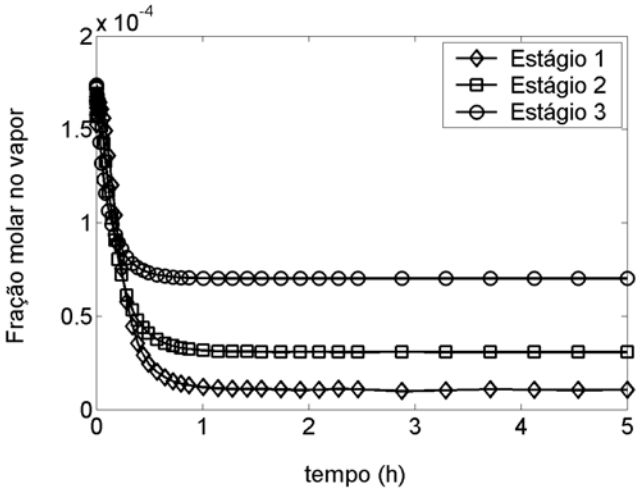

(C)

Figura A4. Frações molares no vapor para (a) água, (b) ácido oléico e (c) trioleína.

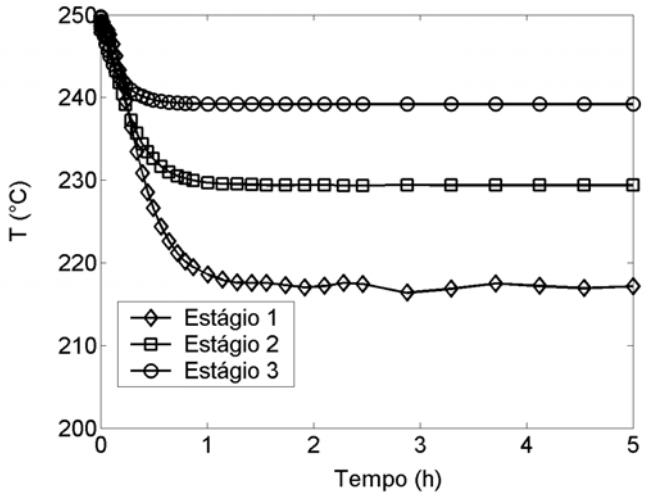

Figura A5. Perfil da temperatura de equilíbrio.

Como era de se esperar, a concentração da acidez livre no líquido aumentou, atingindo um novo estágio estacionário. Os perfís das temperaturas nos estágios cairam, como conseqüência do aumento da concentração de água dissolvida no líquido. Embora os resultados tenham sido coerentes, é difícil avaliar sua veracidade, uma vez que as hipóteses feitas são comumente utilizadas em colunas de destilação.

Referências

TAYLOR, R., KRISHNA, R. Modeling Reactive Distillation. *Chem. Eng. Sci.*, v.55, p.5183-5229, 2000.

OSORIO, D., PÉREZ-CORREA, R., BELANCIC, A., AGOSIN, E. Rigorous Dynamic Modeling and Simulation of Wine Distillations. *Food Control*, v.15, p.515-521, 2004.

GROSSER, J.H., DOHERTY, M.F., MALONE, M.F. Modeling Reactive Distillation. *Ind. Eng. Chem. Res.*, v.26, p.983-989, 1987.

APÊNDICE II: BANCO DE DADOS DE PRESSÃO DE VAPOR DE COMPOSTOS GRAXOS (REFERENTE AO CAPÍTULO 3)

TAG e MAG

Comp.*	T (°C)	P (mmHg)	Comp.	T (°C)	P (mmHg)	Comp.	T (°C)	P (mmHg)
BBB	45	0,001	**CCC**	213	0,05	**CCC**	159	0,001
BBB	91	0,05	**CCC**	232,5	0,09	**CLM**	223	0,001
BBB	123	0,27	**LLL**	188	0,001	**CLM**	280	0,05
BBB	129	0,45	**LLL**	244	0,05	**C--**	175	1
BBB	186,5	10	**MMM**	216	0,001	**L--**	186	1
BBB	190	15	**MMM**	275	0,05	**M--**	199	1
BBB	317,4	760	**PPP**	239	0,001	**P--**	211	1
BBB	315	760	**PPP**	298	0,05	**S--**	190	0,2
BBB	307,5	760	**SSS**	253	0,001	**O--**	186	0,2
CoCoCo	85	0,001	**SSS**	313	0,05			
CoCoCo	135	0,05	**OSS**	254	0,001			
CoCoCo	157,5	0,25	**OSS**	315	0,05			
CoCoCo	368,2	760	**MPS**	237	0,001			
CoCoCo	368,1	760	**MPS**	297	0,05			
CpCpCp	128	0,001	**PLS**	223	0,001			
CpCpCp	162,5	0,03	**PLS**	282	0,05			
CpCpCp	179	0,05	**MLS**	215	0,001			
CpCpCp	233,25	1	**MLS**	274	0,05			
CpCpCp	385,2	760	**PCS**	232	0,001			
CpCpCp	385,3	760	**PCS**	290	0,05			

* Comp.= abreviação para composto graxo

Álcoois graxos

Comp.	T (°C)	P (mmHg)	Comp.	T (°C)	P (mmHg)	Comp.	T (°C)	P (mmHg)	Comp.	T (°C)	P (mmHg)
C6OH	24,4	1,0	**C6OH**	85	40,7	**C6OH**	138	400,0	**C7OH**	76,1	10,9
C6OH	47,2	5,0	**C6OH**	90,83	54,6	**C6OH**	141,67	456,8	**C7OH**	80,58	14,3
C6OH	52,2	5,7	**C6OH**	91,1	55,3	**C6OH**	144,5	500,0	**C7OH**	81,5	15,0
C6OH	56,8	7,5	**C6OH**	92	60,0	**C6OH**	152,77	659,8	**C7OH**	85,8	20,0
C6OH	58,2	10,0	**C6OH**	97,3	75,0	**C6OH**	157,1	750,1	**C7OH**	87,6	21,1
C6OH	60,4	9,7	**C6OH**	98,7	80,0	**C6OH**	157	760,0	**C7OH**	90,83	25,7
C6OH	60,11	9,8	**C6OH**	101,16	90,0	**C6OH**	157,3	757,3	**C7OH**	94,3	30,2
C6OH	67,4	15,3	**C6OH**	102,8	100,0	**C7OH**	42,4	1,0	**C7OH**	99,9	40,2
C6OH	70,29	17,7	**C6OH**	107,6	120,8	**C7OH**	60,11	3,8	**C7OH**	99,8	40,0
C6OH	70,3	20,0	**C6OH**	120,55	207,2	**C7OH**	63,6	4,7	**C7OH**	101,16	44,1
C6OH	72,6	20,5	**C6OH**	119,6	200,0	**C7OH**	64,3	5,0	**C7OH**	106,4	55,5
C6OH	80,58	31,6	**C6OH**	119,7	201,0	**C7OH**	70,1	7,5	**C7OH**	108	60,0
C6OH	79,2	29,8	**C6OH**	130,88	309,8	**C7OH**	70,29	7,5	**C7OH**	110,19	68,0
C6OH	83,7	40,0	**C6OH**	130,1	301,8	**C7OH**	74,7	10,0	**C7OH**	112,5	75,0

Álcoois graxos (continuação)

Comp.	T (°C)	P (mmHg)	Comp.	T (°C)	P (mmHg)	Comp.	T (°C)	P (mmHg)	Comp.	T (°C)	P (mmHg)
C7OH	114,5	80,5	**C9OH**	113,8	20,0	**C10OH**	149,9	56,0	**C12OH**	146	14,6
C7OH	119,5	100,0	**C9OH**	114,4	20,3	**C10OH**	152	60,0	**C12OH**	150	20,0
C7OH	120,55	107,2	**C9OH**	122,4	30,2	**C10OH**	157,3	75,0	**C12OH**	152,57	19,9
C7OH	124,1	122,4	**C9OH**	128,8	40,6	**C10OH**	159,2	81,1	**C12OH**	155,67	22,9
C7OH	130,88	163,6	**C9OH**	129	40,0	**C10OH**	159,21	81,0	**C12OH**	160,33	28,1
C7OH	136,5	201,0	**C9OH**	135,8	55,5	**C10OH**	163,69	96,3	**C12OH**	162,5	30,1
C7OH	136,6	200,0	**C9OH**	139	60,0	**C10OH**	165,8	100,0	**C12OH**	164,47	33,5
C7OH	141,67	246,5	**C9OH**	141	75,0	**C10OH**	168,65	115,8	**C12OH**	167,2	40,0
C7OH	147,8	303,5	**C9OH**	144,7	80,4	**C10OH**	169,9	121,3	**C12OH**	168,25	39,2
C7OH	152,77	364,5	**C9OH**	151,3	100,0	**C10OH**	174,65	143,6	**C12OH**	169,5	40,9
C7OH	155,6	400,0	**C9OH**	152,15	95,1	**C10OH**	177,57	159,0	**C12OH**	172,64	46,9
C7OH	162,8	501,0	**C9OH**	155	120,7	**C10OH**	182,74	189,4	**C12OH**	177,03	55,7
C7OH	175,8	760,0	**C9OH**	169	201,4	**C10OH**	183,9	198,0	**C12OH**	177,1	55,6
C7OH	176,4	760,8	**C9OH**	170,2	190,1	**C10OH**	186,2	200,0	**C12OH**	177,8	60,0
C8OH	54	1,0	**C9OH**	170,5	200,0	**C10OH**	189,38	235,2	**C12OH**	181,89	66,9
C8OH	76,5	5,0	**C9OH**	181	302,4	**C10OH**	194,48	276,1	**C12OH**	185	75,0
C8OH	78,9	5,3	**C9OH**	181,03	278,6	**C10OH**	197,4	303,0	**C12OH**	186,69	79,9
C8OH	88,3	10,0	**C9OH**	187,49	345,8	**C10OH**	201,04	336,6	**C12OH**	187,1	81,2
C8OH	88,8	10,2	**C9OH**	192,1	400,0	**C10OH**	207,35	404,3	**C12OH**	192	100,0
C8OH	95,4	15,0	**C9OH**	194,8	437,6	**C10OH**	208,8	400,0	**C12OH**	192,07	96,7
C8OH	101	20,0	**C9OH**	198	502,5	**C10OH**	213,12	475,3	**C12OH**	197,47	116,5
C8OH	101,5	21,0	**C9OH**	203,95	580,2	**C10OH**	215,3	504,8	**C12OH**	198,7	122,3
C8OH	108,4	30,0	**C9OH**	207,76	649,9	**C10OH**	218,92	556,1	**C12OH**	203,45	142,1
C8OH	114	39,5	**C9OH**	213	750,1	**C10OH**	225,49	660,0	**C12OH**	207,66	162,7
C8OH	115,2	40,0	**C9OH**	213,44	764,7	**C10OH**	230,47	749,2	**C12OH**	213	200,0
C8OH	120,9	54,4	**C9OH**	213,5	760,0	**C10OH**	230,6	750,1	**C12OH**	213,44	194,8
C8OH	123,8	60,0	**C9OH**	213,6	763,9	**C10OH**	231	757,6	**C12OH**	214,5	201,3
C8OH	128,2	75,0	**C10OH**	69,5	1,0	**C10OH**	231	760,0	**C12OH**	220,14	238,3
C8OH	131,2	85,4	**C10OH**	97,3	5,0	**C11OH**	71,1	1,0	**C12OH**	225,80	280,8
C8OH	135,2	100,0	**C10OH**	105	5,6	**C11OH**	99	5,0	**C12OH**	228,4	300,2
C8OH	140,3	123,8	**C10OH**	111,3	10,0	**C11OH**	112,8	10,0	**C12OH**	232,76	341,2
C8OH	152	200,0	**C10OH**	114,5	10,2	**C11OH**	127,5	20,0	**C12OH**	235,7	400,0
C8OH	166,1	315,5	**C10OH**	121,7	15,0	**C11OH**	143,7	40,0	**C12OH**	238,46	397,9
C8OH	173,8	400,0	**C10OH**	125,8	20,0	**C11OH**	153,7	60,0	**C12OH**	245,20	474,3
C8OH	181,2	507,6	**C10OH**	127,3	20,1	**C11OH**	167,6	75,0	**C12OH**	247,7	499,0
C8OH	194,8	750,1	**C10OH**	127,26	19,9	**C11OH**	167,2	100,0	**C12OH**	247,8	503,7
C8OH	195,2	760,0	**C10OH**	129,53	22,3	**C11OH**	187,7	200,0	**C12OH**	250,87	547,2
C8OH	195,3	760,0	**C10OH**	133,57	27,0	**C11OH**	209,8	400,0	**C12OH**	258,05	651,8
C9OH	59,5	1,0	**C10OH**	135,6	29,9	**C11OH**	244,1	750,1	**C12OH**	263,57	742,7
C9OH	86,1	5,0	**C10OH**	138,24	33,5	**C11OH**	232	760,0	**C12OH**	264,1	750,1
C9OH	91,7	5,6	**C10OH**	141,82	39,3	**C12OH**	91	1,0	**C12OH**	265,4	766,0
C9OH	96,9	7,5	**C10OH**	142,1	40,0	**C12OH**	120,2	5,0	**C12OH**	259	760,0
C9OH	99,7	10,0	**C10OH**	142,2	40,1	**C12OH**	126,5	5,3	**C13OH**	192,3	75,0
C9OH	102,1	10,5	**C10OH**	145,86	46,9	**C12OH**	134,7	10,0	**C13OH**	273,1	750,1
C9OH	108,9	15,3	**C10OH**	149,41	54,5	**C12OH**	138,3	9,8	**C14OH**	205,3	75,0

Álcoois graxos (continuação)

Comp.	T (°C)	P (mmHg)	Comp.	T (°C)	P (mmHg)	Comp.	T (°C)	P (mmHg)	Comp.	T (°C)	P (mmHg)
C14OH	286,7	750,1	**C16OH**	295,90	339,5	**C18OH**	216,95	17,2	**C18OH**	349,5	760,0
C16OH	122,7	1,0	**C16OH**	305,9	502,4	**C18OH**	218,79	18,4	**C20OH**	270	75,0
C16OH	158,3	5,0	**C16OH**	312,7	400,0	**C18OH**	220	20,0	**C20OH**	355,1	750,1
C16OH	172,1	5,9	**C16OH**	311,7	750,1	**C18OH**	221,94	20,4			
C16OH	177,8	10,0	**C16OH**	325,1	759,2	**C18OH**	222,25	20,7			
C16OH	185,3	10,3	**C16OH**	344	760,0	**C18OH**	225,43	23,3			
C16OH	193,4	15,1	**C17OH**	240,1	75,0	**C18OH**	225,59	23,5			
C16OH	197,8	20,0	**C17OH**	323,3	750,1	**C18OH**	229,23	26,9			
C16OH	201	19,8	**C18OH**	150,3	1,0	**C18OH**	229,71	27,4			
C16OH	211	30,1	**C18OH**	162,8	1,3	**C18OH**	235,06	33,3			
C16OH	218,6	40,4	**C18OH**	171,56	2,1	**C18OH**	239,96	39,6			
C16OH	219,8	40,0	**C18OH**	177,21	2,8	**C18OH**	239,6	39,6			
C16OH	225,31	52,2	**C18OH**	181,47	3,4	**C18OH**	240,04	39,7			
C16OH	227,3	55,3	**C18OH**	184,82	4,0	**C18OH**	240,4	40,0			
C16OH	231,21	63,8	**C18OH**	185,6	5,0	**C18OH**	245,49	47,9			
C16OH	234,3	60,0	**C18OH**	187,54	4,6	**C18OH**	245,53	47,9			
C16OH	229	75,0	**C18OH**	189,29	5,0	**C18OH**	249,85	55,4			
C16OH	238,7	80,3	**C18OH**	191,33	5,5	**C18OH**	252,7	60,0			
C16OH	242,60	74,1	**C18OH**	193,13	6,0	**C18OH**	255,74	67,1			
C16OH	250,10	95,4	**C18OH**	194,72	6,4	**C18OH**	257,3	75,0			
C16OH	251,6	120,3	**C18OH**	195,14	6,6	**C18OH**	261,45	80,3			
C16OH	251,7	100,0	**C18OH**	196,47	7,0	**C18OH**	268,04	98,3			
C16OH	257	116,6	**C18OH**	197,73	7,4	**C18OH**	269,4	100,0			
C16OH	261,02	143,0	**C18OH**	199,4	8,0	**C18OH**	273,59	115,8			
C16OH	265,53	160,6	**C18OH**	200,5	7,5	**C18OH**	281,28	144,3			
C16OH	269,3	200,5	**C18OH**	200,91	8,5	**C18OH**	285,36	162,0			
C16OH	274,19	182,4	**C18OH**	202	10,0	**C18OH**	292,47	196,2			
C16OH	280,2	200,0	**C18OH**	204,97	10,7	**C18OH**	293,5	200,0			
C16OH	281,08	230,9	**C18OH**	210,5	13,2	**C18OH**	301,15	246,1			
C16OH	285	302,1	**C18OH**	212,67	14,1	**C18OH**	320,3	400,0			
C16OH	289,13	276,7	**C18OH**	214,89	15,7	**C18OH**	343	750,1			

Ácidos graxos saturados

Comp.	T (°C)	P (mmHg)	Comp.	T (°C)	P (mmHg)	Comp.	T (°C)	P (mmHg)	Comp.	T (°C)	P (mmHg)
C6:0	11,5	0,01	**C6:0**	94,6	8	**C6:0**	117	26,6	**C6:0**	133,46	58,22
C6:0	34	0,1	**C6:0**	98,1	9,4	**C6:0**	118,33	28,73	**C6:0**	133,3	60
C6:0	59	0,7506	**C6:0**	99,5	10	**C6:0**	120,8	32	**C6:0**	136	64
C6:0	61,7	1	**C6:0**	98,5	10	**C6:0**	122,28	34,79	**C6:0**	136,6	67,3
C6:0	71,9	2	**C6:0**	107,3	16	**C6:0**	123,3	36,3	**C6:0**	137,51	69,51
C6:0	82,8	4	**C6:0**	108,8	17,5	**C6:0**	125	40	**C6:0**	139,3	75,06
C6:0	86,5	5	**C6:0**	111,8	20	**C6:0**	125,71	40,95	**C6:0**	141,1	82,1
C6:0	89,5	5	**C6:0**	113,12	22,14	**C6:0**	126,2	41,4	**C6:0**	141,431	82,23
C6:0	93	7,506	**C6:0**	115,42	24,86	**C6:0**	129,76	49,32	**C6:0**	144	94,3

Ácidos graxos saturados (continuação)

Comp.	T (°C)	P (mmHg)	Comp.	T (°C)	P (mmHg)	Comp.	T (°C)	P (mmHg)	Comp.	T (°C)	P (mmHg)
C6:0	145,56	97,59	**C7:0**	162	100	**C8:0**	169,4	78	**C9:0**	210	200
C6:0	145,5	99,8	**C7:0**	168,2	128	**C8:0**	172,2	100	**C9:0**	217,4	256
C6:0	144	100	**C7:0**	179,5	200	**C8:0**	174,7	100	**C9:0**	227,5	400
C6:0	146,5	100	**C7:0**	180,7	200	**C8:0**	176,5	103,4	**C9:0**	232,7	400
C6:0	149,74	115,67	**C7:0**	187,5	256	**C8:0**	176,6	103,5	**C9:0**	240,9	512
C6:0	152,5	128	**C7:0**	199,6	400	**C8:0**	183,3	128	**C9:0**	246,7	600
C6:0	154	141,8	**C7:0**	202	400	**C8:0**	186,8	153	**C9:0**	255,1	750,06
C6:0	159,01	165,93	**C7:0**	209,3	512	**C8:0**	193,8	198,4	**C9:0**	253,5	760
C6:0	160,8	180,3	**C7:0**	215,3	600	**C8:0**	190,3	200	**C9:0**	255,6	760
C6:0	160,8	200	**C7:0**	222,6	750,06	**C8:0**	194,7	200	**C10:0**	108	0,7506
C6:0	163,5	202,6	**C7:0**	221,5	760	**C8:0**	200,3	248,7	**C10:0**	110,3	1
C6:0	166,7	222,4	**C7:0**	223	760	**C8:0**	203	256	**C10:0**	121,1	2
C6:0	168,63	235,96	**C8:0**	32,5	0,01	**C8:0**	206,3	305,5	**C10:0**	132,7	4
C6:0	170,3	255,9	**C8:0**	57,5	0,1	**C8:0**	213,9	400	**C10:0**	137	5
C6:0	171,5	256	**C8:0**	77,9	0,5	**C8:0**	216,7	400	**C10:0**	145	7,506
C6:0	170,3	255,9	**C8:0**	85	0,7506	**C8:0**	225,6	512	**C10:0**	145,5	8
C6:0	174,7	298,2	**C8:0**	87,5	1	**C8:0**	230,7	600	**C10:0**	148,7	10
C6:0	179,1	348,8	**C8:0**	92,3	1	**C8:0**	238,4	750,06	**C10:0**	152,2	10
C6:0	181	400	**C8:0**	97,9	2	**C8:0**	237,5	760	**C10:0**	159,4	16
C6:0	192,5	512	**C8:0**	109,1	4	**C8:0**	239,7	760	**C10:0**	163,3	20
C6:0	202	760	**C8:0**	113,5	5	**C9:0**	45	0,01	**C10:0**	165	20
C6:0	204,5	750,06	**C8:0**	114,1	5	**C9:0**	69	0,1	**C10:0**	174,6	32
C6:0	205,8	760	**C8:0**	120	7,506	**C9:0**	89,2	0,5	**C10:0**	178,7	40
C7:0	45,5	0,1	**C8:0**	121,3	8	**C9:0**	97	0,7506	**C10:0**	179,9	40
C7:0	65,2	0,5	**C8:0**	124	10	**C9:0**	98,9	1	**C10:0**	189,8	60
C7:0	72	0,7506	**C8:0**	125,3	10	**C9:0**	109,6	2	**C10:0**	191,3	64
C7:0	74,9	1	**C8:0**	130,2	12	**C9:0**	121,2	4	**C10:0**	202	100
C7:0	78	1	**C8:0**	131,9	13,1	**C9:0**	126	5	**C10:0**	254,9	512
C7:0	85,3	2	**C8:0**	134,6	16	**C9:0**	133	7,506	**C10:0**	261,3	600
C7:0	96,3	4	**C8:0**	136,4	20	**C9:0**	134	8	**C10:0**	269,5	750,06
C7:0	100	5	**C8:0**	139,3	20	**C9:0**	137,4	10	**C10:0**	268,4	760
C7:0	101,3	5	**C8:0**	140,12	20,9	**C9:0**	138,7	10	**C10:0**	270	760
C7:0	107	7,506	**C8:0**	142,8	24,2	**C9:0**	147,5	16	**C11:0**	118	0,7506
C7:0	108,3	8	**C8:0**	147,8	29,8	**C9:0**	149,8	20	**C11:0**	119,8	1
C7:0	113,2	10	**C8:0**	149,2	32	**C9:0**	152	20	**C11:0**	131,1	2
C7:0	118,3	10	**C8:0**	150,2	33,5	**C9:0**	162,4	32	**C11:0**	143,3	4
C7:0	121,1	16	**C8:0**	150,6	40	**C9:0**	163,7	40	**C11:0**	156	7,506
C7:0	125,3	20	**C8:0**	153,3	40	**C9:0**	167,3	40	**C11:0**	156,5	8
C7:0	135,2	32	**C8:0**	154	40,6	**C9:0**	172,3	60	**C11:0**	170,8	16
C7:0	139,5	40	**C8:0**	159,6	51,2	**C9:0**	178,8	64	**C11:0**	186,1	32
C7:0	140	40	**C8:0**	161,5	55,6	**C9:0**	182,7	75,06	**C11:0**	185,6	40
C7:0	148,5	60	**C8:0**	160	60	**C9:0**	184,4	100	**C11:0**	197,2	60
C7:0	150,8	64	**C8:0**	165,3	64	**C9:0**	190	100	**C11:0**	203,1	64
C7:0	154,6	75,06	**C8:0**	165,5	75,06	**C9:0**	196,9	128	**C11:0**	207,2	75,06
C7:0	160	100	**C8:0**	169,3	77,9	**C9:0**	203,1	200	**C11:0**	212,5	100

Ácidos graxos saturados (continuação)

Comp.	T (°C)	P (mmHg)	Comp.	T (°C)	P (mmHg)	Comp.	T (°C)	P (mmHg)	Comp.	T (°C)	P (mmHg)
C11:0	268,7	512	**C13:0**	195,8	20	**C14:0**	272,7	200	**C16:0**	257,1	64
C11:0	283,6	750,06	**C13:0**	207,9	32	**C14:0**	281,5	256	**C16:0**	261,9	75,06
C11:0	284	760	**C13:0**	212,4	40	**C14:0**	294,6	400	**C16:0**	270	100
C12:0	52	0,001	**C13:0**	222	60	**C14:0**	299,3	400	**C16:0**	271,5	100
C12:0	66,2	0,00515	**C13:0**	225,8	64	**C14:0**	309	512	**C16:0**	278,7	128
C12:0	72	0,01	**C13:0**	230,3	75,06	**C14:0**	325,6	750,06	**C16:0**	298,7	200
C12:0	91	0,05	**C13:0**	236	100	**C14:0**	318	760	**C16:0**	303,6	256
C12:0	98	0,1	**C13:0**	245,9	128	**C14:0**	326,2	760	**C16:0**	332,6	512
C12:0	98,5	0,1	**C13:0**	255,2	200	**C15:0**	157,8	1	**C16:0**	350,2	750,06
C12:0	119,6	0,5	**C13:0**	268,6	256	**C15:0**	169,7	2	**C17:0**	175,1	1
C12:0	128	0,7506	**C13:0**	276,5	400	**C15:0**	182,8	4	**C17:0**	187,6	2
C12:0	130,2	1	**C13:0**	295,4	512	**C15:0**	196,8	8	**C17:0**	200,8	4
C12:0	141,8	2	**C13:0**	299	760	**C15:0**	201,1	9,976	**C17:0**	214,9	8
C12:0	154,1	4	**C14:0**	84	0,0058	**C15:0**	212	16	**C17:0**	219,7	9,976
C12:0	158	5	**C14:0**	89,5	0,01	**C15:0**	228,1	32	**C17:0**	230,7	16
C12:0	166	7,506	**C14:0**	99,7	0,027	**C15:0**	246,4	64	**C17:0**	247,9	32
C12:0	167,4	8	**C14:0**	109,6	0,0583	**C15:0**	268	128	**C17:0**	266,6	64
C12:0	172	10	**C14:0**	116	0,1	**C15:0**	292,7	256	**C17:0**	288,4	128
C12:0	201,4	40	**C14:0**	116,5	0,1	**C15:0**	321,2	512	**C17:0**	314,3	256
C12:0	202,7	40	**C14:0**	120	0,13	**C15:0**	339,1	760	**C17:0**	343,8	512
C12:0	214,6	64	**C14:0**	137,8	0,5	**C16:0**	98,7	0,0055	**C17:0**	363,8	760
C12:0	219,1	75,06	**C14:0**	147	0,7506	**C16:0**	104,8	0,01	**C17:0**	363,8	760
C12:0	226,7	100	**C14:0**	144,5	0,77	**C16:0**	120	0,04	**C18:0**	96	0,001
C12:0	227,5	100	**C14:0**	149,2	1	**C16:0**	122	0,0445	**C18:0**	113	0,00575
C12:0	234,3	128	**C14:0**	161,1	2	**C16:0**	132	0,1	**C18:0**	119	0,01
C12:0	247,3	200	**C14:0**	173,9	4	**C16:0**	132,5	0,1	**C18:0**	141,8	0,0596
C12:0	249,8	200	**C14:0**	174,1	5	**C16:0**	143,5	0,225	**C18:0**	144,2	0,077
C12:0	256,6	256	**C14:0**	177,5	5	**C16:0**	154,7	0,5	**C18:0**	147,5	0,1
C12:0	272,7	400	**C14:0**	186	7,506	**C16:0**	165	0,7506	**C18:0**	148	0,1
C12:0	273,8	400	**C14:0**	187,6	8	**C16:0**	167,4	1	**C18:0**	183	0,7506
C12:0	282,5	512	**C14:0**	191,4	9,9758	**C16:0**	179	2	**C18:0**	183,6	1
C12:0	289,3	600	**C14:0**	190,8	10	**C16:0**	192,2	4	**C18:0**	195,9	2
C12:0	298,1	750,06	**C14:0**	192	10	**C16:0**	197	5	**C18:0**	209,2	4
C12:0	298,9	760	**C14:0**	202,4	16	**C16:0**	205	7,506	**C18:0**	213	5
C12:0	299,2	760	**C14:0**	207,3	20	**C16:0**	206,1	8	**C18:0**	223	7,506
C13:0	109	0,0751	**C14:0**	207,8	20	**C16:0**	210,6	9,9756	**C18:0**	224,1	8
C13:0	138	0,7506	**C14:0**	218,3	32	**C16:0**	205,8	10	**C18:0**	228,7	9,976
C13:0	137,8	1	**C14:0**	223,5	40	**C16:0**	210,7	10	**C18:0**	225	10
C13:0	139,9	1	**C14:0**	224	40	**C16:0**	221,5	16	**C18:0**	228,7	10
C13:0	151,5	2	**C14:0**	237,2	60	**C16:0**	223,8	20	**C18:0**	240	16
C13:0	164,2	4	**C14:0**	236,3	64	**C16:0**	226,7	20	**C18:0**	243,4	20
C13:0	166,3	5	**C14:0**	241,3	75,06	**C16:0**	238,4	32	**C18:0**	245,3	20
C13:0	176	7,506	**C14:0**	249,3	100	**C16:0**	244,4	40	**C18:0**	257,1	32
C13:0	177,8	8	**C14:0**	250,5	100	**C16:0**	244,7	40	**C18:0**	263,3	40
C13:0	181	10	**C14:0**	257,3	128	**C16:0**	244,7	40	**C18:0**	263,3	40
C13:0	192,2	16	**C14:0**	272,3	200	**C16:0**	256	60	**C18:0**	275,5	60

Ácidos graxos saturados (continuação)

Comp.	T (°C)	P (mmHg)	Comp.	T (°C)	P (mmHg)	Comp.	T (°C)	P (mmHg)	Comp.	T (°C)	P (mmHg)
C18:0	276,8	64	**C18:0**	237,4	9,975	**C22:0**	142	0,0053	**C22:0**	390	750,06
C18:0	281,6	75,06	**C19:0**	121,6	0,0028	**C22:0**	145,4	0,0075	**C24:0**	257	3,9975
C18:0	290,7	100	**C20:0**	135	0,01	**C22:0**	148	0,01	**C26:0**	271	3,9975
C18:0	291	100	**C20:0**	152,8	0,0415	**C22:0**	176,5	0,0751	**C28:0**	285	3,9975
C18:0	299,7	128	**C20:0**	204	1	**C22:0**	213,7	0,7506	**C30:0**	299	3,9975
C18:0	316,5	200	**C20:0**	214,5	2	**C22:0**	213,7	0,7506			
C18:0	324,8	256	**C20:0**	245,9	9,976	**C22:0**	259,3	7,506			
C18:0	343	400	**C22:0**	122	0,001	**C22:0**	316,2	75,06			

Ácidos graxos insaturados

Comp.	T (°C)	P (mmHg)	Comp.	T (°C)	P (mmHg)	Comp.	T (°C)	P (mmHg)	Comp.	T (°C)	P (mmHg)
C11:1 c	114	1	**C18:1 c**	224	10	**C18:1 t**	273	60	**C22:1 c**	306,5	75,006
C11:1 c	142,8	5	**C18:1 c**	233,5	15	**C18:1 t**	288	100	**C22:1 c**	314,4	100
C11:1 c	156,3	10	**C18:1 c**	240	20	**C18:1 t**	312,4	200	**C22:1 c**	336,5	200
C11:1 c	172	20	**C18:1 c**	250	30	**C18:1 t**	337	400	**C22:1 c**	358,8	400
C11:1 c	188,7	40	**C18:1 c**	257,2	40	**C18:1 t**	362	760	**C22:1 c**	381,1	750,06
C11:1 c	199,5	60	**C18:1 c**	264	49	**C18:2 c,c**	133	0,07	**C22:1 c**	381,5	760
C11:1 c	213,5	100	**C18:1 c**	269,8	60	**C18:2 c,c**	224	9,976	**C22:1 t**	209,6	1
C11:1 c	232,8	200	**C18:1 c**	277	75,006	**C18:2 c,c**	224	10	**C22:1 t**	241,7	5
C11:1 c	254	400	**C18:1 c**	286	100	**C18:2 c,c**	230	16	**C22:1 t**	256	10
C11:1 c	275	760	**C18:1 c**	309,8	200	**C18:3 c,c,c**	231	17	**C22:1 t**	272,9	20
C14:1 c	184,5	14,025	**C18:1 c**	334,7	400	**C18:3 t,t,t**	224	9,976	**C22:1 t**	285	30
C16:1 c	219	15	**C18:1 c**	359,7	750,06	**C18:3 t,t,t**	224,5	10	**C22:1 t**	290	40
C16:1 t	179	0,8251	**C18:1 c**	360	760	**C18:3 c,t,t**	235	12,0010	**C22:1 t**	301,5	60
C16:1 t	180	0,8251	**C18:1 t**	171,3	1	**C22:1 c**	239,7	5	**C22:1 t**	316,2	100
C16:1 t	181	0,8251	**C18:1 t**	206,7	5	**C22:1 c**	247,4	7,5006	**C22:1 t**	336,8	200
C16:1 t	182	0,8251	**C18:1 t**	226	9,976	**C22:1 c**	264,5	15	**C22:1 t**	359,6	400
C16:1 t	183	0,8251	**C18:1 t**	227	9,976	**C22:1 c**	270,6	20	**C22:1 t**	382,5	760
C18:1 c	176,5	1	**C18:1 t**	228	9,976	**C22:1 c**	285	30,0024	**C22:5 c,c,c,c,c**	236	5,025
C18:1 c	208,5	5	**C18:1 t**	223,5	10	**C22:1 c**	281	31,5			
C18:1 c	214,5	7,5006	**C18:1 t**	242,3	20	**C22:1 c**	289,1	40			
C18:1 c	223	9,976	**C18:1 t**	260,8	40	**C22:1 c**	300,2	60			

Ésteres graxos

Comp.	T (°C)	P (mmHg)	Comp.	T (°C)	P (mmHg)	Comp.	T (°C)	P (mmHg)	Comp.	T (°C)	P (mmHg)
M-C6:0	5	1	**M-C6:0**	42	10	**M-C6:0**	49,9	15,5	**M-C6:0**	55,7	20,8
M-C6:0	30	5	**M-C6:0**	44,5	11,8	**M-C6:0**	55,4	20	**M-C6:0**	60	25,5

Ésteres graxos (continuação)

Comp.	T (°C)	P (mmHg)	Comp.	T (°C)	P (mmHg)	Comp.	T (°C)	P (mmHg)	Comp.	T (°C)	P (mmHg)
M-C6:0	60,3	26,2	**M-C8:0**	91,5	21	**M-C10:0**	108	10	**M-C12:0**	167,4	40,1
M-C6:0	62,7	30	**M-C8:0**	94,6	24	**M-C10:0**	107,3	10,8	**M-C12:0**	174,8	53,1
M-C6:0	64,2	31,7	**M-C8:0**	97,6	28,5	**M-C10:0**	114,1	14,5	**M-C12:0**	177,8	59,1
M-C6:0	66,6	36	**M-C8:0**	100,3	32,7	**M-C10:0**	118,2	17,4	**M-C12:0**	176,8	60
M-C6:0	69	39,8	**M-C8:0**	101,6	33,5	**M-C10:0**	123	20	**M-C12:0**	181,1	66,4
M-C6:0	70	40	**M-C8:0**	105,5	40	**M-C10:0**	122,8	21,5	**M-C12:0**	184	74,2
M-C6:0	70,6	44	**M-C8:0**	105,3	40	**M-C10:0**	126,5	25,1	**M-C12:0**	187,4	82,7
M-C6:0	73,8	49,7	**M-C8:0**	105,5	40,8	**M-C10:0**	128,8	27,8	**M-C12:0**	191	93,4
M-C6:0	75,9	54,4	**M-C8:0**	108,8	46,5	**M-C10:0**	130,6	29,9	**M-C12:0**	190,8	100
M-C6:0	75,5	54,5	**M-C8:0**	110	49	**M-C10:0**	137,3	39,3	**M-C12:0**	194,2	103,7
M-C6:0	77,6	58,9	**M-C8:0**	109,8	49	**M-C10:0**	139	40	**M-C12:0**	198,1	117,9
M-C6:0	79,7	60	**M-C8:0**	112,2	54	**M-C10:0**	142	47,3	**M-C12:0**	204,5	144,4
M-C6:0	78,8	62,5	**M-C8:0**	114,7	59,9	**M-C10:0**	147,8	59,7	**M-C12:0**	208,1	160,7
M-C6:0	81,5	69,7	**M-C8:0**	115,3	60	**M-C10:0**	148,6	60	**M-C12:0**	212,3	182,2
M-C6:0	84,9	80,3	**M-C8:0**	115	60,8	**M-C10:0**	148,6	61,4	**M-C14:0**	115	1
M-C6:0	86,1	84,5	**M-C8:0**	118,5	69,6	**M-C10:0**	151,1	67,4	**M-C14:0**	145,7	5
M-C6:0	87	88	**M-C8:0**	120,3	74,8	**M-C10:0**	155	77,9	**M-C14:0**	160,8	10
M-C6:0	88,5	93,1	**M-C8:0**	121	77	**M-C10:0**	156,2	81,1	**M-C14:0**	166	13
M-C6:0	91,4	100	**M-C8:0**	124	86,3	**M-C10:0**	158,8	89	**M-C14:0**	171,1	15,9
M-C6:0	93,9	115,6	**M-C8:0**	126,9	96,1	**M-C10:0**	161,5	100	**M-C14:0**	177,8	20
M-C6:0	94,1	117	**M-C8:0**	128	100	**M-C10:0**	162,2	100,1	**M-C14:0**	179,2	22,2
M-C6:0	99,6	144	**M-C8:0**	128,1	100,7	**M-C10:0**	164,2	107,6	**M-C14:0**	179,6	22,7
M-C6:0	101	153,5	**M-C8:0**	131,5	101,6	**M-C10:0**	164,3	108	**M-C14:0**	185	27,9
M-C6:0	101,3	154	**M-C8:0**	128,6	102,5	**M-C10:0**	167,1	118,4	**M-C14:0**	192,3	36,9
M-C6:0	104,8	174,8	**M-C8:0**	129,4	105,5	**M-C10:0**	169	126,3	**M-C14:0**	195,8	40
M-C6:0	105,4	180,5	**M-C8:0**	131,1	112,5	**M-C10:0**	174,3	150,9	**M-C14:0**	197,1	44
M-C6:0	109,8	200	**M-C8:0**	131,4	113,8	**M-C10:0**	177,8	168,7	**M-C14:0**	202,9	53,9
M-C6:0	109,9	211,5	**M-C8:0**	131,5	113,9	**M-C10:0**	181,4	188,7	**M-C14:0**	207,5	60
M-C6:0	112,7	234	**M-C8:0**	131,5	114,2	**M-C10:0**	181,6	200	**M-C14:0**	207,3	62,8
M-C6:0	117,5	275,5	**M-C8:0**	135,1	130,5	**M-C10:0**	184,7	209,1	**M-C14:0**	210,5	70
M-C6:0	121,5	316	**M-C8:0**	137,3	141,4	**M-C10:0**	188,2	232,2	**M-C14:0**	214,7	80,3
M-C6:0	128,6	395	**M-C8:0**	137,6	142,6	**M-C10:0**	202,9	400	**M-C14:0**	218,8	98,7
M-C6:0	129,8	400	**M-C8:0**	138,8	148	**M-C12:0**	87,8	1	**M-C14:0**	222,6	100
M-C6:0	134,4	472	**M-C8:0**	141	159,6	**M-C12:0**	102,8	2,003	**M-C14:0**	221,6	100,4
M-C6:0	148,6	730	**M-C8:0**	145,7	186,5	**M-C12:0**	116	3,998	**M-C14:0**	225,6	114,1
M-C6:0	150	760	**M-C8:0**	148,1	200	**M-C12:0**	117,9	5	**M-C14:0**	228	123,1
M-C8:0	34,2	1	**M-C8:0**	170	400	**M-C12:0**	120,7	5,003	**M-C14:0**	230,6	133
M-C8:0	61,7	5	**M-C10:0**	63,7	1	**M-C12:0**	124,4	6,000	**M-C14:0**	234,7	150,8
M-C8:0	73,2	8	**M-C10:0**	78,7	2,003	**M-C12:0**	130,4	8,003	**M-C14:0**	237,8	165,2
M-C8:0	74,9	10	**M-C10:0**	90,8	3,998	**M-C12:0**	135	9,998	**M-C14:0**	245,3	200
M-C8:0	78,1	10,5	**M-C10:0**	93,5	5	**M-C12:0**	133,2	10	**M-C14:0**	269,8	400
M-C8:0	83,3	14	**M-C10:0**	93,4	5,003	**M-C12:0**	149	20	**M-C14:0**	295,8	760
M-C8:0	86,9	17	**M-C10:0**	98,1	6,000	**M-C12:0**	157,8	27,4	**M-C16:0**	134,3	1
M-C8:0	89	20	**M-C10:0**	103,3	8,003	**M-C12:0**	166	40	**M-C16:0**	148	2,003

Ésteres graxos (continuação)

Comp.	T (°C)	P (mmHg)	Comp.	T (°C)	P (mmHg)	Comp.	T (°C)	P (mmHg)
M-C16:0	162	3,998	**B-C10:0**	176,4	40	**P-C10:0**	179,6	80,002
M-C16:0	166,8	5	**B-C10:0**	182,6	50	**P-C10:0**	185,6	99,998
M-C16:0	172	5,003	**B-C10:0**	187,4	60	**P-C18:0**	186,8	2,003
M-C16:0	177	6,000	**B-C10:0**	195,6	80	**P-C18:0**	200,8	3,998
M-C16:0	184	8,003	**B-C10:0**	201,8	100	**P-C18:0**	206	5,003
M-C16:0	184,3	10	**P-C8:0**	70,5	2,003	**P-C16:0**	166	2,003
M-C16:0	193,6	14,3	**P-C8:0**	82,3	3,998	**P-C16:0**	181,6	3,998
M-C16:0	194,7	16,9	**P-C8:0**	86	5,003	**P-C16:0**	187	5,003
M-C16:0	202	20	**P-C8:0**	90	6,000	**P-C16:0**	191,4	6,000
M-C16:0	204,6	23,2	**P-C8:0**	94,1	8,003	**P-C16:0**	198,2	8,003
M-C16:0	208,6	26,9	**P-C8:0**	100	9,998	**P-C16:0**	203,6	9,998
M-C16:0	214,8	33,9	**P-C8:0**	114,1	19,997	**M-C18:1**	155,57	1,04
M-C16:0	219,5	40	**P-C8:0**	129,8	40,001	**M-C18:1**	162,77	1,541
M-C16:0	222,9	44,9	**P-C8:0**	135	49,999	**M-C18:1**	166,2	2,003
M-C16:0	225,1	48,6	**P-C8:0**	139,5	59,997	**M-C18:1**	169,56	2,188
M-C16:0	227,3	52,7	**P-C8:0**	147	80,002	**M-C18:1**	170,18	2,247
M-C16:0	229,9	57,5	**P-C8:0**	152,6	100,007	**M-C18:1**	175,46	2,94
M-C16:0	232,5	62,2	**P-C12:0**	123,7	2,003	**M-C18:1**	177,51	3,235
M-C16:0	235,8	69,7	**P-C12:0**	138,1	3,998	**M-C18:1**	182	3,998
M-C18:0	169,4	2,003	**P-C12:0**	143	5,003	**M-C18:1**	185,37	4,727
M-C18:0	184,6	3,998	**P-C12:0**	147	6,000	**M-C18:1**	192	6,000
M-C18:0	189,4	5,003	**P-C12:0**	155,3	8,003	**M-C18:1**	191,85	6,32
M-C18:0	193,6	6,000	**P-C12:0**	156,8	9,998	**M-C18:1**	194,74	7,258
M-C18:0	198,8	8,003	**P-C12:0**	173,8	19,997	**M-C18:1**	199,5	8,003
M-C18:0	204,1	9,5	**P-C12:0**	194	40,001	**M-C18:1**	198,46	8,498
M-C18:0	205,8	10,2	**P-C12:0**	200,2	49,999	**M-C18:1**	205,3	9,998
M-C18:0	208,4	11,1	**P-C12:0**	205,4	59,997	**M-C18:1**	202,96	10,147
M-C18:0	212,1	12,9	**P-C14:0**	147	2,003	**M-C18:1**	205,96	11,743
M-C18:0	216,6	15,3	**P-C14:0**	161,7	3,998	**M-C18:1**	208,93	13,247
M-C18:0	222,3	19	**P-C14:0**	166,8	5,003	**M-C18:1**	212,07	15,083
M-C18:0	227,3	23,1	**P-C14:0**	171	6,000	**M-C18:2**	166,5	2,003
M-C18:0	229,4	25,1	**P-C14:0**	177,6	8,003	**M-C18:2**	182,4	3,998
M-C18:0	230,7	26	**P-C14:0**	182,8	9,998	**M-C18:2**	193	6,000
M-C18:0	237,9	31,7	**P-C14:0**	200,2	19,997	**M-C18:2**	199,9	8,003
M-C18:0	239,7	36,2	**P-C10:0**	96,8	2,003	**M-C18:2**	206	9,998
E-C8:0	87	10	**P-C10:0**	109,7	3,998			
E-C8:0	101,8	20	**P-C10:0**	114,2	5,003			
E-C8:0	117,6	40	**P-C10:0**	117,8	6,000			
E-C8:0	123	50	**P-C10:0**	123,7	8,003			
E-C8:0	127,6	60	**P-C10:0**	128,5	9,998			
E-C8:0	134,8	80	**P-C10:0**	144,3	19,997			
E-C8:0	140,8	100	**P-C10:0**	161,2	40,001			
B-C10:0	143,3	10	**P-C10:0**	166,6	49,999			
B-C10:0	159,3	20	**P-C10:0**	171,6	59,997			

Os resíduos entre os valores experimentais e os preditos pelo modelo sugerido no Capítulo 3 (vide Equações 3.2.1 a 3.2.5) estão graficados na Figura A6 abaixo. Vale ressaltar que o maior desvio relativo foi igual a 135,5%, referente a um resíduo de 1,89 mmHg entre o valor experimental da pressão de vapor do ácido linoléico (1,4 mmHg a 202 °C) e o valor predito pelo modelo (3,29 mmHg).

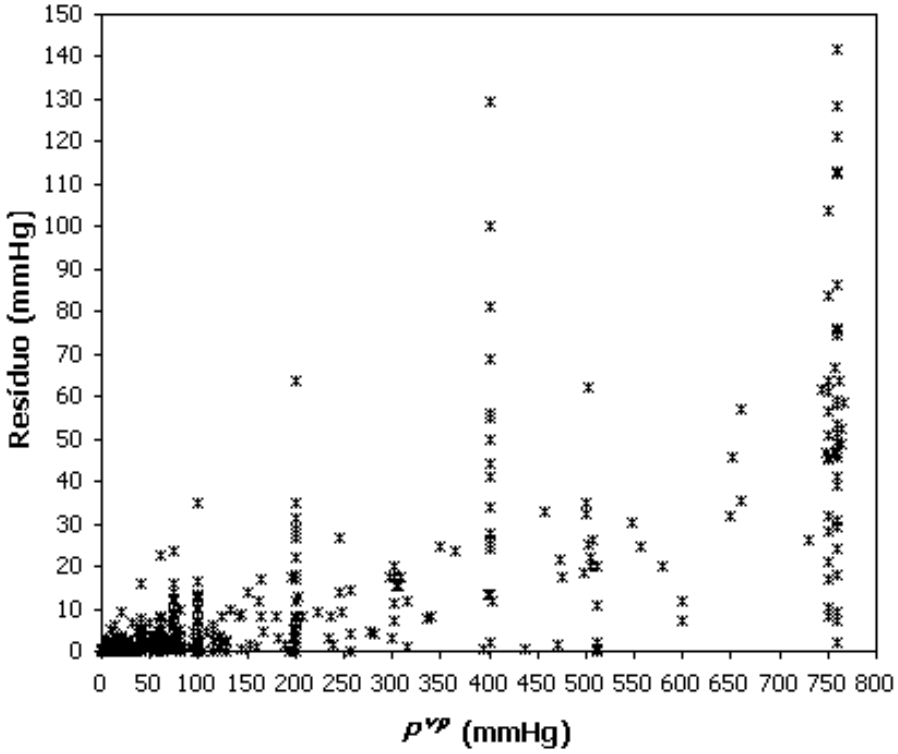

Figura A6. Resíduos para o banco de dados de pressão de vapor utilizado no Capítulo 3.

APÊNDICE III: INFORMAÇÕES A RESPEITO DOS PROGRAMAS DE SIMULAÇÃO

Este apêndice apresenta algumas informações relevantes a respeito do desenvolvimento dos programas de simulação utilizados neste projeto, que podem vir a ser úteis para um futuro trabalho do leitor.

De uma maneira geral, pode-se dizer que todos os programas foram desenvolvidos utilizando o software MatLab®, devido a maior facilidade na programação e na visualização dos resultados, na opinião da autora.

O programa de cálculo do ponto de bolha necessário no desenvolvimento do Capítulo 3 seguiu o algoritmo de resolução apresentado na Figura A7 abaixo.

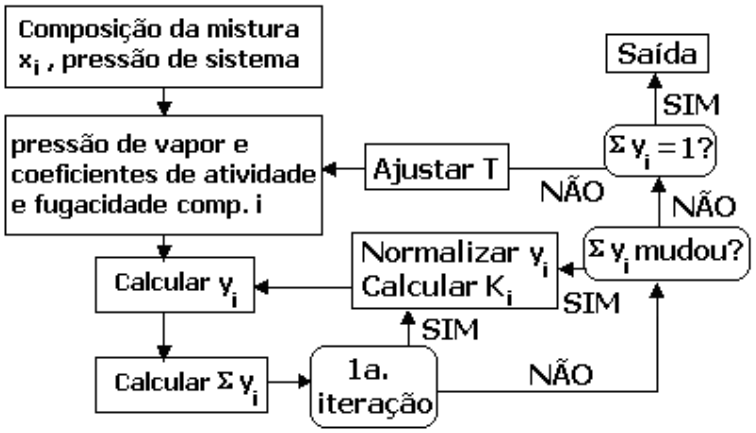

Figura A7. Algoritmo de resolução: cálculo do ponto de bolha.

Para se obter os resultados apresentados no Capítulo 4, foi necessário desenvolver um programa com três possibilidades diferentes do cálculo do equilíbrio líquido-vapor, que satisfizessem os três modelos desenvolvidos para a função objetivo $\sum_i y_i - 1 \leq \varepsilon$ (vide Equações 4.2.7, 4.2.8 e 4.2.9).

O algoritmo de resolução do problema está colocado na Figura A8. O tempo total de processo foi dividido em intervalos de um minuto. O algoritmo apresentado na Figura A8 é seguido a cada minuto, até que o tempo total do processo seja atingido. A subrotina do ponto de bolha segue o mesmo

procedimento descrito na Figura A7. Os dados de entrada necessários para inicializar o programa são:

- Carga inicial e composição do líquido;
- Parâmetros operacionais;
- Divisão dos compostos envolvidos em grupos, de acordo com os métodos disponíveis para coeficiente de atividade, propriedades críticas e pressão de vapor.

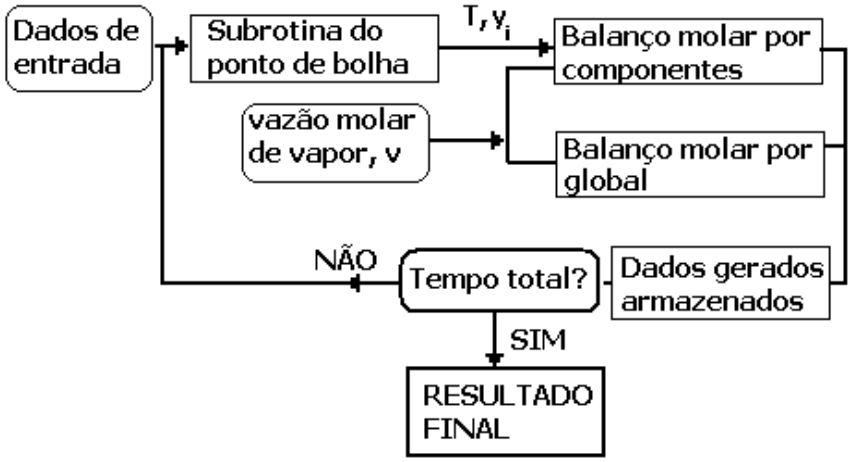

Figura A8. Algoritmo de resolução: destilação diferencial.

O algoritmo de resolução, apresentado na figura anterior, foi ligeiramente modificado para a inclusão da cinética de reações químicas e do balanço de energia, de forma que pudesse ser feita a investigação da isomerização de ácidos graxos polinsaturados durante a desodorização do óleo de canola e ser calculada a quantidade de vapor formada a cada tempo. O novo algoritmo pode ser visualizado na Figura A9.

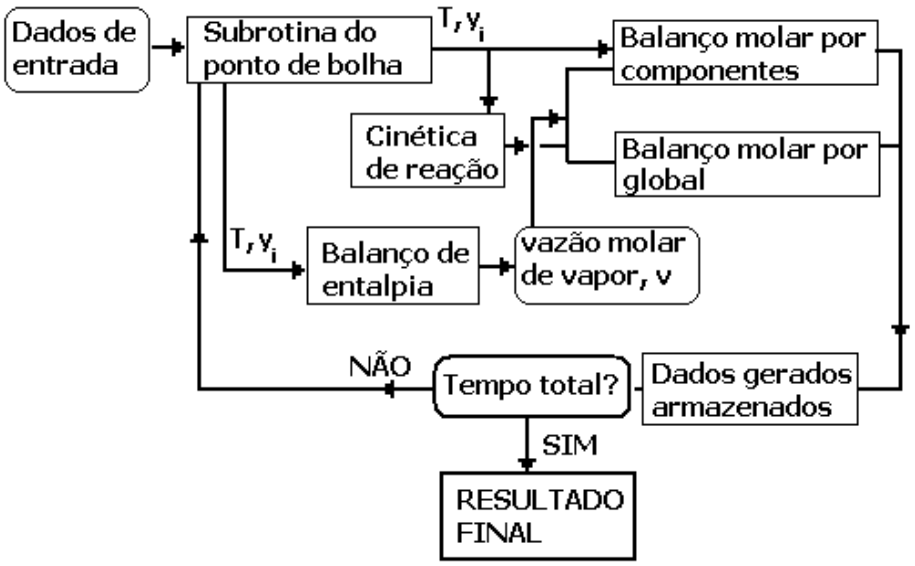

Figura A9. Algoritmo de resolução: destilação diferencial com reação química e balanço de energia.

Em relação ao programa desenvolvido para a simulação dos processos contínuos de desodorização e/ou desacidificação física em estado estacionário, o livro *Vapor-liquid equilibria using UNIFAC* (Amsterdam: Elsevier, 1977), de A. FREDENSLUND, J. GMEHLING e P. RASMUSSEN, é a melhor referência para quem deseja entender os detalhes da programação do algoritmo de NAPHTALI & SANDHOLM (1971) aplicado à uma coluna de destilação. Uma vez que o equipamento estudado neste trabalho não apresenta refervedor ou refluxo vindo do condensador, algumas pequenas modificações nas equações dos balanços de massa e energia, além das derivadas dos mesmos, necessárias no cálculo da matriz Jacobiana do método de convergência, foram feitas. O algoritmo de resolução (FREDENSLUND et al., 1977) está colocado a seguir na Figura A10.

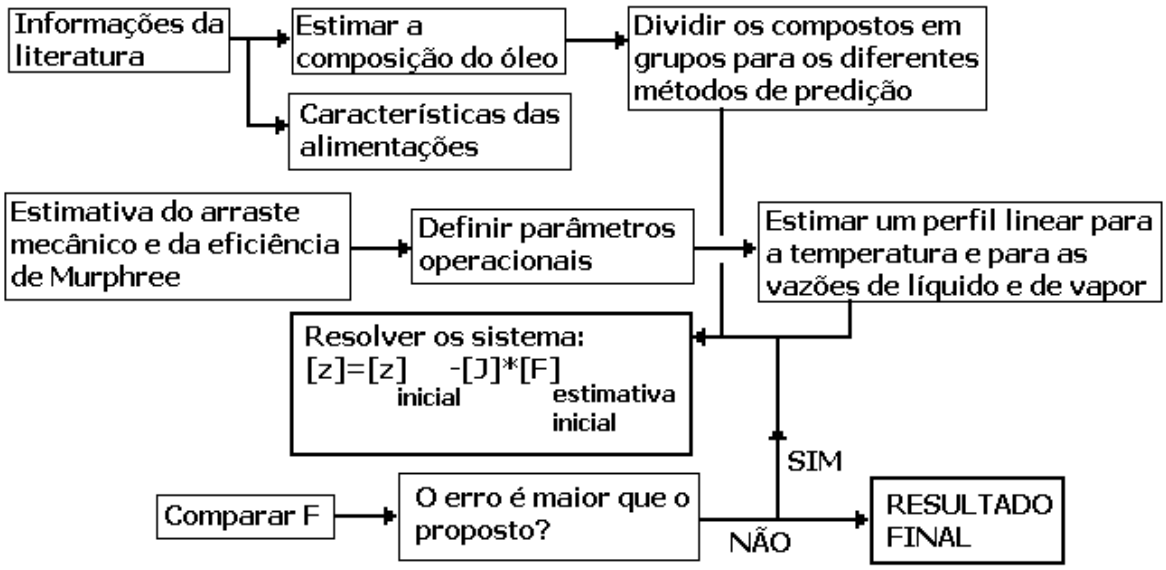

Figura A10. Algoritmo de resolução: processo contínuo em regime permanente.

onde z= vetor da variáveis desconhecidas; $z_{inicial}$ = vetor da estimativa inicial das variáveis desconhecidas; J = matriz Jacobiana do método de Newton-Raphson; F= vetor funções discrepância avaliadas com a estimativa inicial.

Em relação ao programa feito para a análise dinâmica, os detalhes já foram apresentados no Capítulo 2 de revisão bibliográfica e no Apêndice I desta tese.